High-frequency climate variability and forcing mechanisms in the western Mediterranean during the last 20,000 yrs: reconstructing atmospheric and oceanic responses

Tesis Doctoral

Marta Rodrigo Gámiz

Instituto Andaluz de Ciencias de la Tierra
Consejo Superior de Investigaciones Científicas -
Universidad de Granada (CSIC - UGR)

High-frequency climate variability and forcing mechanisms in the western Mediterranean during the last 20,000 yrs: reconstructing atmospheric and oceanic responses

Variabilidad climática de alta frecuencia y mecanismos asociados en el oeste del Mediterráneo durante los últimos 20.000 años: reconstrucción de la respuesta atmosférica y oceánica

Memoria de Tesis presentada por la Licenciada en Geología Dña. Marta Rodrigo Gámiz para optar al Grado de Doctor por la Universidad de Granada.

Esta Tesis Doctoral ha sido dirigida por la Dra. Francisca Martínez Ruiz, Investigadora Científica del CSIC, del Instituto Andaluz de Ciencias de la Tierra (CSIC-UGR).

Granada, 5 de diciembre de 2011

Vº Bº de la Directora

Francisca Martínez Ruiz

La Doctoranda

Marta Rodrigo Gámiz

Editor: Editorial de la Universidad de Granada
Autor: Marta Rodrigo Gámiz
D.L.: GR 1731-2012
ISBN: 978-84-9028-029-4

Instituto Andaluz de Ciencias de la Tierra
Consejo Superior de Investigaciones Científicas -
Universidad de Granada (CSIC - UGR)

Tesis Doctoral

High-frequency climate variability and forcing mechanisms in the western Mediterranean during the last 20,000 yrs: reconstructing atmospheric and oceanic responses

Variabilidad climática de alta frecuencia y mecanismos asociados en el oeste del Mediterráneo durante los últimos 20.000 años: reconstrucción de la respuesta atmosférica y oceánica

Marta Rodrigo Gámiz

Esta tesis ha sido desarrollada dentro de los proyectos del Plan Nacional CGL2006-13327-C04-04 y CGL2009-07603, financiados por el Ministerio de Ciencia e Innovación (MICINN) del Gobierno de España. También se agradece la financiación de los Fondos Europeos de Desarrollo Regional (FEDER) de la Comunidad Económica Europea, los proyectos RNM 05212 y Grupo de Investigación 0179 de la Junta de Andalucía, MARM 200800050084447 del Ministerio de Medioambiente y Medio Rural y Marino, y al programa Consolider-Ingenio CSD2006-00041 del Ministerio de Ciencia e Innovación del Gobierno de España. Igualmente es de agradecer la colaboración del Training Through Research Program UNESCO-IOC/MSU para la obtención de los testigos de sedimento marino estudiados. Se ha contado con una beca-contrato (2+2) de Formación de Personal Investigador (FPI) (referencia BES-2007-16814) y cuatro ayudas complementarias para le realización de Estancias Breves en el Extranjero concedidas por el Ministerio de Ciencia e Innovación. El trabajo de investigación ha sido mayormente desarrollado en el Instituto Andaluz de Ciencias de la Tierra (IACT) del Consejo Superior de Investigaciones Científicas (CSIC), en el Departamento de Mineralogía y Petrología de la Universidad de Granada (UGR), y en el Centro de Instrumentación Científica (CIC), todos ellos en Granada.

Parte del trabajo también fue realizado durante las estancias en el extranjero en “Section of Earth and Environmental Science” (octubre a diciembre de 2008), y “Department of Mineralogy, Isotopes Geochemistry and Geochonology” (octubre y noviembre de 2009) ambos en la Universidad de Ginebra (Suiza), así como en “The Royal Netherlands Institute for Sea Research”, NIOZ (septiembre y octubre de 2010, y mayo a julio de 2011) en Holanda.

“Investigar es el arte de indagar para descubrir las relaciones entre causa y efecto,

profundizar en el conocimiento, revelar lo que se desconoce,

la aproximación a una verdad.”

Aprender, realizar, experimentar, montar un modelo y concluir.

Bases del método científico (1604), Galileo Galilei

TABLE OF CONTENTS

Abstract

This Thesis provides a high-resolution paleoclimate reconstruction over the last 20,000 yrs obtained from marine records in the westernmost Mediterranean. Such reconstruction has provided new insights regarding millennial- to centennial-time scale atmospheric and oceanographic oscillations during this time interval. Thus, this multi-proxy approach allowed identifying abrupt climate oscillations and forcing mechanisms since the Last Glacial Maximum. Such oscillations have also been correlated with Greenland ice records but also with monsoonal low latitude variations, suggesting a strong connection of western Mediterranean climate with North Atlantic changes.

Over the last 20,000 yrs major climate intervals studied have been: the last Heinrich event, the Bölling-Alleröd period, the Younger Dryas, and the Holocene, when significant climate oscillations were also recognized.

Cold and dry conditions, supported by enhanced palygorskite and quartz contents, and significant increases in some detrital ratios (Si/Al, Zr/Al, and Ti/Al), characterize the last Heinrich event. At this time, major eolian dust contribution derived from the nowadays Senegal and Guinea regions. Such fluctuations also coincided with major oscillations in deep-water ventilation and current intensity associated with the impact of large volumes of Atlantic meltwater inflow. This has been further supported by the oxygen isotope record and lower SST (around 12ºC) derived from two organic paleothermometers (*haptophyte algae*-$U^{k'}_{37}$ and *thaumarchaeota*-TEX^{H}_{86}). Paleoproductivity proxies within this interval also indicate enhanced productivity and a subsequent organic enrichment prior to the last Organic Rich Layer described in the Alboran Sea basin.

During the interstadial Bölling-Alleröd period, progressively more humid conditions are denoted by typical fluvial proxies, and short-term climate oscillations such as the Intra-Alleröd Cold Period are also recognized. Concerning the oceanographic realm, lower oxygenation conditions favoured the onset of the last Organic Rich Layer deposition, thus evidencing stable thermohaline Mediterranean circulation. This warmer period is subsequently characterized by an increase in SST (up to around 18ºC) although exhibiting rapid variations (±3.0º-4.0ºC) in the *haptophyte*/alkenone paleothermometer ($U^{k'}_{37}$) supporting the definition of the Older Dryas period.

The Younger Dryas interval presents a remarkable feature; an early dry phase and more humid conditions towards the end. These distinct time-periods are also inferred by changes in paleoceanographic conditions, exhibiting high productivity levels at the onset and also an abrupt and brief cooling, reaching minimum values of 13ºC and 16ºC, using *haptophyte* and *thaumarchaeota* thermometers respectively.

Major divergence in SST-estimation ($U^{k'}_{37}$-18º-20ºC; TEX^{H}_{86}-23º-26ºC) with the respective biomarkers is recorded throughout the Holocene as well as slightly warmer *haptophyte*-derived temperatures (by ca. 1.5º-2ºC) in the westernmost Alboran Sea basin. These differences suggest a seasonal response in the organic proxies, as well as the influence of the hydrographic configuration of the Alboran Sea.

During the Holocene, significant detrital fluctuations are prominent at around 8.9 kyr cal. BP, correlating with forest cover declines in the Alboran borderlands, and suggest an intense eolian input from the southern African sources (Guinea and/or Senegal). At the same time, the demise of the last Organic Rich Layer deposition is recognized, which seems to be linked with major restructuration of the intermediate and deep-water circulation. A progressive decrease in values of fluvial proxies points to an early decline of the African Humid Period at 7.4 kyr cal. BP, with drier conditions prevailing up to 4.5 kyr cal. BP.

Within this context, increasing detrital input during cold events, deriving from the intensification of Saharan dust export from the present Guinea and Senegal regions across the western Mediterranean, has been related to a predominant positive index of the North Atlantic Oscillations, and southward migrations of the Inter-Tropical Convergence Zone over North Africa, involving variations in the African monsoon system. Conversely, radiogenic isotopes from detrital material deposited during warmer periods support a dominant provenance from present regions of Morocco, Mali and Mauritania.

Regarding climate forcing mechanisms, proxies used for reconstructing fluctuations in terrigenous input and paleoceanographic conditions, set in four paleoenvironmental groups (detrital, redox, paleoproductivity, and paleotemperature-paleosalinity) for spectral analysis, have

revealed major cycles at 1,300, 1,515, 2,000, and 5,000 yrs plus secondary harmonics. Obtained periodicities at 2,000 and 5,000 yrs support a global connection with records distributed at high-, mid-, and low-latitudes linked with the solar activity and monsoonal variations, while the 1,300 and 1,515 yr cycles appear to be linked with North Atlantic climate fluctuations. Spectral periodicities reinforce the strong connection between North Atlantic climate and monsoonal variations in the western Mediterranean context, and further support the extreme sensitivity of this region to cyclic climate changes as well as the climate teleconnections triggered by the North Atlantic Oscillations, the Inter-Tropical Convergence Zone migrations and monsoon activity, probably exacerbated by solar activity variations.

Resumen

En esta Tesis se aborda la reconstrucción de la variabilidad climática acaecida en los últimos 20.000 años, a partir del análisis de alta resolución de sedimentos marinos del Mediterráneo más occidental, cuenca del mar de Alborán. La utilización e integración de diversos indicadores mineralógicos, geoquímicos y de tamaño de grano, ha permitido interpretar la respuesta de los distintos componentes del sistema climático, fundamentalmente la de la atmósfera y océano a lo largo del intervalo temporal estudiado. Asimismo, se han caracterizado cambios climáticos rápidos ocurridos a escala de los cientos y miles de años, y los mecanismos asociados a sus causas y efectos. Estas oscilaciones rápidas se han correlacionado con las registradas en Groenlandia y en el Atlántico Norte y con cambios en el sistema monzónico africano, lo cual pone de manifiesto la alta sensibilidad del Mediterráneo occidental en respuesta a la variabilidad climática global.

A lo largo de los últimos 20.000 años se han podido caracterizar los periodos climáticos más significativos de este intervalo. En orden cronológico son los siguientes: el último evento Heinrich (H1), el periodo Bölling-Alleröd (B-A), el Younger Dryas (YD), y diversas fluctuaciones que tuvieron lugar durante el Holoceno.

El último evento Heinrich se reconoce como un periodo frío y seco caracterizado por altos valores de las relaciones geoquímicas típicamente eólicas, Si/Al, Zr/Al, y Ti/Al, y de los contenidos de cuarzo y paligorskita. Durante este intervalo se confirman condiciones áridas con un mayor aporte de material detrítico procedente del Norte de África, lo que unido a una intensificación de la circulación atmosférica favoreció el transporte de material desde las regiones africanas correspondientes a las actuales de Guinea y Senegal. Al mismo tiempo, también se han interpretado importantes oscilaciones en la circulación oceánica, condiciones de elevada oxigenación y mayor intensidad de las corrientes de fondo. Se pone de manifiesto, además, la entrada de aguas atlánticas procedentes del deshielo de los glaciares, con temperaturas superficiales de unos 12ºC. Durante este periodo también tuvo lugar un aumento de la productividad biológica, que contribuyó al depósito de una capa rica en materia orgánica previa a la última descrita en Alboran.

El periodo Bölling-Alleröd se registra como un intervalo más cálido, con aumento progresivo de las relaciones geoquímicas indicadoras de condiciones fluviales y, por tanto, de mayor humedad. También se produjeron algunas interrupciones rápidas de mayor aridez como el "Intra-Alleröd Cold Period (IACP)". Respecto a las condiciones paleocenográficas durante este intervalo de tiempo, una mayor estabilidad en la circulación y una menor ventilación del fondo favorecieron el depósito de la "última capa rica en materia orgánica" descrita en la cuenca del mar de Alborán. Durante este tiempo se registran temperaturas superficiales de unos 18ºC, aunque con algunas oscilaciones rápidas hacia valores menores durante el periodo conocido como "Older Dryas".

El Younger Dryas corresponde a un evento frío, pero no tan árido como el último evento Heinrich. Se caracteriza por una primera fase más fría con valores de temperaturas superficiales en torno a unos 13º-16ºC según los indicadores orgánicos utilizados (*Haptophyta algae* y *Thaumarchaeota* respectivamente) y una mayor aridez, que dio paso a unas condiciones progresivamente más cálidas y de mayor humedad.

Durante el Holoceno, aunque tradicionalmente ha sido definido como un periodo de estabilidad climática, se han puesto de manifiesto diversas oscilaciones tanto en el régimen sedimentario como en el contexto oceánico. Entorno a los 8.900 años BP se registra un aporte de material eólico similar al reconocido durante el último evento Heinrich, así como un progresivo descenso de humedad a partir de los 7.400 años BP, determinando el deterioro del "Período Húmedo Africano" y un cambio hacia condiciones áridas y semi-áridas equivalentes a las reconocidas actualmente. En relación a las condiciones paleoceanográficas, se produjo un aumento de ventilación en torno a los 8.900 años BP que marca el fin del depósito de la "última capa rica en materia orgánica". Una mayor divergencia en los valores absolutos de las temperaturas de las aguas superficiales obtenidas con los dos paleotermómetros orgánicos usados, sugiere una inversión en la estación de máxima producción de *Thaumarchaeota*, que reflejaría temperaturas de la estación de verano. Además, las temperaturas registradas en la cuenca Oeste presentan valores mayores, en torno a 1,5º-2,0ºC más elevadas que en la cuenca Este, sugiriendo una mayor influencia de la circulación oceánica superficial en esta cuenca.

El incremento de material eólico procedente de las regiones actuales de Guinea y Senegal durante periodos fríos estaría condicionado por las migraciones meridionales de la Zona de

Convergencia Inter-Tropical, así como por un índice positivo de la Oscilación del Atlántico Norte. Contrariamente, durante los periodos más cálidos la Zona de Convergencia Inter-Tropical estaría en una posición más septentrional y la Oscilación del Atlántico Norte presentaría un índice negativo, favoreciendo así unas condiciones más húmedas con una procedencia del material detrítico del Sur de la Peninsula Ibérica y del Norte de África, como serían las regiones actuales de Marruecos, Mauritania y Mali.

El análisis espectral integrado de los diferentes indicadores, detríticos de régimen sedimentario, productividad, oxigenación y condiciones paleoceanográficas, ha puesto de manifiesto oscilaciones climáticas de carácter cíclico, con periodicidades de 1.300, 1.515, 2.000 y 5.000 años. Los ciclos a mayor escala, 2.000 y 5.000 años, se correlacionan con ciclos reconocidos en otros registros climáticos situados a latitudes altas, medias y bajas, y se relacionan con variaciones orbitales y en la actividad solar. Los ciclos de 1.300 y 1.515 años estarían relacionados con las variaciones climáticas en el Atlántico Norte así como con las oscilaciones del sistema monzónico Africano. Todo ello confirma la influencia de las fluctuaciones climáticas del Atlántico Norte y la actividad monzónica en el Mediterráneo más occidental.

1. Motivation

Climate variability at high frequency scale is a disturbing current topic motivating an intense debate around global warming, its impact on present day society, and its linkage with the anthropogenic activities such as greenhouse gases emissions (e.g., Ruddiman, 2001; Overpeck and Cole, 2006; IPCC, 2007; Wanner et al., 2008).

However, many aspects of the functioning of the Earth's climate system remain still unknown. Climate has changed abruptly in the past, and is likely to change abruptly in the future, even in the absence of significant anthropogenic climate forcing (Overpeck and Cole, 2006). Thus, in order to assess the significance of modern climate change it is essential to place our recent observed changes in a longer-term context.

Furthermore, the understanding of Earth's climate, its variations and eventual prediction of future changes, requires the knowledge of the response of the different constituents conforming the climate system and their controlling factors (e.g., Ruddiman, 2001). This complex system includes various components, such as the atmosphere, oceans, ice and snow cover, land surface, as well as the interactions among them, which involve a large variety of physical, chemical and biological processes on a wide range of space and time scales (e.g., Rahmstorf, 2001).

At orbital time-scales, the oscillations of the climate system are relatively well understood, being mainly related to perturbations of the Earth's orbit around the Sun, determining "Milankovitch cycles". However, at shorter time-scales, climate variability is poorly comprehended. Addressing the climate change at the high frequencies requires longer observations than the present time. Consequently, appropriate natural climate archives are essential to constrain the functioning of the climate system in the past at longer time-scale than historical archives.

In this sense, marine records from high-sedimentation rate settings are of special relevance for paleoclimate reconstructions. Marine sediments have revealed as excellent paleoarchives providing a comprehensive overview of past climate variability. In particular, the westernmost Mediterranean fulfils this goal, offering exceptional high-resolution records of climate oscillations. Additionally, the role of atmospheric and oceanic systems, their interrelation and their interlatitudinal climatic transmission in this area are of especial interest to understand their rapid response to climate changes. The western Mediterranean region is also one of the most sensitive areas to climate change at regional and global scales due to its intermediate latitudinal position interplaying the tropical and the polar climate influences, the interconnection between Atlantic and Mediterranean water masses, as well as the large contribution of North African eolian dust.

Within this context, this Thesis was intended to reconstruct the past climate variability registered in marine sediments from the western Mediterranean in order to further understand the complex picture of the climate change and climate responses from the atmosphere and the ocean.

Regarding the selected time interval, although climate shifts have been more dramatic at glacial/interglacial frequencies, abrupt paleoenvironmental changes occurred since the Last Glacial Maximum (last 20,000 yrs) represent our immediate past climate, and their reconstruction is essential for further understating of present conditions. Furthermore, such significant climate oscillations are also the key to elucidate climate responses, cyclic changes and forcing processes in the context of future oscillations.

2. Introduction

The Earth has experienced drastic climate fluctuations for billions of years, being the forcing factors of much of these major climatic oscillations related to external (orbital) and internal parameters of the Earth's climate system. Even though climate has been in continuous change, the rapid rates of change at present time, involving both natural and anthropogenic factors, have led to increasing concerns on global effects. Indeed climate change is already beginning to transform life on Earth. Around the globe, seasons are shifting, temperatures and sea levels are raising, whereas at the same time ecosystems, natural resources, and modern societies are threaten by such rapid alterations. Major efforts and actions are being taken to face such a global concern. Furthermore, the society is also becoming aware of climate change effects and vast information is now available from the literature and web resources (e.g., http://www.ipcc.ch/, http://www.climate.noaa.gov/, http://www.usgcrp.gov/usgcrp/, http://www.globalchange.gov/). Despite growing research efforts and economic investments, the functioning of the climate system is far from being understood. Other than the uncertainties regarding the consequences of global change in the future, the interactions of the different climate components (atmosphere, lithosphere, biosphere, hydrosphere and cryosphere) and respective climate responses to climate variability are not yet fully understood. For this understanding, it is necessary to address climate oscillations at larger scales than instrumental and historical data, which implies natural archives providing information on past climate change and climate variability. Diverse paleoarchives have been used for this purpose, including continental records (e.g., tree rings, speleothemes, lakes sediments) ice cores and marine archives (e.g., corals, sediments). In this context, paleoclimate data provide the necessary constrains on the functioning of the climate systems and a comprehensive overview of the climate variability. Particularly, marine sediments have revealed as excellent records of past climate variability and constitute the base for paleoclimate reconstructions in this research.

Regarding the timing and scales of climate variations, even though our changing planet has experienced significant climate changes over Earth’s history, our immediate past climate, involving similar ocean circulation patterns to present times, is the most directly related to current climate conditions thus being the immediate precedent to the intensively debated “climate change problem”. Furthermore, the significant climate oscillations occurred since the Last Glacial Maximum (LGM) may offer climate scenarios and valuable information on nowadays changes, also serving to better understand and predict potential future effects.

As far as spatial variability is concerned, paleoclimate archives from highly sensitive regions provide most valuable information for high-frequency climate variations and enable the identification of the causes and the driving mechanisms of past rapid climate oscillations, thus providing an accurate knowledge of the components of the climate system and an understanding of internal climate feedbacks (e.g., Menviel et al., 2011). In this sense, the westernmost Mediterranean has revealed as an exceptional region for paleoclimate reconstruction since high sedimentation rates in the basin have resulted in remarkably high-resolution records. The identification of both climate components and feedbacks from these records is essential to evaluate the significance of present and future climate variability (e.g., Jasen et al., 2007; Solomon et al., 2007). Thus, high-resolution paleoclimate reconstructions of high-frequency climate oscillations, millennial- to centennial- time scale, allow addressing past trends and are necessary in order to understand the future evolution.

In summary, this research has been designed to analyze paleoclimate information by using high-resolution marine records from a highly sensitive region, and spanning an appropriate time window to investigate the factors that control the spatial and temporal patterns of climate variability.

2.1. Climate variability since the Last Glacial Maximum

Prior to the LGM (115 to 21 kyr BP), climate conditions have been characterized by abrupt glacial–interglacial oscillations over periods of about 100,000 years, broadly recorded in the Greenland ice-cores and North Atlantic sediments. These included the Dansgaard–Oeschger events (D/O events) as a progressive coolings (stadials) interrupted by rapid warmings (interstadials) (e.g., Bond et al., 1993; Grootes et al., 1993), and the Heinrich events (H events) (Heinrich, 1988). The mechanism driving the D/O events probably involves changes in the thermohaline circulation, though the ultimate causes are still unknown. In contrast, the mechanism leading to Heinrich events are much better understood; the presence of ice-rafted debris (IRD) layers in North Atlantic marine records has been explained by the melting of icebergs in this region, which additionally provided a large freshwater input to the North Atlantic. Modelling studies showed that such an input would cause the thermohaline circulation (THC) to collapse and the cooling of North Atlantic surface waters (e.g., Paillard et al., 1994; Rahmstorf, 1995; Seidov and Maslin, 1999).

The LGM (23,000 – 18,000 yrs) is identified as a critical major manifestation of natural climate changes. This period is also recognized as the most recent maximum in globally integrated ice volume (Mix et al., 2001), with a low-stand sea level (130m lower). Other known abrupt climate oscillations have also taken place after this last ice age, i.e. last Heinrich event (H1, ~16,500 – 15,700 yr cal. BP) (Heinrich, 1988), Bölling-Alleröd period (B-A, 14,670 - 12,890 yr cal. BP) (e.g., Von Grafenstein et al., 1999; Brauer et al., 2000; Liu et al., 2009), Younger Dryas (YD, 12,890 - 11,650 yr cal. BP) (e.g., Dansgaard et al., 1989; Alley et al., 1993; Peteet, 1995), and several short-term variations during the Holocene (e.g., Alley et al., 1997; Mayewsky et al., 2004; Alley and Ágústsdóttir, 2005; Wanner et al., 2008).

In particular, the last glacial-interglacial transition (around 15,000 – 9,000 yr cal. BP) has been of special interest since many processes and components of the climate system were involved in a total restructuring of the climate at a global scale (e.g., von Grafenstein et al., 1999; Denton et al., 2006). That transition occurred in several steps, some of them still poorly known in terms of their hydrological signal or internal structure, such as the Mystery Interval (MI) (17,500 – 14,500 yr cal. BP) defined as the time period between the beginning of the H1 and the onset of the B-A, representing the onset of the most recent glacial termination (Denton et al., 2006).

Much progress in the study of climate changes of the LGM has occurred in the last 40 years since the end of the CLIMAP project of the 1970s (Climate Long-range Investigation, Mapping and Prediction) (CLIMAP-Project-Members, 1979, 1981). Since 1999, the EPILOG project is the scientific committee in charge of giving continuation to this document and synthesizing the progress of the LGM knowledge. However, in spite of this amount of research, some interactions of the climate system remain yet uncertainties for the scientific community claiming its continuous study.

In this sense, the geological marine record from the western Mediterranean offers well preservation conditions of the past climate variations, allowing a detail study of paleoclimate fluctuations, their consequences and the forcing mechanisms associated.

2.2. Marine archives from the westernmost Mediterranean: the Alboran Sea record

The highly sensitive western Mediterranean area provides useful information for understanding patterns of the climate variability and paleoclimate responses. Numerous records have demonstrated the westernmost Mediterranean environment responses to climatic fluctuation during the last glacial period (e.g., Cacho et al., 2001; Moreno et al., 2002, 2005; Martrat et al., 2004, 2007; Sierro et al., 2005).

The hydrodynamic response of the western Mediterranean Sea to rapid climate variability has been previously described in terms of oxygenation conditions and marine productivity during the last deglaciation (e.g., Jiménez-Espejo et al., 2007, 2008; Rogerson et al., 2008). Sea surface temperature (SST) reconstructions have been derived from marine and terrestrial biomarker, and planktonic foraminifera assemblages for the last 52 kyr BP (e.g., González-Donoso et al., 2000; Cacho et al., 2001; Martrat et al., 2004, 2007). Similarly, deep-water temperatures (DWT) have been reconstructed for the last 50 kyr based on the analysis of Mg/Ca ratios and stable oxygen isotopes in benthic foraminifera showing the link with Dansgaard-Oeschger (D-O) variability, i.e., cold temperatures associated with stadial intervals (Cacho et al., 2006).

In the context of oceanic and atmospheric interconnections, variations in fluvial and eolian inputs during cold stadial periods have demonstrated an increase in aridity in southern Iberia and North Africa, with stronger Saharan winds (Moreno et al., 2002, 2005). Moreover, palynological studies have shown the synchronism between the vegetation response on the Mediterranean region and rapid climate variability during the last glacial period, with rapid forest development during interstadials and forest contractions accompanied by the expansion of semi-desert vegetation during D-O stadials and H events (Sánchez Goñi et al., 2000, 2002; Combourieu Nebout et al., 2002; Fletcher et al., 2008). Pollen records have also demonstrated the possible relationships between African faunal variations and climatic change (deMenocal et al., 2004).

The comparison of model-data including Heinrich Event 1 (H1) and the Last Glacial Maximum with palynological records presents major changes in vegetation distribution occurring simultaneously with shifts in the ocean state (surface temperature, circulation), showing colder temperature and increasing dryness during this events (Kageyama et al., 2005).

2.3. Range of proxies: mineralogical and geochemical approach

The inorganic fraction and organic components of marine sediments have been widely used as proxies for changes in paleoenvironmental conditions. Considerable effort has been devoted to identify specific sedimentary components that have been unambiguously transported to the ocean via the atmosphere or by river runoff in order to gain insight into the geochemistry of sedimentary deposits.

Bulk mineralogy composition of deep-sea sediments has been successfully used to trace the source areas, the climate conditions and the transport mechanisms of detrital particles (e.g., Caquineau et al., 1998). Serving as an example, palygorskite is found in calcareous pedogenic crusts in areas with arid and semi-arid climates that favoured evaporation and chemical concentration (e.g., El Mouden et al., 2005). Thus, this fibrous clay mineral is recognized as a tracer of desert sources, especially as a source marker for the Saharan eolian dust in the western Mediterranean (Coudé-Gaussen et al., 1987; Chamley, 1989; Rognon et al., 1989; Molinaroli, 1996; Bout-Roumazeilles et al., 2007). Kaolinite is also commonly found in aerosols, evidencing that the source areas have undergone intense leaching, typical of the central and southern Sahara and abundant in the Sahel and equatorial regions (Caquineau et al., 1998). In general, North Africa eolian minerals include quartz, feldspars, calcite, dolomite, illite, kaolinite, smectite, mixed layers clay minerals and palygorskite. (Chester et al., 1984; Coudé-Gaussen et al., 1987). Specifically, quartz is the most abundant mineral in Saharan dust being easily quantified because it has a much wider range of particle size compared to other minerals commonly found in deep-sea sediments (Beltagy et al., 1972; Kolla et al., 1979). Thus, higher eolian mineral contents must have been caused by changes in the prevailing atmospheric patterns, resulting from drier and colder climatic conditions in the source areas and/or more frequent and intense outbreaks of dust transport (Hoogakker et al., 2004).

Paleoenvironmental changes are also reflected in the bulk chemical composition of marine sediments. Thus, element/Al ratios reflect chemical weathering conditions depending on physical erosion in the surrounding areas, as well as the oceanographic conditions at time of sediments deposition. Al concentrations in marine sediments generally can be assigned to the fine-grained aluminosilicate detrital fraction (Calvert and Pedersen, 2007). This has led to its use as a

normalizing parameter for the assessment of the relative degrees of enrichment or depletion of specific elements in a given sample, or to estimate the "background" contribution of an element derived from crustal sources (Van der Weijden, 2002).

Geochemical ratios such as Si/Al, Ti/Al, Zr/Al, K/Al, Mg/Al, Rb/Al have been extensively used as proxies for terrigenous fluctuations (eolian and riverine inputs) in the Mediterranen region (Wehausen and Brumsack, 1999; Martínez-Ruiz et al., 2000; Moreno et al., 2002; Weldeab et al., 2003; Frigola et al., 2007, 2008; Jiménez-Espejo et al., 2007, 2008). Si mostly derives from alumino-silicates and quartz since biogenic opal content is of minor importance in this area due to its oligotrophic conditions and the dissolution of silica (Masqué et al., 2003). Zr and Ti reside within heavy minerals such as zircon, ilmenite and rutile (both TiO2). Zr/Al ratio is a reliable proxy for eolian input used to discriminate the input from the African margin (Hamroush and Stanley, 1990), reflecting changes in the prevailing atmospheric circulation over the area. Clay minerals (illite, chlorite) and feldspars are mainly responsible for the higher K/Al, Mg/Al and Rb/Al ratios mainly reflect clay minerals (illite, chlorite) and feldspars, which are predominantly found in sediments derived from rivers (Wehausen and Brumsack, 1998, 2000; Foucault and Mélières, 2000; Weldeab et al., 2003), indicating the intensity of physical/chemical weathering.

Similarly, redox-sensitive trace element ratios, such as V, Cr, Cu, Co, Zn, Fe, Mn, U, provide further information about bottom-water oxygenation conditions due to their solubility dependence on their valence and hence on the prevailing redox conditions at time of sediment deposition (e.g., Böttcher et al., 2003; Martínez-Ruiz et al., 2003; Moreno et al., 2004; Tribovillard et al. 2006; Brumsack, 2006; Jiménez-Espejo et al., 2007; Rogerson et al., 2008).

Therefore, terrigenous deposition and oceanographic conditions are controlled by a complex and subtle combination of processes that can exert a strong influence on the paleoclimatic marine record which are reflected in a diversity of proxy indicators.

3. Scope and framework of the Thesis

As mentioned in previous sections, the particular latitudinal position and the high-sedimentation rates of the westernmost Mediterranean made of this region a key location for paleoclimate reconstructions. On the basis of high-resolution analyses of marine sediment records from this area, this Thesis aims the recognition of climate oscillations since the LGM, establishing the marine and atmospheric responses to climate variability.

Within this context, specific objectives of the Thesis focus on:

- Reconstruction of rapid climate changes over the last 20,000 yrs.
- Assessment of the marine response to climate variability, which will include paleoproductivity, oxygen conditions, paleocirculation, and sea surface temperatures.
- Reconstructing atmospheric responses to climate variability on the basis on terrigenous input fluctuations associated with cold/dry and warm/humid periods, identifying source areas for eolian dust and atmospheric circulation patterns.
- Identification of cyclic climate oscillations as well as the main forcing mechanism associated to each climate cycle.

A wide suite of mineralogical, sedimentological and geochemical proxies was applied, encompassing the different results in four main Chapters.

Chapter I present a complete and high-resolution mineralogical, geochemical and grain size distribution records from a sediment core (293G) recovered on the East Alboran Sea basin. This multi-proxy approach allowed the reconstruction of the atmospheric and oceanic variability in this region in terms of eolian input fluctuations, and paleoceanographic conditions to rapid climate variability since the LGM. Paleoproductivity conditions and deep-water current intensity at time of major paleoclimate oscillations have also been addressed in this chapter.

After a detailed description of detrital material fluctuations in the marine record 293G, Chapter II focuses on a further characterization of the eolian terrigenous provenance and the paleoatmospheric transport pathways during the last 20,000 yrs in the western Mediterranean. For this purpose radiogenic isotopes have revealed as appropriate tracers to identify source areas of

terrigenous material. This study provides valuable insights into past atmospheric circulation, geographic provenance of the eolian dust and the climate conditions over the surrounding continents.

Chapter III includes a detailed cyclostratigraphic analysis using different paleonvironmental proxies (those for detrital input, redox conditions, paleoproductivity, and paleotemperature-paleosalinity) to determine high-frequency periodicities over the last 20,000 yrs and the forcing mechanisms associated. The conspicuous climate cycles recognized at the millennial- to centennial-climate spectrum scale have revealed the excellence and sensitivity of this continuous and high-resolution multi-proxy record for evidencing cyclic climate changes in the oceanic-atmospheric circulation in the western Mediterranean as well as its strong link with the North Atlantic climate system.

Chapter IV envisages the oceanic response to rapid climate oscillations in terms of Sea Surface Temperatures (SST) by using an organic geochemical approach. For that, two marine records have been analyzed; record 293G from the Eastern basin and a second core, 434G, from the Western Alboran basin. The integration and comparison of two paleothermometers used in both selected marine records also extend the discussion of molecular markers distribution over the studied time interval. The high-resolution paleoceanographic evolution reconstruction at millennial- to centennial-time scales along western Mediterranean have further demonstrated the North Atlantic influence in this region as well as the complex Mediterranean thermohaline circulation.

Furthermore, other works derived from different collaborations are also mentioned in Appendix III, which relates to:

- The integration of terrestrial and marine paleoclimate records for reconstructing climate variability in the Iberian Peninsula during the Late Holocene.
- The impact of major climate fluctuations and environmental conditions on human cultural evolution.

4. Chapter I.- Impact of climate variability in the western Mediterranean during the last 20,000 years: oceanic and atmospheric responses

Rodrigo-Gámiz, M., Martínez-Ruiz, F., Jiménez-Espejo, F.J., Gallego-Torres, D., Nieto-Moreno, V., Romero, O., Ariztegui, D.

Quaternary Science Reviews 30 (15-16), 2018-2034. doi:10.1016/j.quascirev.2011.05.011

Abstract

Eolian input fluctuations and paleoceanographic conditions in the western Mediterranean have been reconstructed by using a multi-proxy approach to infer climate variability for the last 20,000 yr. A sediment core from the East Alboran Sea basin provides high-resolution geochemical, mineralogical and grain size distribution records from the Last Glacial Maximum onward. The accurate chronology obtained, closely related with the North Greenland Ice core Project, has provided a detailed paleoclimate reconstruction at the centennial-millennial time scale. Mineral and chemical compositions as well as sediment grain size distribution have been used to establish both fluvial and eolian input variations, deep-water current intensity, and ventilation and productivity conditions at the time of deposition. During the cold period Greenland Stadial-2a, the analyzed proxies evidence significant climate oscillations. Redox proxies, showing marked Mn/Al and Fe/Al peaks, as well as granulometric parameters, support major changes in thermohaline circulation, with active circulation triggered by the Western Mediterranean Deep Water formation. Ba/Al ratios and the presence of authigenic barite point to high productivity during the Last Heinrich event. At this time, Zr/Al, Si/Al and Ti/Al ratios as well as quartz and palygorskite contents also corroborate dryer conditions in the Alboran borderlands, with a major reorganization of atmospheric circulation at the beginning of the deglaciation and during the Last Heinrich event. In contrast, a decreasing trend in the Zr/Al ratio and increasing Mg/Al, K/Al and illite + chlorite/kaolinite ratios would indicate enhanced river runoff and supporting lower eolian dust input and wetter periods during the Bölling-Alleröd. Short-term and abrupt climate oscillations such as the Intra-Alleröd Cold Period are likewise reflected by minor yet conspicuous changes in eolian proxies. During the Younger Dryas, we distinguish an initial cold and dry phase, with major westerlies intensity, thermohaline reactivation, and high productivity levels, and a second wetter phase characterized by sporadic rainfalls over poorly vegetated surrounding continental areas. Then, during the Holocene, alternating phases of major humidity and aridity were recorded by major fluctuations in detrital input. These are also correlated with recurrent forest cover declines reported from pollen records, with a noteworthy early decline in the African Humid Period. During the Holocene, an initial demise of the Last Organic-Rich Layer is also evidenced, tentatively associated with aspiration forces promoted by intense thermohaline circulation through the Gibraltar Strait.

1. Introduction

Understanding ocean-atmospheric interactions is essential when interpreting changes in the climate system and to further identify past climate variations. The atmospheric response to climate oscillations has been mainly reconstructed to date from fluctuations in atmospheric dust fluxes and circulation patterns (e.g., Pye, 1987; Guerzoni et al., 1997; Moulin et al., 1998; Bar-Or et al., 2008). Eolian dust transported in the atmosphere from the desert areas is known to be a major contributor to oceanic sedimentation in certain regions (Loÿe-Pilot and Martin, 1996; Molinaroli, 1996; Prospero, 1981). Thus, well-dated marine sediments can be used to reconstruct past variations in atmospheric circulation throughout the Mediterranean region (e.g., Moreno et al., 2002; Weldeab et al., 2003; Bout-Roumazeilles et al., 2007). In particular, the western Mediterranean is an exceptional region because it has received a significant volume of eolian dust from the African margin during cold periods as a result of stronger wind transportation and/or availability of the material (Moreno et al., 2002; Bout-Roumazeilles et al., 2007).

The latitudinal position of the western Mediterranean makes this region especially sensitive to past climate oscillations. Therefore, several westernmost Mediterranean records serve to demonstrate the connection between oceanographic and atmospheric oscillations during the last glacial cycle, supporting a strong link between the Mediterranean and North Atlantic climates (e.g., Rohling et al., 1998; Cacho et al., 1999, 2000; Combourieu Nebout et al., 2002, 2009; Martrat et al., 2004). Some recent terrestrial records from diverse lake sequences distributed in the Iberian Peninsula suggest the interplay of Atlantic and Mediterranean influences on the hydrology and vegetation fluctuations (e.g., Carrión and van Geel, 1999; González-Sampériz et al., 2006; Morellón et al., 2009a; Moreno et al., 2011b; and references therein).

Various geochemical and mineralogical proxies have been successfully used to recognize past climate conditions. Fluctuations in quartz, palygorskite and kaolinite contents have been used to mark Saharan dust provenance (e.g., Kolla et al., 1979; Coudé-Gaussen et al., 1987; Caquineau et al., 1998, 2002; Bout-Roumazeilles et al., 2007). Analogously, Si/Al, Ti/Al, K/Al, Zr/Al ratios in the Mediterranean region have been extensively used as proxies for terrigenous input or sediment supply that can be linked to environmental conditions in the source areas (e.g., Wehausen and Brumsack, 1999; Martínez-Ruiz et al., 2000; Moreno et al., 2002; Weldeab et al., 2003; Frigola et al., 2007, 2008; Jiménez-Espejo et al., 2007, 2008). Variations in some redox-sensitive elements have also been used to describe oxygenation conditions in the westernmost Mediterranean (Jiménez-Espejo et al., 2007, 2008; Rogerson et al., 2008). However, a continuous high-resolution record of

the last 20,000 yr integrating a wide suite of proxies (geochemical, mineralogical and grain size) was lacking for this region.

This contribution therefore presents an integrated multi-proxy study with a robust chronology that provides a much more detailed reconstruction of past environmental changes for the westernmost Mediterranean since the Last Glacial Maximum (LGM). It aims to reconstruct both atmospheric and oceanographic responses to rapid climate variability in the Alboran Sea basin, which is a key region for paleoclimate archives due to its high sedimentation rates. Additionally, the time period spanning the last 20,000 yr is punctuated by significant climate events, i.e. last Heinrich event (H1), Bölling-Alleröd period (B-A), Younger Dryas (YD), and short-term variations during the Holocene, all of which make the interval crucial for a comprehension of climate variability at centennial-millennial time-scales.

2. Oceanographic setting and present climate conditions

The Alboran basin, located in the westernmost Mediterranean Sea, has a semi-enclosed configuration connected to the Atlantic Ocean through the Strait of Gibraltar to the West and to the Algero-Balearic basin to the East. As a transitional area between the Atlantic Ocean and the Mediterranean Sea, the hydrodynamics of the Alboran Sea basin is characterized by the entrance of a 200–300-m-thick jet of Atlantic Surface Water (ASW), which becomes more saline by mixing with water of Mediterranean origin thus forming the Modified Atlantic Water (MAW) travelling into the western Mediterranean (Fig. 1). This Atlantic jet forms two almost permanent anticyclonic gyres, namely the Western Alboran Gyre (WAG) and the Eastern Alboran Gyre (EAG), before it flows eastwards along the Algerian coast. The deeper water layers are filled by the Levantine Intermediate Waters (LIW) coming from the eastern Mediterranean and the Western Mediterranean Deep Water (WMDW) originating in the Gulf of Lion due to intense northwesterly winds. Both water masses form the Mediterranean outflowing water, or MOW (Send et al., 1999). This complete thermohaline circulation system is the result of climatic conditions over the entire Mediterranean that produce an excess of evaporation over precipitation plus river runoff, that in turn generates dense water masses (Béthoux 1979, 1980; Lacombe et al., 1981).

Regarding present climate conditions, the western Mediterranean Sea is surrounded by a catchment area under continental, alpine and Mediterranean climate regimes in the North, and Mediterranean to semi-arid climates in the South. The atmospheric circulation over North Africa is mainly controlled by the E-W winds denominated Saharan Air Layer (SAL) and its northern branch

(NSAL) (Kalu, 1979). The relative intensity of the winds system is seasonally modulated by the migration of the Inter-Tropical Convergence Zone (ITCZ) and the resulting oscillations of the African monsoon rain belt. Still active today are two major seasonal dust plumes over the ocean: one centered around 20ºN during summer, and the other around 10ºN in winter (Prospero, 1981; Pye, 1987). Satellite observations show contributions in eolian Saharan dust transport and deposition over the western Mediterranean ranging from 10% to 50% (Dulac et al., 1992; Loÿe-Pilot et al., 1986; Prospero, 1996). Most direct measurements indicate average present-day Saharan dust fluxes of ~1 mg/cm2 x yr (Guerzoni et al., 1997) with the maxima of fallout activity in spring and summer (Loÿe-Pilot and Martin, 1996; Moulin et al., 1998). Furthermore, the transmission of heat and moisture between low and high latitudes is controlled by the displacements of the Azores high. The North Atlantic Oscillation (NAO) is based on fluctuations in the sea-level atmospheric pressure between the Icelandic low and the Azores high-pressure centers (Hurrell, 1995). This pattern, the NAO, oscillates at decadal scale and controls present-day climate variability in the entire region (Rodó et al., 1997; Trigo et al., 2002). Variations in African dust export at interannual or at major time-scale show a significant relationship with the climatic variability defined by the NAO (Moulin et al., 1997). A positive mode of the NAO, i.e. a major pressure difference, is characterized by stronger westerlies and a northward displacement of storm tracks, leading to dry and cold winters in southern Europe, the Mediterranean Sea and northern Africa, with large aerosol loads over the region; and warm, wet winters in the northern Europe. Contrariwise, during the negative phase of the NAO or lower pressure difference, northwesterly winds are weaker and shift to mid-latitudes, bringing greater precipitation to the Mediterranean and North African areas (Wanner et al., 2001).

3. Materials and methods

3.1. Core description

The gravity core 293G was recovered in the East Alboran Sea basin (Fig. 1) (Lat. 36´10.414N, Long. 2´45.280W, depth 1,840 mbsl) during the oceanographic cruise Training Through Research-12 (R/V Professor Logachev). The lithology is dominated by homogeneous green-brownish hemipelagic mud-clays with some foraminifera and shell fragments (Comas and Ivanov, 2003). This 402 cm long core was sampled continuously every 1.5 cm obtaining 267 samples which were split into three representative portions. One subsample was dried and homogenized in agate mortar for mineralogical and geochemical analysis; a second portion was used to separate marine planktonic foraminifera for stable isotope analysis and radiocarbon dating; and the third one underwent grain size analysis.

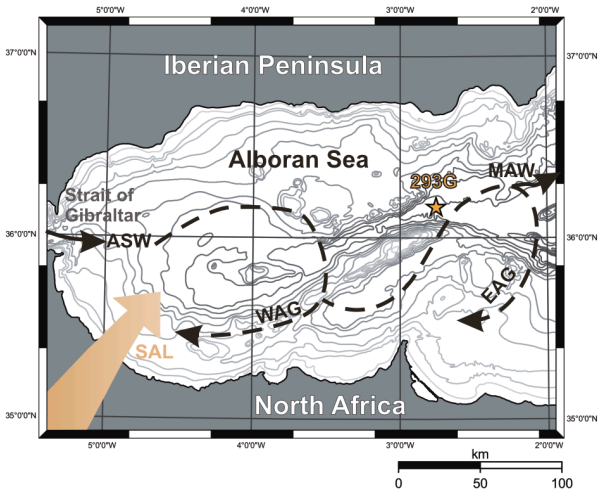

Figure 1. Geographical setting of the study area. Bathymetric map of the Alboran Sea showing the location of gravity core 293G (orange star). Black arrows represent the theoretical surface circulation in the Alboran Sea: Atlantic Surface Water (ASW), Western Alboran Gyre (WAG), Eastern Alboran Gyre (EAG) and Modified Atlantic Water (MAW). Thick arrow indicates northern branch of Saharan winds (SAL).

3.2. Mineralogical analysis

Bulk and clay mineral compositions were obtained by X-ray diffraction (XRD) following the international recommendations compiled by Kisch (1991). X-ray diffractograms were obtained using a PANalytical X´Pert PRO diffractometer with Cu-Kα radiation and automatic slit. Scans were run from 4º-70º 2θ for bulk-sample diffractograms, from 3-50º 2θ for untreated clay preparations, and from 3º-30º 2θ for glycolated samples. They were interpreted using Xpowder software developed by Martin (2004) (available at http://www.xpowder.com). Precise quantitative analysis for the different mineral contents was obtained developing our own standard patterns to create a specific database for this purpose. Standard patterns were produced using a mixture of each individual mineral phase adding a known amount of fluorite as internal standard in order to set the intensities on a common scale. Quantitative analysis was adjusted using the least squares method between each experimental diffractogram and the best-weighted combination of the standard pattern. The best fit quality was controlled by the agreement factor R, giving values <1% for bulk mineralogy and <4% for clay mineral assemblages. Amorphous constituents were not taken into account in the calculations.

Reference Intensity Ratio (RIR) values of each mineral phase were calculated using the equation:

$$RIRm = (\%\ Xtal_m\ /\ \%Xtal_{St}) * (Weight(mg)_m\ /\ Weight(mg)_{St})$$

where,

Xtal: intensity of cristal with RIR initial = 1

Weight (mg): each component in the standard pattern

m: each mineral phase

St: fluorite

The following RIR values were obtained for each mineral phase: quartz (2.80); calcite (0.50); dolomite (1.52); feldspar (0.26); illite (0.40); smectite (0.50); kaolinite (1.00); chlorite (1.00); palygorskite (1.70).

Previous research has used marine barite and Ba/Al ratios to establish export production fluxes (e.g., Dehairs et al., 1980; Dymond et al., 1992; Paytan et al., 1996; Martínez-Ruiz et al., 2000; Gallego-Torres et al., 2007; Jiménez-Espejo et al., 2007, 2008). Barite was separated by sequential leaching (as described in Eagle et al., 2003) in selected samples from the Ba-rich intervals to qualitatively determine if Ba enrichments correspond to authigenic marine barite (Paytan et al., 2002).

Morphological and compositional studies in selected samples, including barite separates, were performed using field emission scanning electron microscopy (FESEM), LEO (Carl Zeiss), mod. GEMINI-1530. Quantitative geochemical microanalysis of fibrous clay minerals (palygorskite) was obtained by transmission electron microscopy (TEM) using a Philips CM-20 equipped with an EDAX microanalysis system.

3.3. Grain size analysis

Grain size distribution was obtained using a Micromeritics SediGraph 5100 at a 3 cm sampling resolution. The coarse fraction (>63μm) was removed by wet sieving and weighed after cooling to room temperature. About 5 g of each sample were treated to remove the carbonate fraction with an acetic acid solution whereas organic matter was removed with 10% hydrogen peroxide. Samples were dispersed with a sodium hexametaphosphate solution (concentration of 0.02-0.1g/mL) followed by mechanical and ultrasonic stirring. SediGraph 5100 determined the particle grain size spectrum between 0.1 and 63μm with satisfactory resolution above about 1μm and precision of 0.1μm.

The fine grain size or “mud” distribution was divided accordingly into three terrigenous fractions; <2μm dominated by clay minerals, 2–10μm called fine silt or cohesive silt with the same properties of a cohesive material, and 10–63μm called coarse silt or sortable silt (SS) with non-cohesive behavior. The percentage of sortable silt (SS) in the total <63μm terrigenous fraction has been suggested as an index of current-controlled grain size selection (McCave et al., 1995). The silt/clay ratio (S/C) also provides information about changes in paleocurrent intensity (Hall and McCave, 2000). In this study, both values were used as current speed proxies, equivalent to the UP10 parameter applied in some western Mediterranean studies (Frigola et al., 2007, 2008;

Rogerson et al., 2008) rather than the sediment fraction susceptible to transport by wind as previously described by Moreno et al. (2002).

3.4. Geochemical analysis

Major elements (Si, Al, Ti, K, Mg, Fe, Mn) and Zr measurements were obtained by X-Ray Fluorescence (XRF). For the major elements, samples were prepared as fused beads using glass discs prepared by melting about 0.3 g of ground bulk sediment with lithium tetra borate flux; Zr was measured using pressed pellets prepared by pressing about 5 g of ground bulk sediment into a briquet with boric acid backing. The quality of the analysis was monitored with reference materials showing high precision with 1 sigma 1.0-3.4% on 16 data-sets at the 95% confidence level.

Trace element analysis was performed using inductively coupled plasma-mass spectrometry (ICP-MS) previous HNO3+HF digestion. Measurements were taken in triplicate through spectrometry (Perkin-Elmer Sciex Elan 5000) using Re and Rh as internal standards. The instrumental error is ± 2% and ± 5% for elemental concentrations of 50 ppm and 5 ppm respectively (Bea, 1996).

The determination of total organic carbon (TOC) was performed using a Horiba Carbon/Sulfur Analyzer EMIA-320V Series. All samples were subjected to acid leaching (HCl) onto glass fiber filters in order to remove inorganic carbon. Treated samples were oxidized by the high frequency induction furnace method under an oxygen stream and CO2 gases evolved were detected by calibrated infra-red (IR) cells. Total carbon (C) contents were measured as mg and calculated as percentages of the sample weights. The respective precision and accuracy of the method are approximately 0.01% and 92%.

The stable oxygen isotope ratio was measured using a Finnigan MAT 252 mass spectrometer over approximately 10 specimens of Globigerina bulloides from the >125μm fraction avoiding senescent forms. Foraminifera were cleaned in an ultrasonic bath to remove fine-fraction contamination, rinsed with distilled water, and thoroughly washed in alcohol. The results are reported in the conventional notation with reference to the V-PDB standard. Analytical reproducibility of the method, based on repeated standards, is approximately <0.07‰ (Solnhofen Limestone is calibrated against NBS 19 as internal standard).

4. Age model and oxygen isotope stratigraphy

A robust age model was obtained by linear interpolation between ten ^{14}C-AMS radiocarbon ages (Accelerator Mass Spectrometry, AMS) recorded in approximately 20 mg of monospecific planktonic foraminifera *Globigerina bulloides* from the size fraction >125μm (Table 1, Fig. 2) (National Centre for Accelerators, CNA, Spain). In order to compare our data with other paleoclimatic records, all ^{14}C-AMS ages were calibrated to calendar years using Calib 6.0.2 software (Stuiver and Reimer, 1993) and the Marine09 calibration curve, with a correction for ocean surface reservoir effects of 400 yr (Reimer et al., 2009). The dates in Figs. 3, 5-7 and 9-10 are given in reference to calibrated years before present (yr cal. BP), 0 BP being equivalent to AD 1950, and they are presented with a 2σ standard deviation of the age uncertainty (Table 1).

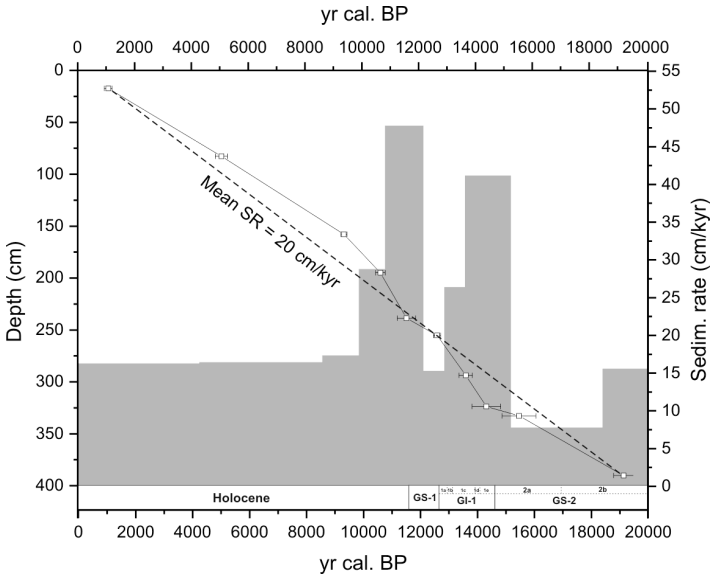

Figure 2. Sedimentation rates along 293G sediment core calculated linearly by ten AMS ^{14}C ages (open squares) calibrated with Calib 6.0.2 software (Reimer et al., 2009) (see Table 1 for details). The mean sedimentation rate (SR) of 20 cm/kyr is represented by dashed line.

The validity of the age model is further strengthened by stable isotope stratigraphy. This chronology is moreover verified by comparison with other well-dated records in the western Mediterranean Sea (Cacho et al., 2001; Jiménez-Espejo et al., 2008) and correlation of the stable isotope data with Greenland ice-core δ^{18}O records from the Greenland Ice-Sheet Project II (GISP2) (Stuiver and Grootes 2000), North Greenland Ice core Project (NGRIP) (Lowe et al., 2008). The model is likewise consistent with regional sea surface isotope and thermohaline circulation changes. The event stratigraphy used timings from the INTIMATE group (Lowe et al., 2008). The temporal resolution of each sample taken from the studied core is ~75 years, given the high sedimentation rates at the core site which makes possible to distinguish centennial to millennial climate oscillations.

Table 1. Results of AMS ^{14}C carbon dating of single planktonic foraminifera G. bulloides (>125 μm) taken from TTR-12 core 293G

Sample description	Core depth (cm)	Laboratory code	^{14}C AMS age (BP)	Calibrated age (yr cal. BP) (range 2σ)
293G/01/16.5-18	17.25	CNA467	1,520 ± 60	1,075 ± 141.5
293G/02/24-25.5	82.75	CNA468	4,780 ± 80	5,056 ± 215
293G/03/40.5-42	157.75	CNA469	8,705 ± 45	9,371 ± 108
293G/04/19.5-21	194.75	CNA470	9,760 ± 60	10,655 ± 166
293G/05/6-7.5	238.75	CNA471	10,440 ± 90	11,573,5 ± 324.5
293G/05/22.5-24	255.25	CNA472	11,120 ± 70	12,653 ± 124
293G/06/3-4.5	293.75	CNA473	12,230 ± 110	13,656 ± 238
293G/06/33-34.5	323.75	CNA474	12,680 ± 100	14,384.5 ± 503.5
293G/06/42-4.35	332.75	CNA475	13,280 ± 90	15,537 ± 591
293G/07/40.5-42	390.25	CNA476	16,540 ± 160	19,213.5 ± 345.5

* Calibration was done using Calib 6.0.2 software. We used the Marine09 calibration curve with standard marine correction of 400 years (data from two sigma probability interval).

5. Results

5.1. Detrital input fluctuations

Selected mineral phases and elemental/Al ratios were used as indicators of detrital input fluctuations. Al normalization allowed us to avoid any lithological effect on trace and major element concentration (Calvert and Pedersen, 2007).

Sediments are mainly composed of clay minerals (35-60%), calcite (30-48%), quartz (6-14%), and minor proportions of dolomite and feldspars (<5% and <8%, respectively; Fig. 3). Likewise, clay mineral assemblages contain high quantities of illite (42-56%) and lower proportions of smectites (18-31%), kaolinite and chlorite (both 8-14%) and palygorskite (4-7%) (Fig. 3), that have also been observed by TEM (Fig. 4). Typical eolian minerals (quartz, palygorskite) show maximum proportions from the LGM to the Oldest Dryas (18,000-14,670 yr cal. BP), at the onset of the YD, and at the early Holocene. During the Holocene, palygorskite started to increase at 4,600 yr cal. BP, while quartz shows increasing trends at 7,400 and 1,700 yr cal. BP (Fig. 3).

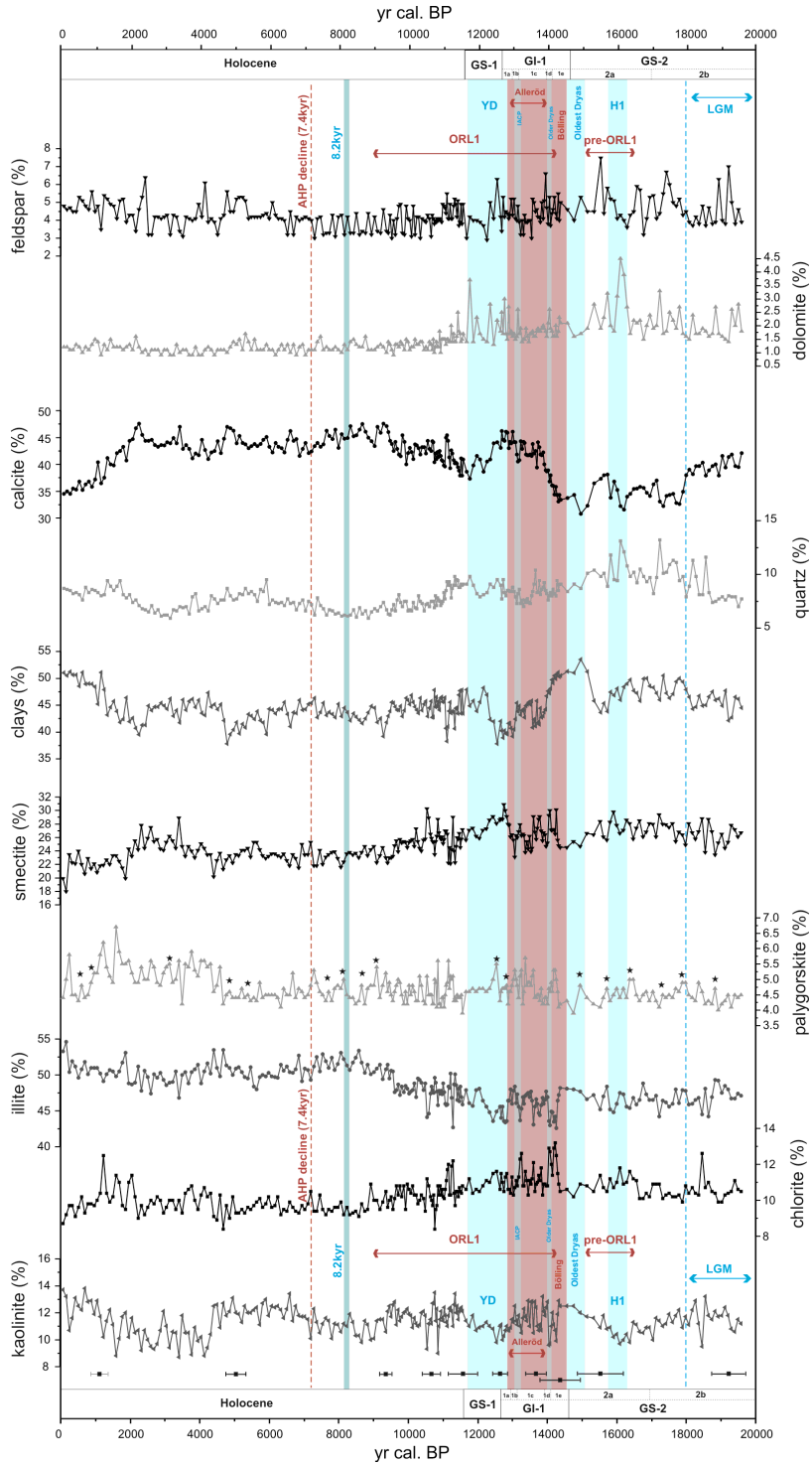
yr cal. BP
Holocene
GS-1
GI-1
GS-2
YD
Alleröd
H1
LGM
ORL1
pre-ORL1
Oldest Dryas
Bölling
Older Dryas
IACP
AHP decline (7.4kyr)
8.2kyr
feldspar (%)
dolomite (%)
calcite (%)
quartz (%)
clays (%)
smectite (%)
palygorskite (%)
illite (%)
chlorite (%)
kaolinite (%)

Figure 3. Bulk and clay mineral composition obtained by quantitative XRD in 293G core (see text for details). Black stars correspond to palygorskite identified and analyzed by TEM.

The selected detrital/Al ratios (Si/Al, Mg/Al, K/Al, Rb/Al, Ti/Al, Zr/Al) and mineral ratios (illite+chlorite/kaolinite) show major terrigenous fluctuations over the last 20,000 yr (Fig. 5). Zr/Al ratio shows a significant increase from the end of LGM to the Oldest Dryas (18,000-14,670 yr cal. BP, Greenland Stadial 2 (GS-2) in NGRIP terminology, Lowe et al., 2008) with two peaks distinguished at 17,800 yr and 16,100 yr cal. BP. A considerable decrease in this ratio occurs during the B-A period (Greenland Interstadial 1,GI-1), whereas a slight rise coincides with both the Intra-Alleröd Cold Period (IACP, GI-1b) and the onset of the YD. A more uniform pattern characterizes the Holocene. The Ti/Al ratio shows one significant peak at 16,200 yr cal. BP, also seen in the Si/Al ratio, which displays another peak at 12,650 yr cal. BP that coincides with the Alleröd-YD transition (from GI-1a to GS-1).

A different history is recognized for Rb/Al, Mg/Al and K/Al ratios. The Rb/Al ratio shows a noteworthy increase from the IACP offset to the early YD. Both Mg/Al and K/Al ratios show similar profiles, with an increasing trend from the Bölling to the Alleröd periods. A decrease in K/Al ratio is observed between 7,400 and 4,500 yr cal. BP, followed by a sharp increase, maintaining high values until around 2,000 yr cal. BP and a decreasing trend to present time. The clay minerals ratio of illite+chlorite/kaolinite shows an identical trend during the Holocene.

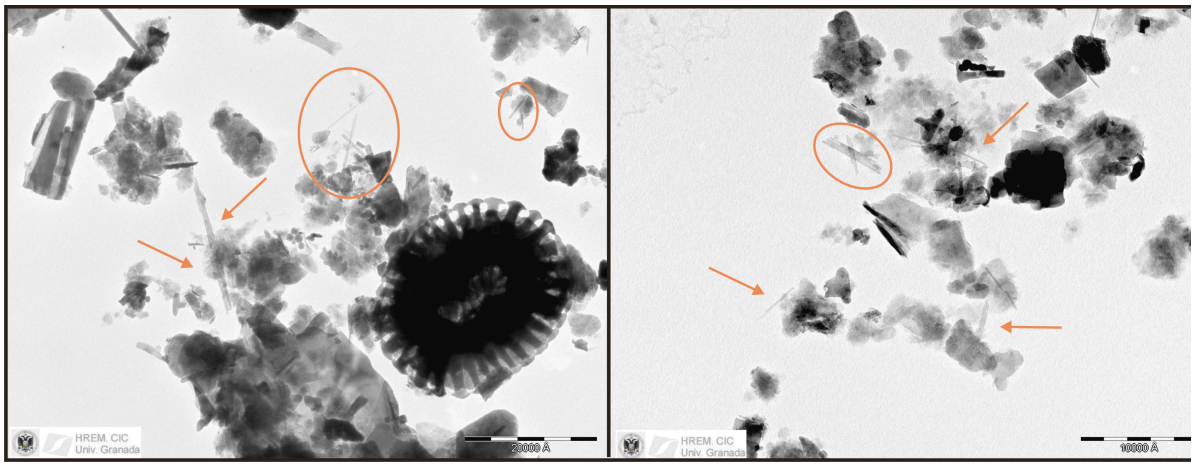

Figure 4. Palygorskite fibers observed by TEM.

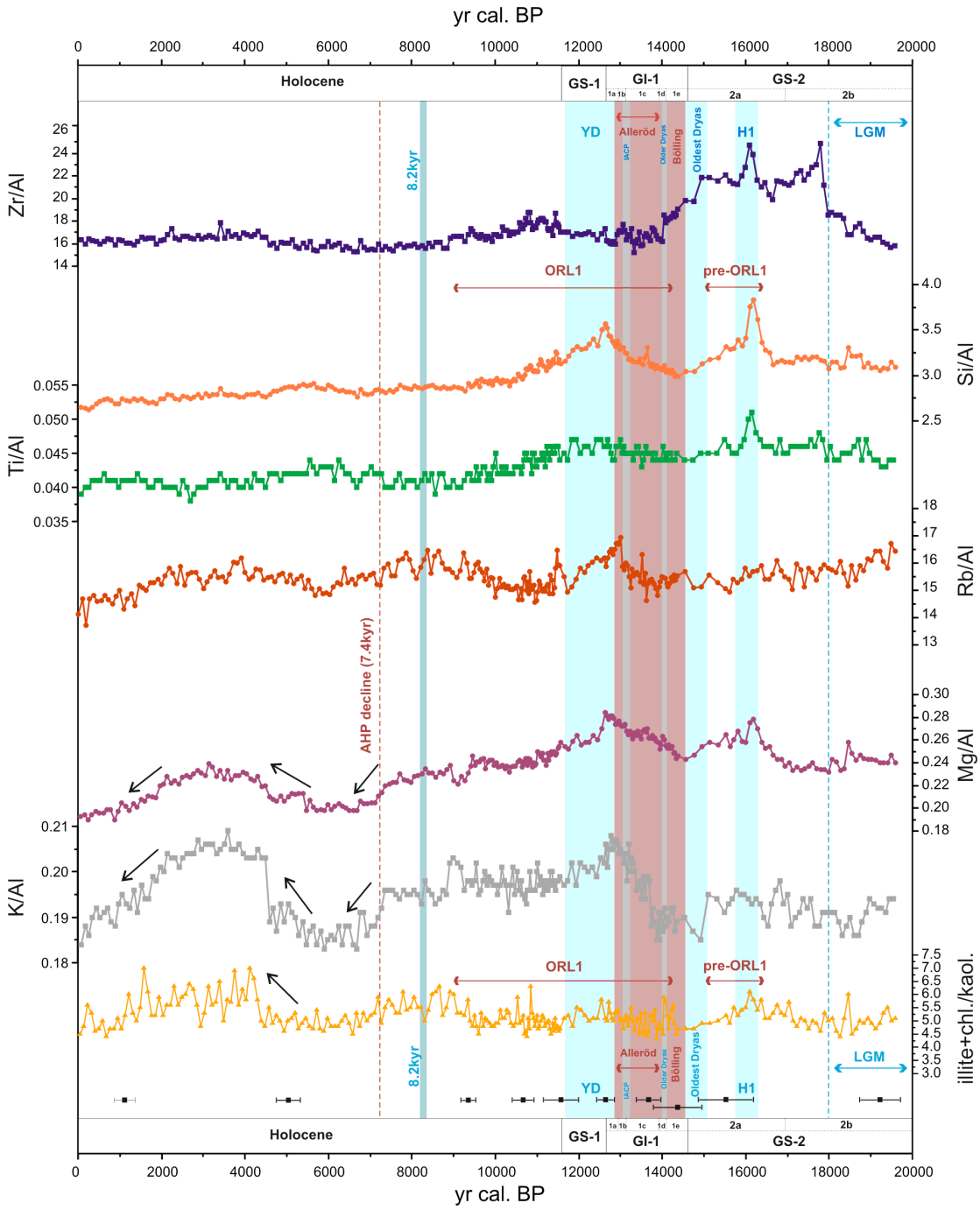
yr cal. BP
Holocene
GS-1
GI-1
GS-2
1a 1b 1c 1d 1e
2a
2b
YD
Alleröd
IACP
Older Dryas
Bölling
Oldest Dryas
H1
LGM
8.2kyr
ORL1
pre-ORL1
AHP decline (7.4kyr)
Zr/Al
Si/Al
Ti/Al
Rb/Al
Mg/Al
K/Al
illite+chl./kaol.

Figure 5. Age profiles of terrigenous proxies/Al ratios (Element/Al ratio for major elements and Element/Al ratio $*10^{-4}$ ppm for trace elements) and mineralogical proxies (illite+chlorite/kaolinite ratio). Light red vertical bars indicate warm periods such as Alleröd (A), and Bölling (B) time intervals. Light blue bars indicate main cold periods, "8,200 yr" cold event (Alley et al., 1997), Younger Dryas (YD), Intra-Alleröd Cold Period (IACP), Older Dryas, Oldest Dryas, and the last Heinrich event (H1) time intervals. Short dashed blue vertical line indicates the offset of the Last Glacial Maximum (LGM) time interval. Dark red horizontal arrows show Organic-Rich Layers (pre-ORL1, ORL1) time intervals, and the vertical one shows the early decline of the African Humid Period (AHP). White horizontal boxes indicate Greenland Stadials (GS-1, GS-2), Interstadials (GI-1) and Holocene. Chronostratigraphy timing subdivisions are based on ^{14}C AMS dates and stable oxygen isotope stratigraphy from Greenland ice-cores published by Stuiver and Grootes (2000), and Lowe et al., (2008).

5.2. Deep-water ventilation, isotopes, productivity and grain size distribution

Variations in certain redox-sensitive trace metal ratios (Zn/Al, Cu/Al, V/Al, Mn/Al, Fe/Al, U/Th) indicate fluctuations in deep-water oxygen contents at the time of sediment deposition (Fig. 6). Thus, Zn/Al, Cu/Al, V/Al ratios show an interval characterized by low oxygen conditions during the GS-2a (15,914-15,630 yr cal. BP), reaching the lowest deep-water ventilations during the Alleröd-YD boundary (from GI-1a to GS-1), when the lowest deep-water ventilations are reached; and then again from the early Holocene to around 7,800 yr cal. BP. The U/Th ratio displays the same pattern recording general low ventilation conditions from GS-2a until the onset of YD, and again from the early Holocene onward. The highest values for deep-water oxygenation, however, were reached during the GS-2 —the Mn/Al and Fe/Al ratios display a noticeable maximum prior to and after the H1 event, and a nearly flat pattern for the rest of the time period.

The oxygen isotope profile shows that glacial-interglacial amplitude in the 293G core ranges from 3.76‰ to 0.36‰ with a total oscillation of 3.40‰ (Fig. 7). The $\delta^{18}O$ profile records the maximum values during the LGM and GS-2a but with a sudden depletion within the H1 event. This general tendency of higher values abruptly decreases at the onset of the B-A period, followed by another slight increase during the YD. In general, the Holocene is characterized by low $\delta^{18}O$ values, with a slight depletion in the heavy isotope during the 8,200 yr cal. BP event (Alley et al., 1997).

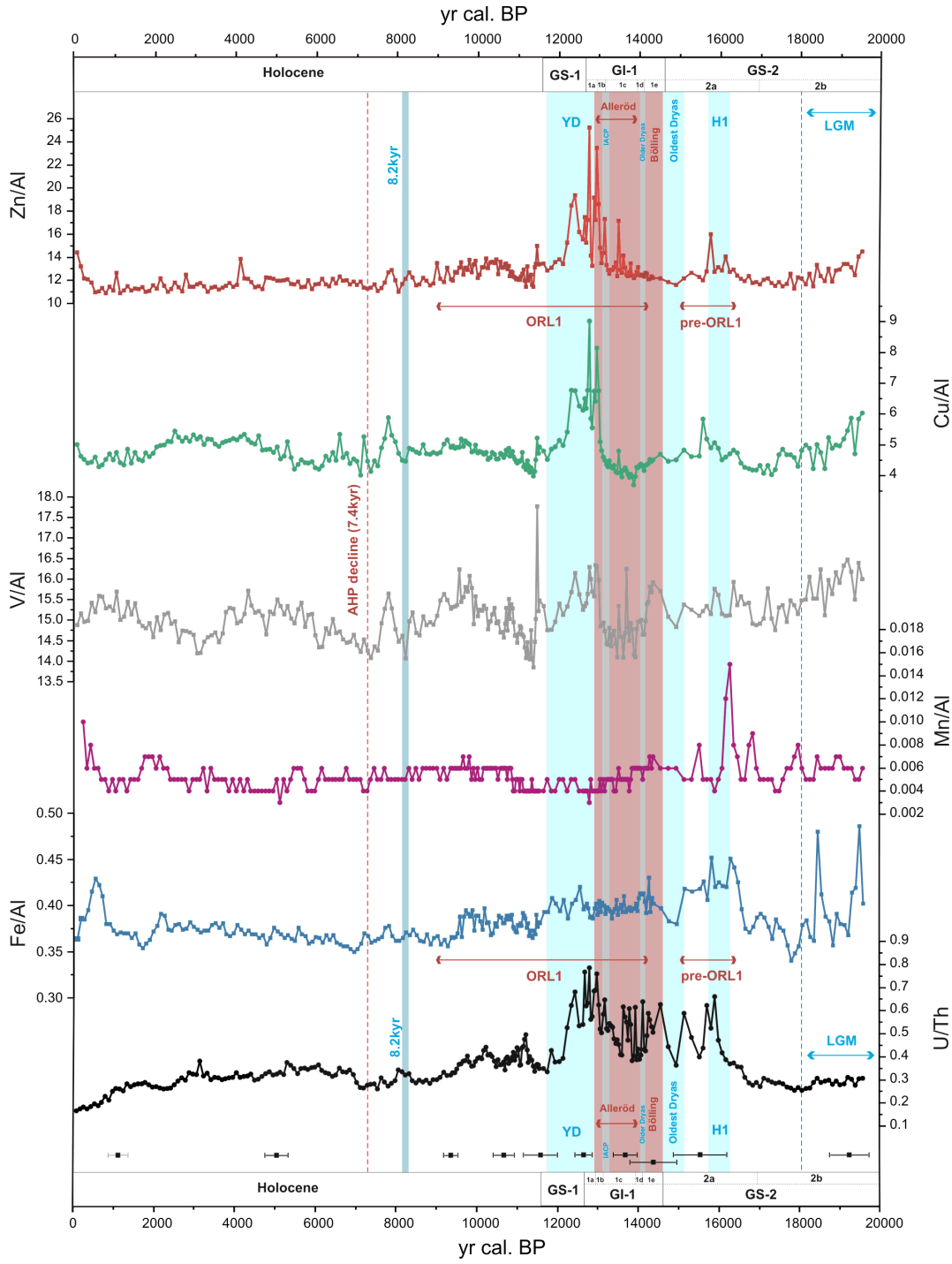
yr cal. BP
Holocene
GS-1
GI-1
GS-2
1a 1b 1c 1d 1e
2a
2b
YD
Alleröd
IACP
Older Dryas
Bölling
Oldest Dryas
H1
LGM
8.2kyr
ORL1
pre-ORL1
AHP decline (7.4kyr)
Zn/Al
Cu/Al
V/Al
Mn/Al
Fe/Al
U/Th

Figure 6. Age profiles of redox proxies/Al ratios (*10^{-4} ppm). Color-coded vertical bars indicate warm and cold periods as described in Fig. 5.

Regarding productivity proxies, the Ba/Al ratio indicates two main enrichments corresponding to the middle GS-2a period and to the boundary between the offset of Alleröd and the onset of YD (Fig. 7). FESEM observations of selected samples from Ba-enriched intervals revealed the presence of authigenic marine barite just in these intervals (Fig. 7). Observed barite crystals showed 1–5µm sizes and elliptical morphologies corresponding to typical marine barite originated in high productivity regions (Fig. 8). The TOC profile evidences three main enrichments whose values are between 0.60% and 1.05% (Fig. 7). The first and second peaks coincide with the two Ba peaks, and the third enrichment is reached during the early Holocene, with the most significant decrease at about 8,900 yr cal. BP.

Grain size distribution (median, mode and mean) and terrigenous fraction contents used for paleoenvironmental reconstruction reflect a poorly sorted material (Fig. 9). The coarse fraction (>63µm) content is very low (<3%). Mean is always lower than 6µm. Clay and fine silt are the major components of the sediments with median grain size values about 1µm. SS and S/C ratio display high values during the H1 and the YD, and around 8,000 and 4,500 yr cal. BP.

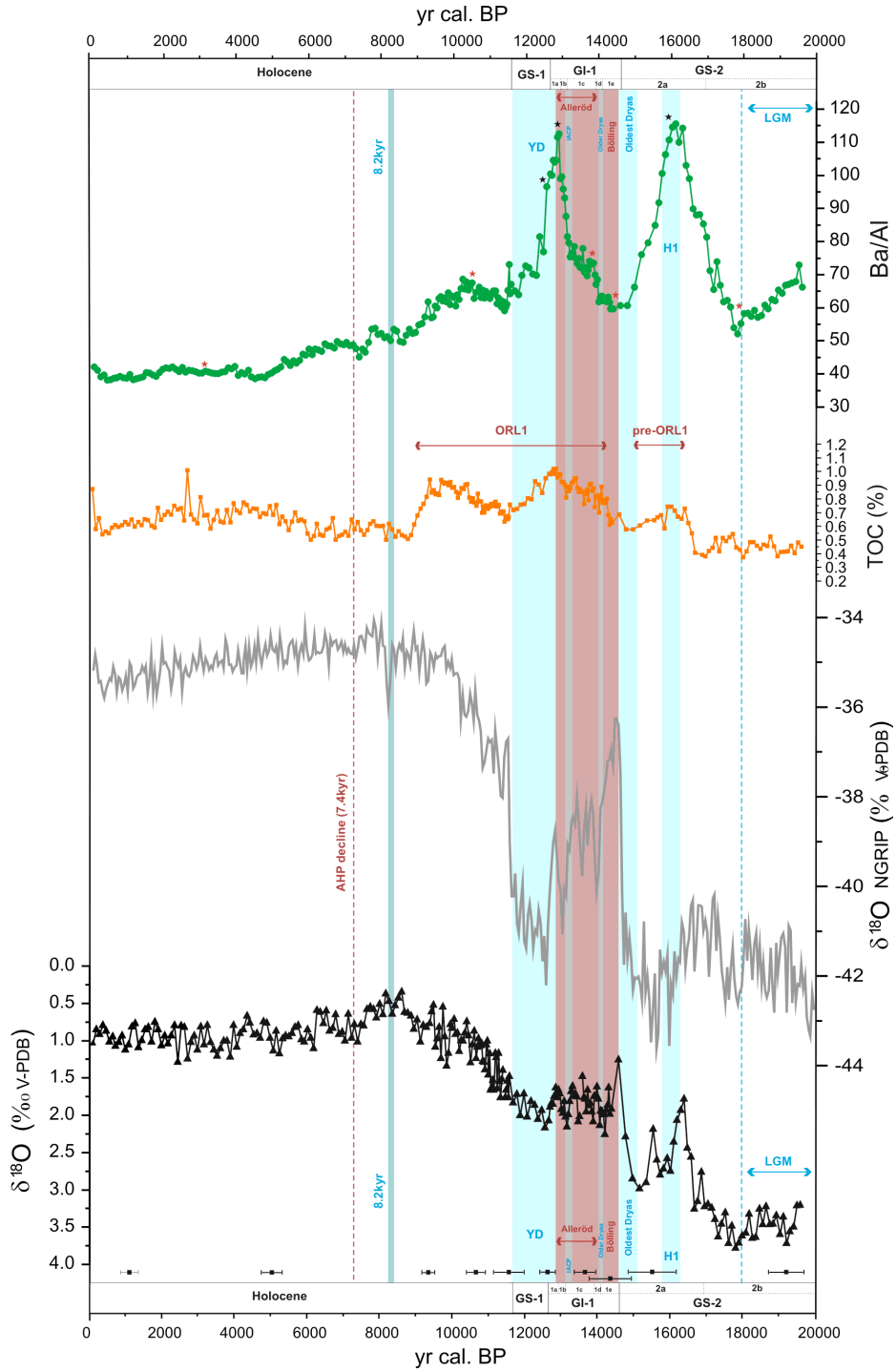
yr cal. BP
Holocene
GS-1
GI-1
GS-2
1a 1b 1c 1d 1e
2a
2b
Alleröd
YD
8.2kyr
Oldest Dryas
Bölling
LGM
H1
ORL1
pre-ORL1
AHP decline (7.4kyr)
Ba/Al
TOC (%)
δ18O NGRIP (‰ V-PDB)
δ18O (‰ V-PDB)

Figure 7. Stable oxygen isotope profile, TOC content and Ba/Al ratio (*10^{-4} ppm) show paleoclimate and paleoproductivity conditions for the time studied respectively. Stars indicate selected samples separated by sequential leaching, where only the black ones correspond to authigenic marine barite identified. Well-marked correlation is observed between our stable isotope profile and the NGRIP $\delta^{18}O$ ice core record (Lowe et al., 2008) suggesting an accurate age model obtained and the connection with the Atlantic climate variability. Color-coded vertical bars indicate warm and cold periods as described in Fig. 5.

6. Discussion

The multi-proxy analysis performed provides a high-resolution time window reconstruction of paleoceanographic and atmospheric oscillations since the LGM. Some of the major paleoclimatic evidence closely correlates with climatic oscillations recorded in Greenland ice cores, and with European and Mediterranean records, supporting the connection between high and mid-latitude climates (Fig. 11).

6.1. Last Heinrich event

During the cold period GS-2a, the analyzed proxies support major paleoclimatic changes, especially in connection with the H1, from 16,200 to 15,700 yr cal. BP (Sierro et al., 2005) (Fig. 7). The H1 has been previously identified in the western Mediterranean as a cold and arid event, with elevated percentages of the cold-water foraminifera N. pachyderma (sinistral), a marked drop in sea surface temperatures (Cacho et al., 1999, 2006; Sierro et al., 2005) and semi-desert vegetation expansion in the surrounding continental regions (Combourieu Nebout et al., 2002, 2009; Sánchez-Goñi et al., 2002; Baudin et al., 2007; Fletcher and Sánchez Goñi, 2008).

Paleoproductivity proxies such as Ba/Al and enrichment in TOC content point to high productivity during the H1 event (Fig. 7). Meanwhile, recent studies of coastal northwest Africa have linked Ba increases during this period with glacial meltwater pulses via dissolved Ba input through the Azores Front and changes in the Ba/Al ratio during the GS-2a period (Plewa et al., 2006). Although dissolved Ba could potentially have affected Ba profiles in the Alboran Sea (e.g., Jiménez-Espejo et al., 2008; Rogerson et al., 2008), the identification of authigenic marine barite in H1 Ba-enriched interval supports the likelihood that marine productivity also increased at this time (Figs. 7, 8). Furthermore, the Ba/Al and TOC profiles from this record indicate an organic enrichment prior to the Organic Rich Layer 1 (pre-ORL1, Fig. 7) that has been documented in the Alboran Sea basin (e.g., Cacho et al., 2002). Such a productive enrichment coincides with the strong shift toward lower $\delta^{18}O$ values (Fig. 7) resulting from Atlantic freshwater influx from North Atlantic iceberg melt

in the western Mediterranean, an input intense enough to cause a decrease in sea surface salinity, reducing the Mediterranean thermohaline circulation during a short period of time, less than 1,000 yr (Sierro et al., 2005). We also found evidence of major changes in thermohaline circulation in some redox proxies, with marked Mn/Al and Fe/Al peaks associated with reoxidation events (Fig. 6). The SS and S/C granulometric parameters (Fig. 9) point to enhanced ventilation in bottom waters and major paleocurrent intensity just prior to H1. This suggests an active circulation during the GS-2a triggered by the WMDW formation and induced by the northwesterlies, which would have filled the deepest area of the western Mediterranean, followed by fresher AMW inflow during the H1, which injected large volumes of water from melting icebergs, causing a decrease in sea surface salinity.

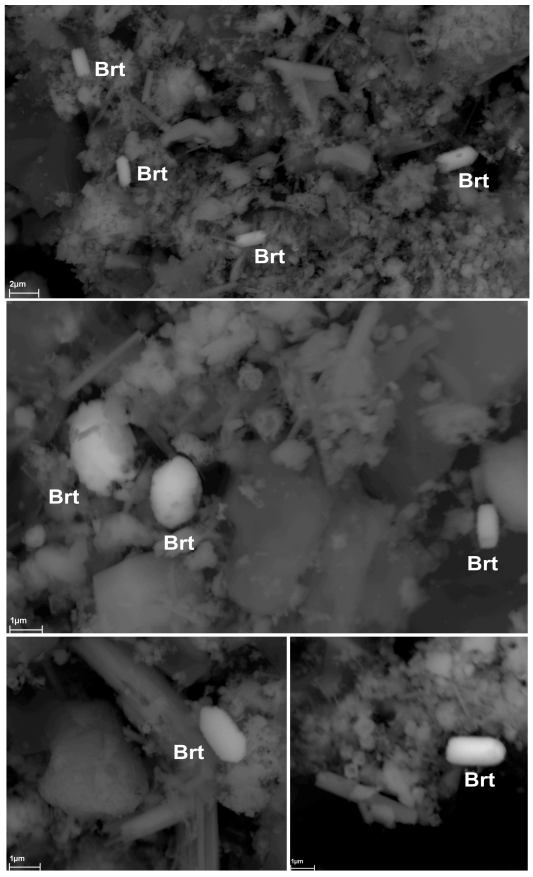

Figure 8. Authigenic marine barite observed in Ba-enriched intervals with backscattered images (FESEM).

At the same time, increases in eolian proxies, Zr/Al, Si/Al and Ti/Al ratios, and quartz and palygorskite contents (Figs. 3, 5) point towards dryer conditions in the Alboran borderlands and a major reorganization of atmospheric circulation at the beginning of the deglaciation and during the H1. This observation is partially correlated with the peak identified in the non-sea-salt ion series in the Greenland ice core GISP associated with periods of high atmospheric dust connected to a rise in wind-blown particles and sea-salt (Mayewski et al., 1994). Therefore, a more northern position of the westerlies could bring high pressures at mid-latitudes and hence dry conditions during North Atlantic cold events. In addition, the southward migration of the ITCZ, a weak regional rainfall system, and a reduction in the Atlantic meridional overturning circulation, have been proposed as a possible mechanism behind the aridity conditions recorded in the Mediterranean and African region (Sarnthein et al.,

1982; Mulitza et al., 2008; Stager et al., 2011). A combination of these atmospheric changes could have promoted an increase in cyclonic activity and a stronger thermal gradient between high and low latitudes with major eolian input from North Africa to the Alboran Sea basin (Fig. 11).

6.2. Bölling-Alleröd period

The B-A period, between the offset of GS-2a and the onset of the YD (14,670-12,890 yr cal. BP), is characterized by a stable water column and low deep-water ventilation (Fig. 6,7) as evidenced by the onset of the last ORL1 described in the Alboran basin (Cacho et al., 2002). Previous works argue that the ORL1 was deposited in the Alboran basin between 14,500 and 8,200 yr cal. BP, spanning the B-A, the YD, and the early Holocene (Cacho et al., 2002; Rogerson et al., 2008). Our data indicate a well-developed pattern for the organic matter enrichment in the Alboran Sea from the H1 (pre-ORL1) to around 8,900 yr cal. BP, with two major enrichments that coincide with corresponding Ba enrichments and also signal increasing productivity (Fig. 7). Former physical oceanographic models explain the origin of this organic enrichment as a result of the strong reduction in surface water density and a shoaling of the interface between intermediate and deep water during the deglacial period (Rogerson et al., 2008). Furthermore, the onset of the ORL1 is registered in parallel with $\delta^{18}O$ depletion, promoted by the general northern atmospheric warming of the last Greenland Interstadial, characterized by a weakened wind pattern evidenced by the fall of eolian input proxies (Figs. 5, 7). Conversely, fluctuations in Mg/Al, K/Al and illite+chlorite/kaolinite ratios suggest progressively humid conditions during the B-A period (Fig. 5). The growing humidity is also recognized in Iberian lake records (e.g., González-Sampériz et al., 2006; Morellón et al., 2009a) and speleothem sequences from northern Iberian (Moreno et al., 2010) and southern Europe (Genty et al., 2006). The onset of North African humidity during this time has been characterized as a “green-Sahara” period (Gasse and Van Campo, 1994; deMenocal et al., 2000). The development of this warm interstadial is made manifest in other marine records by the elevated abundance of temperate pollen taxa from Mediterranean forests (Combourieu Nebout et al., 2002, 2009; Sánchez-Goñi et al., 2002) and by the reduced contents of some clay mineral associations such as palygorskite and illite-to-kaolinite (Bout-Roumazeilles et al., 2007). The B-A atmospheric conditions could be attributed to a negative NAO index with southward westerlies migration (Fig. 11).

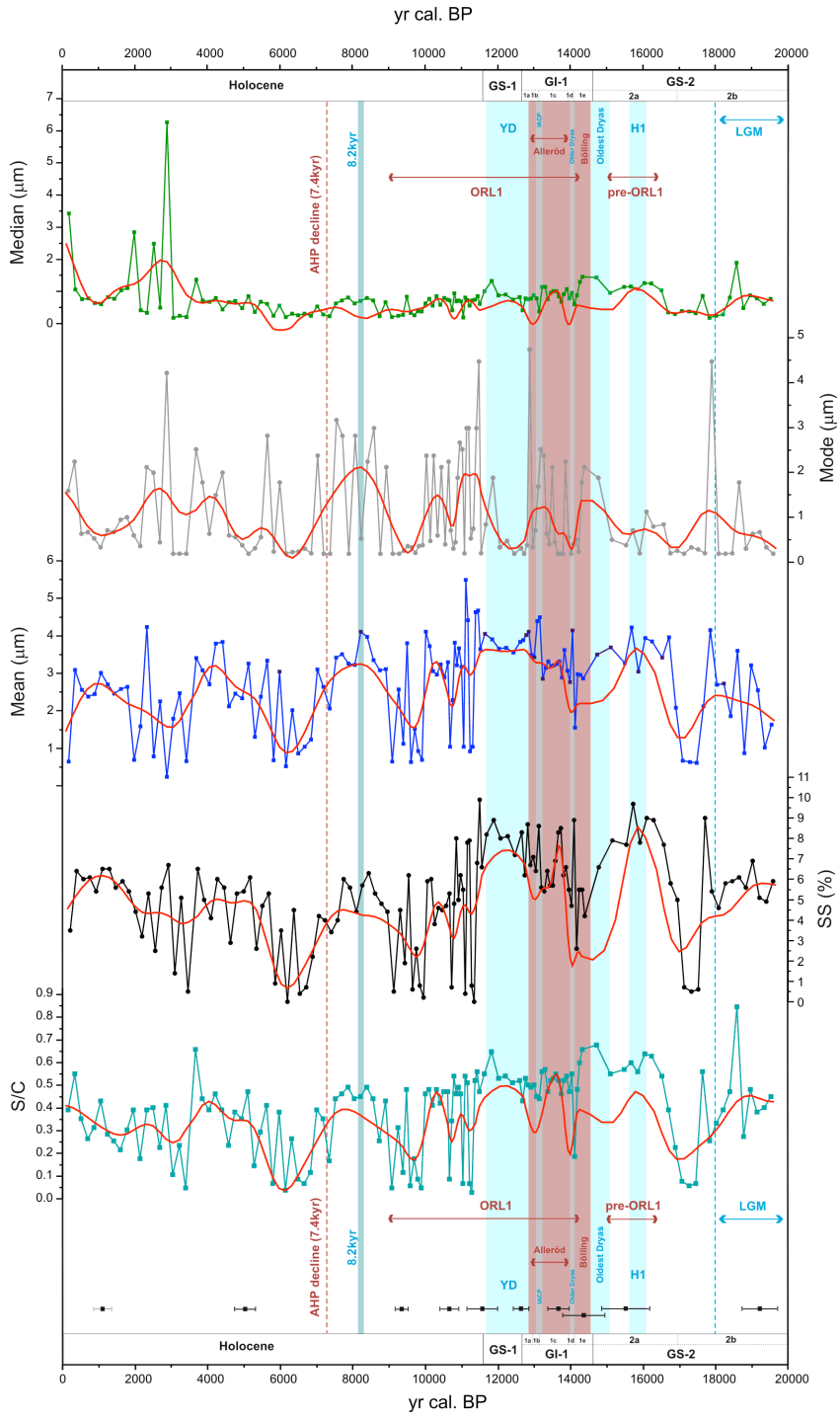
yr cal. BP
Holocene
GS-1
GI-1
GS-2
YD
Alleröd
Bölling
Oldest Dryas
H1
LGM
ORL1
pre-ORL1
AHP decline (7.4kyr)
8.2kyr
Median (μm)
Mode (μm)
Mean (μm)
SS (%)
S/C

Figure 9. Particle size distribution profiles (median, mode, mean) versus age. Sortable silt (SS) and silt/clay ratio (S/C) used as paleocurrents indicators. Red lines are 3-point smoothing average. Color-coded vertical bars indicate warm and cold periods as described in Fig. 5.

One marked terrigenous variation recorded during this time period is the IACP. It gives rise to an increase in eolian proxies such as Zr/Al, quartz and palygorskite contents (Figs. 3, 5). The IACP detected in the Greenland ice-cores during high-latitude Atlantic cooling events is generally difficult to identify in mostly paleoclimate records. The Alboran record studied here, however, presents the resolution required to evidence such a short-term cold variation. An intensification of the paleocurrent speed with a later increase of ventilation are also suggested by the different proxies used (Figs. 6, 9), pointing to cooling conditions and intense thermohaline circulation throughout the Alboran region. The IACP is also reflected in forest record variations in lake sequences in Western Europe and the Mediterranean sector of the Iberian Peninsula, with increases in steppe taxa (González-Sampériz et al., 2006; Magny et al., 2006; Fletcher et al., 2010), a pronounced shift in δ13C, and high Mg/Ca and Ba/Ca ratios in cave records from the Atlantic Iberian region (Moreno et al., 2010).

6.3. Younger-Dryas

The YD (12,890-11,650 yr cal. BP) has been proposed as a cold snap of millennial duration that punctuated the end of the last glacial period, involving ice sheet growth and subsequent meltwater discharge in high latitudes of the North Atlantic (e.g., Alley, 2000; Alley et al., 2007). Despite intensive research devoted to this interval, its origin is still a subject of debate. Recent evidence provided by Broecker et al., (2010) suggests that this cold snap was simply part of the deglacial sequence of events that produced the termination of the last glacial period. In the context of the last four terminations, these authors argue that cold reversals equivalent to the YD may be integral parts of global switches from glacial to interglacial climates, without invoking any catastrophic events for such abrupt climate changes. In our record, this period is also revealed as a cold snap entailing significant paleoceanographic and paleoclimate changes from its onset through its termination. Thus, a prominent feature of the YD onset is a productivity increase (Fig. 7) also supported by the presence of marine barite (Fig. 8). A previous diatom record from this same region accordingly indicates high sea surface productivity during GI-1a and YD as a result of increased westerlies (Bárcena et al., 2001). Following the lower deep-water ventilation recorded at the offset of

Alleröd period, paleocurrent proxies show an increase through the YD indicating a reactivation of thermohaline circulation in the Mediterranean (Figs. 6, 9). Even though extreme cold and dry conditions are recognized at high latitudes, only slight changes in values of eolian proxies such as the Zr/Al ratio, palygorskite and quartz proportions are recorded at the onset of this period in the East Alboran basin (Figs. 3, 5). This suggests that main paleoclimatic changes mostly involved fluvial input over this period. In fact, high-resolution pollen diagrams evidence an alternation of warm/humid and cool/arid conditions in the northwest Mediterranean during the YD (Allen and Huntley, 2000; Naughton et al., 2007), including a first period with very dry conditions and an increase in semi-desert taxa, and a second period that was more humid, with a slight forest increase (Combourieu Nebout et al., 2009). Furthermore, in the northeastern Iberian, no major palynological evidence has been recorded in relation with this arid and cold period (González-Sampériz et al., 2006). Carbon and oxygen isotopic signals in stalagmites from Southern France and Northern Tunisia also recorded a climatic amelioration trend after the cooling YD onset (Genty et al., 2006). Thus, the recorded detrital fluctuations corroborate these observations and support an initial cold and dry phase, with intense major westerlies, thermohaline reactivation, and high productivity levels. A second wetter phase then took place, characterized by sporadic rainfalls over poorly vegetated surrounding continental areas that prevented water seepage, or else freshwater injections caused by glacier melt from the southern European high mountain ranges (Fig. 11). Such a scenario could have promoted an increase in local river discharge over the Alboran margin, with major fluvial erosion at the offset of YD. These climate oscillations further support a major reorganization of atmospheric circulation with regional changes in the Mediterranean pluviosity regime that were closely related to ITCZ migrations over North Africa and monsoonal variations (Gasse and Van Campo, 1994).

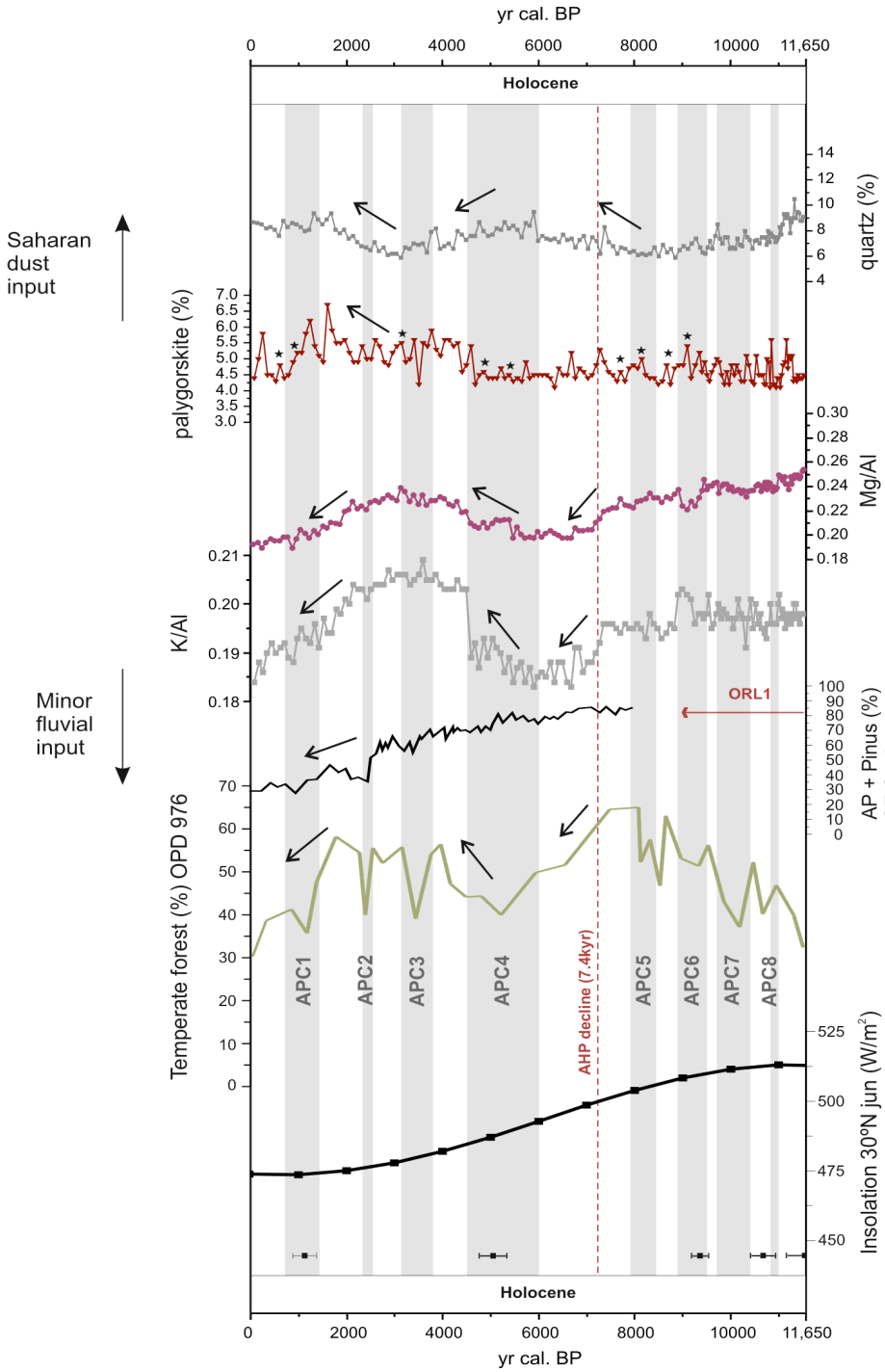
yr cal. BP
0
2000
4000
6000
8000
10000
11,650
Holocene
Saharan dust input
Minor fluvial input
quartz (%)
palygorskite (%)
Mg/Al
K/Al
ORL1
AP + Pinus (%) SE Spain
Temperate forest (%) OPD 976
APC1
APC2
APC3
APC4
APC5
APC6
APC7
APC8
AHP decline (7.4kyr)
Insolation 30°N jun (W/m²)
Holocene
yr cal. BP

Figure 10. Selected eolian (quartz and palygorskite content) and river runoff (Mg/Al, K/Al ratios) proxies record arid and humid condition variations over the Holocene (last 11,650 yr cal. BP), integrated with: percentages of arboreal pollen (AP) and pinus from South-eastern Spain (Sierra de Baza) (Carrión et al., 2007), abundances in temperate forest recorded in western Mediterranean marine sediments of ODP site 976 (Combourieu Nebout et al., 2009), and Summer insolation curve (June) for 30ºN (Berger and Loutre, 1991). Light gray vertical bars indicate short-lived arid climate events at 11-10.8, 10.5-9.8, 9.6-8.9, 8.5-7.9, 6-4.5, 3.7-3.1, 2.6-2.3, and 1.5-0.7 kyr, named APC 1-8, interpreted as rapid forest curve oscillations registered in ODP 976 pollen record.

6.4. Holocene

The early Holocene Northern hemisphere paleoenvironmental records point to a general trend towards more humid conditions, linked with greater insolation and moisture-flux from the ocean to the African continent, but punctuated by significant climate oscillations associated with monsoonal intensification or weakness (Berger and Loutre, 1991; Ganopolski et al., 1998; Mayewsky et al., 2004). In the Alboran Sea borderlands, such climate oscillations resulted in recurrent declines of forest cover (APC 1 to 8) (Combourieu Nebout et al., 2009) (Fig. 10) and SST Mediterranean coolings (Cacho et al., 2001), that can be correlated with the North Atlantic Bond events (Bond et al., 2001). Similarly, our detrital proxy record supports the existence of diverse phases of major humidity and aridity in the western Mediterranean borderlands (Figs. 3, 5, 10). From 11,650 to 10,000 yr cal. BP, the increase in palygorskite and quartz contents and declining trend in Mg/Al and K/Al ratios (Figs. 3, 5, 10) reflect a slight increase in eolian input and comparatively dryer conditions. The increase in eolian dust during this period could be associated with a preboreal oscillation previously defined in the Alboran Sea (Cacho et al., 2001), and partially correlated with the Mediterranean APC 8-7 declines in temperate forest (Combourieu Nebout et al., 2009) (Fig. 10). The shift towards dry and cold conditions may also be coeval with cooling signals detected in Greenland ice cores (Rasmussen et al., 2007) and with a sudden increase in dry pollen taxa in other western Mediterranean sequences (Carrión, 2002; Fletcher et al., 2010). In the marine setting, this atmospheric situation was accompanied by low deep-water ventilation (high V/Al, Cu/Al and Zn/Al ratios) and lower bottom currents (low SS, and S/C ratio), which favored TOC preservation and contributed to enhanced TOC contents despite decreasing paleoproductivity levels (Figs. 6, 7, 9).

Another short-term dry period is supported by higher palygorskite and lower Mg/Al ratios, probably linked to APC 6 (Fig. 10). Just at the offset of this period, at 8,900 yr cal. BP, a sharp increase in paleocurrents is seen (Fig. 9), coinciding with the demise of ORL1 deposition. This takes place 500-700 years before its occurrence in other western Mediterranean areas, where deep-water mass formation (WMDW) prevented dysoxic conditions (e.g., Rogerson et al., 2008). One plausible

explanation for the local ORL1 demise is an increase in aspiration forces promoted by intense circulation through the Gibraltar Strait. Subsequent ventilation in the Alboran Sea basin would have prevented TOC preservation and resulted in a non-isochronous ORL1 collapse. Such observations point to a link between the paleocurrents proxies employed here and deep water formation in the western Mediterranean, yet also with the complex deep and intermediate water masses formed in the eastern Mediterranean (e.g., Schmield et al., 2010).

Following the ORL1 deposition, one of the most significant early Holocene climate events is the cold and dry phase that occurred at 8,200 yr cal. BP (e.g., Alley et al., 1997; Lowe et al., 2008). In our record, minor detrital input oscillations are recognized. The most significant are those related to redox sensitive elements (Figs. 5, 6), certain current intensification (Fig. 9), and a slight increase in $\delta^{18}O$ values (Figs. 7, 9).

At 7,400 yr cal. BP a slight decrease in $\delta^{18}O$ values, low paleocurrent intensity and oxygen conditions reflect substantial changes in paleoceanographic conditions (Figs. 6, 7, 9). Furthermore, a significant terrigenous variation is recorded at this time as a progressively decreasing trend in the K/Al ratio, which reaches its lowest values at 4,500 yr cal. BP (Fig. 10). Such oscillations were accompanied by a decrease in other typical fluvial proxies such as the Mg/Al and illite+chlorite/kaolinite ratios (Fig. 5). The significant decrease in illite content is documented in other Alboran Sea records (Martínez-Ruiz et al., 2003). Such conditions could be related with an early decline of the African Humid Period (AHP) at 7,400 yr cal. BP. Although records from the western coast of North Africa support the end of the AHP at approximately 5,500 yr cal. BP (deMenocal et al., 2000), diatom records from paleolakes in the Western Sahara and Sahel show a mid-Holocene arid episode over northwest Africa by 6,000-4,000 yr cal. BP (Gasse and Van Campo, 1994; Gasse, 2002) and a subsequent lake-level decline (Hoelzmann et al., 2004). This shift toward drier conditions is also registered in the northern and northeastern Iberian records as intermediate or ephemeral lake levels (e.g., Morellón et al., 2008; Moreno et al., 2011a), or minor oscillations in terrigenous input and deep-water circulation in the Balearic Islands (Frigola et al., 2007). Altogether, these observations suggest a decline in humidity and progressive lower river discharge that is further supported by enhanced palygorskite content and increasing arid conditions in the surrounding borderlands (Figs. 4, 10, 11). The runoff downward trend could be explained by a particular atmospheric situation over South Iberian-North African regions related with a gradual decrease in the monsoon system and progressively lower insolation (Berger and Loutre, 1991), which led to a monsoonal precipitation decline and changes in the subtropical vegetation as suggested by the long-term temperate forest decline (APC 4, Fig. 10) in Alboran pollen records (Combourieu Nebout et al., 2009).

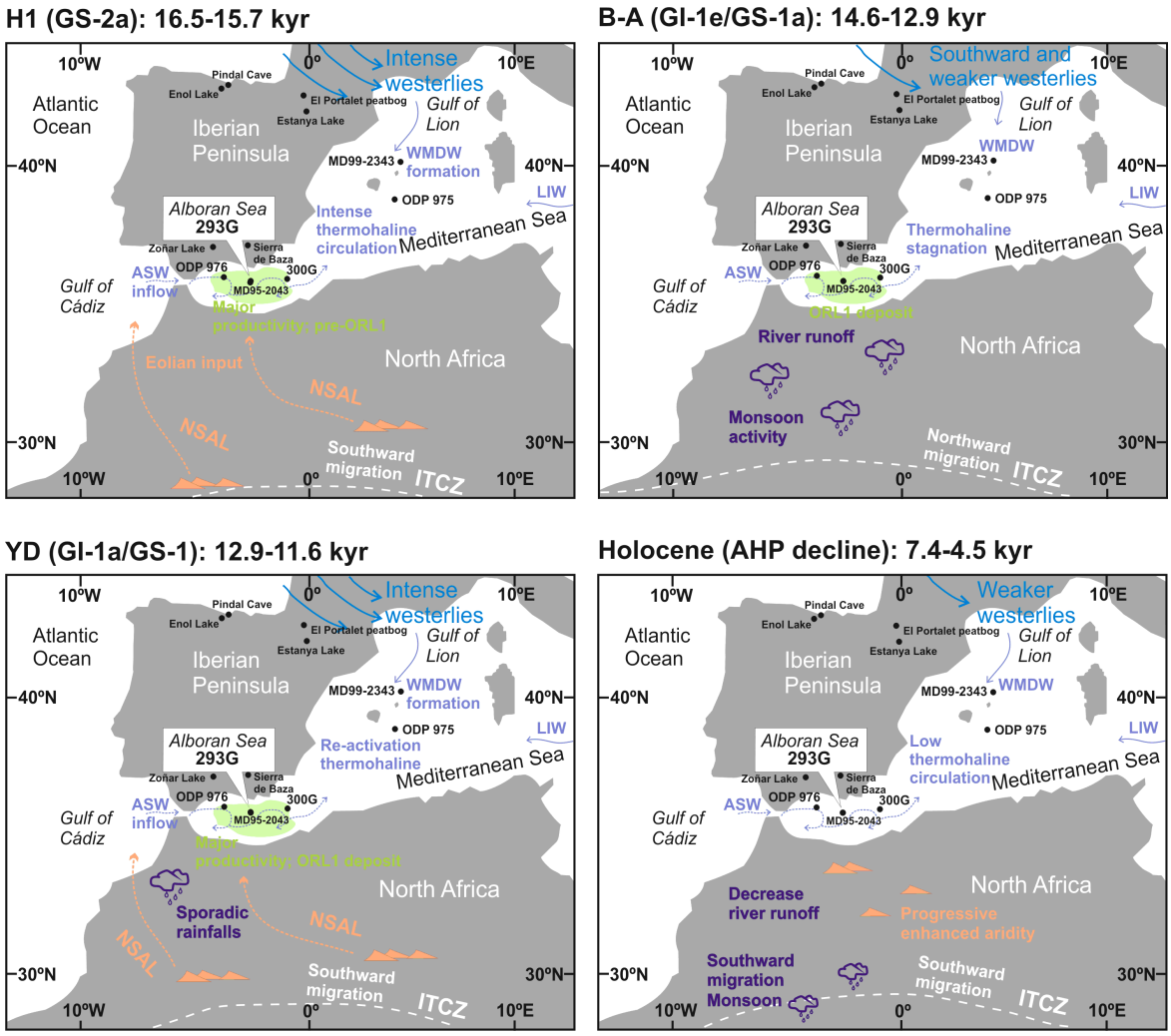

Figure 11. Schematic representation of atmospheric and oceanographic conditions recorded in the gravity core 293G from the Alboran Sea during the climatic periods Last Heinrich event (H1: 16.5-15.7 kyr), Bölling-Alleröd period (B-A: 14.6-12.9 kyr), the Younger Dryas (YD: 12.9-11.6 kyr), and the African Humid Period decline in the Holocene (AHP: 7.4-4.5 kyr) (see references in the text for other paleoclimate records). Green areas show productivity conditions. Blue arrows indicate the westerlies, Levantine Intermediate Water (LIW) and Western Mediterranean Deep Water (WMDW). Dashed blue arrows indicate the theoretical superficial water circulation in the Alboran Sea, Atlantic Surface Water (ASW) and Modified Atlantic Water (MAW). Dashed brown arrows represent the northern branch of the wind system Saharan Air Layer (NSAL). White dashed line shows the location of the Inter-Tropical Convergence Zone (ITCZ).

A rapid shift in the K/Al values at 4,500 yr cal. BP points to a return to more humid conditions (Fig. 10). Other southern Iberian marine and continental records signal the Roman Humid Period (RHP) (2,600-1,600 yr cal. BP) as the most humid period in the late Holocene (Martín-Puertas et al., 2010; Nieto-Moreno et al., 2011). In addition, some fluvial and lacustrine records from North Africa register a brief period of humid conditions at about 3,000-2,000 yr cal. BP (Swezey, 2001).

Around 2,200 yr cal. BP, the humidity began again to decrease, up to present times. The main forest depletion and consequent establishment of the current dominant grazed areas in southeast Iberia has been recorded from 2,500 yr cal. BP onward (Fig. 10) (Carrión et al., 2007), while palynological sequences also show an increase in anthropogenic fire activity (Carrión, 2002; Carrión et al., 2007). Additionally, Sahara eolian dust proxies (quartz and palygorskite contents) show a clear drying trend from around 1,700 yr cal. BP onward (Fig. 10), reaching higher values during the Medieval Warm Period (MWP) at around 1,150-650 yr cal. BP, as suggested by the compilation of different Iberian paleorecords (Moreno et al., submitted) and the equivalent last forest pollen decline (APC 1, Fig.10). Following these climate events, different paleoclimatic records of the last millennium also evidence a rapid cooling event known as the Little Ice Age (LIA) (650-150 yr cal. BP), linked to orbital forcing, and coinciding with solar activity minima and several strong tropical volcanic eruptions (Wanner et al., 2008). Increasing values in our eolian proxies and lower summer insolation (Fig. 10) indicate progressive dryness and desertification in the western Mediterranean as a result of a southward shift of the ITCZ coinciding with a pronounced weakening of the African monsoon system.

7. Conclusions

The high time resolution obtained from the sediment record analyzed here provides new insights regarding centennial to millennial paleoceanographic and atmospheric oscillations since the LGM. Such oscillations suggest a strong connection of western Mediterranean climate not only with North Atlantic changes but also with monsoonal low latitude variations. Cold and dry conditions involving major eolian input characterize the H1 event. Ba/Al ratios and the presence of authigenic marine barite within this interval indicate enhanced productivity and a subsequent organic enrichment prior to the ORL1 previously described in the Alboran Sea basin. Paleoredox proxies also evidence major oscillations in deep-water ventilation and current intensity accompanying the pronounced shift in planktonic $\delta^{18}O$ associated with the injection of large volumes of Atlantic meltwater. During the interstadial B-A period, redox-sensitive proxies and a prominent decrease in the speed of deep-sea bottom currents evidence lower oxygen conditions,

which favored ORL deposition. This warm period is further characterized by progressive humid conditions denoted by fluvial proxies, although a short-term IACP dry oscillation is also recognized. The YD interval is seen in this region as a two-phase period, characterized by a slightly dry onset and more humid conditions towards the end. The YD onset is also characterized by enhanced productivity, as indicated by Ba/Al ratios and the presence of authigenic marine barite. Then, during the Holocene, major detrital input fluctuations corroborate the previously reported forest cover declines in the Alboran borderlands. In the marine realm, the ORL1 demise at 8,900 yr cal. BP appears to be related to aspiration forces between intermediate and deep water in the westernmost Mediterranean. An early decline of the African Humid Period (AHP) at 7,400 yr cal. BP is also made manifest in oscillations in typical fluvial input proxies such as K/Al and illite+chlorite/kaolinite, with drier conditions prevailing around 4,500 yr cal. BP. In general, increasing detrital input during cold events deriving from the intensification of Saharan dust export across the western Mediterranean could be related to a predominant positive NAO index. Hydrological oscillations also appear to be linked with migrations of the ITCZ over North Africa, involving variations in the African monsoon system.

Acknowledgments

This work was supported by Projects CGL2009-07603, CTM2009-07715, CSD2006-00041 (Ministerio de Ciencia e Innovación), 200800050084447 (MARM), Project RNM 05212, Research Group 0179 (Junta de Andalucía). We thank the Training-Through-Research Programme (UNESCO-Moscow State University) for core material recovery. F. J. Jiménez-Espejo acknowledges funding from the CSIC "JAE-Doc" postdoctoral program. We are very grateful to Dr. D. Martin Ramos for such great help with the quantitative mineral analysis and with the Xpowder software. We are likewise grateful to E. Holanda, E. Abarca, C. Niembro, L. López, J. Santamarina and D. Ortega for their laboratory assistance. Analyses were performed at the "Centro de Instrumentación Científica", University of Granada, Granada (Spain), at National Centre for Accelerators (CNA), Sevilla (Spain), at the SGS Minerals Services Analytical, Lakefield, Ontario (Canada), and at Isotope Laboratory, Marum, Bremen University, Bremen (Germany). The manuscript was greatly improved by the instructive comments and suggestions of two anonymous reviewers. J. L. Sanders post-edited the English style.

5. Chapter II.- Reconstructing weathering history and eolian input provenances in the western Mediterranean since the Last Glacial Maximum

Rodrigo-Gámiz, M., Martínez-Ruiz, F., Chiaradia, M., Jiménez-Espejo, Ariztegui, D.

To be submitted to Earth and Planetary Science Letters

Abstract

Eolian dust from the North Africa margin has significantly contributed to the terrigenous sedimentation in the Mediterranean. Reconstruction of oscillations in eolian input provides information on atmospheric fluxes and consequently on the atmospheric response to climate change. We present a high-resolution record of such oscillations in the westernmost Mediterranean (Alboran Sea basin) for the last 20 kyr based on radiogenic isotope proxies. Neodymium, strontium and lead profiles, obtained from carbonate-free samples from the <37μm size fraction, have been used to characterize paleoenvironmental fluctuations, sediment provenance and eolian input oscillations. These isotope compositions have been further integrated with previous geochemical and mineralogical data. Substantial variations in Nd, Sr, and Pb isotopic signatures throughout the studied time interval support climate oscillations related to short-term cold periods at 8.9 kyr cal. BP and just about the last Heinrich event (H1). In addition, enhanced palygorskite and quartz contents with significant increases in Si/Al, Zr/Al, and Ti/Al ratios reveal dominant arid conditions during the same periods. Furthermore, radiogenic isotope compositions indicate an Archaean rock source during these colder periods located in the present Senegal and Guinea regions. Conversely, the dust source during warmer periods records a dominant provenance from Morocco, Mali and Mauritania. Thus, these oscillations in composition and source of eolian dust support fluctuations in wind intensity modulated by the migration of the Inter-Tropical Convergence Zone and hence fluctuations in the African monsoon system.

1. Introduction

The Western Sahara dry land in North Africa is recognized as the major dust source (Prospero, 1999). Numerical simulations concluded that North Africa is the largest single source region of dust on Earth providing 58 wt% of total dust emissions (Tanaka and Chiba, 2006). Extrapolating this flux to the total western Mediterranean basin area (840,000 km2) yields an average total atmospheric flux of 10.9 ± 0.6 x 1012 g/yr (Bergametti et al., 1989b; Löye-Pilot et al., 1989). The source of the North African margin terrigenous particles includes a large area extending from Morocco to north Mauritania and south Algeria, Mali and Niger (Molinaroli, 1996). Therefore, dust source areas from North Africa have changed along the past times according to the boundaries of different wind systems, their intensities, as well as the paleo-positioning and migrations of the Inter-Tropical Convergence Zone (ITCZ). Furthermore, at the scale of Quaternary climatic oscillations, eolian dust fluxes to the ocean have been suggested to be higher during glacial (Greenland Stadial, GS) than

interglacial (Greenland Interstadial, GI) periods (nomenclature based on INTIMATE group, Lowe et al., 2008), as result of a general southward displacement of the ITCZ (e.g., Reader et al., 1999; Elenga et al., 2000). At present, the relative amount of sediment input from the Sahara and Sahelian regions to the western Mediterranean is low and occurs in winter (Bergametti et al., 1989b; Dulac et al., 1992). The terrigenous particles deflated from the surface depend on several factors, such as the wind speed, the instability of the atmosphere, the particle size, the degree of particle exposure, the soil moisture, the vegetation cover, and the mineralogical composition, among others (e.g., deMenocal, 1995, 2004; Mulitza et al., 2008).

It has also been recognized that the mineral dust is mainly composed of quartz, feldspar, clay minerals (palygorskite, kaolinite), carbonates (calcite and dolomite), oxides (e.g., hematite, magnetite, rutile), and evaporites (halite, gypsum) (Kolla et al., 1979; Foucault and Mélières, 2000; Caquineau et al., 2002; Bout-Roumazeilles et al., 2007). Eolian pulses can occur as individual grains or as aggregates, from less than 2 micrometres to 30 micrometres (μm) in diameter (Kolla et al., 1979).

Therefore, the composition of marine sediments in marginal marine basins mainly derives from riverine and eolian inputs, thus reflecting the climatic conditions over adjacent continental regions (Kolla et al., 1979; Jeandel et al., 2007). In the case of the western Mediterranean, eolian materials from arid and semi-arid regions in North Africa are the main source of terrigenous marine sediments (e.g., Chester et al., 1971; Bergametti et al., 1989a, 1989b; Loÿe-Pilot and Martin, 1996; Molinaroli, 1996; Prospero, 1996), although a small fraction of suspended particulate matter from South Iberian rivers runoff should also be considered (Grousset et al., 1988; Stumpf et al., 2011).

In general, the identification of terrigenous particles provenance in Mediterranean marine sediments has been based on geochemical and mineralogical data (e.g., Coudé-Gaussen et al., 1987; Foucault and Mélières, 2000; Wehausen and Brumsack, 2000; Caquineau et al., 2002; Moreno et al., 2002; Weldeab et al., 2002a, 2002b, 2003; Díaz-Hernández et al., 2011) as well as on remote sensing methods, analysis of surface dust observations, back-trajectory analysis, and the use of mineral tracers (e.g., Goudie and Middleton, 2001). Another recently developed method to detect dust source regions is the Total Ozone Mapping Spectrometer (TOMS), which is currently carried on board the Earth Probe Satellite (e.g., Goudie and Middleton, 2001).

Stable radiogenic isotopes are another suitable tracers for identifying and quantifying source(s) areas of terrigenous matter, which may in turn give us additional information about the provenance of eolian dust and its atmospheric transport patterns (e.g., Grousset et al., 1988, 1992, 1998; Revel et al., 1996b; Hemming et al., 1998; Tütken et al., 2002; Grousset and Biscaye, 2005). The variability

of stable radiogenic isotope composition of rocks occurring on the Earth's surface, which are ultimately the source of the particulate matter suspended and transported by winds, is essentially the result of chemical fractionation between radioactive parents and radiogenic daughters operated by large-scale geological processes and of age. This makes that rocks of different ages and of different provenance in terms of large-scale reservoirs (e.g., mantle versus crust) have significantly and measurably different isotopic compositions. The isotopic composition of the material (sediment, soil) that is the weathering product of the source rocks may coincide or not with that of the source rock, as explained further below.

Previous research in a west-east Mediterranean transect have characterized the spatial distribution of detrital flux and the provenance of surface and Late Pleistocene sediments, obtaining as main end members Saharan dust and Nile particulate matter (e.g., Weldeab et al., 2002a, 2002b, 2003). In the westernmost Mediterranean area, however, there is less work concerning the identification of eolian dust provenance and atmospheric pathways. Thus, a detailed estimation of the eolian input in marine sediments from the western Mediterranean will provide valuable insight into past atmospheric circulation, terrigenous provenance and climate variability over the surrounding continents. Previous mineralogical, geochemical and sedimentological analyses over gravity core 293G recovered in the westernmost Mediterranean, Alboran Sea basin, have been used to reconstruct the climate variability in term of atmospheric and oceanic responses as well as to identify the eolian input oscillations since the LGM (Rodrigo-Gámiz et al., 2011). In this study, we used the radiogenic isotopes of Strontium (Sr), Neodymium (Nd), and Lead (Pb) in the same marine core to constraint the geographic provenance of the eolian dust and its paleo-atmospheric transport pathways during the last 20 kyr.

2. Alboran Sea sediment record and present-day atmospheric pattern

The Alboran Sea, located in the westernmost Mediterranean Sea, is a semi-closed basin surrounded by the Iberian Peninsula in the North and the North Africa margin in the South, which determines its interest for paleoclimate studies. In 2002, a gravity core (293G) was recovered in the East part (Fig. 1) (36´10.414N, 2´45.280W, depth 1,840 m, long. 402 cm) during the oceanographic cruise Training Through Research-12 (R/V Professor Logachev) (Comas and Ivanov, 2003).

Modern climate conditions over the western Mediterranean are governed by the Azores high-pressure system and by the African monsoonal dynamics. Summertime climates usually are dry and hot due to the influence of the atmospheric subtropical high-pressure belt (Sumner et al., 2001).

During winter the subtropical high is shifted to the south, allowing mid-latitude storms to enter the region from the open Atlantic and bring enhanced amounts of rainfall to the western Mediterranean. In addition, local climatology is seasonally modulated by the latitudinal shift over North Africa of the Inter-Tropical Convergence Zone (ITCZ) and hence the African monsoon front. The ITCZ directly controls the location of precipitation over North Africa and changes in its position affect how much rainfall occurs and therefore the degree of river runoff. The recent revision by Nicholson (2009) suggested an ITCZ complex pattern, especially for the boreal summer situation. In winter, the equatorward displacement of the ITCZ (10° N) causes a southward shift of dry subtropical air masses and is associated with the development of strong easterly Saharan Air Layer (SAL) winds and its northern branch (NSAL). The dust plume is generally located between 15 and 25° N along an E–W axis over the tropical Atlantic Ocean (Holz, 2004). During boreal summer, dry subtropical air is shifted northward as the ITCZ is located around 20° N (Fig. 1). It represents the onset of the rainy season (summer monsoon) with heavy rainfall and changes in atmospheric circulation (Peyrillé and Lafore, 2007). Nicholson (2009) suggested that three quasi-independent mechanisms control precipitation development over West Africa in summer: ascent of air masses linked to the upper-level jet streams, convergence associated with the surface ITCZ, and a coastal circulation cell linked to sea-breeze effects. Complex parameters and mechanisms actually modulate precipitation. Surface temperature anomalies of adjacent oceanic basins could also balance the northward expansion of the monsoon, primarily by changes in the evaporation budget (e.g., Rowell, 2003; Hall and Peyrillé, 2006).

3. Analytical techniques

3.1. Sediment core description and samples selection

The marine gravity core 293G contains homogeneous green-brownish hemipelagic mud-clays with some nannofossils. The results of high-resolution geochemical, mineralogical and sedimentological analyses at about 75 yr/1.5 cm (n= 267 samples) from this sediment record have been reported in Rodrigo-Gámiz et al., (2011). A previously developed age model indicates that this marine core spans the last 20 kyr (see Rodrigo-Gámiz et al., 2011, for a detailed description), which a mean sedimentation rate of 20 cm/kyr allowing to resolve millennial to centennial-scales variability in this record.

A total of 37 samples of plausible eolian material was chosen throughout the last 20 kyr using typical eolian proxies recognized in the marine core 293G such as quartz content, Si/Al, Zr/Al, and

the exceptional signal obtained in this continuous record based on the Zr/Al profile (Fig. 1). Changes in grain-size can have a substantial influence in Sr-isotope compositions when used as provenance indicators. Thus, it is necessary to always work on the same grain-size fraction that for this study is <37µm.

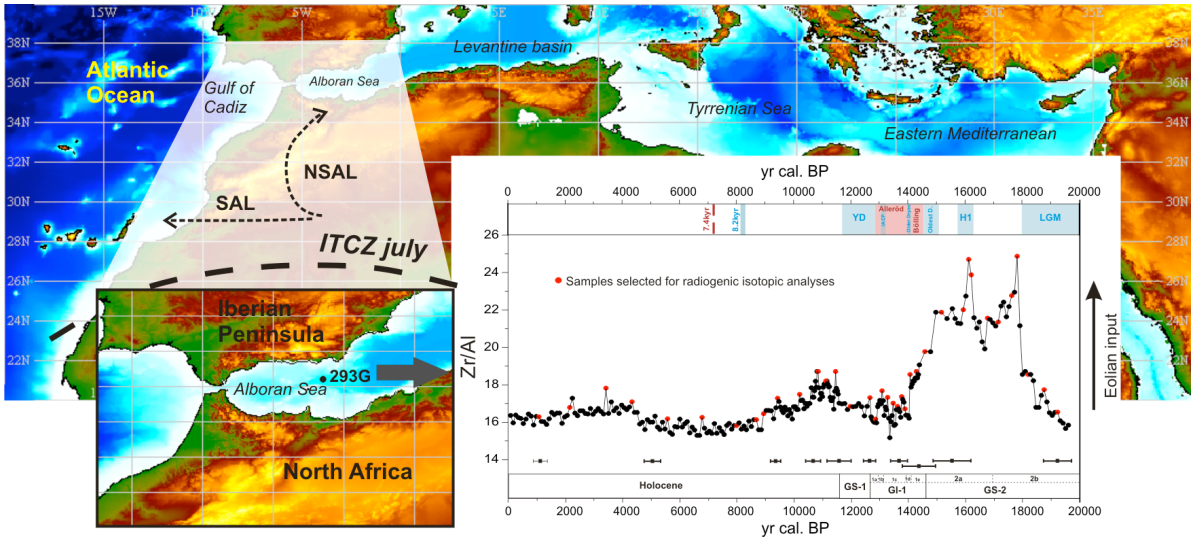

Figure 1. Map of the studied area showing the location of gravity core 293G retrieved in the Alboran Sea. The Inter-Tropical Convergence Zone (ITCZ) is represented in its northern position in summer (July). Zr/Al profile a proxy for eolian input has been used to select 37 samples for radiogenic measurements covering the last 20 kyr.

3.2. Sediment digestion procedure, elements separation and isotope analysis

Chemical extractions for Sr, Nd and Pb isotopes were carried out at the Department of Mineralogy of the University of Geneva (Switzerland). Each sample was treated to leach the carbonate fraction with acetic acid solution followed by a triple rinse with water. The >37µm fraction was removed by dry sieving. Around 100-150 mg of each dried alumino-silicate residual fraction was mineralized in pure acids in Teflon bombs heated on an electrical hotplate (140 ºC), in a two-step procedure: a mixture of 1 ml HNO_3 15M with 4 ml HF at 140ºC during 7 days, after evaporation 3 ml HNO_3 15M at 140 ºC during 2 days, and after evaporation the samples were finally diluted to 1.9 ml with HNO_3 1M for chemical separation.

Sr and Nd separation from the solutions prepared was carried out using cascade columns with Sr-Spec, TRU-Spec and Ln-Spec resins following a modified method after Pin et al., (1994). Pb was further purified by anion exchange chromatography using an AG-MP1-M clean resin in hydrobromic medium and small volume columns (0.08 ml).

Pb was loaded on Re filaments using the silica gel technique (Gerstenberger and Haase, 1997) and Pb isotope ratios of all samples and standards were measured in static mode on Faraday cups on a multicollector Thermo TRITON mass spectrometer (Department of Mineralogy, University of Geneva, Switzerland). Pb isotope ratios were corrected for instrumental fractionation by a factor of 0.1% per amu based on more than 100 measurements of the SRM981 standard and using the standard values of Todt et al., (1996). External reproducibility (2σ) of the standard ratios is 0.05% for $^{206}Pb/^{204}Pb$, 0.08% for $^{207}Pb/^{204}Pb$, 0.10% for $^{208}Pb/^{204}Pb$, 0.006% for $^{206}Pb/^{207}Pb$, 0.007% for $^{208}Pb/^{207}Pb$ and 0.008% for $^{208}Pb/^{206}Pb$.

Sr was loaded on single Re filaments with a Ta oxide solution and measured on the multicollector Thermo TRITON mass spectrometer (Department of Mineralogy, University of Geneva, Switzerland) at a pyrometer controlled temperature of 1480 ºC in static mode using the virtual amplifier design to cancel out biases in gain calibration among amplifiers. $^{87}Sr/^{86}Sr$ values were internally corrected for fractionation using a $^{88}Sr/^{86}Sr$ value of 8.375209. Raw values were further corrected for external fractionation by a value of +0.03‰, determined by repeated measurements of the SRM987 standard ($^{87}Sr/^{86}Sr$=0.710250). External reproducibility (1σ) of the SRM987 standard is <7 ppm.

Nd was loaded on double Re filaments with 1M HNO_3 and measured on a 7-collector Finnigan MAT 262 thermal ionization mass spectrometer with extended geometry and stigmatic focusing (Department of Mineralogy, University of Geneva, Switzerland). $^{143}Nd/^{144}Nd$ ratios were measured in dynamic mode (quadruple collector) and internally corrected for fractionation using a $^{146}Nd/^{144}Nd$ value of 0.721903 and normalized to the JNdi1 standard. Our mean of 19 replicated analyses of this standard in dynamic mode was 0.512097 ± $3x10^{-6}$ (2σ) during the period of analysis. The $^{143}Nd/^{144}Nd$ ratio is commonly expressed as $\varepsilon Nd(0) = [(^{143}Nd/^{144}Nd)sample / (^{143}Nd/^{144}Nd)CHUR - 1] \times 10^4$ with present day Chondritic Uniform Reservoir (CHUR) being 0.512638 (Wasserburg et al., 1981).

4. Results: isotopic composition

The Sr and Nd isotope results of the carbonate-free <37μm and sediment fraction are shown in Table 1, and plotted against age in Figure 2. Likewise, the Pb isotope values are presented in Table 2, and various Pb isotope ratios are plotted against age in Figure 3.

The Sr isotope signature for the last 20 kyr in the westernmost Mediterranean shows eight periods with less radiogenic values recorded at 18.7, 17.2-16.7, 14.3-13.9, 13.5, 13.1, 10.2-8.9, 6.8-4.3, and 1.1 kyr cal. BP (Fig. 2). The $^{87}Sr/^{86}Sr$ ratio value ranges from 0.713110 to 0.718042, reaching the minimum value at 16.6 kyr cal. BP.

Some of these oscillations in the $^{87}Sr/^{86}Sr$ signature are also evidenced in the $^{143}Nd/^{144}Nd$ and εNd(0) profile with more negative εNd(0) values, i.e., less radiogenic (Fig. 2). The $^{143}Nd/^{144}Nd$ isotopic signature ranges between 0.512037 and 0.512099 (Fig. 2). Maximum and minimum values are dated at 9.4 and 8.7 kyr cal. BP, respectively. The $^{143}Nd/^{144}Nd$ ratio displays less radiogenic values at 17.6, 16.2-15.9, 14.5, 13.9, 13.6, 8.9-8.7, 5.5, and 2.2 kyr cal. BP (Fig. 2). The εNd(0) signature oscillates between -11.7 and -10.5 recording the most negative values around 17.6, 16.2-15.9, 14.5, 8.9-8.7, 5.5, and 2.2 kyr cal. BP (Fig. 2). Typical εNd(0) values from fluvial sediments in the western Mediterranean oscillate between -10.8 and -9.7, and between -12.2 and -10.2 from European atmospheric input (Henry et al., 1994).

Regarding the Pb isotopic composition, in particular $^{206}Pb/^{204}Pb$, $^{207}Pb/^{204}Pb$, and $^{208}Pb/^{204}Pb$ ratios show almost the same oscillation pattern, ranging from 18.8275 to 18.6929, 15.755 to 15.595, and 39.081 to 38.681, respectively (Fig. 3). Higher Pb isotope ratio values during the last 20.0 kyr, are observed at 17.6, 13.5, 11.1, 4.3-3.4 kyr cal. BP (Fig. 3). Conversely, lower values of Pb isotope ratios are recorded at 18.7, 16.7, 14.6, 12.8, 11.5, 8.9, and 2.2 kyr cal. BP (Fig. 3). These periods are also represented by more negative values of εNd(0) (i.e. lower $^{143}Nd/^{144}Nd$) and lower values of $^{87}Sr/^{86}Sr$ (Fig. 2). The $^{207}Pb/^{206}Pb$ values oscillate between 0.83788 and 0.83286, the $^{208}Pb/^{206}Pb$ ratio shows variations between 2.07794 and 2.06768, and $^{208}Pb/^{207}Pb$ ratio between 2.48654 and 2.47854 (Fig. 3), displaying more radiogenic signatures at 18.7, 15.9, 13.5, 11.1, 9.4, 4.3-2.2 kyr cal. BP.

Table 1. Sr and Nd isotopic composition on the carbonate-free fraction below 37μm from the marine core 293G. $^{87}Sr/^{86}Sr$ and $^{143}Nd/^{144}Nd$ ratios, εNd(o) values and Sr concentrations of all samples analyzed.

Samples	Depth (cm)	Age (yr cal. BP)	Sr (ppm)	$^{87}Sr/^{86}Sr$	$1\sigma*10^{-6}$	$^{143}Nd/^{144}Nd$	$1\sigma*10^{-6}$	εNd(0)
293G 1 16.5-18	17.25	1075	449.3253	0.716771	2	0.512088	2	-10.7
293G 1 34.5-36	36.75	2160	565.6682	0.717964	2	0.512068	3	-11.1
293G 1 55.5-57	56.25	3427	610.5798	0.717332	2	0.512081	2	-10.9
293G 2 12-13.5	70.75	4332	557.265	0.717776	2	0.512096	2	-10.6
293G 2 33-34.5	91.75	5574	538.1959	0.716461	2	0.512066	4	-11.2
293G 2 54-55.5	112.75	6782	581.7916	0.717616	2	0.512087	8	-10.7
293G 3 16.5-18	133.75	7990	628.3586	0.717816	5	0.512077	2	-10.9
293G 3 28.5-30	145.75	8681	652.7198	0.717795	2	0.512037	8	-11.7
293G 3 33-34.5	150.25	8940	642.6469	0.714397	2	0.512041	6	-11.6
293G 3 42-43.5	159.25	9422	651.0137	0.717152	3	0.512099	166	-10.5
293G 4 6-7.5	181.25	10193	645.0884	0.716134	1	0.512095	23	-10.6
293G 4 28.5-30	203.75	10839	581.7589	0.717591	2	0.512071	14	-11.1
293G 4 42-43.5	217.25	11114	565.881	0.717651	2	0.512078	2	-10.9
293G 5 0-1.5	232.75	11451	553.4159	0.717110	3	0.512059	7	-11.3
293G 5 12-13.5	244.75	11966	556.2425	0.717639	2	0.512057	6	-11.3
293G 5 22.5-24	255.25	12653	582.626	0.716945	3	0.512068	1	-11.1
293G 5 30-31.5	262.75	12846	596.618	0.716280	2	0.512062	7	-11.2
293G 5 39-40.5	271.75	13078	581.3984	0.715134	3	0.512068	1	-11.1
293G 5 46.5-48	279.25	13271	561.8477	0.717187	3	0.512079	7	-10.9
293G 5 54-55.5	286.75	13464	588.6822	0.716166	1	0.512064	4	-11.2
293G 6 1.5-3	292.25	13618	579.8712	0.717347	3	0.512052	18	-11.4
293G 6 7.5-9	298.25	13765	543.2918	0.717056	3	0.512064	1	-11.2
293G 6 12-13.5	302.75	13874	526.5423	0.716427	2	0.512053	6	-11.4
293G 6 19.5-21	310.25	14056	503.9568	0.715899	2	0.512062	7	-11.2
293G 6 28.5-30	319.25	14275	445.8737	0.716152	2	0.512076	2	-11.0
293G 6 34.5-36	325.25	14577	429.9046	0.717414	2	0.512060	25	-11.3

Samples	Depth (cm)	Age (yr cal. BP)	Sr (ppm)	$^{87}Sr/^{86}Sr$	$1\sigma*10^{-6}$	$^{143}Nd/^{144}Nd$	$1\sigma*10^{-6}$	εNd(0)
293G 6 39-40.5	329.75	15153	403.8799	0.717045	4	0.512080	2	-10.9
293G 6 48-49.5	338.75	15914	385.3481	0.716053	2	0.512047	5	-11.5
293G 6 51-52.5	341.75	16103	425.2311	0.716376	3	0.512062	1	-11.2
293G 6 52.5-54	343.25	16197	456.4441	0.715867	2	0.512044	3	-11.6
293G 7 1.5-3	351.25	16669	447.8152	0.713110	3	0.512067	1	-11.1
293G 7 7.5-9	357.25	17140	423.3665	0.715785	2	0.512057	8	-11.3
293G 7 15-16.5	364.75	17612	375.6393	0.717949	2	0.512041	9	-11.6
293G 7 18-19.5	367.75	17800	414.3141	0.717095	3	0.512060	2	-11.3
293G 7 24-25.5	373.75	18177	539.771	0.718042	2	0.512057	26	-11.3
293G 7 33-34.5	382.75	18743	641.7128	0.714939	2	0.512074	3	-11.0
293G 7 40.5-42	390.25	19214	603.5997	0.717840	2	0.512060	14	-11.3

Table 2. Pb isotopic data measured on the carbonate-free fraction below 37μm from the marine core 293G.

Samples	Depth (cm)	Age (yr cal. BP)	$^{206}Pb/^{204}Pb$	$1\sigma*10^{-4}$	$^{207}Pb/^{204}Pb$	$1\sigma*10^{-4}$	$^{208}Pb/^{204}Pb$	$1\sigma*10^{-4}$
293G 1 16.5-18	17.25	1075	18.733		15.688		38.909	
293G 1 34.5-36	36.75	2160	18.6947	1	15.664	2	38.824	5
293G 1 55.5-57	56.25	3427	18.8039	74	15.723	62	39.057	158
293G 2 12-13.5	70.75	4332	18.803	76	15.713	147	39.070	356
293G 2 33-34.5	91.75	5574	18.7776	4	15.669	5	38.888	14
293G 2 54-55.5	112.75	6782	18.7737	104	15.680	87	38.902	214
293G 3 16.5-18	133.75	7990	-	-	-	-	-	-
293G 3 28.5-30	145.75	8681	18.7632	3	15.668	3	38.876	10
293G 3 33-34.5	150.25	8940	18.7429	1	15.667	1	38.865	3
293G 3 42-43.5	159.25	9422	18.7564	71	15.684	58	38.928	144
293G 4 6-7.5	181.25	10193	18.7703	3	15.683	3	38.929	7
293G 4 28.5-30	203.75	10839	18.7879	18	15.678	15	38.933	37
293G 4 42-43.5	217.25	11114	18.823	124	15.755	107	39.081	264

Samples	Depth (cm)	Age (yr cal. BP)	$^{206}Pb/^{204}Pb$	$1\sigma*10^{-4}$	$^{207}Pb/^{204}Pb$	$1\sigma*10^{-4}$	$^{208}Pb/^{204}Pb$	$1\sigma*10^{-4}$
293G 5 0-1.5	232.75	11451	18.7524	20	15.649	16	38.834	41
293G 5 12-13.5	244.75	11966	18.7799	3	15.675	3	38.915	10
293G 5 22.5-24	255.25	12653	18.757	69	15.663	57	38.891	143
293G 5 30-31.5	262.75	12846	18.7095	117	15.612	97	38.749	237
293G 5 39-40.5	271.75	13078	-	-	-	-	-	-
293G 5 46.5-48	279.25	13271	18.7358	2	15.668	2	38.847	4
293G 5 54-55.5	286.75	13464	18.7814	34	15.723	31	39.022	83
293G 6 1.5-3	292.25	13618	18.7699	3	15.668	3	38.874	10
293G 6 7.5-9	298.25	13765	18.799	21	15.688	19	38.938	47
293G 6 12-13.5	302.75	13874	18.7685	2	15.667	2	38.872	5
293G 6 19.5-21	310.25	14056	18.7699	52	15.676	43	38.905	105
293G 6 28.5-30	319.25	14275	-	-	-	-	-	-
293G 6 34.5-36	325.25	14577	18.7525	3.1	15.670	3.1	38.871	9.3
293G 6 39-40.5	329.75	15153	18.788	19	15.677	16	38.893	39
293G 6 48-49.5	338.75	15914	18.7803	20	15.672	17	38.876	39
293G 6 51-52.5	341.75	16103	18.757	41	15.689	32	38.907	82
293G 6 52.5-54	343.25	16197	18.7557	2	15.660	2	38.844	5
293G 7 1.5-3	351.25	16669	18.692	151	15.595	124	38.681	308
293G 7 7.5-9	357.25	17140	18.7852	1.7	15.656	1.8	38.855	5.8
293G 7 15-16.5	364.75	17612	18.8275	79	15.687	66	38.953	164
293G 7 18-19.5	367.75	17800	18.8065	13	15.663	10	38.885	27
293G 7 24-25.5	373.75	18177	18.7850	77	15.661	65	38.874	161
293G 7 33-34.5	382.75	18743	18.7384	104	15.641	89	38.794	218
293G 7 40.5-42	390.25	19214	18.7875	2.1	15.662	2.4	38.858	7.7

Table 2 cont. Pb isotopic data measured on the carbonate-free fraction below 37μm from the marine core 293G.

Samples	Depth (cm)	Age (yr cal. BP)	$^{207}Pb/^{206}Pb$	$1\sigma*10^{-5}$	$^{208}Pb/^{206}Pb$	$1\sigma*10^{-5}$	$^{208}Pb/^{207}Pb$	$1\sigma*10^{-5}$
293G 1 16.5-18	17.25	1075	0.83754		2.07703		2.48018	
293G 1 34.5-36	36.75	2160	0.83788	0	2.07673	1	2.47854	1
293G 1 55.5-57	56.25	3427	0.83607	4	2.07706	13	2.48395	10
293G 2 12-13.5	70.75	4332	0.83572	8	2.07794	14	2.48654	18
293G 2 33-34.5	91.75	5574	0.83447	1	2.07094	3	2.48174	2
293G 2 54-55.5	112.75	6782	0.83512	4	2.07190	10	2.48079	14
293G 3 16.5-18	133.75	7990	-	-	-	-	-	-
293G 3 28.5-30	145.75	8681	0.83507	1	2.07193	3	2.48117	2
293G 3 33-34.5	150.25	8940	0.83591	0	2.07359	1	2.48064	1
293G 3 42-43.5	159.25	9422	0.83620	3	2.07553	6	2.48211	9
293G 4 6-7.5	181.25	10193	0.83551	0	2.07395	1	2.48228	1
293G 4 28.5-30	203.75	10839	0.83444	1	2.07216	3	2.48328	4
293G 4 42-43.5	217.25	11114	0.83701	6	2.07673	22	2.48085	14
293G 5 0-1.5	232.75	11451	0.83457	1	2.07092	2	2.48140	3
293G 5 12-13.5	244.75	11966	0.83468	1	2.07214	3	2.48255	2
293G 5 22.5-24	255.25	12653	0.83506	3	2.07334	6	2.48275	7
293G 5 30-31.5	262.75	12846	0.83442	4	2.07104	7	2.48191	10
293G 5 39-40.5	271.75	13078	-	-	-	-	-	-
293G 5 46.5-48	279.25	13271	0.83623	0	2.07342	1	2.47947	1
293G 5 54-55.5	286.75	13464	0.83714	3	2.07786	12	2.48212	8
293G 6 1.5-3	292.25	13618	0.83475	1	2.07105	3	2.48105	2
293G 6 7.5-9	298.25	13765	0.83454	1	2.07161	7	2.48229	5
293G 6 12-13.5	302.75	13874	0.83473	0	2.07109	1	2.48116	1
293G 6 19.5-21	310.25	14056	0.83535	3	2.07293	4	2.48151	6
293G 6 28.5-30	319.25	14275	-	-	-	-	-	-
293G 6 34.5-36	325.25	14577	0.83564	0	2.07285	2	2.48054	1
293G 6 39-40.5	329.75	15153	0.83444	1	2.07012	2	2.48080	3

Samples	Depth (cm)	Age (yr cal. BP)	$^{207}Pb/^{206}Pb$	$1\sigma*10^{-5}$	$^{208}Pb/^{206}Pb$	$1\sigma*10^{-5}$	$^{208}Pb/^{207}Pb$	$1\sigma*10^{-5}$
293G 6 48-49.5	338.75	15914	0.83448	1	2.06999	3	2.48060	3
293G 6 51-52.5	341.75	16103	0.83646	2	2.07435	8	2.47984	7
293G 6 52.5-54	343.25	16197	0.83496	0	2.07102	1	2.48039	1
293G 7 1.5-3	351.25	16669	0.83433	6	2.06950	10	2.48048	15
293G 7 7.5-9	357.25	17140	0.83340	0	2.06839	1	2.48187	1
293G 7 15-16.5	364.75	17612	0.83323	4	2.06894	6	2.48311	9
293G 7 18-19.5	367.75	17800	0.83286	1	2.06768	2	2.48261	2
293G 7 24-25.5	373.75	18177	0.83375	3	2.06953	6	2.48228	8
293G 7 33-34.5	382.75	18743	0.83464	4	2.07029	7	2.48050	9
293G 7 40.5-42	390.25	19214	0.83363	0	2.06830	2	2.48108	1

5. Discussion

5.1. Weathering conditions in the westernmost Mediterranean since the Last Glacial Maximum

Neodymium is a relatively immobile element during weathering and, as mentioned above, its isotopic composition in weathering products is not affected by changes in the evaporation/precipitation (E/P) balance and variations in soil formation during transition from wet to dry periods (e.g., Nesbitt et al., 1980; Braun et al., 1998). Thus, the $^{143}Nd/^{144}Nd$ ratio of weathered material retains the character of the source whereas the Sr isotope variations are associated with changes in weathering (Nesbitt et al., 1980). During chemical weathering the radiogenic Sr fraction of a rock is extracted from the source faster than the non-radiogenic Sr fraction due to the preferential breakdown of Rb-rich phases such as mica and K-feldspar (Nesbitt et al., 1980). Thus, radiogenic Sr enters into solution and is removed from the source region (Blum and Erel, 1997).

Therefore, the Sr-Nd isotopes variations (Fig. 2) could reveal two types of processes or a combination of both: one in which changes in the source area are the predominant signal recorded, and the other in which periods with a major influence of chemical weathering degree, e.g., enhanced rainfall, intensification of the African monsoon, major river runoff, are recorded. This last phenomenon is strongly related with prevailing environmental factors over the source area, such as the vegetation cover, aridity and wind intensity.

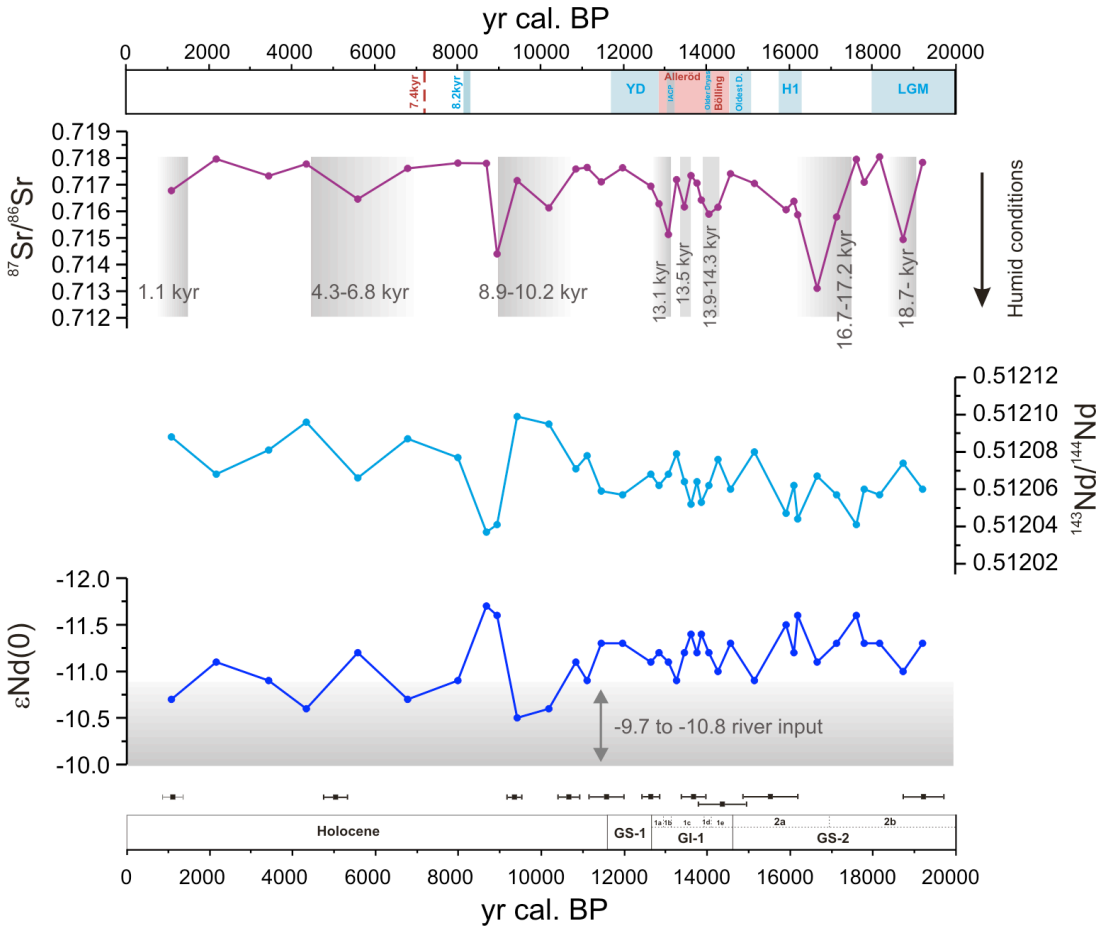

Figure 2. $^{87}Sr/^{86}Sr$ ratio, $^{143}Nd/^{144}Nd$ ratio and εNd(0) distribution plotted against age.
Vertical grey bars show lower $^{87}Sr/^{86}Sr$ signatures could reflect major chemical weathering. Shaded grey area in εNd(0) profile shows typical values from fluvial sediments in the western Mediterranean (Henry et al., 1994).
Upper panel: light red vertical bars indicate the Allërod (A), and the Bölling (B) warm time intervals. Light blue vertical bars indicate main cold periods, such as the last Heinrich event (H1), Oldest Dryas, Older Dryas, Intra-Alleröd Cold Period (IACP), the Younger Dryas (YD), and the "8.2 kyr" cold event. Short dashed red vertical bar show the demise of the African Humid Period (AHP). Lower panel: Greenland Stadials (GS-1, GS-2) and Interstadials (GI-1) and Holocene time intervals according to the event stratigraphy timing proposed by the INTIMATE group (Lowe et al., 2008). Black squares indicate ten ^{14}C-AMS dates with two-sigma probability interval using Calib 6.0.2 software (Stuiver and Reimer, 1993) and the Marine09 calibration curve (Reimer et al., 2009).

Furthermore, taking into account the oscillation in the different Pb isotope ratios (Fig. 3), more information can be extracted concerning the type of phenomenon recorded. This is so because non-radiogenic Pb signatures have been associated with cold or glacial periods, while radiogenic Pb sources with warm or interglacial periods (Abouchaimi and Zabel, 2003).

As result, combining the Sr, Nd and Pb isotopes, the first intervals with low radiogenic Sr signatures are recorded during the LGM at 18.7 kyr cal. BP., and just about the last Heinrich event (H1), at 16.7 kyr cal. BP. Both periods could suggest enhanced humid conditions during the Greenland Stadial 2 (GS-2, from 20.0 to 14.7 kyr cal. BP) at a time where generally arid conditions and semi-desert vegetation cover prevailed over the continental areas surrounding the western Mediterranean basin (e.g., Fletcher and Sánchez Goñi, 2008; Combourieu Nebout et al., 2009). Contemporaneous Nd and Pb isotopic fluctuations suggest that the Sr isotope signature would reflect variations in the eolian dust provenance rather than major washed-soils over the source area. This observation is further supported by the increase of typical eolian proxies such as the Zr/Al ratio and the presence of palygorskite fibers in coherence with cold and arid conditions during both time periods (e.g., Bout-Roumazeilles et al., 2007; Jullien et al., 2007; Rodrigo-Gámiz et al., 2011).

Sr and Nd isotopic signatures have been documented in ice rafted detritus originated during Heinrich events (Hemming et al., 1998), contributing to radiogenic excursions in the clay-size fraction in marine sediments from the Gulf of Cadiz (Stumpf et al., 2011). However, in the western Mediterranean the $^{87}Sr/^{86}Sr$ ratio and εNd(0) values recorded at this time are comparable with Saharan eolian dust signatures (Jeandel et al., 2007).

Thereafter, the Bölling-Alleröd period (from 14.67 to 12.89 kyr cal. BP) shows rapid shifts in the Sr-Nd-Pb signatures supporting the high-resolution of environmental short-term changes recorded during the last deglaciation in the westernmost Mediterranean record (Rodrigo-Gámiz et al., 2011). Intervals of plausible wetter conditions are dated at 14.3-14.06, 13.5, and 13.1 kyr cal. BP interrupted by short-term cold and arid periods such as the Older Dryas (14.09-14.01 kyr cal. BP) and the Intra-Alleröd Cold Period (IACP, 13.25-13.07 kyr cal. BP). Assuming the onset of the African Humid Period (AHP) in North Africa around 14.5 kyr cal. BP (deMenocal et al., 2000), the progressive increase of tropical vegetation and major humid conditions over a hyper-arid desert could favour the loss of the radiogenic Sr fraction but this would not be the case for Nd and Pb. In addition, at 14.2 and 13.1 kyr cal. BP the εNd(0) values point to a signature of river input sediments (between -10.8 and -9.7) (Henry et al., 1994). This onset has been described as synchronous with the end of

cold, glacial conditions in Europe and the North Atlantic (Bond et al., 1993; Broecker et al., 1993; Dansgaard, 1993).

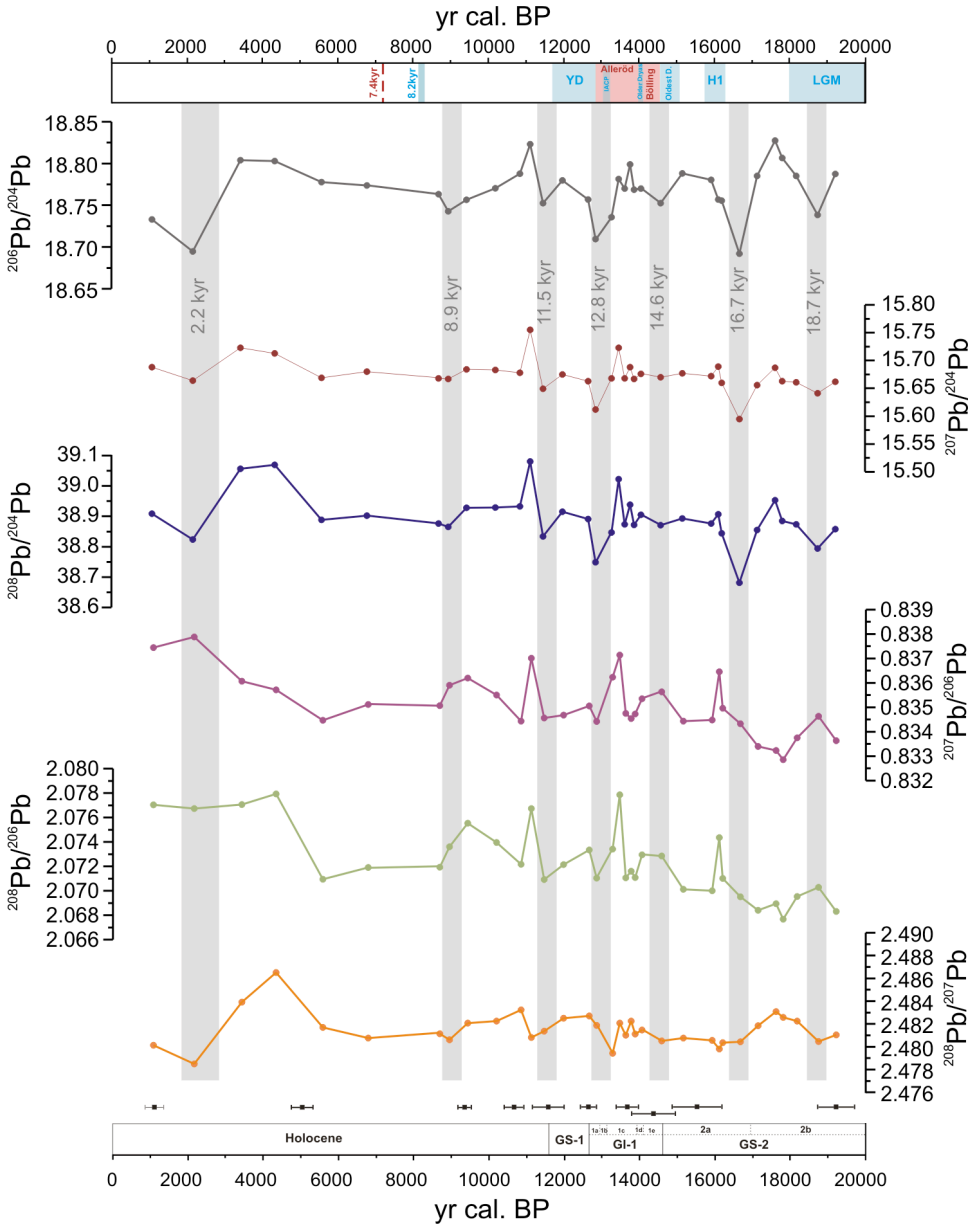

Figure 3. $^{208}Pb/^{204}Pb$, $^{206}Pb/^{204}Pb$ and $^{207}Pb/^{206}Pb$ ratios for core 293G (<37 μm fraction) plotted against age. Gray bars show periods with more unradiogenic Pb ratios. For upper and lower panel code see Fig. 3.

The Younger Dryas (YD) cold period presents major non-radiogenic Pb signatures at the onset (12.89 kyr cal. BP) with more homogenous Sr, Nd, and Pb ratios towards the end (11.65 kyr cal. BP). Previous records in subtropical Africa have been associated with the YD as a sharp increase in regional aridity that interrupted the AHP (e.g., deMenocal et al., 2000; Gasse, 2000). Such paleoenvironmental scenario is coherent with previous geochemical and mineralogical data from this core (Rodrigo-Gámiz et al., 2011) involving a combination of dry and wetter conditions over poorly vegetated continental areas. Palynological records from the western Mediterranean region also evidenced a first period with very dry conditions and an increase in semi-desert taxa, and a second period that was more humid, with a slight forest increase (e.g., Combourieu Nebout et al., 2009).

During the Holocene, major Sr-Nd-Pb oscillations in the westernmost Mediterranean marine record around 10.2-8.9, 6.8-4.3, and 2.2-1.1 kyr cal. BP can be correlated with other well-dated continental and marine archives from the surrounding areas. They all reveal periods of wetness and phases of dry spells with eolian sediments mobilization.

In general, the “lacustrine hydrological optimum” has been recorded by water-level variations in several lake records from northern Africa and the Sahel around 10.5 to 8.5-8 and 7.5-4.5 kyr cal. BP (Gasse and Van Campo, 1994; Gasse, 2002). However, after a rapid sub-humid period at ca. 6.0-4.0 kyr cal. BP over the northwest Africa, an abrupt change from the “green Sahara” to the present hyperarid desert and the end of the AHP has been generalized as shown by diatoms, terrigenous records and Sr isotope ratios (e.g., Gasse and Van Campo, 1994; Gasse, 2002; Kuhlmann et al., 2004; Cole et al., 2009). Moreover, paleoenvironmental reconstruction from northern Chad shows a strong reduction in tropical trees and Sahelian grassland cover allowing large-scale dust mobilization from 4.3 kyr cal. BP (Kröpelin et al., 2008). During the Late Holocene, around 2.7 kyr cal. BP, desert ecosystem and regional wind regime were established, and periods of extremely severe droughts, were recorded especially at 2-1.2 kyr cal. BP (Gasse, 2002; Kröpelin et al., 2008).

Regarding the Iberian Mediterranean area, several pollen sequences have shown a great environmental variability during the Holocene (Carrión et al., 2010 and references therein). However, the major period of transition from mesophytic optimum (warm and humid conditions) with a relatively high lake levels to xerophytic conditions and high fire activity, has been punctuated from 7.5 to 5.0 kyr cal. BP (Carrión et al., 2001a, 2002b).

Additionally, lake sediments from the southern Iberian and Alboran box cores have recorded progressive drier environmental conditions during the transition between the Roman Humid Period

and the Medieval Warm Period (1.6-0.65 kyr cal. BP) with a decrease in fluvial input (Martín-Puertas et al., 2010; Nieto-Moreno et al., 2011).

In the eastern Africa region, however, these climatic changes seem to be more gradually (Jung et al., 2004). Sr isotope ratios from Arabian Sea off Somalia reflect a first aridification step occurred at 8.5 kyr cal. BP followed by a second aridification step at 6.0 kyr cal. BP which ceased at 3.8 kyr cal. BP when modern-day dry climate over North Africa was established (Jung et al., 2004).

Therefore, despite that the chronological control between different paleoclimate archives is not always simple, the Sr, Nd and Pb isotope oscillations punctuated at 8.9-8.6, 5.5, and 2.2 kyr cal. BP reveal a progressive drying of the regional continental areas surrounding the westernmost Mediterranean, and probably a decrease of the rain-belt African monsoon.

5.2. Variability of eolian dust provenance

The Sr, Nd and Pb isotopic composition measured on the <37mm carbonate-free fraction demonstrates eolian dust provenance oscillations for the last 20 kyr. The fact that much of the radiogenic signatures variations in the marine record change in parallel must be related to variations in the sediment provenance rather than to chemical weathering effects which would merely cause a change in Sr isotopic composition without significant changes in eNd(0) values. Differences in Nd isotopic ratios in the western Mediterranean marine sediment core 293G are primarily caused by input from source regions with different Sm-Nd systematics. The combination of Sr, Nd, and Pb isotopic composition, therefore, provide more information about the sedimentary history allowing for a distinction of provenance and atmospheric transport processes as has been described in other marine areas (e.g., Revel et al., 1996a; Tütken et al., 2002). This should be verified by sediment samples where all size fractions definitely come from the same crustal source to avoid different provenance of the grain-size fractions.

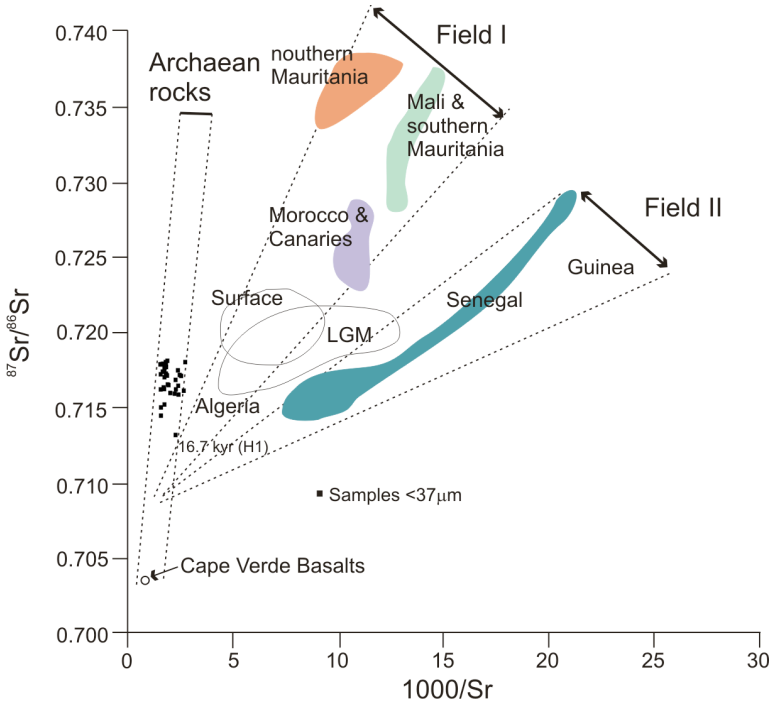

Figure 4. $^{87}Sr/^{86}Sr$ ratio with error bars vs. 1000/Sr. Error bars are smaller than symbol size (Table 1). Modified from Grousset et al., (1998).

The Sr–Nd isotopic composition of the eolian dust flux originating from the Saharan region can be explained according to the most recent literature by a mixture of three main end-members: an almost constant contribution of a volcanic end-member that can be considered as a background, and two crustal end-members: the Archean (2.3-to-3 Ga) and the post-Archean "Birimian" (2.3-to-1.7 Ga) geological formations (Grousset and Biscaye, 2005). The "North Africa" domain roughly encompasses the three-mixture aerosol domain. Three sub-provinces can be also distinguished according to the geology of the source areas: Northern sources (Morocco, Algeria, Mauritania and Mali); Eastern/southern sources (Lybia, Chad, Guinea, Senegal) and the Archean Saharan shield, with its main outcrops located in Mauritania (Grousset and Biscaye, 2005).

The $^{87}Sr/^{86}Sr$ ratio against the 1000/Sr ratio plot in Fig. 4 shows that all the samples measured clustered in the same source area. Lower 1000/Sr values and Sr signatures from 0.713 to 0.718 correspond to the Archaean rocks (Grousset and Biscaye, 2005). Additional discrimination can be seen combining $^{87}Sr/^{86}Sr$ with εNd(0) values in Fig. 5 showing sub-clusters in Field I and II. Field I comprises northern Africa regions, such as Morocco, Mauritania, and Mali, as well as western regions such as Niger and Guinea. Conversely, Field II is represented by isotopic signatures from the present Senegal region (Grousset et al., 1998). Specifically, those samples matched in the Field II are dated at 16.7 kyr and 8.9 kyr cal. BP supporting that these $^{87}Sr/^{86}Sr$ ratio shifts recorded along the last 20 kyr cal. BP (Fig. 2) can be interpreted as a change in the source area rather than a change in

the degree of chemical weathering of the same source region. Furthermore, taking into account the εNd(0) documented by Henry et al., (1994) some Holocene samples which are matched in the Field I (10.2, 9.4, 6.8, 4.3 and 1.1 kyr cal. BP) could be related with typical values of river input provenance.

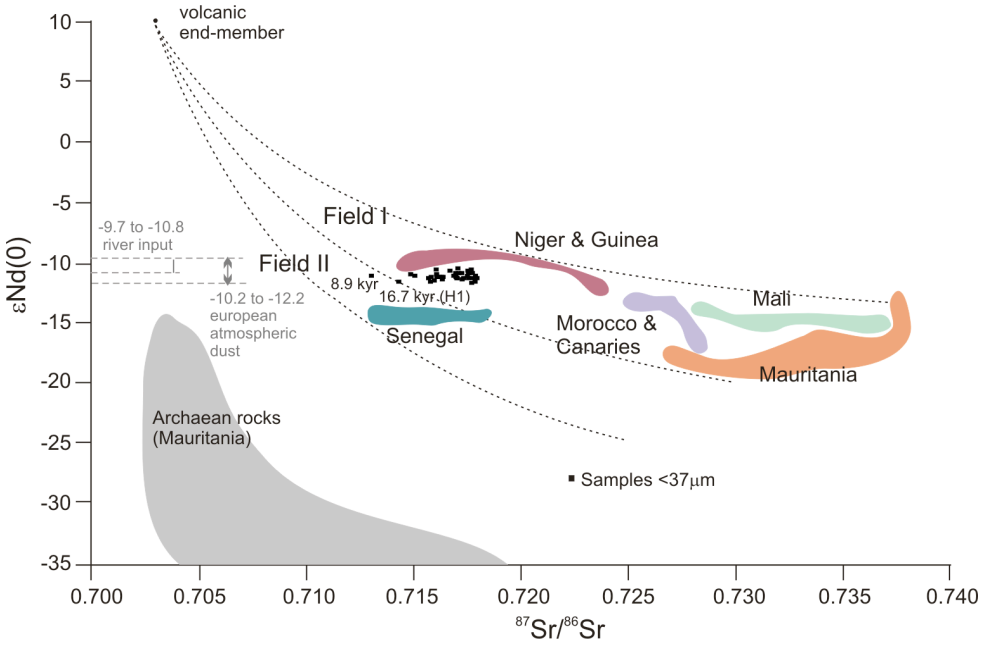

Figure 5. εNd(0) distribution vs. $^{87}Sr/^{86}Sr$ ratio. Error bars are smaller than symbol size (Table 1). Modified from Grousset et al., (1998). Typical εNd(0) values from fluvial sediments in the western Mediterranean (-10.8 and -9.7), and from European atmospheric input (-12.2 and -10.2) are also indicated (Henry et al., 1994).

Pb isotope ratios are plotted in Figure 6 (a, b, c). Pb isotope ratios reflect in general the Pb signature described in Saharan Al-silicates (Erel and Torren, 2010). However, $^{207}Pb/^{204}Pb$ vs. $^{206}Pb/^{204}Pb$ (Fig. 6a) and $^{208}Pb/^{204}Pb$ vs. $^{206}Pb/^{204}Pb$ (Fig. 6b) show that the less radiogenic Pb signatures correspond to a typical composition of granites from North Africa, $^{206}Pb/^{204}Pb$ = 18.74, $^{207}Pb/^{204}Pb$ = 15.66, and $^{208}Pb/^{204}Pb$ = 38.80 (Juteau et al., 1986; Abouchaimi and Zabel, 2003), whereas the signatures outside this group could be associated with an European source related with granites from the Italian Alps (Juteau et al., 1986).

Although the geochemical behaviour of Nd and Pb in the sedimentary cycle is different, both isotopes are correlated in suspended loads of rivers draining post-Archean areas, reflecting the isotopic composition of the average crustal source rocks (Asmeron and Jacobsen, 1993). According to potential European Pb sources described by Fagel et al., (2004), the Pb signature could

correspond to Upper and post-Paleozoic materials related to the Variscan orogeny from the western Europe.

Data in the $^{208}Pb/^{206}Pb$ vs. $^{207}Pb/^{206}Pb$ plot exhibit a linear correlation (R^2 = 0.8244) with the exception of a few samples. These samples correspond to 4.3 and 3.3 kyr cal. BP, and also coincide with high radiogenic values over the last 20 kyr as we described in the previous section (Fig. 3). More radiogenic Sr and Pb isotopic signatures transported by river runoff from Iberian area with respect to Saharan sources have been described in sediments deposited in the Gulf of Cadiz and Portuguese margin (Stumpf et al., 2011). Therefore, the Pb isotopic signatures in the marine record from the westernmost Mediterranean could be explained in terms of simple binary mixing between North Africa and European sources. Variations along the mixing line reflect changes in the relative mixing proportions of the two-natural Pb end-member sources. The more radiogenic Pb source corresponds to an European source, and the less radiogenic end member to a North Africa provenance. Enhanced inputs from the less radiogenic Pb source occurred during the colder periods such as the last H1 event (16.7 kyr cal. BP), while the radiogenic Pb inputs correspond to warm intervals such as Alleröd period (13.5 kyr cal. BP), and some Holocene periods (11.1, 9.4, 1.1 kyr cal. BP).

Radiogenic Pb variations in Atlantic marine records have also been described in terms of two end-members source during stadial and interstadial periods (Abouchaimi and Zabel, 2003).

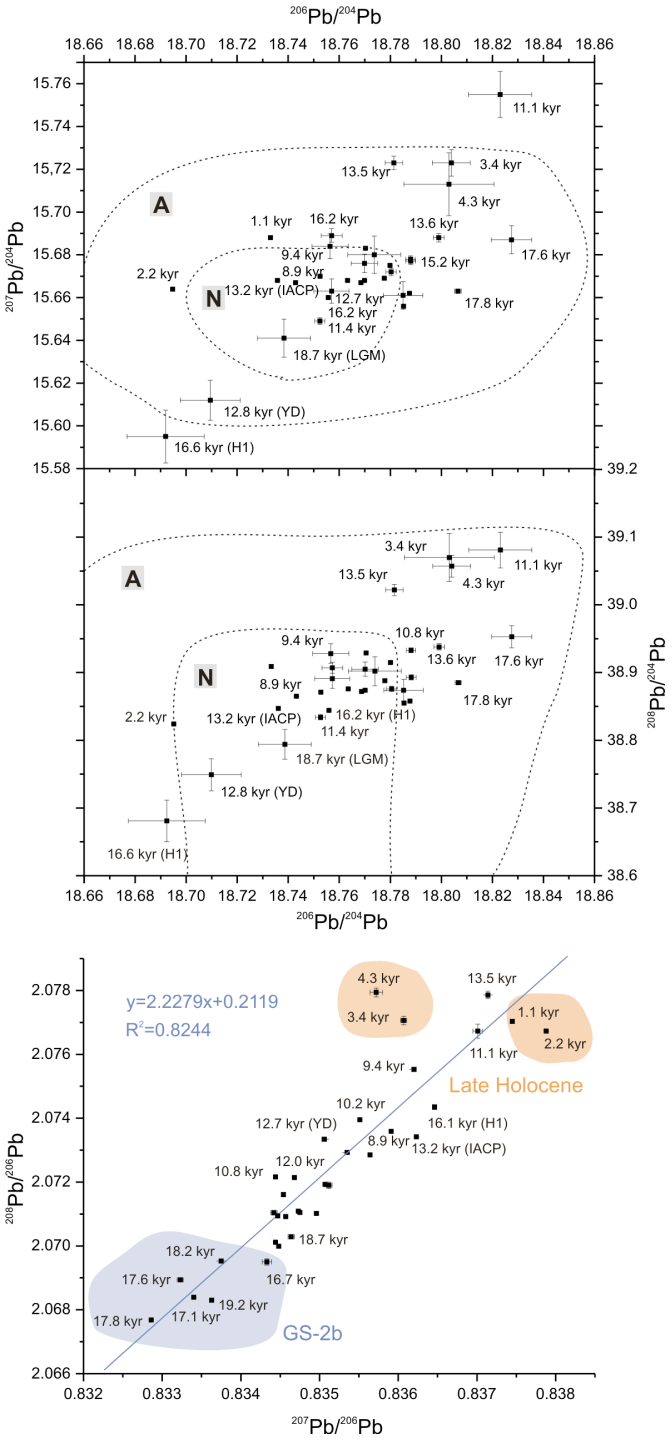
206Pb/204Pb
207Pb/204Pb
208Pb/204Pb
A
N
11.1 kyr
13.5 kyr
3.4 kyr
4.3 kyr
1.1 kyr
16.2 kyr
13.6 kyr
17.6 kyr
9.4 kyr
15.2 kyr
2.2 kyr
8.9 kyr
13.2 kyr (IACP)
12.7 kyr
17.8 kyr
16.2 kyr
11.4 kyr
18.7 kyr (LGM)
12.8 kyr (YD)
16.6 kyr (H1)
10.8 kyr
16.2 kyr (H1)
y=2.2279x+0.2119
R2=0.8244
Late Holocene
GS-2b
12.0 kyr
18.2 kyr
16.7 kyr
19.2 kyr
17.1 kyr
208Pb/206Pb
207Pb/206Pb

Figure 6. (a) $^{207}Pb/^{204}Pb$ vs. $^{206}Pb/^{204}Pb$, (b) $^{208}Pb/^{204}Pb$ vs. $^{206}Pb/^{204}Pb$ and (c) $^{208}Pb/^{206}Pb$ vs. $^{207}Pb/^{206}Pb$ ratios for 293G core (<37 μm fraction). Error bar values are showed in Table 2.
Dashed contour represents Pb isotope composition of granitic K-feldspars from North Africa (N) (Juteau et al., 1986).

Terrigenous material from European sources could be transported by river runoff or atmospheric input. Taking into account the low fluvial discharge of the Alboran Rivers, the main contributor to the radiogenic Pb signature to the westernmost Mediterranean could be: (1) the Rhône River draining detrital sediments from the Alps (Juteau et al., 1986), being further transported from the Gulf of Lion to the Alboran Sea by the western Mediterranean deep waters (Millot, 1999); (2) the southwestern Iberian rivers, i.e., Guadiana and Guadalquivir, which transport particulate matter from the Gualdalquivir basin (Erel and Torrent, 2010) flowing into the western Mediterranean by the surface Atlantic waters (Grousset et al., 1988).

However, according to the εNd(0) values obtained in some of these samples, it is not possible to distinguish between fluvial sediments sources or atmospheric input provenance (Henry et al., 1994). Therefore, the provenance discrimination is primarily based on the Nd and Sr, and not the Pb isotopic composition. As a result, Pb isotopic compositions do not themselves discriminate among potential North Africa sources in western Mediterranean marine sediments as readily as the Nd and Sr isotopic data. A more detailed Pb isotopic sampling in some continental areas from the Africa margin will provide new insight for a more accurate discrimination.

5.3. Atmospheric circulation patterns

The radiogenic isotopes (Sr, Nd, Pb) signals obtained in the marine sediment from the westernmost Mediterranean can be associated with particular atmospheric trajectories, which favoured the eolian dust transport from different source areas during the last 20 kyr.

Several pressure system configurations have been described to produce the transport of Saharan dust air masses to the Iberian Peninsula: (1) low pressures over West and/or Southwest of Portugal; (2) high pressure over East or Southeast of Iberian Peninsula; and (3) the combination of both low and high pressure systems (Avila et al., 1998; Rodríguez et al., 2001). Interannual variations in dust transport in the Atlantic Ocean have been also well correlated with the climatic variability defined by the North Atlantic Oscillation (NAO) (Hurrell, 1995; Moulin et al., 1997).

Furthermore, according to our isotopic signatures, the predominance of certain dust sources is mainly controlled by the migrations of the ITCZ, which also determines the position of the subtropical Azores anticyclone. The anticyclone centre, in turn, determines the southward extent of the incursion of cold polar air masses (Bergametti et al., 1989a). Moreover, the ITCZ migrations are associated with alternating dry and wet periods according to the monsoon activity fluctuations. They are accompanied by changes in wind regime and intensity, variable coverage of land by vegetation, and variations in rainfall amount and river discharge (Clemens and Prell, 1990; Gasse and Van Campo, 1994; Gasse, 2000).

During summer the displacements of the North African anticyclone over Algeria and the distance of the Azores high would favour the incursion of a depression trench between these two anticyclones gyres (e.g., Bergametti et al., 1989a; Moulin et al., 1997; Rodríguez et al., 2001; Torres-Padrón et al., 2002), originating eolian dust transport from Morocco and central part of the Sahara to western and central part of the Mediterranean (Moulin et al., 1997). Moreover, a more northerly ITCZ position during summer, could led to a more northerly position of the monsoon system decreasing the aridity over North Africa and/or the wind intensity. A combination of wind intensity oscillations, displacement and distance of the anticyclone centres, and availability of the eolian material, could be the cause of the different atmospheric trajectories recorded during warmer periods passing over the presents Western Sahara, Morocco, Mauritania, Mali, Niger, Algeria (Fig. 7).

In contrast, the southernmost position of the ITCZ in winter led to enhance of eolian dust from latitudes 10º-20ºN to the westernmost Mediterranean. This configuration causes a more southerly position of the anticyclone centre and the monsoon system increasing the aridity over North Africa and/or major wind intensity (e.g., Matthewson et al., 1995). This could be the case of the eolian dust from the actual Senegal recorded during colder periods such as the H1 (16.7 kyr cal. BP), and at 8.9 kyr cal. BP (Fig. 7).

Therefore, the atmospheric back-trajectories associated with such Sr-Nd isotopic signatures of the eolian fraction deposited in the western Mediterranean since the LGM indicate a clear predominance of two distinguished source areas during colder or warmer periods modulated by the ITCZ migrations and the position of the anticyclones centres. In general, most of the samples analyzed are clustered in a northwestern Africa provenance, located in Morocco, Mauritania and Mali (Fig. 7). The atmospheric trajectories related imply that the ITCZ was in a northern position, around 20º-30ºN, likely to the actual summer shift. In addition, nowadays atmospheric situation and major eolian dust transported to the ocean present a similar transport pattern (e.g., Kalu, 1979). However, a south-easterly African area (Niger, Algeria), could act as a source area during

migrations in the winter period. In a second group of eolian material provenance are the samples matched with more unradiogenic old Archaean rocks in the present Guinea and Senegal fields (Fig. 7), induced by a southward migration of the ITCZ during colder periods.

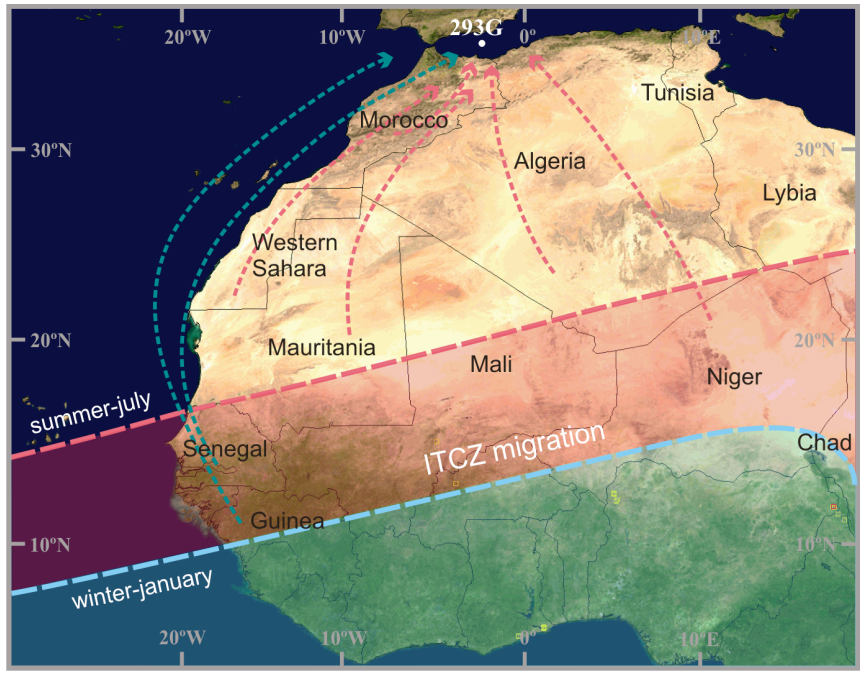

Figure 7. Potential source areas from North Africa during the Last Glacial Maximum according to the radiogenic isotopic composition of the marine core 293G recovered in the westernmost Mediterranean Sea. Dashed blue lines represent the main atmospheric trajectories from Senegal and Guinea for different dust events at 16.7 kyr (H1), and 8.9 kyr cal. BP. Dashed red lines show diverse atmospheric trajectories from Morocco, Mauritania, Mali, South of Algeria and Niger, recorded as most frequent source areas during the last 20 kyr cal. BP. Red and blue areas indicate the seasonal northward in summer (july) and southward in winter (january) position of the Inter-Tropical Convergence Zone (ITCZ) respectively.

5. Conclusions

Radiogenic isotope (Sr, Nd, Pb) signatures from a western Mediterranean high-resolution marine record have allowed recognizing weathering history, eolian input provenance and atmospheric transport patterns since the Last Glacial Maximum. Nd, Sr and Pb isotope compositions from carbonate-free sample sediments on the <37μm size fraction have been integrated with previous geochemical and mineralogical data. Diverse periods with lower $^{87}Sr/^{86}Sr$ signatures reflect the

chemical weathering influence on the isotopic composition. Some of these oscillations are also evidenced in εNd(0) with more negative values, suggesting oscillations in source area provenance of terrigenous material. These events dated just about the last Heinrich event and at 8.9 kyr correspond to arid and cold conditions associated with eolian input provenance from the present Senegal and Guinea regions. Warmer periods, in contrast, are characterized by radiogenic signatures from northern and northwestern Africa regions (Morocco, Mauritania and Mali). Furthermore, although Pb ratios do not themselves discriminate among potential sources in North Africa, they reflect a possible mixture between two-natural Pb end-member sources, i.e., the European more radiogenic source transported by river runoff or atmospheric input mainly during the Holocene, and the less radiogenic North Africa source.

The different dust provenance recorded in the western Mediterranean marine sediments reveals millennial fluctuations in both weathering conditions and atmospheric circulation patterns. We suggest the northern and southern oscillations of the Inter-Tropical Convergence Zone as main control for the African dust source along with changes in the intensity and regime of the wind system and the position of the subtropical Azores anticyclone.

Acknowledgements

This work was supported by Projects CGL2009-07603, CTM2009-07715, CSD2006-00041 (Ministerio de Ciencia e Innovación), 200800050084447 (MARM), Project RNM-5212, and Research Group RNM-179 (Junta de Andalucía). We are also grateful to the oceanographic cruise Training- Through-Research Programme (UNESCO-Moscow State University). F. J. Jiménez-Espejo acknowledges funding from the CSIC "JAE-Doc" postdoctoral program. We likewise thank Michèle Senn-Gerber and Denis Fontignie for their laboratory assistance.

6. Chapter III.- Forcing mechanisms of climate variability in the western Mediterranean: millennial- to centennial-scale periodicities for the past 20,000 yrs

Rodrigo-Gámiz, M., Martínez-Ruiz, F., Rodríguez-Tovar, F.J., Jiménez-Espejo, F.J., Pardo-Igúzquiza, E.

Submitted to Global and Planetary Change

Abstract

Cyclostratigraphic analysis conducted on a continuous high-resolution marine record from the westernmost Mediterranean reveals well-identified paleoclimate cycles since the Last Glacial Maximum. Here, we present innovative high-frequency climate periodicities for the last 20,000 yrs using a range of proxies, including major and trace element/Al ratios and stable oxygen isotopes. The detrital proxies used (Si/Al, Ti/Al, Zr/Al, Mg/Al, K/Al, Rb/Al) are related to different sediment transport mechanisms, including eolian dust pulses and fluvial runoff, that involve fluctuations in the atmosphere-hydrosphere systems. These fluctuations are accompanied by changes in marine productivity (Ba/Al) and bottom-water redox conditions (Cu/Al, V/Al, Zn/Al, Fe/Al, Mn/Al, U/Th). Spectral analysis conducted using the Lomb-Scargle periodogram and the achieved significance level implemented with the permutation test allowed us to establish climate oscillations where different proxies are statistically significant. Major periodicities were obtained at 1,300, 1,515, 2,000, and 5,000 yrs, and their secondary peaks at 650, 1,087, and 3,000 yrs. Some of these cycles agree with those previously described in the North Atlantic Ocean, coupled with ocean-atmosphere fluctuations. The periodicities obtained at 2,000 and 5,000 yrs support a global connection with records distributed at high-, mid-, and low-latitudes associated with solar activity and orbital forcing. The 1,300 and 1,515 yr cycles appear to be linked with the North Atlantic climate and the African monsoon system. Thus, the analyzed record provides evidence of climate changes and their teleconnections in oceanic-atmospheric circulation. Comparison with other circum-Mediterranean records points to the North Atlantic Oscillations, Inter-Tropical Convergence Zone migrations and monsoon activity, probably exacerbated by solar activity variations, as main forcing mechanisms.

1. Introduction

A range of different paleorecords (i.e., ice cores, terrestrial and marine sediments) globally distributed (i.e., Greenland, North Atlantic and Pacific Oceans) have shown climate oscillations on diverse timescales, resulting from interactions among the different elements of the Earth's environmental system during the last glacial cycle (e.g., Broecker, 1994; Bond and Lotti, 1995; Stuiver et al., 1995; Sirocko et al., 1996; Chondrogianni et al., 2004). Most periodic variations in the Earth's climate system on long timescales have been directly related to Milankovitch forcings (mainly 20 to 400 kyr) and caused by variations in the orbital cycles (i.e., due to changes in the seasonal and latitudinal pattern of insolation). Nevertheless, most cyclic patterns recognized at sub-Milankovitch timescales (<20 kyr) during the Late Pleistocene and Holocene in the North Atlantic regions correspond to Dansgaard-Oeschger (D-O) oscillations and Bond cycles. Extreme events of

ice-rafted detritus (IRD) deposition (Heinrich events, H) took place at the culminations of progressive coolings (Stadials) followed by rapid warmings (Interstadials) in the context of D-O oscillations during the last glacial interval, showing a periodicity of about 7,000 to 10,000 yrs (Heinrich, 1988; Bond et al., 1993; Dansgaard et al., 1993; Grousset et al., 1993). Furthermore, the climate quasiperiodic slowdown of North Atlantic Deep Water (NADW) production and the cold climate in Europe recorded at the millennial timescale, every 1,470±500 yrs, have been described as Bond cycles (Bond et al., 1993, 2001; Broecker, 1994).

At higher frequency timescales, interannual to decadal or even centennial climate oscillations appear to be associated with the El Niño-Southern Oscillation (ENSO), changes in the intensity of the Inter-Tropical Convergence Zone (ITCZ) —and consequently in the monsoon variability— and oceanic-atmospheric processes related to the North Atlantic Oscillation (NAO) (e.g., Sirocko, 1996; Marshall et al., 2001; Wanner et al., 2001; Marchitto et al., 2010).

However, the forcing mechanisms of these climatic variations at higher time-scales are still poorly understood. Possible causes may entail non-linear responses to orbital cycles (i.e., variations in solar output/activity) (Van Geel et al., 1999; Bond et al., 2001; Kodera and Kuroda, 2005) amplified by a wide range of internal factors of the climate system, such as changes in ice extent or in the sea surface freshwater balance, which would produce reorganizations of the thermohaline circulation (e.g., Denton and Karlén, 1973; Bond et al., 1997; Broecker, 2000; deMenocal et al., 2000; Gasse, 2000; Stocker, 2000; Mayewski et al., 2004). The only possibly linear response to orbital forcing would be the double insolation maximum described in tropical regions over the course of a year, producing 11,000 yr and 5,500 yr periods of equatorial insolation (Berger et al., 2006). Therefore, pronounced variations are found in the monsoonal runoff in response to precessional forcing; that is, during precession maxima (low summer insolation) precipitation is low and deserts expand, and vice versa (Tuenter et al., 2003, 2007).

In the case of the Iberian Peninsula, previous paleoclimatic studies in both the western Mediterranean and western Iberian margin have shown significant climate variations related with D-O oscillations and H events (e.g., Cacho et al., 1999, 2000, 2001; von Grafenstein et al., 1999; Moreno et al., 2004, 2005; Sierro et al., 2005; Naughton et al., 2009), demonstrating a strong link between the Mediterranean and North Atlantic climates, and with the monsoon regimen (e.g., Sánchez Goñi et al., 2008). Furthermore, other paleoenvironmental changes such as vegetation cover, aridity conditions, productivity oscillations and the cooling of sea surface temperature (SST) show a clear D-O variability with statistically significant cycles at 730, 1,470, 3,300, 5,000, and

8,000 yrs, and harmonics for the time interval spanning 48,000 to 28,000 yr cal. BP (Cacho et al., 1999; Moreno et al., 2005).

Nevertheless, climatic periodicity studies at the millennial- to centennial-scale require a high-resolution proxy record as well as high continuity of the paleoclimatic archive to identify potential signals. This paper presents a detailed cyclostratigraphic analysis using a range of statistically significant paleoenvironmental proxies (detrital input, redox conditions, paleoproductivity, and paleotemperature-paleosalinity) on a marine record from the Alboran Sea, to determine high-frequency climate oscillations over the last 20,000 yrs. Previous data from this core (Rodrigo-Gámiz et al., 2011) have revealed the excellence and interest of this record for the cyclostratigraphic approach. Some of the conspicuous cycles recognized in the climate spectrum analyzed reveal periodicities similar to those of previously registered North Atlantic cycles. In addition, new cycles registered in the spectral analysis offer novel insights into the timing and effect of global factors such as monsoon variability, NAO and solar activity in the westernmost Mediterranean region.

2. Material and methods

2.1. Alboran Sea geochemical record: paleoenvironmental proxies

For this study we used high-resolution geochemical data from core 293G, recovered in the East Alboran Sea basin (Fig. 1) (Lat. 36´10.414N, Long. 2´45.280W, Depth 1,840 m) during the oceanographic cruise Training Through Research-12 (Comas and Ivanov, 2003). This allowed for a detailed paleoclimate reconstruction over the last 20,000 yr (Rodrigo-Gámiz et al., 2011), revealing the exceptional worth of this continuous high-resolution record for cyclostratigraphic analyses.

The Alboran Sea, located in the westernmost Mediterranean Sea, is the natural connection to the Atlantic Ocean through the Strait of Gibraltar. Thus, the oceanographic conditions in this transitional area are characterized by three main water masses: a) a thick water layer of about 200–300m of Modified Atlantic Water (MAW) that forms two almost permanent anticyclonic gyres (e.g., Millot, 1999), b) an intermediate water layer named the Levantine Intermediate Waters (LIW), formed in the eastern Mediterranean, and c) a deeper water layer known as the Western Mediterranean Deep Water (WMDW), originating in the Gulf of Lion as a result of the northwesterlies. The two water masses form the Mediterranean outflowing water (Millot, 2009).

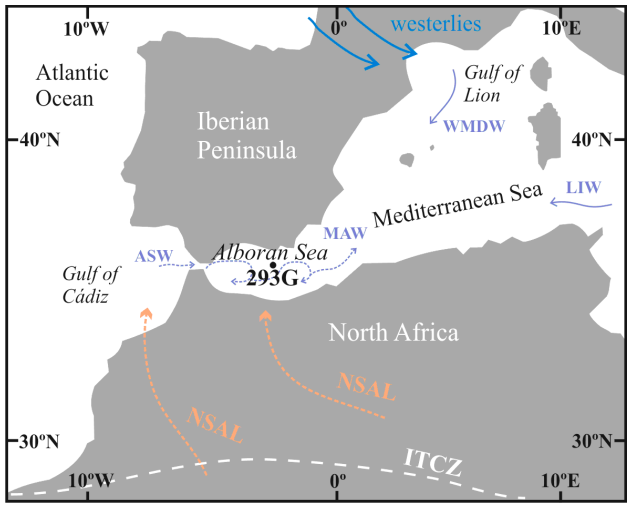

Figure 1. Iberian Peninsula map with setting of gravity core 293G in the Alboran Sea. Blue dashed arrows represent theoretical surface circulation in the Alboran Sea, influxes of Atlantic Surface Water (ASW) and Modified Atlantic Water (MAW) in the basin. Blue arrows represent westerly winds and Western Mediterranean Deep Water (WMDW) formation in the Gulf of Lion. Orange dashed arrows indicate the main wind system over North Africa, the northern branch of Saharan Air Layers (NSAL). White dashed line show northern position of the Inter-Tropical Convergence Zone (ITCZ).

At present, Mediterranean climate conditions are mainly driven by the position of the Azores high-pressure system. Summertime climates are usually dry and hot due to the influence of the atmospheric subtropical high-pressure belt (Sumner et al., 2001). In winter the subtropical high shifts to the south, allowing mid-latitude storms to enter the region from the open Atlantic and bringing enhanced amounts of rainfall to the western Mediterranean. The North Atlantic Oscillation (NAO) oscillates at an interannual to decadal scale and represents fluctuations in the sea-level atmospheric pressure between the Icelandic low and the Azores high-pressure centers (Hurrell, 1995). A high (positive) NAO index produces wetter winters over northern Europe and drier winters over southern Europe, the Mediterranean and northern Africa (Trigo et al., 2002; Wanner et al., 2001). A low (negative) index of the NAO causes the opposite pattern, driving more rainfall to southern latitudes. Regional climatology is moreover seasonally modulated by the migration of the Inter-Tropical Convergence Zone (ITCZ), and hence the monsoon front, over North Africa. The ITCZ directly controls both the intensity and direction of the main winds such as the Northern Saharan Air Layer (NSAL) and the location of precipitation over North Africa (Kalu, 1979). Changes in its position affect the amount of rainfall and therefore the degree of eolian input or river runoff as well (e.g., Prospero, 1981).

2.2. Paleoenvironmental proxies

The multiproxy approach permittted us to select a range of proxies that configure the four main groups used in this study:

1) Detrital group: consisting of major and trace elements/Al ratios (Si/Al, Mg/Al, K/Al, Rb/Al, Ti/Al, Zr/Al). Eolian dust from the Sahara, which contributes significantly to Mediterranean sedimentation, is relatively high in Zirconium (Zr), Silicium (Si) and Titanium (Ti) (Pye, 1987; Grousset et al., 1989; Brumsack and Wehausen, 1999). These elements reside in heavy minerals (zircon, quartz and Ti oxides, respectively) that are chemically resistant in the weathering profile, surviving multiple cycles of erosion and deposition. These ratios are transported with the silt and fine sand fractions of marine sediments, and thus can be successfully used as eolian proxies (Calvert and Pedersen, 2007, and references therein). Clay minerals (illite, chlorite) and feldspars are mainly responsible for the higher K/Al, Mg/Al and Rb/Al ratios, and they are predominantly found in sediments derived from rivers (Chester et al., 1977; Böttcher et al., 2003). In particular, changes in the K/Al ratio are interpreted as an increase in the relative proportions of illite formed at intermediate precipitation rates, in the general sequence of clay mineral formation, and transported via rivers (Meunier and Velde, 2004). Chlorite (contributing to the Mg/Al ratio) is found mainly in sediments derived from the northern Mediterranean rivers (Foucault and Mélières, 2000). More feldspar survives in poorly weathered soils reflecting higher Rb/Al ratios (Pastouret et al., 1978).

2) Redox group: variations in certain redox-sensitive trace metal ratios used (Zn/Al, Cu/Al, V/Al, Mn/Al, Fe/Al, U/Th) indicate fluctuations in deep-water oxygen content at the time of sediment deposition (Böttcher et al., 2003; Brumsack, 2006; Tribovillard et al., 2006; Calvert and Pedersen, 2007). In general, Vanadium (V) is reduced to insoluble species of lower valence under anoxic conditions, and together with Zinc (Zn) and Copper (Cu) enrichments, it indicates anoxic bottom waters (Calvert and Pedersen, 2007, and references therein). Uranium (U) may also form a complex with dissolved fulvic acid in hemipelagic sediments (Nagao and Nakashima, 1992) that would concentrate under anoxic conditions. Manganese (Mn) is used to identify reventilation fronts (e.g., Mangini et al., 2001; Powell et al., 2003). Iron (Fe) could be considered a detrital element, but it can also precipitate with authigenic phases, as an oxide or as sulfide, in the form of pyrite (e.g., Calvert and Pedersen, 2007; Powell et al., 2003). Enrichments in both Mn and Fe could be promoted by the diffusion of Mn^{2+} and Fe^{2+} in pore waters from anoxic to oxic layers in which such cations are immobilized. On reaching an oxidative front, these elements can precipitate into other solid phases. Such Fe/Al and Mn/Al enrichments are usually distanced as a result of differences in

thermodynamics and kinetic processes (e.g., Thomson et al., 1995; Martinez-Ruiz et al., 2000; Rutten and de Lange, 2003).

3) Paleoproductivity group: the Ba/Al ratio is used as a productivity proxy since Barium (Ba) excess derives from marine barite in the Ba-rich intervals; it can thus be considered as a reliable indication of export production fluxes. This proxy has been successfully used in the Mediterranean for paleoproductivity reconstructions (e.g., Dehairs et al., 1987; Martínez-Ruiz et al., 2000, 2003; Wehausen and Brumsack, 2000; Paytan et al., 2004; Gallego-Torres et al., 2007, 2010, and references therein). In the particular case of the westernmost Mediterranean, enhanced productivity during cold periods such as the Younger Dryas (YD) and the last Heinrich event (H1) has been recorded by Ba enrichments (e.g., Moreno et al., 2004; Jiménez-Espejo et al., 2008; Rodrigo-Gámiz et al., 2011).

4) Paleotemperature-paleosalinity group: major $\delta^{18}O$ changes in planktonic foraminifera reveal paleoceanographic oscillations, including global ice volume, surface-water salinities and temperature conditions (e.g., von Grafenstein et al., 1999). Indeed, ice-sheets are the main suppliers of the lighter (16O) isotope into the ocean during interglacial stages, and their response to rapid climate change is almost instantaneous on the millennial scale (Rogerson et al., 2006 and references therein).

2.3. Power spectral analysis

Even though the sampling space interval along the core is constant (1.5 cm sampling resolution), variations in the sedimentation rate lead to an uneven sampling time interval. Accordingly, cyclostratigraphic analysis of the studied time series was performed for the different proxies by means of the Lomb-Scargle periodogram (Lomb, 1976; Scargle, 1982). With this method, the power spectrum is evaluated for a high number of frequencies, larger than the number of experimental data. This is a very appropriate spectral methodology when working with uneven sampling data, providing a higher resolution than the main alternatives (obtaining an even time series by interpolation, or considering the uneven time series as even with an average sampling interval equal to the mean interdistance between data). Previous research has underlined the usefulness of this methodology in applications to paleoclimatic/paleoceanographic time series with uneven sampling records, even when dealing with short time series (Jiménez-Moreno et al., 2007; Rodríguez-Tovar et al., 2010). In evaluating the significance of the registered spectral peaks, one appropriate method is the implemented achieved significance level using the permutation test (see Pardo-Igúzquiza and Rodríguez-Tovar, 2000, 2005, for a detailed description). Subsequently, the peaks obtained through the achieved significance level can be considered as primary, and not secondarily generated by the

applied methodology. Thus, out of all the peaks registered by means of the Lomb-Scargle procedure, only those also registered in the achieved significance level were interpreted in our study.

As a conservative strategy, in order to interpret only those peaks especially significant or primary —thereby avoiding consideration of secondary cycles that could be a consequence of the spectral methodology— our analysis is focused on the cycles registered in the frequency band that shows higher possibilities of registering primary cycles. Therefore, taking into account that the sediment core spans around 20,000 yrs, the cycles at the lowest frequencies, registered close to the vertical axis in the achieved significance level and calibrated as higher than 7,000 yrs (around 1/3 of the total time interval), were not considered. On the other hand, given the sampling interval, the cycles in the highest frequency band, calibrated as lower than 500 yrs, were likewise not interpreted. That is, we took into consideration only those cycles corresponding to periodicities between 500 and 7,000 yrs.

3. Results

3.1. Spectral treatment: achieved significance level

In general, the four main groups of proxies distinguished show a well-developed cyclic pattern in their power spectrum (Figs. 2-5). Nevertheless, different patterns of general incidence are recorded for each proxy in their power spectra, with different cycles of variable significance summarized in Table 1. Of the different groups, detrital and redox groups exhibit the best-defined cyclic patterns, with numerous peaks of high confidence levels (usually above 99% CL).

The detrital group evidences a cyclic pattern that is particularly well developed in the lower frequency bands, corresponding to cycles calibrated from 1,515 to 5,000 yrs (Table 1); cycles at frequencies above those corresponding to cycles shorter than 1,515 yrs go unrecorded for the most part. The typical fluvial proxies of this group (Mg/Al, K/Al, and Rb/Al) show peaks in different frequency bands (Fig. 2 A-C, Table 1). In particular, the Mg/Al ratio reflects cycles of 2,000 yrs (90.1-95% CL), around 3,000 yrs (>99% CL), and 5,000 yrs (>99% CL; Fig. 2 A). The K/Al ratio shows a cycle at 1,515 yrs (90.1-95% CL), and two close peaks around 3,000 yr (>99% CL) (Fig. 2 B). The Rb/Al ratio shows main cycles at 1,515 yrs, 2,000 yrs, and 5,000 yrs with a relatively high CL (90.1 and mainly >99%) (Fig. 2 C). The main eolian input proxies (Si/Al, Zr/Al, and Ti/Al ratios) point to a less-developed cyclicity, with just a few registered peaks of minor significance and different temporal calibration (Fig. 2 D-F, Table 1). The lowest frequency cycle at 5,000 yrs is only characterized by the

Si/Al ratio (>99% CL; Fig. 2 D). Meanwhile, the Zr/Al ratio presents a cycle at 3,000 yrs (95.1-99% CL; Fig. 2 E), and Ti/Al ratio shows 1,515 yrs and 2,000 yrs cycles, yet with a low CL (70-80%; Fig. 2 F).

Table 1. Major peaks in dark gray and their probable secondary peaks in light gray obtained for each selected proxy from core 293G. Confidence levels (in %) for the particular peak (in year, yr) obtained with spectral analysis are indicated.

Group	Variable	Temporal cycles (yr)						
		5,000	3,000	2,000	1,515	1,300	1,087	650
Detrital	K/Al		>99 (3,125, 2778)		90.1-95 (1,515)			
	Ti/Al			70-80 (2,000)	70-80 (1,515)			
	Zr/Al		95.1-99 (3,125)					
	Si/Al	>99 (5,000)						
	Mg/Al	>99 (5,000)	>99 (2,778)	90.1-95 (2,000)			70-80 (1,087)	
	Rb/Al	>99 (5,000)		90.1-95 (1,923)	>99 (1,515)			
Redox	Fe/Al	95.1-99 (5,000)	>99 (2,941)	>99 (1,923)			>99 (1,087)	
	V/Al				>99 (1,515)	>99 (1,282)		>99 (649-1)
	Zn/Al	90.1-95 (4,545)	>99 (3,125)			95.1-99 (1,282)		
	U/Th		>99 (2,778)		95.1-99 (1,471)			
	Mn/Al	>99 (5,000)	>99 (3,125)	>99 (2,000)				
	Cu/Al	>99 (5,000)	>99 (2,778)			>99 (1,282)	>99 (1,087)	95.1-99 (649-1)
Paleoproductivity	Ba/Al		>99 (3,125)		<70 (1,515)	70-80 (1,316)		
Paleotemperature-	$\delta^{18}O$	>99 (5,556)		70-80% (2,000)		<70 (1,316)		

The redox group reveals the best cycle pattern (Fig. 3 A-F). An outstanding feature recognized for this group is the generalized peak at 3,000 yrs, represented at high CL (>99%) in all of the redox-sensitive elements (Table 1). Thus, this group is characterized by all the main cycles obtained (1,300, 1,515, 2,000, and 5,000 yrs) to quite a significant degree, although no exclusive frequency band was observed (Fig. 3 A-F, Table 1). In particular, Cu/Al and Zn/Al ratios reveal 1,300 and 5,000 yrs cycles with high CL (Fig. 3 A, B). The V/Al ratio shows cycles at higher frequency bands at 1,300 and 1,515 yrs (>99% CL; Fig. 3 C). In turn, the U/Th ratio is recorded only in the main cycle at 1,515

yrs (Fig. 3 D). Both Fe/Al and Mn/Al ratios characterize the 2,000 and 5,000 yrs cycles with high significance (>95.1% CL; Fig. 3 E, F).

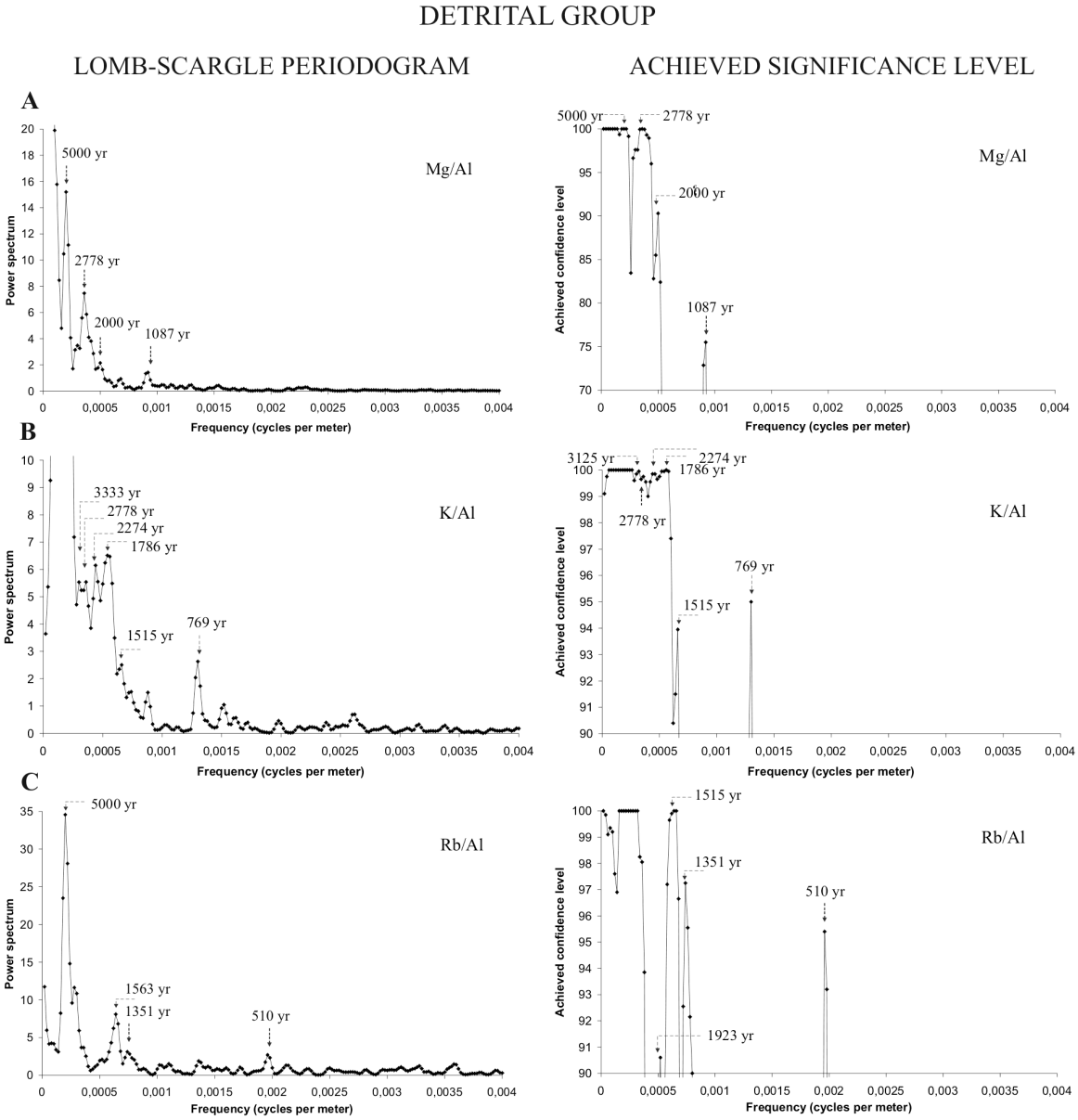

Figure 2. Power spectra for the detrital group proxies (A-F) studied according to multi-proxy analysis of marine core 293G. Spectral peaks registered with Lomb-Scargle Periodogram are shown on the left; significant spectral

peaks obtained with Achieved Significance Level are shown on the right.

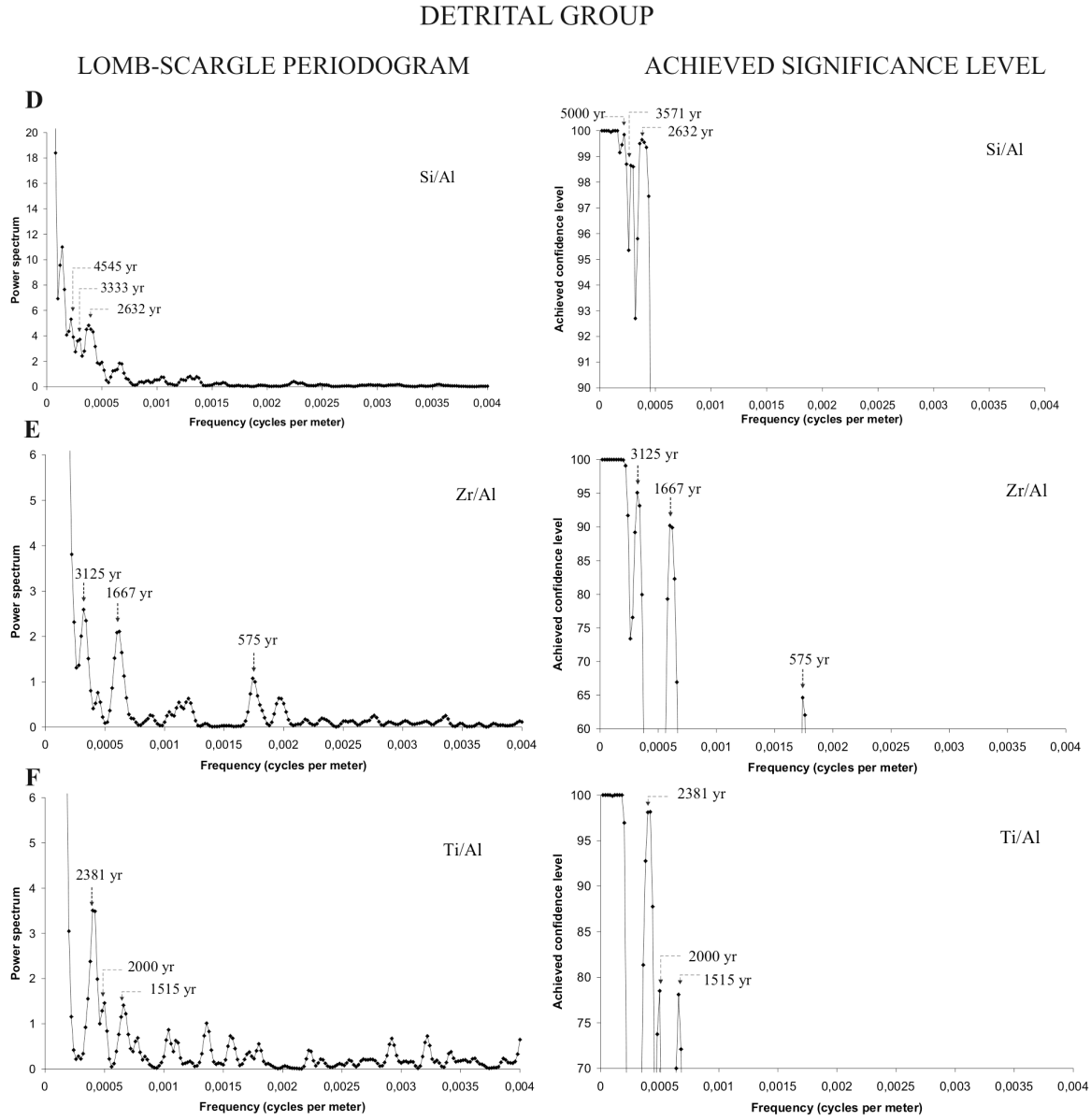

Figure 2 cont.

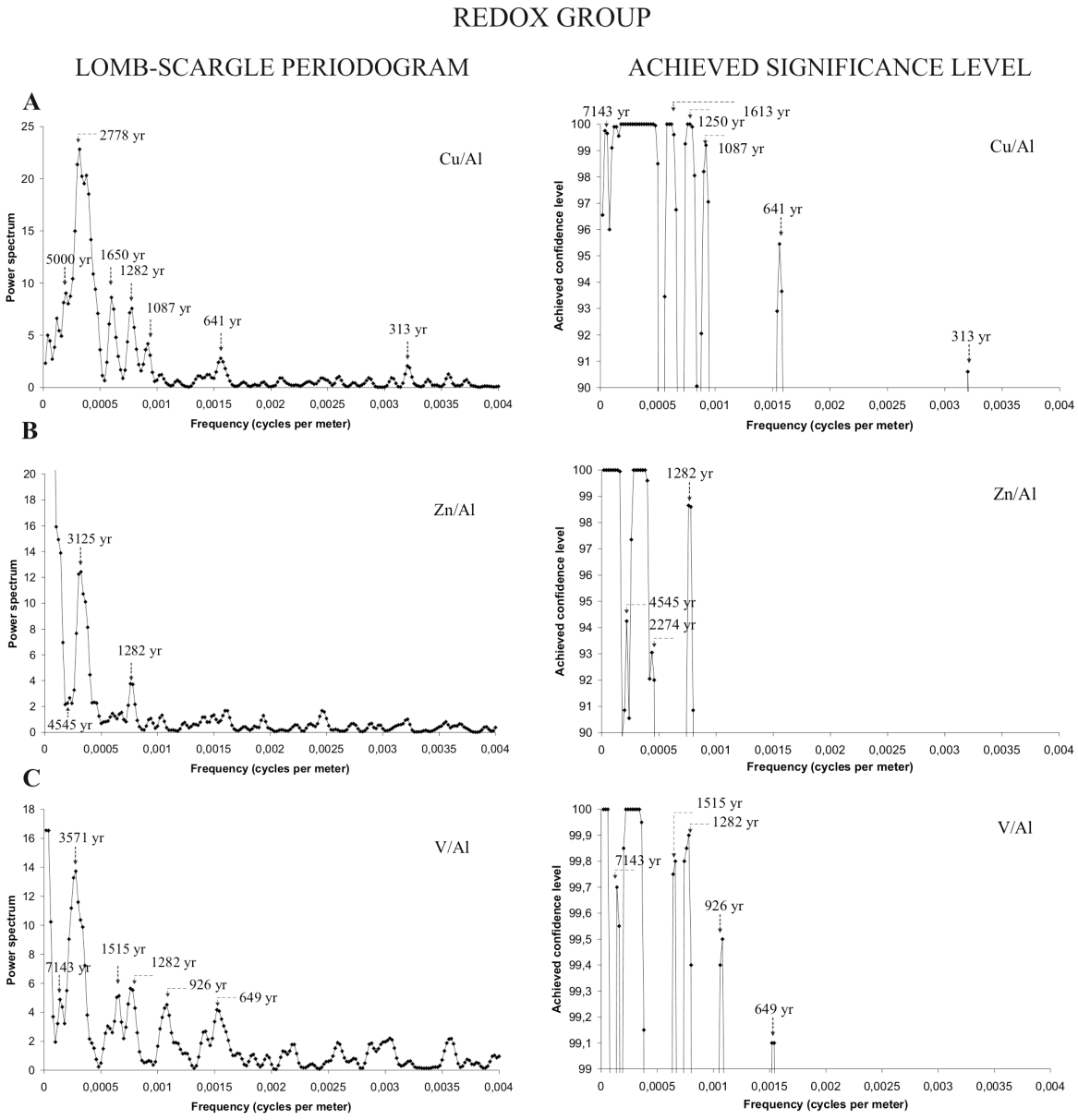

Figure 3. Power spectra for the redox group proxies (A-F) studied according to multi-proxy analysis of marine core 293G. Spectral peaks registered with Lomb-Scargle Periodogram are shown on the left; significant spectral peaks obtained with Achieved Significance Level are shown on the right.

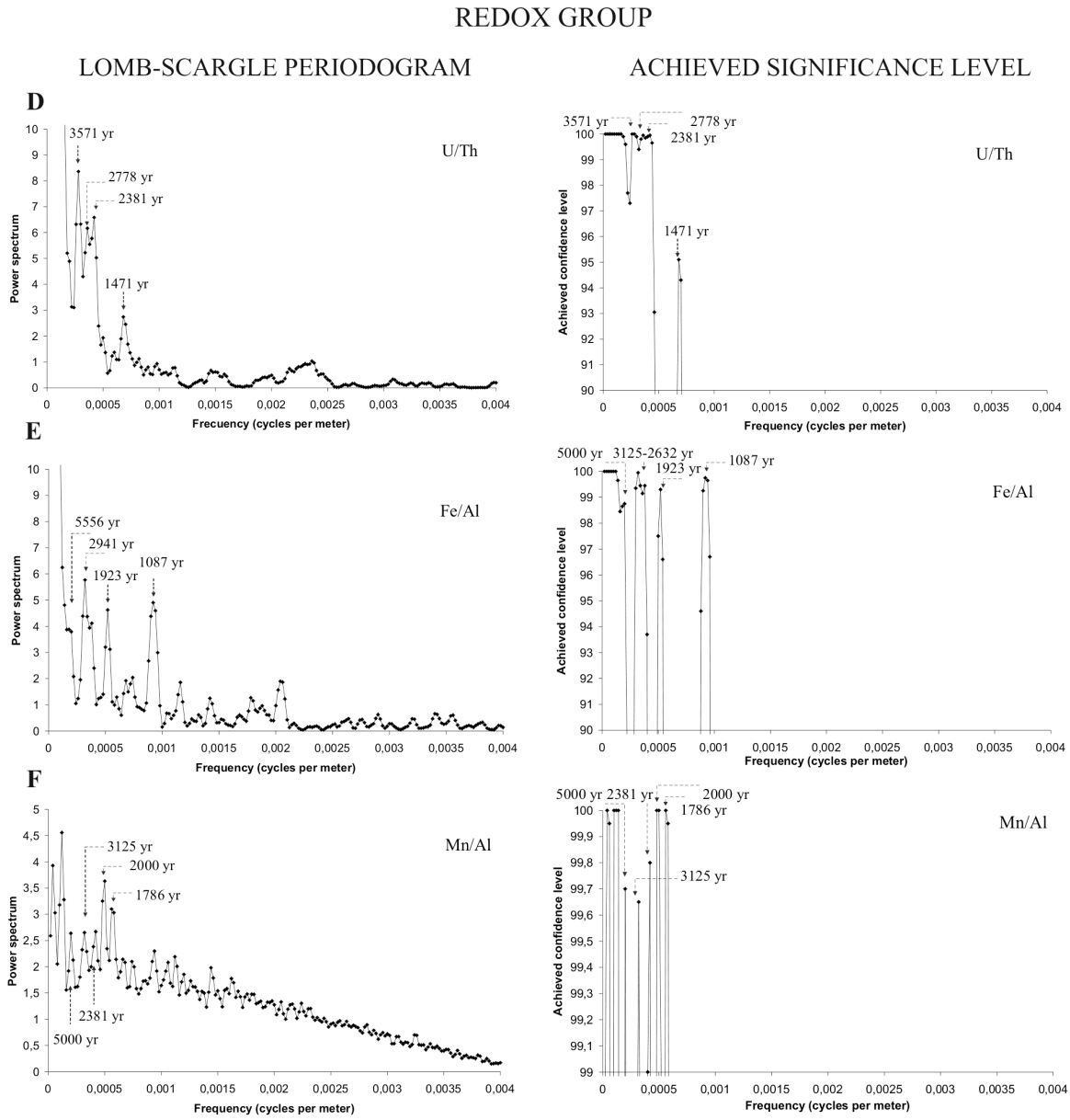

Figure 3 cont.

In terms of paleoproductivity and paleotemperature-paleosalinity, cycles were scarcely observed, with irregular significance. The Ba/Al ratio characterizes the paleoproductivity group that shows cycles at 1,300 and 1,515 yrs, with a significance level over 70% (Fig. 4). Finally, the paleotemperature-paleosalinity group records $\delta^{18}O$ cycles at periodicities of 1,300, 2,000 and 5,000 yrs, their significance oscillating from 70% to >99% CL (Fig. 5).

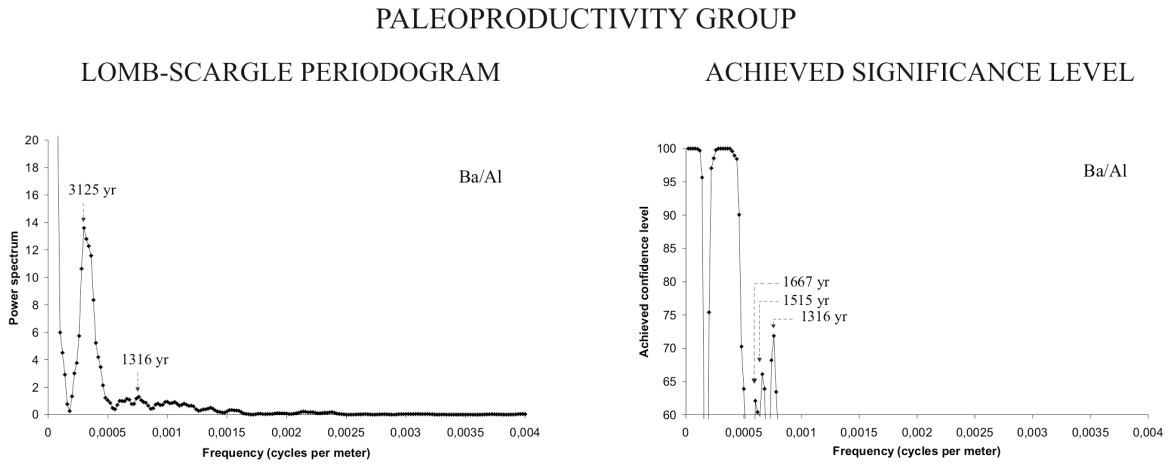

Figure 4. Power spectra for the paleoproductivity group studied according to multi-proxy analysis of marine core 293G. Spectral peaks registered with Lomb-Scargle Periodogram are shown on the left; significant spectral peaks obtained with Achieved Significance Level are shown on the right.

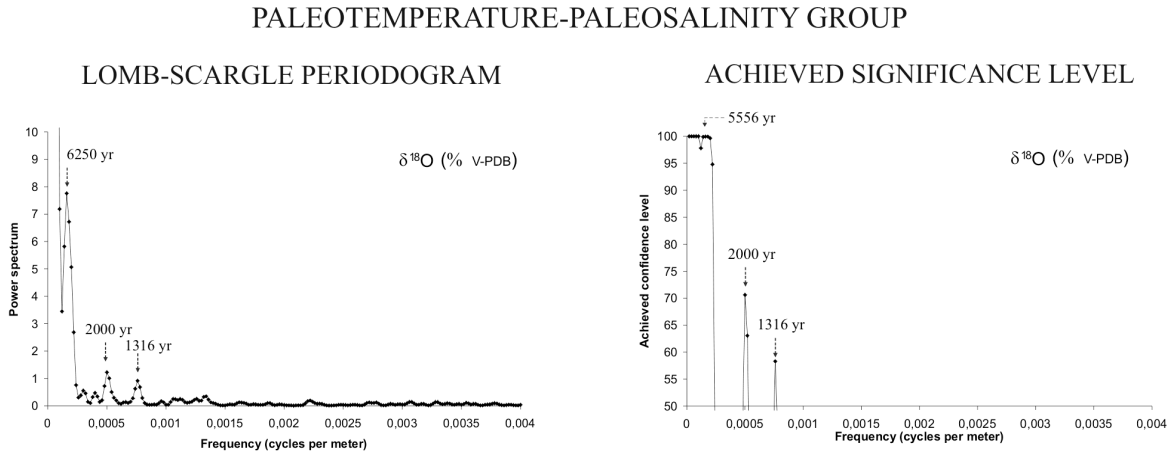

Figure 5. Power spectra for the paleotemperature-paleosalinity group studied according to multi-proxy analysis of marine core 293G. Spectral peaks registered with Lomb-Scargle Periodogram are shown on the left; significant spectral peaks obtained with Achieved Significance Level are shown on the right.

4. Discussion

4.1. Relevance of the climatic cycles obtained from the cyclostratigraphic approach

Before interpreting the cycles registered at periodicities of 5,000, 3,000, 2,000, 1,515, 1,300, 1,087, and 650 yrs (Table 1, Figs. 2-5), it is necessary to differentiate between primary cycles and secondary harmonics, or the artifacts of primary cycles. The cycles detected at 5,000 yrs, 2,000 yrs and 1,515 yrs show a constant periodicity as well as a generalized record in most of the four differentiated groups (Table 1), together with a high significance level (always >90.1%, and usually >99% CL). We may therefore interpret them as primary in origin. Other peaks having a variable temporal calibration, less frequent record, or lower CL, such as those around 3,000 yrs (in the range of 2,778 yrs and 3,125 yrs) or 1,087 yrs, are considered to be secondary manifestations of the primary peaks at 1,515 yrs and 2,000 yrs, respectively. Interpretation of the cycles at 1,300 yrs and 650 yr is no easy matter; yet according to their temporal calibration, as well as the corresponding record and CL, we may infer that the cycle at around 1,300 yrs (between 1,282 yrs and 1,316 yrs) is primary in origin, whereas the one at 650 yrs would be secondary.

Thus, detailed analysis of the interpreted primary peaks at 1,300 yrs, 1,515 yrs, 2,000 yrs, and 5,000 yrs, and the secondary harmonics, leads us to envisage significant paleoenvironmental implications and different forcing mechanisms when analyzing, accordingly, the groups of proxies differentiated (Figs. 6-8).

4.2. Forcing mechanisms

4.2.1. The 1,300 yr cycle: influence of the North Atlantic waters

Paleoproductivity and paleotemperature-paleosalinity groups as well as some proxies included in the redox group (V/Al, Zn/Al, Cu/Al ratios) display a 1,300 yr cycle and its secondary 650 yr harmonics (Figs. 7, 8A-B), but this cycle is not registered in the detrital group (Fig. 6). We therefore note similar periodicity between certain periods of major oxygen-depleted bottom water conditions reflected by highly significant V/Al, Zn/Al, Cu/Al ratios (Fig. 7) and major paleotemperature and paleosalinity variations ($\delta^{18}O$) (Fig. 8A). The fact that these millennial- to centennial-scale oscillations in the paleoceanographic context only affect the described proxies would point to oceanographic variations as the main origin for such cyclicity in the western Mediterranean, where this type of periodicity has not been recorded yet.

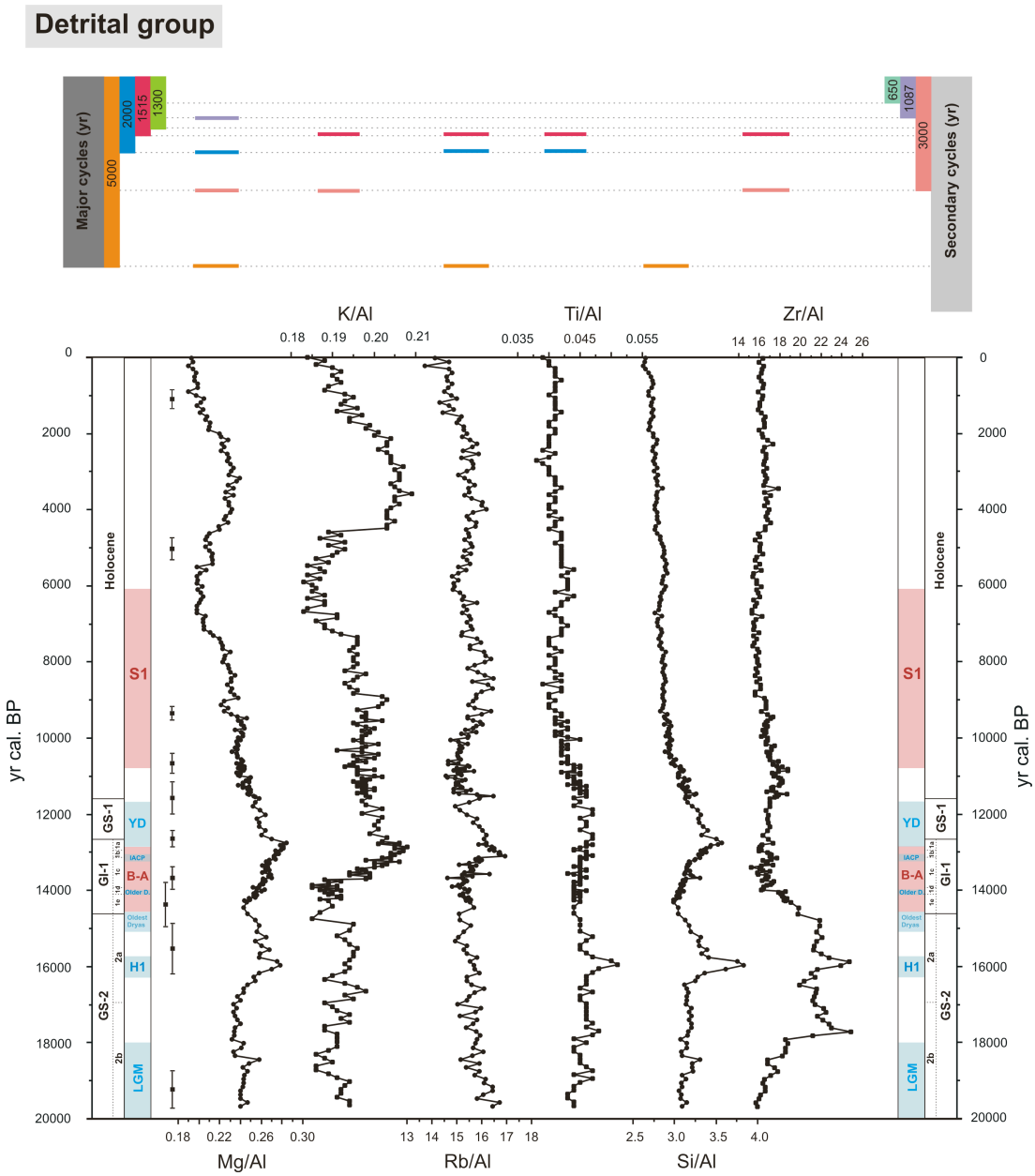
Detrital group
Major cycles (yr)
5000
2000
1515
1300
650
1087
3000
Secondary cycles (yr)
K/Al
Ti/Al
Zr/Al
0.18 0.19 0.20 0.21
0.035 0.045 0.055
14 16 18 20 22 24 26
yr cal. BP
Holocene
S1
GS-1
YD
GI-1
IACP
B-A
Older D.
Oldest Dryas
H1
GS-2
LGM
Mg/Al
Rb/Al
Si/Al
0.18 0.22 0.26 0.30
13 14 15 16 17 18
2.5 3.0 3.5 4.0

Figure 6. Major and secondary peaks obtained in the Detrital group presented as geochemical proxy profiles versus calibrated ^{14}C ages (Element/Al ratios for major elements and Element/Al ratios $*10^{-4}$ for trace elements). Horizontal colored lines refer to the cycles recognized in the proxies below. Black squares show the ten AMS 14C dates with 2σ error bars. Light red boxes indicate warm periods Bölling-Alleröd (B-A) and last Sapropel deposition (S1) in the eastern Mediterranean time interval. Light blue boxes indicate main cold periods, Last Glacial Maximum (LGM), last Heinrich event (H1), Oldest Dryas, Older Dryas, Intra-Alleröd Cold Period (IACP) and Younger Dryas (YD) time intervals. According to NGRIP terminology (Lowe et al., 2008), white boxes indicate Greenland Stadials (GS-1, GS-2) and Interstadials (GI-1).

The 1,300 yr cycle is not evident in most of the circum-North Atlantic climate records (Debret et al., 2007), although when recognized, it has been associated with the North Atlantic IRD events during the Holocene (Bond et al., 1997; Bütikofer, 2007), as well as with solar forcing (Berner et al., 2011). It is noteworthy that similar cycles around 1,100 yr have been recorded by oceanographic proxy records near Iceland (Bianchi and McCave, 1999), and by summer temperature records in North American for the past 14 kyr (Viau et al., 2006).

Lower oxygen levels recorded in the western Mediterranean, in turn, suggest stratification of the water column. This less intense thermohaline circulation could be triggered by different processes, such as increased riverine runoff due to an intensification of the African monsoon activity, or by a negative NAO index, among others. However, the absence of significance in any proxy that defined the detrital group leads us to discard any substantial atmospheric influence, meaning that oceanographic oscillations would be the main climate response to this cycle. Previous research suggests that a fresher Atlantic water inflow reduced the formation of the Levantine Intermediate Water (LIW) and/or the Western Mediterranean Deep Water (WMDW), weakening the Mediterranean thermohaline circulation (Rogerson et al., 2008). Lower thermohaline circulation intensity would reduce bottom-water ventilation, thereby increasing the contents in certain redox elements at this periodicity. Moreover, strong similarities with the secondary peak at 650 yrs are reflected by the short SST cooling events (of about 730±40 yrs) previously observed during the Holocene in this region in association with short freshwater influxes (Cacho et al., 2001). One explanation for this cyclic phenomenon at 1,300 yrs, then, could be variations in the North Atlantic thermohaline circulation with a temporary incursion of fresher subpolar Atlantic surface water into the western Mediterranean.

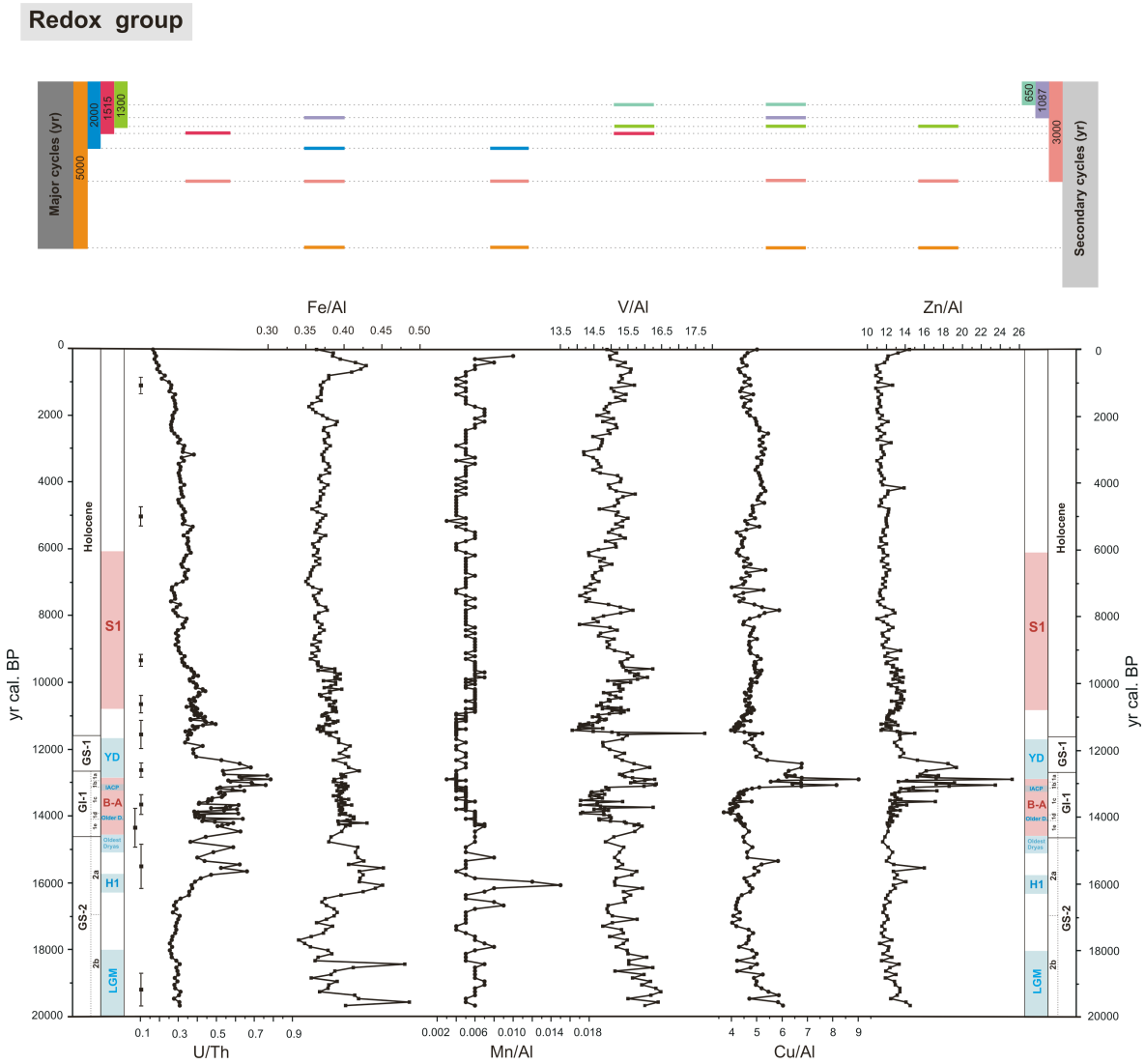

Figure 7. Major and secondary peaks obtained in the Redox group presented as geochemical proxy profiles versus calibrated ^{14}C ages (Element/Al ratios for major elements and Element/Al ratios $*10^{-4}$ for trace elements). Horizontal colored lines refer to the cycles recognized in the proxies below. Black squares show the ten AMS 14C dates with 2σ error bars. Light red boxes indicate warm periods Bölling-Alleröd (B-A) and last Sapropel deposition (S1) in the eastern Mediterranean time interval. Light blue boxes indicate main cold periods, Last Glacial Maximum (LGM), last Heinrich event (H1), Oldest Dryas, Older Dryas, Intra-Alleröd Cold Period (IACP) and Younger Dryas (YD) time intervals. According to NGRIP terminology (Lowe et al., 2008), white boxes indicate Greenland Stadials (GS-1, GS-2) and Interstadials (GI-1).

The paleoproductivity group moreover displays a statistically significant 1,300 yr cycle (Fig. 8B). In this case, the paleoproductivity proxy (Ba/Al ratio) was able to record high productivity levels as well as major preservation conditions. The main factors giving rise to the increase in primary productivity could be: (1) major terrigenous input, of both fluvial and eolian provenances, and an ensuing increase in nutrient fluxes; (2) major oceanographic variations such as meltwater pulses or reorganizations of main oceanographic currents in the area and/or upwelling and active productivity fronts, among others. Again, due to the fact that no increase of terrigenous material was observed in relation to the 1,300 yr cycle the most likely phenomenon behind the paleoproductivity significance of this cycle is nutrient enhancement related with oceanographic variations (e.g., Packard et al., 1988; Fernández de Puelles et al., 2007). Thus, oceanic variations can be put forth as the main forcing mechanism for this cycle, promoted by changes in the nature and tempo of the North Atlantic freshwater inflow through the Strait of Gibraltar in the western Mediterranean, leading to stratification of the water column due to a reduction of WMDW formation, and hence a weakening of the thermohaline circulation (Fig. 9A).

4.2.2. The 1,515 yr cycle: North Atlantic thermohaline circulation, global ice volume and/or NAO and ITCZ migrations

The primary cycle at 1,515 yrs —as well as a corresponding secondary cycle at 3,000 yrs— is clearly detected in all the main proxy groups described (Fig. 6, 7, 8B). This cycle might be the equivalent of the Bond cycle described in North Atlantic ice-core records, with a periodicity of 1,470±500 yrs (Bond et al., 1992, 1993). Cycles with this short-term periodicity have been reported as millennial-scale changes superimposed on the orbital climate evolution in the circum-North Atlantic region (Bond et al., 1997, 2001; Mangini et al., 2007), and have been described previously in the western Mediterranean during the last glacial cycle (Cacho et al., 1999, 2000; Moreno et al., 2005). Gasse (2000) proposed such fluctuations to be feedbacks between changes in insolation and oceanic or atmospheric circulation. Despite being well recognized in the Northern Hemisphere, the origin of such periodicities during the Holocene remains unclear (Debret et al., 2007). Wavelet analysis recently performed over Atlantic, circum-Antarctic and Pacific paleorecords spanning the Holocene indicates that the 1,500 yr climate cycles may be associated with oceanic internal forcing, and not only with variations in solar output (Debret et al., 2007, 2009).

All the proxies included in the redox group signal this cycle as having a high degree of significance (Table 1, Fig. 7). Redox proxies have proven to be particularly sensitive to variations in the Mediterranean thermohaline circulation over the last 20 kyr (Jiménez-Espejo et al., 2008). This

circulation is a key factor for our understanding of the evolution of the MOW, which could play a major role in North Atlantic circulation resumption (Voelker et al., 2006; Toucanne et al., 2007). Rogerson et al. (2008) proposed that changes in surface layer buoyancy, the Gibraltar Strait section and sea level could be a main mechanism underlying the aspiration of deep water and thermohaline circulation during the last glacial cycle. Yet according to this model, only two major changes in deep water ventilation might be expected, one during the increase of deglacial meltwaters at 14.5 kyr cal. BP (Termination 1a), and the other related to the deep water formation during the 8.2 kyr cal. BP cold event (Rogerson et al., 2008). The presence of significant 1,500 yr periodicity therefore suggests a more complex scenario involving cyclic changes in deep and/or intermediate waters in the Alboran Sea.

Among the detrital group, typical fluvial proxies (K/Al, Mg/Al and Rb/Al ratios) display these periodicities, and some eolian input proxies (Ti/Al and Zr/Al ratios) also record the major cycle and its secondary peak (Fig. 6). The presence of some minerals formed at low weathering conditions indicates enhanced aridification over the Sahara region and further supports an atmospheric intensification of the northern branch of the African wind system transporting, latitudinally, eolian dust to the western Mediterranean. Such an interpretation of the detrital mineral oscillations recorded is thus supported by recent models where low rainfall conditions in North Africa are triggered by the southward migration of the ITCZ (Lee et al., 2011), and fluvial proxies come from poorly-drained soils of the lower sectors of equatorial and tropical rivers.

The ITCZ northward/southward displacements have been identified in diverse paleorecords, including African lakes (Tierney and Russell, 2007) and Asian monsoon precipitation (Wang et al., 2001; Cai et al., 2010). Other atmospheric perturbations with high wind intensities at this frequency oscillation were documented in Greenland ice-core records by an increased concentration of sea salt and terrestrial dust in the atmosphere during the Holocene (O´Brien et al., 1995).

Periodical changes between wet-dry conditions observed in the western Mediterranean can be explained by variations in the position of the Atlantic jet-stream, and the equivalent negative and positive NAO modes (Trigo et al., 2002). NAO variations have been described at centennial scales (Trouet et al., 2009) and NAO-like mechanisms have been also invoked to explain SST-cooling events recorded in the western Mediterranean (Cacho et al., 1999). This teleconnection may be related with the presence of cold or warm surface waters over the North Atlantic region, affecting the northward/southward westerlies displacements, and coupled with Atlantic inflow salinity and temperature changes (Trigo et al., 2002; Moreno et al., 2005; Trouet et al., 2009). In addition, Atlantic SST cooling bears an impact on the African climate by strengthening the subtropical cell

pressure, affecting both the aridity of dust source areas and the intensity of the dust-transporting trade winds (deMenocal and Rind, 1993). This SST record from northwestern Africa (deMenocal et al., 2000) demonstrates a clear oceanic imprint with the 1,500 yr internal period, well expressed during the Late Holocene (Debret et al., 2009). The same periodicity has been reported in sea surface salinity oscillations and rainfall patterns in Asian monsoon areas (Wang et al., 1999; Sarkar et al., 2000).

The 1,515 yr periodicity can also be seen in the Ba/Al ratio of the studied sediments (Fig. 8B). Though the $\delta^{18}O$ signal was not recorded as significant in this cycle (Fig. 8A), redox sensitive elements, detrial fluctuations and paleoproductivity conditions suggest a strong oceanic-atmospheric impact. These productivity variations could be associated with a greater supply of nutrients and a well mixed water column triggered by the formation of surface cold water that increased oxygenation of the water column linked to the intensification of wind systems over the western Mediterranean (Bassetti et al., 2010). The spectral $\delta^{18}O$ values are in agreement with a lack of relationship between Bond cycles and ice sheet volume, as proposed previously by Debret et al. (2007). Moreover, the proposed collapse of thermohaline circulation during Heinrich 1 (H1) in the western Mediterranean (Sierro et al., 2005), the presence of African surface currents in the Gulf of Cadiz during the Last Glacial Maximum and YD (Rogerson et al., 2006), and local isotopic gradients in the western Mediterranean (Jiménez-Espejo et al., 2008) could mask the $\delta^{18}O$ signature of the 1,515 yr periodicity. Minor oxygen variability in the Gulf of Cadiz has additionally been related with long-term stable temperature and salinity properties of the LIW (Voelker et al., 2006).

For all these reasons, the 1,515 yr cycle registered in the western Mediterranean record would evidence a rapid response in the oceanic and atmospheric systems given the different proxies described, though to a lesser extent on the isotopic signal since the Last Glacial Maximum (LGM). The forcing mechanisms related to this noteworthy period may very well be directly linked to North Atlantic thermohaline circulation and atmospheric changes in the North Atlantic realm. Aside from altering the properties and volume of the inflowing North Atlantic surface waters, the trigger mechanism would have modified the intensity and position of atmospheric pressure gradients as determined by the NAO influence and the ITCZ migrations in North Africa, with the consequent displacement of the monsoon rain-belt, thereby changing the Mediterranean pluviosity regimen and the wind systems (Fig. 9B). These atmospheric and oceanographic changes hence affect the WMDW and LIW formation, and they leave their imprint in redox proxies with better or poorer deep-water ventilation, as well as in the productivity conditions.

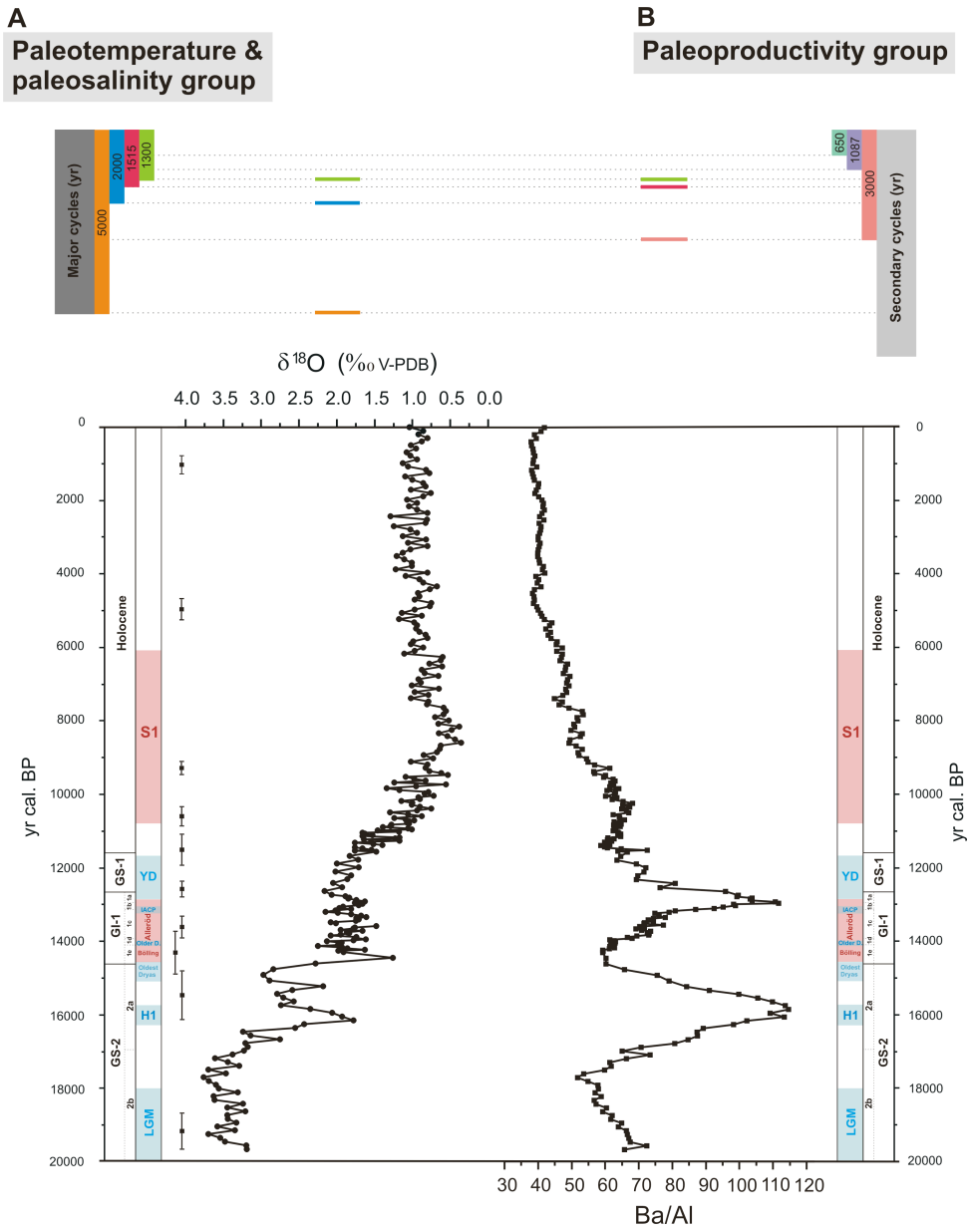

Figure 8. Major and secondary peaks obtained in the Redox group presented as geochemical proxy profiles versus calibrated ^{14}C ages (Element/Al ratios for major elements and Element/Al ratios $*10^{-4}$ for trace elements). Horizontal colored lines refer to the cycles recognized in the proxies below. Black squares show the ten AMS 14C dates with 2σ error bars. Light red boxes indicate warm periods Bölling-Alleröd (B-A) and last Sapropel deposition (S1) in the eastern Mediterranean time interval. Light blue boxes indicate main cold periods, Last Glacial Maximum (LGM), last Heinrich event (H1), Oldest Dryas, Older Dryas, Intra-Alleröd Cold Period (IACP) and Younger Dryas (YD) time intervals. According to NGRIP terminology (Lowe et al., 2008), white boxes indicate Greenland Stadials (GS-1, GS-2) and Interstadials (GI-1).

4.2.3. The 2,000 yr cycle: high- to low- latitude climate variability linked to variations in solar activity

The 2,000 yr cycle, and its secondary peak at 1,087 yrs, is significant in three groups, i.e. detrital, redox, and paleotemperature-paleosalinity, yet it hardly explains the proxies (Figs. 6, 7, 8A). The fluvial proxies in particular (Mg/Al, Rb/Al) are significant among the detrital element group, though the Ti/Al ratio is also characterized (Fig. 6). Elevated Ti/Al ratios are expected in eolian-derived material from North Africa. However, the increase in this ratio in conjunction with typical fluvial proxies suggests a combined transport phenomenon. Chemical cycles during Pliocene sapropel formation reveal the same Ti/Al ratio anomaly, attributing the increase to westward-directed transport from continental sources of basaltic rocks rich in Ti contents located in the east (Wehausen and Brumsack, 2000). The cycle could thus be interpreted as prevailing humid conditions with major terrigenous input due to river run-off (Mg/Al, Rb/Al) and dust pulses from the eastern Mediterranean borderlands.

During the Holocene, similar millennial-scale climate oscillations have been recognized in locations from the North Atlantic area and elsewhere, most likely related to long-term solar forcing variations (Debret et al., 2009, and references therein). Spectral analyses of diverse paleorecords (Bütikofer, 2007) determine periodic surface temperature variations at around 2,000 yrs in the Tropical Pacific Ocean (Stott et al., 2004; Bütikofer, 2007). In this sense, recent models highlight the role of the Atlantic Multidecadal Oscillation and the natural fluctuation of the Atlantic Meridional Overturning Circulation (AMOC) in modulating the variation of the ENSO-monsoon system (Chen et al., 2010). During older periods, frequency spectra from lacustrine records in central Italy (Lake Albano) and northern Greece respectively evidence cyclic periods at 2,000 yrs and 2,500 yrs (Chondrogianni et al., 2004; Kloosterboer-van Hoeve et al., 2006). This cycle and its secondary peak at 1,087 yrs present similarities with periodicities recorded in $\delta^{18}O$ values from the GISP2 ice-core during the Late Pleistocene, with periodicities of 1,050 yrs (Stuiver et al., 1995). Likewise, the 1,150 yr period is reportedly characteristic of SW monsoonal variability in the Arabian Sea (Sirocko et al., 1996). In northwestern Africa, marine records present a periodicity in the terrigenous signal of 900 yrs over the past 9,000 yrs, comparable to the temperature variation in Greenland, suggesting a transitional area between the influences of the African monsoonal system and the North Atlantic climate (Kuhlmann et al., 2004).

In addition, a 2,300 yr spacing is recorded in the Aegean SST and winter/spring intensity of the Siberian High (GISP2 K+ record), which suggests solar modulation of the climate recognized in the δ14C record and in worldwide Holocene glacier advance phases (Rohling et al., 2002). Moving

toward the Southern Hemisphere (SE Australia), SST oscillations in the Pacific Ocean also record a significant cycle at 2,100 yrs in relation with solar irradiance variations (McGowan et al., 2010). Therefore, the Mediterranean cycle recognized at 2,000 yrs, and at around half this time span, suggests a direct atmospheric link with high- (North Atlantic), mid- (monsoon region), and low-latitude (Pacific Ocean) climate variability, supposedly influencing the whole Mediterranean region. The reasons underlying this regular climatic fluctuation are not clear. Yet a recurrence of cold climatic phases in Greenland ice-cores, and in terrestrial records from Europe, North Africa and the Southern Hemisphere, could be linked to variations in solar activity (Maunder-type oscillations) (Van Geel et al., 1999). Accordingly, the coincidence of variations in cosmogenic isotopes (14C and 10Be) with climate changes during the Holocene, and the upper part of the last Glacial, imply that the climate system is far more sensitive to small variations in solar activity than is generally believed. Simulation models also show that the response in atmospheric parameters to irradiance forcing can be characterized as the direct response of a system with a large thermal inertia in parameters such as surface air temperature, monsoon precipitation and glacier length (Weber et al., 2004).

In terms of paleoceanographic and climate conditions, the redox group presents the highest confidence level for this cycle, and $\delta^{18}O$ oscillations are also highly significant (Figs. 7, 8A). The $\delta^{18}O$ oscillations may result from the high sensitivity of ice-sheets to increasing solar radiation as a main forcing mechanism triggering this periodicity. SST variations, especially higher during summer, would intensify Mediterranean cyclogenesis and associated floodings (Trigo et al., 2002), reinforcing the oceanic-atmospheric teleconnections. Obtained detrital proxies are also coherent with northerly moisture transport toward the Saharan-Sahelian belt and the monsoonal front displacement (Gaetani et al., 2010). The influence of the African monsoon fluctuations has been seen in flux oscillations of the Nile (Skliris et al., 2007). A major Nile input would reduce the formation of LIW, whereas low Nile input would reduce surface dilution in the Levantine basin, increasing LIW formation. Such changes in temperature and related salinity could also strongly affect the seasonal stability of the Mediterranean water column (e.g., Sparnocchia et al., 1994; Skliris et al., 2007; Cartes et al., 2011), altering the bottom-water oxygen conditions. Therefore, the oceanic response to insolation forcing due to solar irradiance variations is strongly modified by internal feedback processes, as Holocene climate models would indicate (Weber et al., 2004).

In summary, the obtained 2,000 yr cycle in the western Mediterranean appears to be forced by solar-derived activity variations and consequent monsoonal intensification. The African monsoon regime would bear an impact on Mediterranean thermohaline circulation, affecting intermediate and deep-water formation as well as water column stabilization (Fig. 9C).

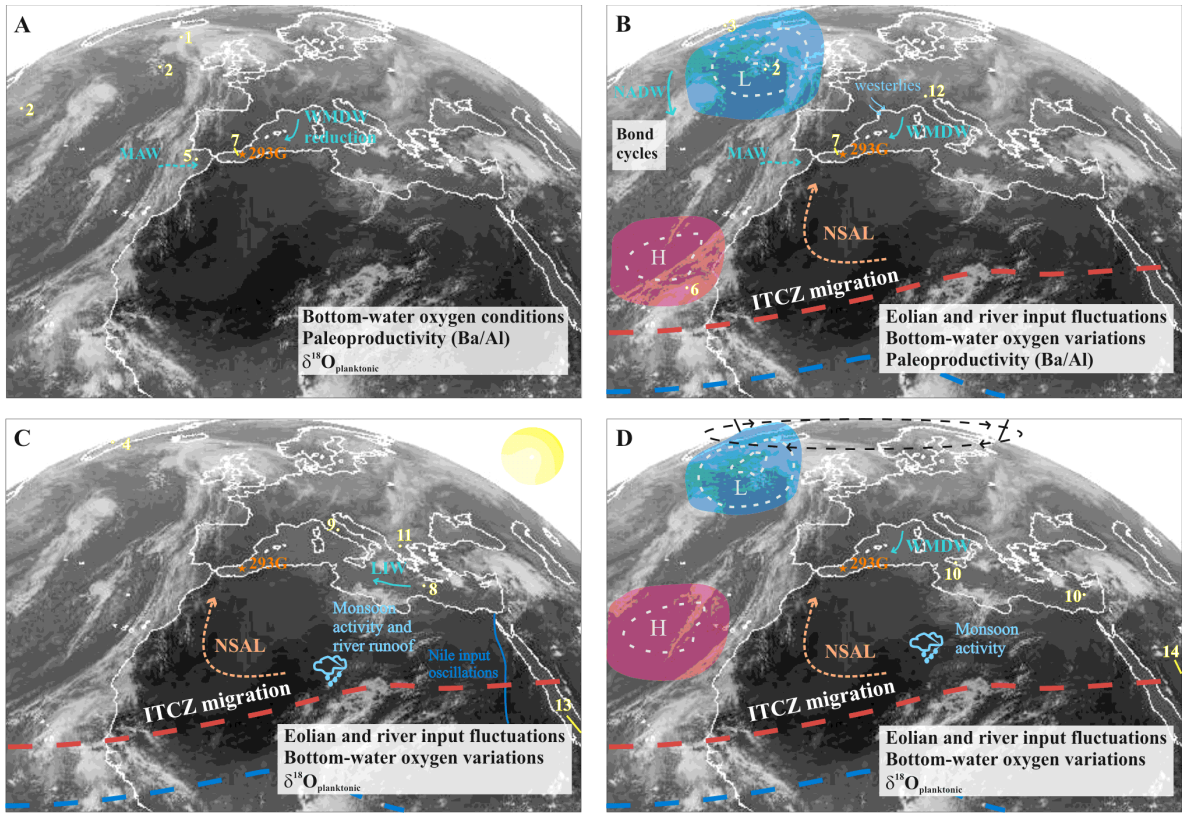

Figure 9. Scheme of the main climate teleconnections and proxies associated with (A) 1,300 yrs, (B) 1,515 yrs, (C) 2,000 yr, and (D) 5,000 yrs periodicities obtained in the power spectra on marine record 293G from the westernmost Mediterranean Sea. A) The 1,300 yr cycle appears to be mainly driven by changes in the nature of the Atlantic water inflow and the Western Mediterranean Deep Water formation. B) The 1,515 yr cycle is associated to variations in North Atlantic thermohaline circulation, ice volume and atmospheric conditions. C) The 2,000 yr cycle suggests variations in solar activity as the main driving factor, affecting moonsonal regime, riverine input and Deep and Intermediate Mediterranean Water formation. D) The 5,000 yr cycle is directly linked to orbital forcing influence and monsoon dynamics. Numbers indicates other paleorecord locations cited in the manuscript that recognize similar periodicities. Greenland and North Atlantic Ocean: (1) Bianchi and McCave, 1999, (2) Bond et al., 1997, 2001, (3) O'Brien et al., 1995, (4) Stuiver et al., 1995; Gulf of Cadiz: (5) Voelker et al., 2006; Tropical West Africa: (6) deMenocal et al., 2000; Europe and Mediterranean Sea: (7) Cacho et al., 2001, Moreno et al., 2005, (8) Rohling et al., 2002, (9) Chondrogianni et al., 2004, (10) Becker et al., 2005, (11) Kloosterboer-van Hoeve et al., 2006, (12) Mangini et al., 2007; Arabian region: (13) Sirocko et al., 1996, (14) Fleitmann et al., 2003. NADW: North Atlantic Deep Water. MAW: Modified Atlantic Water. WDMW: Western Mediterranean Deep Water. LIW: Levantine Intermediate Water. ITCZ: Intertropical Convergence Zone.

4.2.4. The 5,000 yr cycle: orbital forcing influence and monsoon dynamics

The 5,000 yr cycle presents high significance in the detrital, redox, and paleotemperature-paleosalinity groups (Figs. 6, 7, 8A). Once again, this periodicity corresponds to an important generalized mechanism, affecting both oceanic and atmospheric response systems at high- and mid-latitudes. This cycle is in agreement with significant temperature oscillations and changes of the polar circulation index recorded in the GISP2 ice-core (Grootes and Stuiver, 1997; Mayewski et al., 1997). This comes to further support the existence of a strong link between the rates of deep-water ventilation (with significant high Fe/Al and Mn/Al ratios) and the intensity of high-latitude atmospheric circulation reflected in major eolian input (Si/Al ratio) in the western Mediterranean region (Figs. 6, 7). In addition, changes in the deep-water convection produced in the Gulf of Lion by cold and arid conditions can be detected using the n-hexacosanol/n-nonacosane index, directly influenced by the intensity of northwesterly winds as previously described in this region (Cacho et al., 2000).

In the monsoonal areas (Asia and Africa), pronounced variations at periods of about 10,000 yrs and 5,000 yrs have been related with runoff variations in response to the precessional forcing (Berger et al., 2006; Tuenter et al., 2007). Climate model simulations have also shown that wetter conditions were probably caused by changes in the Earth's orbital parameters that increased the amplitude of the seasonal cycle of solar radiation in the Northern Hemisphere, enhanced the land-ocean temperature contrasts, and thereby strengthened the African summer monsoon (Kutzbach et al., 1996). Therefore, this cycle is the only one that could have a direct relationship with an orbital forcing response. During precession maxima, insolation is low and the desert area expands, as reflected by the Si/Al ratio; thus, the surface albedo increases whereas the surface air temperature decreases (lower temperature contrast between land and ocean). In contrast, the African monsoon response is a general reduction in precipitation and hence in runoff (Tuenter et al., 2007). Minor amounts of precipitation during precession maxima can, however, increase river runoff input as well, meaning statistically significant Mg/Al and Rb/Al ratios as fluvial proxies, since the soil retains less water. Such a scenario —where major desert expansion implies major Saharan dust export/supply but with some sporadic rainfall— could be the main reason why we observe a significant response in the detrital group, especially in the two fluvial proxies (Mg/Al, Rb/Al ratios) and the typically eolian-delivered elements such as Si/Al ratio (Fig. 6). These runoff oscillations at sub-Milankovitch time-scales, every 5,000 yrs, produce variations in $\delta^{18}O$ within the western Mediterranean as well, and in the redox conditions, particularly in terms of Fe/Al, Mn/Al, Zn/Al, and Cu/Al ratios, due to oscillations of the water column stratification (Figs. 7, 8A). A decrease in precipitation or African monsoons could give rise to major salinity in the surface water lens of the

western Mediterranean, together with lower temperatures and a drier climate favoring the WMDW formation; this implies more ventilated bottom water conditions during preccesion maxima. The opposite situation would be reflected during precession minima, favoring stagnant bottom water in conjunction with the African monsoon increase.

High-frequency climate variability at 3,000-5,000 yr timescales in the eastern Mediterranean has been previously related to changes in Saharan dust supply (Becker et al., 2005). Enhanced dust deposition over the Mediterranean, correlated with the cold intervals of the millennial-scale D-O oscillations, suggests that the Atlantic pressure system (NAO) may also have played a critical role in varying the wind strength and/or aridification of northern Africa. In addition, the establishment of the modern ENSO band characterized by increased El Niño frequency could have caused significant monsoon weakening by the southward migrations of the ITCZ after around 5,400 yr cal. BP (Haug et al., 2001), which may in turn be regulated by orbitally induced insolation in the tropical oceans (Fleitmann et al., 2003). The 5,000 yr cycle is therefore strongly related to orbital forcing as the main mechanism, while also accompanied by monsoon variations due to ITCZ migrations and NAO oscillations that influence the western Mediterranean cyclicity (Fig. 9D).

4.3. Sub-Milankovitch scale cycles in other related paleorecords

Spectral analysis of diverse marine paleoclimate records worldwide has also evidenced cycles at the sub-Milankovitch band, from millennial to multi-decadal time-scales. In general, these climate cycles have been interpreted as a result of several forcing factors, solar activity being the main external factor responsible for higher-frequency climate cycles at sub-Milankovitch scales. These cycles are also associated to internal factors such as the nature of the proxy records, local forcing mechanisms, sampling intervals and paleorecord resolution. Even though it was demonstrated long ago that significant climate changes also occur at these scales (e.g., Willis et al., 1999), there has been little research into sub-Milankovitch frequencies in the Mediterranean and adjacent regions.

In the westernmost Mediterranean, previous work on high frequencies underlined four significant periodicities at 8,000, 5,000, 3,300 and 1,470 yrs for the time interval 48,000 to 28,000 yr cal. BP, in agreement with those found in Greenland (Moreno et al., 2005). The significance and the variance of these bands are quite different for each group of paleoclimatic proxies considered. The 1,470yr cycle is usually most significant for the records (stable isotopes, molecular biomarkers, proportion of Neogloboquadrina pachyderma, total organic carbon content, grain-size, major and trace elements, and pollen), excepting those proxies that reflect conditions on land. Thus, cycles at 3,300 and 8,000 yrs are registered in proxies related to changes on the terrestrial realm, interpreted

as revealing paleoenvironmental changes that may affect intensity of the North Africa wind systems, continental aridity, and steppic vegetation abundance (Moreno et al., 2005).

In nearby Mediterranean regions such as the Arabian Sea, terrigenous input and REE content evidence monsoonal climate cycles at 1,785, 1,450, and 1,150 yrs (Sirocko et al., 1996). The Globigerina bulloides record also indicates statistically significant periodicities at 1,550 yrs and diverse centennial-scale cycles that fit well with periodicities of sunspot numbers, thus indicating a relationship between solar and summer monsoon variability and induced upwelling (Gupta et al., 2005).

In the North Atlantic area, a marine record from the North Iceland margin shows spectral periodicities on the millennial to multi-decadal scale at 6,000-5,000, 1,250, 200, 140, 125, 118, 88, and 78 yrs, associated overall with solar variability and further controlled by atmospheric and oceanographic changes linked to changes in the relative advection of Atlantic and Polar waters along the North Iceland margin (Andrews et al., 2003). Major changes in Atlantic water flow at a quasi-stationary 2,500 yr periodicity have been also presented in coccolith records from Norway and northern Iceland (Giraudeau et al., 2010), a cycle well recorded in proxy records of solar activity (e.g. Nederbragt and Thurow, 2005). Thus, a potential link between solar activity as an external factor, and Atlantic oceanic forcing to the Nordic Sea as a local factor, appears to gain force throughout the Holocene. Climate models have also shown millennial to multicentennial time-scale oscillations between strong and weak states of the AMOC during the Holocene, with variable recurrence times, ranging from 3,000 to 400 yrs (Schulz et al., 2007).

Diverse circum-North Atlantic records also support a Holocene pattern characterized by an early phase with cycles at 1,000 and 2,500 yrs triggered by solar activity, and a second phase marked by cycles at 1,500 yrs, associated with the Atlantic thermohaline circulation (Debret et al., 2007, 2009, and references therein).

Therefore, the cycles recognized in our record of study lie in agreement with some of those found in other paleoclimatic records, as discussed in previous sections, and further support the significance of high-frequency climate cycles at sub-Milankovitch time-scales over the last 20,000 yrs, even though the amplitude of the Holocene variations appears to be smaller than the pronounced glacial climate variations.

5. Conclusions

The high sedimentation rates of the marine record from the Alboran Sea have allowed us to establish novel high-periodicity cycles at millennial- to centennial-scales for the last 20,000 yrs in this location. The paleoenvironmental cyclicities obtained exhibit noteworthy spectral periodicities of varying statistical significance for the range of the different multi-proxy groups. Main periodicities at 1,300, 1,515, 2,000, and 5,000 yrs plus secondary harmonics at 650, 1,087, and 3,000 yrs suggest different forcing mechanisms triggering paleoclimatic oscillations. The 1,300 yr cycle is principally recorded in the Mediterranean paleoceanographic context, pointing to the influence of North Atlantic freshwater inflow to the Alboran Sea. All the groups described show a 1,515 yr cycle equivalent to the Bond cycle in the North Atlantic; however, it is less significant in the isotopic signal, probably due to a lagged response of the ice-sheets to these cyclic oscillations at the time interval studied. These high frequency bands appear to be linked to North Atlantic thermohaline circulation and changes in the intensity and NAO-like oscillations and ITCZ migrations. Although the 2,000 yr cycle is not reflected by many proxies, it suggests generalized climate variability in the Mediterranean region, with variations in solar activity and monsoonal teleconnections between high- and low-latitudes as the main forcing mechanism. The cycle at 5,000 yrs corresponds, then, to a generalized periodicity and is the only one presenting a direct relationship with an orbital forcing response. Therefore, the obtained spectral periodicities provide evidence that serves to reinforce the strong connection between North Atlantic climate and monsoonal variations in the western Mediterranean context, and further supports the extreme sensitivity of this region to cyclic climate changes.

In general, we may envisage a future climate response entailing cyclical alterations in the hydrographic circulation over the Alboran Sea, highly sensitive to cyclic variations, through oscillations in the water column thermal-salinity stratification and bottom-water oxygenation, along with detrital fluctuations due to river runoff or major eolian dust pulses forced by the NAO and ITCZ migrations over North Africa; yet natural volcanic eruptions and the current warming trend exacerbated by greenhouse emissions should be accounted for in predictions of future climate change.

Acknowledgements

This work was supported by Projects CGL2009-07603, CGL2008-03007, CTM2009-07715, CSD2006-00041 (Ministerio de Ciencia e Innovación), 200800050084447 (MARM), Projects RNM-5212, RNM-3715, and Research Groups RNM-179, RNM-178 (Junta de Andalucía). We are also grateful to the oceanographic cruise Training-Through-Research Programme (UNESCO-Moscow State University). F. J. Jiménez-Espejo acknowledges funding from the CSIC "JAE-Doc" postdoctoral program. We are likewise grateful to E. Holanda, C. Niembro, E. Abarca, D. Ortega, L. López and J. Santamarina for their laboratory assistance. Analyses were performed at the "Centro de Instrumentación Científica", University of Granada, Granada (Spain), at National Centre for Accelerators (CNA), Sevilla (Spain), at the SGS Minerals Services Analytical, Lakefield, Ontario (Canada), and at Isotope Laboratory, Marum, Bremen University, Bremen (Germany).

7. Chapter IV.- **Sea surface temperature variations in the western Mediterranean Sea over the last 20,000 yrs: a biomarker approach ($U^{k'}_{37}$ and TEX^{H}_{86})**

Rodrigo-Gámiz, M., Martínez-Ruiz, F., Schouten, S., Sinninghe Damsté, J.S.

To be submitted to Paleoceanography

Abstract

A high-resolution sea surface temperatures (SST) reconstruction in the western Mediterranean was accomplished using two molecular organic proxies, the $U^{k'}_{37}$ index based on long-chain unsaturated ketones synthesized by haptophyte algae and the TEX^{H}_{86} proxy based on thaumarchaeotal membrane lipids. The two marine records analyzed, from the western and eastern Alboran Sea basin, span the last 14,000 and 20,000 years, respectively. From a previous multi-proxy approach based on mineral and inorganic chemical composition of marine sediments, these two records have revealed millennial- to centennial-scale climate variability for the studied time intervals. Thus, for further paleoceanographic reconstructions, organic proxies are used to establish SST oscillations linked to climate oscillations. The transition from the Last Glacial Maximum to the Holocene is clearly revealed by both temperature records from the eastern basin showing an SST increase of 7º ($U^{k'}_{37}$) and 12ºC (TEX^{H}_{86}). Minimum SSTs are reached at the Last Glacial Maximum offset (10.1ºC-$U^{k'}_{37}$ and 12ºC-TEX^{H}_{86}) with a slight oscillation during the Last Heinrich event (12.2º and 11.4ºC in the respective biomarkers). A progressive SST increase is evidenced during the Bölling-Alleröd period with TEX^{H}_{86}-SST derived from 14.7ºC to 17.9ºC, while $U^{k'}_{37}$-SST shows an abrupt increase just during the Bölling onset (from 12.4ºC to 17.9ºC). Short-term fluctuations are recorded in the haptophyte and stable oxygen isotopes records during the Bölling-Alleröd period comparing with thaumarchaeota denoting rapid climate fluctuations such as the Older Dryas up to another minimum during the Younger Dryas cold event (12.8ºC-$U^{k'}_{37}$ and 16.1ºC-TEX^{H}_{86}). The Younger Dryas is recorded in the two marine basins with a short-time cold event (12.8ºC-$U^{k'}_{37}$ and 16.1ºC-TEX^{H}_{86} in the eastern, and 13.8ºC-$U^{k'}_{37}$ and 17ºC-TEX^{H}_{86} in the western). During the Holocene several SST fluctuations have been supported although with major evidences in haptophyte algae than thaumarchaeota. Higher $U^{k'}_{37}$-derived temperatures (18.9º-22.3ºC) are observed in the western Alboran (by ca. 1.5º-2ºC) comparing to the eastern (17.8º-20.4ºC), suggesting a warmer water influence due to it proximity to the Iberian coast and the surface water circulation of the Western Alboran Gyre. Major TEX^{H}_{86}-SST absolute values derived in both records (around 25ºC) during the Holocene and similar oscillation pattern suggest a seasonal response in the organic proxies reflecting thaumarchaeota summer temperatures.

1. Introduction

A variety of proxies have been used to reconstruct past Sea Surface Temperature (SST) changes due to the rapid influence of the climate oscillations in the past-oceanographic conditions (e.g., Rimbu et al., 2004). The most frequently indicator used has been the stable oxygen isotopes since

their documentation in Greenland ice-core records (e.g., Grootes et al., 2003). Mg/Ca measurements in foraminifera (e.g., Barker et al., 2005 and references therein; Patton et al., 2011), transfer function and modern analogs techniques in fossil assemblages (e.g., González-Donoso et al., 2000; Pérez-Folgado et al., 2003; Serrano et al., 2007 and references therein) have also been commonly used as SST proxies for paleoceanographic studies. Previously, the identification of long-chain alkenones (C_{37}, C_{38}, and C_{39}) in marine sediments was reported for the first time by de Leeuw et al., (1980). Then Volkman et al., (1980) recognized an algal source of these compounds in a specific group of marine phytoplankton, coccolithophorid, i.e., in *Emiliania huxleyi*, although other algae genera contribute to long-chain alkenones (Marlowe et al., 1984). The $U^{k'}_{37}$ index was defined as the proportions of di-($C_{37:2}$), tri-($C_{37:3}$), and tetra-($C_{37:4}$) unsaturated ketones (Brassell et al., 1986) observing similar trends in alkenone unsaturation and the $\delta^{18}O$ records over the past 120 kyrs in the eastern equatorial Atlantic and then suggesting its potential paleotemperature fluctuations. Further subsequent works excluded the $C_{37:4}$ ketone in the paleothemperature equation (Prahl and Wakeham, 1987; Prahl et al., 1988). Thus the currently accepted $U^{k'}_{37}$ index shows that these organisms adjust unsaturation in the alkenone series in response to their growth temperature, decreasing the degree of unsaturation as growth temperature increases.

A more recently paleotemperature proxy is theTEX_{86} that is based on isoprenoid glycerol dialkyl glycerol tetraethers (GDGTs) (Schouten et al., 2002). These compounds are present in the membrane lipids of Marine Group I Crenarchaeota, which are now believed to represent the separate phylum Thaumarchaeota (Brochier-Armanet et al., 2008; Spang et al., 2010), a subgroup of prokaryotic microorganisms archaea, which are ubiquitous in marine environments (e.g., Hoefs et al., 1997; Massana et al., 2000; Karner et al., 2001). The GDGTs biosynthesized by these Thaumchaeota are similar to those of their thermophilic ancestors, except for crenarchaeol, a unique GDGT containing one cyclohexane moiety in addition to the more common cyclopentane moieties (Sinninghe Damsté et al., 2002a). The isoprenoidal GDGTs are biosynthesized in varying amounts depending on growth temperature (Schouten et al., 2002) despite the fact that thaumarchaeota are distributed through the water column (Karner et al., 2001). Therefore there must be mechanisms that transport the surface signal to sediments such as repackaging in fecal pellets, marine snow, or mass falls after phytoplankton blooms. Therefore, variation in the temperature at the surface of the oceans can be determined via the TEX_{86} proxy, i.e., by quantifying the average number of cyclopentane moieties in tetraethers with 86 carbons (Schouten et al., 2002).

TEX_{86} is independent to salinity oscillations, changes in nutrients and light availibility (Wuchter et al., 2004), whereas these factors substantially affect the $U^{k'}_{37}$ index, as well as foraminiferal $\delta^{18}O$ values are influenced by ice volume and salinity.

Alkenone-derived SST and $\delta^{18}O$ records have been previously obtained in marine records along the Mediterranean Sea (e.g., Rohling et al., 1998; Cacho et al., 1999, 2000, 2002; Emeis et al., 2000; Martrat et al., 2004, 2007) denoting the close connection of the short-term climate and oceanographic variability with the North Atlantic fluctuations. Recently, a combination of both organic SST proxies, $U^{k'}_{37}$ and TEX_{86}, has been succesfully applied in the western Mediterranean for the last two millenia (Nieto-Moreno et al., submitted) and for the penultimate climate cycle (Huguet et al., 2011), as well as in the eastern Mediterranean (Castañeda et al., 2010). These studies suggest a posible seasonality divergence between both molecular proxies, particularly with TEX_{86} reflecting the warm summer season rather than annual mean SST, especially accentuated during interestadial periods and the Late Holocene.

Here, we present the paleo-SST reconstruction derived from molecular biomarkers ($U^{k'}_{37}$ and TEX_{86}) in the westernmost Mediterranean for the last 20,000 yrs. Two marine records have been selected from the westernmost Mediterranean, which have revealed as excellent paleoclimate archives (Rodrigo-Gámiz et al., 2011; Rodrigo-Gámiz et al., in prep.). The integration of both paleothermometers has alllowed a continuous and high-resolution SST evolution at millennial- to centennial-time scales, and has demonstrated the seasonal effect on the SST obtained values. We also intend to demonstrate the potential response in these organic proxies to the North Atlantic influence and the Mediterranean thermohaline circulation in the Alboran basin.

2. Material and methods

2.1. Study area

The two analyzed gravity cores were recovered in the two different Alboran basins. The core 293G (402 cm) was recovered in the East Alboran Sea basin (Lat. 36´10.414N, Long. 2´45.280W, depth 1,840 mbsl) (Fig. 1) during the oceanographic cruise Training Through Research (TTR) 12. The inorganic geochemical, mineralogical and grain size distribution records from this record has been reported by Rodrigo-Gámiz et al., (2011). A second gravity core, 434G (252.5 cm), was recovered close to ODP Leg 161 Site 976 (Comas, Zahn, Klaus, et al., 1996) in the West Alboran Sea basin (Lat. 36'12.313N, Long. 4'18.735W, depth 1,108 mbsl) (Fig. 1) during the oceanographic cruise TTR-17 (R/V Professor Logachev) (Sagas-08 Cruise). The lithology of both marine sequences is dominated by homogeneous green-brownish hemipelagic mud-clays with some foraminifera and shell fragments (Comas and Ivanov, 2003).

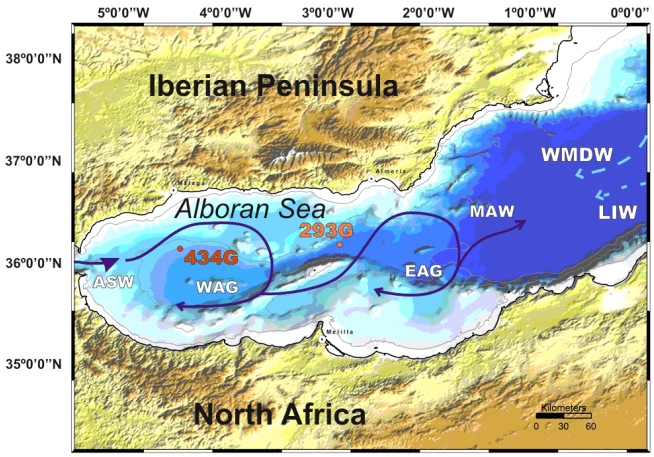

Figure 1. Map of the studied area with localization of the two gravity cores studied, the 434G setting recovered in the eastern Alboran basin, and the 293G setting in the eastern Alboran Sea basin. Black arrows represent the theoretical surface circulation in the Alboran Sea: Atlantic Surface Water (ASW), Western Alboran Gyre (WAG), Eastern Alboran Gyre (EAG) and Modified Atlantic Water (MAW). Grey arrows represent deep water masses circulation: the Levantine Intermediate Water (LIW) and the Western Mediterranean Deep Water (WMDW).

The Alboran Sea basin presents a particular hydrodynamic feature due to its semi-enclosed configuration and its connection to the Atlantic Ocean through the Strait of Gibraltar. The Atlantic Surface Water (ASW) flows into the Alboran from the West at the surface (200 m), which is mixed with the Mediterranean water forming the Modified Atlantic Water (MAW) flowing out the Mediterranean at depth. The ASW, which is almost homothermal (15ºC) (Parrilla and Kinder, 1987), described two almost permanent anticyclonic gyres, namely the Western Alboran Gyre (WAG) and the Eastern Alboran Gyre (EAG) (Millot, 1999), being the most characteristic features of the surface circulation in the Alboran Sea (Fig. 1). These gyres show a high annual-interannual variability driven mainly by the position of the atmospheric pressure cells (La-Violette, 1986). From the East, and below the MAW, comes the Levantine Intermediate Waters (LIW) (200-600 m), and the deeper Western Mediterranean Deep Water (WMDW) (>600 m) originated in the Gulf of Lion by intensification of the westerlies. The intermediate, in major proportion, and deep-water masses form the MOW through the Strait of Gibraltar (Send et al., 1999) implying a strong communication between eastern and western basins (Fig. 1). These two deeper water masses (LIW and WMDW) have high salinities (about 38.5%), although the WMDW is slightly colder (12.9ºC) than the LIW (13.2ºC) (Parrilla and Kinder, 1987). Taking into account the localization and different bathimetric sites of both cores studies in the Alboran basin, the 434G record could be more affected to ASW and hence to the WAG (Fabres et al., 2002), while the core 293G could be more influenced by the cooler and saltier WMDW circulation.

2.2. Chronology

The chronology of core 293G was established by Rodrigo-Gámiz et al., (2011) based on ten AMS ^{14}C measurements and $\delta^{18}O$ profile based on the monospecific planktonic foraminifera *Globigerina bulloides*, which has been well related with Greenland isotopic stratigraphy (Stuiver and Grootes 2000; Lowe et al., 2008) for the last 20,000 yrs.

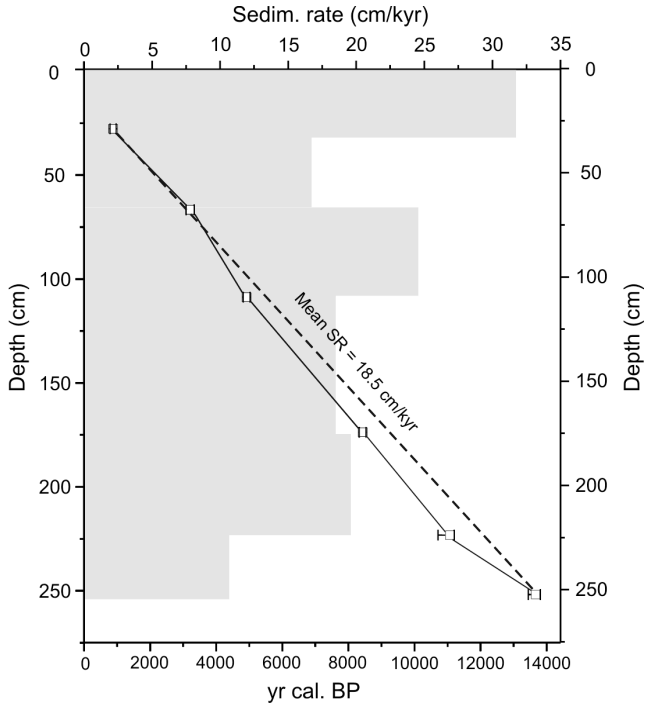

Figure 2. Sedimentation rates along 434G sediment core calculated linearly by six AMS ^{14}C ages (open squares) calibrated with Calib 6.0.2 software (Reimer et al., 2009) (see Table 1 for details). The mean sedimentation rate (SR) of 20 cm/kyr is represented by dashed line.

Similarly, the age model of the gravity core 434G is based on six AMS radiocarbon dates and linear interpolation (Table 1, Fig. 2) analyzed at the Poznan Radiocarbon Laboratory (Poland), using 10 mg of planktonic foraminifera *Globigerina bulloides* over 125 μm size fraction. The radiocarbon ages were calibrated to calendar years (yr cal. BP, being 0 BP equivalent to AD 1950) using Calib 6.0.2 software (Stuiver and Reimer, 1993) and the Marine09 calibration curve, with a correction for ocean surface reservoir effects of 400 yr (Reimer et al., 2009), spanning the last 14,000 yrs. Mean sedimentation rates obtained are 18.5 cm/kyr in core 434G and 20 cm/kyr in core 293G allowing the identification of millennial to centenial time-scale oscillations.

Table 1. Results of AMS ^{14}C carbon dating of single planktonic foraminifera *G. bulloides* (>125 μm) taken from TTR-17 core 433G.

Sample description	Core depth (cm)	Laboratory code	^{14}C AMS age (BP)	Calibrated age (yr cal. BP) (range 2σ)
434G 0 27-28.5	27.75	Poz-40736	1350 ± 35	788 - 970
434G 1 30-31.5	66.75	Poz-40737	3350 ± 40	3,090 - 3,331
434G 2 18-19.5	108.75	Poz-40738	4680 ± 40	4,819 - 5,020
434G 3 27-28.5	173.75	Poz-40739	7960 ± 50	8,329 - 8,535
434G 4 21-22.5	223.25	Poz-40740	10040 ± 90	10,713 - 11,199
434G 4 49.5-51	251.75	Poz-37154	12200 ± 70	13,440 - 13,808

* Calibration was done using Calib 6.0.2 software. We used the Marine09 calibration curve with standard marine correction of 400 years. (Data from two sigma probability interval).

2.3. Biomarker analysis

All the organic geochemistry analyses were conducted at the Royal Netherlands Institute for Sea Research (NIOZ). In core 434, sampling were carried continuously each 3 cm intervals (n = 84), while core 293G was sampled each 6 cm for the time interval spanning the Holocene, and each 3 cm with some interval at higher resolution, 1.5 cm, for the rest of the core (n = 95).

Freeze dried sediment samples were homogenized in agate mortar and subsequently extracted with an Accelerated Solvent Extractor (DIONEX ASE 200) using a solvent mixture of 9:1 (v/v) dichloromethane (DCM) to methanol (MeOH) at 100ºC and 7.6 x 10^6 Pa. The solvent of the extract was removed by rotary evaporation. The extracts were separated into apolar, ketone and polar fractions via pipette column chromatography filled with Al_2O_3 (activated for 2 h at 150ºC) using solvent mixtures of 9:1 (vol/vol) hexane/DCM, 1:1 (vol/vol) hexane/DCM, and 1:1 (vol/vol) DCM/MeOH, respectively.

2.3.1. Determination of alkenone temperatures

The ketone fraction (hexane/DCM 1:1; v/v) was redissolved in a small volume (20-100 μL) of hexane depending of the concentration of ketones in each sample. Identification of the di- ($C_{37:2}$) and tri-unsaturated ($C_{37:3}$) alkenones was performed on a Thermo Finnigan Trace Gas Chromatograph (GC) Ultra coupled to Thermo Finnigan DSQ mass spectrometer (MS). A 25-m CP Sil-5 fused silica capillary column was used (25 m x 0.32 mm; film thickness = 0.12 μm) with helium as the carrier

gas. The column was directly inserted into the electron impact ion source of the DSQ quadrupole mass spectrometer. Mass scans were made in the range of *m/z* = 50–800 with three scans per s and an ionization energy of 70 eV. The temperature program initiated at 70 °C, increased first at a rate of 20 °C per min to 130 °C, and then at a rate of 4 °C min to the final temperature of 320 °C, at which it was held for 10 min. For quantification, samples were analyzed on an HP 6890 GC using a 50-m CP Sil-5 column (0.32-mm diameter, film thickness of 0.12 µm) and helium as the carrier gas. The temperature of the oven was initiated at 70 °C and increased with a rate of 20 °C min^{-1} to 200 °C and subsequently with a rate of 3 °C per min^{-1} to 320 °C at which it was held for 25 min. Compound concentrations were determined by integration of relevant peak areas of alkenones.

The $U^{k'}_{37}$ index, defined as $C_{37:2}/(C_{37:2} + C_{37:3})$, was used to estimate SSTs (Prahl et al., 1988). $U^{k'}_{37}$ values were converted to SSTs by using the core top calibration of Müller et al., (1998):

$$U^{k'}_{37} = 0.033*SST + 0.044$$

Of the 84 samples analyzed from core 434G, 49 were run in duplicate, while 39 of the 95 samples from core 293G were run in duplicate and 4 were run in triplicate.

2.3.2. GDGT analysis

The polar fractions of the extracts, containing the GDGTs, were blown down under a stream of nitrogen, redissolved by sonication (5 min) in 200 µL hexane/propanol (99:1; v/v), and filtered through 0.45 µm polytetrafluoroethylene (PTFE) filters. GDGTs were analyzed by high-pressure liquid chromatography–mass spectrometry (HPLC/MS) following the methods described by Hopmans et al., (2000), with minor modifications (Schouten et al., 2007). Samples were analyzed on an Agilent 1100 series LC/MSD SL with an auto-injector and Chemstation software.

Quantification of the GDGT compounds was achieved by integrating the peak areas at *m/z* = 1300, 1298, 1296, 1292, 1050, 1036 and 1022, and using a C_{46} GDGT internal standard. A Prevail Cyano column (150 mm × 2.1 mm, 3 mm) was used with 99:1 hexane:propanol (vol:vol) as an eluent. After the first 5 min, the eluent increased by a linear gradient up to 1.8% isopropanol (vol) over the next 45 min at a flow rate of 0.2 mL/min. Scanning was performed in single ion monitoring (SIM) mode to increase sensitivity and reproducibility.

The TEX_{86} ratio was calculated following Schouten et al., (2002):

TEX_{86} = [GDGT 2 + GDGT 3 + crenarchaeol regioisomer] / [GDGT 1 + GDGT 2 + GDGT 3 + crenarchaeol regioisomer]

where 1, 2, and 3 are the concentrations of GDGTs with one or more cyclopentane moieties.

TEX_{86} values (TEX^{H}_{86}) were converted to SSTs using the calibration proposed by Kim et al., (2010) where,

$SST = 38.6 + 68.4 * \log(TEX^{H}_{86})$

The Branched and Isoprenoid Tetraether (BIT) index is based on the relative abundance of non-isoprenoidal glycerol dialkyl glycerol tetraethers (GDGTs) derived from organisms living in terrestrial environments versus a structurally related isoprenoid GDGT ‘‘crenarchaeol’’ produced by marine thaumarchaeota; hence representing marine versus soil organic matter input to the sediments. The BIT index was calculated according to Hopmans et al., (2004):

BIT = [GDGT-I + GDGT-II + GDGT-III] / [Crenarchaeol + GDGT-I + GDGT-II + GDGT-III]

where I, II, and III are concentrations of branched GDGTs.

The BIT soil carbon proxy can range between 0 and 1, where 1 means high amounts of soil organic matter input (Hopmans et al., 2004).

In core 434G, 13 of the 84 samples analyzed were run in duplicate, while 4 of the 95 samples measured in core 293G were re-run for TEX^{H}_{86} and the BIT index.

3. Results

3.1. SST estimates in core 293G based on the $U^{k'}_{37}$ index and the TEX^{H}_{86}

$U^{k'}_{37}$-SST estimates vary between 10.1ºC, which is reached at the offset of the Last Glacial Maximum (LGM) (at 17.7 kyr cal. BP), and 20.4ºC registered at 0.1 kyr cal. BP (Fig. 3). The Bölling-Alleröd (B-A) period shows rapid SST fluctuations between 12.8ºC and 17.9ºC in a similar way to the oscillations observed in the $\delta^{18}O$ values of planktonic foraminifera (Rodrigo-Gámiz et al., 2011) (Fig. 3). Holocene SSTs vary by ca. 2ºC with minimum values of 18.8ºC reached at 1.5 kyr cal. BP and maximum of 20.4ºC at present-time (Fig. 3).

The TEX^{H}_{86}-SST record is in comparison with the $U^{k'}_{37}$-SST record rather stable. TEX^{H}_{86}-SSTs range from minimum values of 11.4ºC at 16.0 kyr cal. BP and maximum of 26ºC reached during the Holocene at 3.7 kyr cal. BP (Fig. 3). A progressive increase in SSTs is recorded from the Last Heinrich event (H1) (11.4ºC) to the Bölling-Alleröd period (20.5ºC) and then a progressive decrease to the Younger Dryas onset (YD) (16.1ºC). The YD presents a short cooling period with a sharp SST increase (21.4ºC) and progressive trend to the Holocene onset (22.7ºC).

The BIT index presents similar values since the onset of the deglaciation between 0.01 and 0.08, reaching a maximum value of 0.17 at the LGM offset (Fig. 3).

3.2. SST estimates in core 434G based on the $U^{k'}_{37}$ index and the TEX^{H}_{86}

Core 434G spans the last 14,000 yrs recording SST fluctuations since the Alleröd period. $U^{k'}_{37}$-SST estimates varying between 13.8ºC during the Younger Dryas (YD) at 12.0 kyr cal. BP, and 22.3ºC reached at 4.4 kyr cal. BP (Fig. 4), with Holocene SSTs variations by ca. 2ºC.

The TEX^{H}_{86}-SST derived range between 17ºC recorded at 12.0 kyr cal. BP and 26ºC reached at both 4.7 and 3.7 kyr cal. BP (Fig. 4). The Holocene shows a stable SST-trend with minor-scale fluctuations.

The BIT index presents low values ranging between 0.01 and 0.04 (Fig. 4).

A cross-plot between TEX^{H}_{86}- and $U^{k'}_{37}$-derived SSTs in both cores shows a good correlation but also reveals that the amplitude of SST changes for TEX^{H}_{86} is substantially lager than for $U^{k'}_{37}$ (Fig. 5).

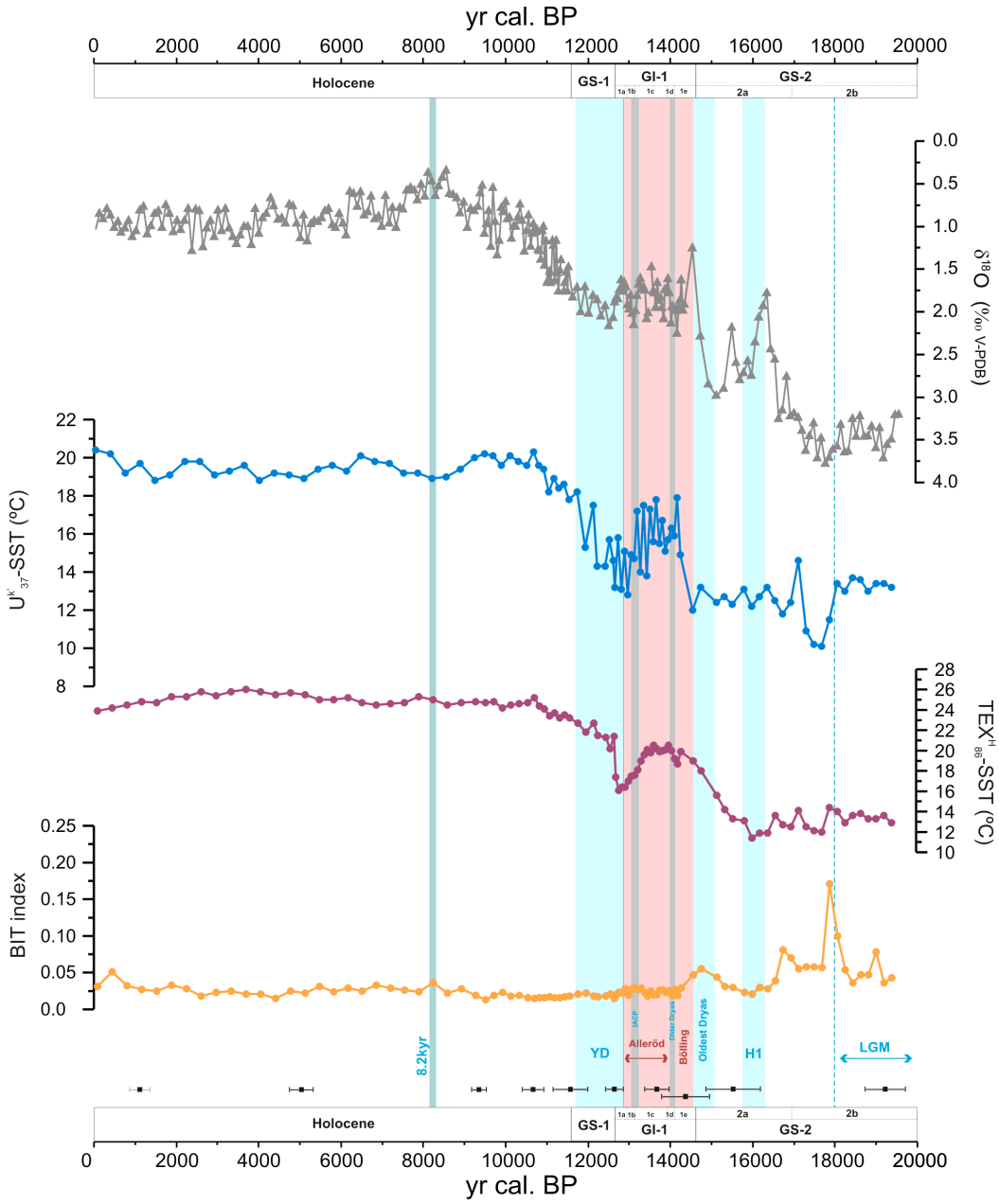
yr cal. BP
0
2000
4000
6000
8000
10000
12000
14000
16000
18000
20000
Holocene
GS-1
GI-1
1a 1b
1c
1d
1e
GS-2
2a
2b
δ18O (‰ V-PDB)
0.0
0.5
1.0
1.5
2.0
2.5
3.0
3.5
4.0
U^k'37-SST (°C)
22
20
18
16
14
12
10
8
TEX^H86-SST (°C)
28
26
24
22
20
18
16
14
12
10
BIT index
0.25
0.20
0.15
0.10
0.05
0.0
8.2kyr
YD
IACP
Alleröd
Older Dryas
Bölling
Oldest Dryas
H1
LGM

Figure 3. Age profiles of stable $\delta^{18}O$ record of the planktic foraminifera *G. bulloides* (Rodrigo-Gámiz et al., 2011), $U^{k'}_{37}$ and TEX^{H}_{86}-SST records, and BIT index from core 293G.
Light red vertical bars indicate warm periods such as Alleröd (A), and Bölling (B) time intervals. Short dashed blue vertical line indicates the offset of the Last Glacial Maximum (LGM) time interval. Light blue bars indicate main cold periods, the last Heinrich event (H1), Oldest Dryas, Older Dryas, Intra-Alleröd Cold Period (IACP), Younger Dryas (YD), and the "8.2 kyr" cold event (Alley et al., 1997). White horizontal boxes indicate Greenland Stadials (GS-1, GS-2), Interstadials (GI-1) and Holocene. Chronostratigraphy timing subdivisions are based on ^{14}C AMS dates and stable oxygen isotope stratigraphy from Greenland ice-cores published by Stuiver and Grootes (2000), and Lowe et al., (2008).

4. Discussion

4.1. Paleo-temperature records in the Alboran basin during the last 20,000 yrs: $U^{k'}_{37}$ and TEX^{H}_{86}

The thermal history along the Alboran Sea basin has been reconstructed using SST-derived from $U^{k'}_{37}$ and TEX^{H}_{86} since the LGM in the eastern area and for the last 14,000 yr cal. BP in the western. TEX^{H}_{86} can be influenced by fluvial input of soil-derived isoprenoid GDGTs, which is denoted by a BIT index >0.3 (Weijers et al., 2006). Particularly, the influence of soil organic matter in both Alboran records is likely negligible, with maximum BIT values of 0.17 in the eastern basin and 0.04 in the western (Figs. 3, 4), being the TEX^{H}_{86} a useful tool to reconstruct SSTs.

Previous studies using both organic paleothermometers in the western and eastern Mediterranean, claim to a seasonal divergence in both proxies, pointing to warmer TEX^{H}_{86}-SST than estimated from $U^{k'}_{37}$ particularly during the MIS7 interglacial and for the Late Holocene (Castañeda et al., 2010; Huguet et al., 2011; Nieto-Moreno et al., submitted).

SST-estimates in core 293G during the LGM (20,000-18,000 yr cal. BP) range between 13.0ºC and 13.7ºC from $U^{k'}_{37}$ and 12.9-14.4ºC from TEX^{H}_{86} (Fig. 3). Thus, alkenones point to absolute temperature variations of ±0.7ºC, while thaumarchaeota indicate slightly major oscillations in a range of ±1.5ºC.

The SSTs amplitude oscillations suggest a similar pattern in both paleothermometer records during the Late Pleistocene in agreement with TEX^{H}_{86}-SSTs recorded in the eastern Mediterranean (Castañeda et al., 2010), although with slightly lower values (15º-17ºC).

However, SST minima are reached at the LGM offset, as previously has been documented by $U^{k'}_{37}$-SST and Mg/Ca in benthic foraminifera in the Alboran basin (Cacho et al., 2001, 2006; Martrat et al., 2004), and by TEX^{H}_{86}-SST in the eastern Mediterranean (Castañeda et al., 2010). The last Heinrich event (H1) depict $U^{k'}_{37}$-SST of 12.2ºC and TEX^{H}_{86}-SST of 11.4ºC (Fig. 3), although alkenones present a minimum value of 10.1ºC at 17.7 kyr cal. BP. This cold period has been proposed as result of North Atlantic icebergs melting inflow through the Strait of Gibraltar (e.g., Cacho et al., 1999, 2002; Sierro

et al., 2005) showing its imprint in the oxygen isotopes profile (Fig. 3) as well as the major percentages of the cold-water foraminifera *N. pachyderma* (sinistral) (Sierro et al., 2005), and maximum peaks of *E. huxleyi* (>4 mm) (Pérez-Folgado et al., 2003). Alkenone unsaturation ratios and planktonic δO^{18} records from the Mediterranean have also revealed SSTs variations between 11º-15ºC prior to 13.0 kyr cal. BP (Emeis et al., 2000).

In general, SST-derived from both biomarkers present one-again similar oscillation patterns from the last 18,000-14,500 yr cal. BP with $U^{k'}_{37}$-SST ranging between 10.1ºC and 14.6ºC, and TEX^{H}_{86}-SST varying from 11.4ºC to 14.2ºC. Thus, it seems improbable seasonal or depth-life differences between both paleothermometers from the last 18,000-14,500 yr cal. BP (Bentaleb et al., 1999; Wuchter et al., 2005; Prahl et al., 2006). Additionally, this is in accordance with the previous reconstructed temperatures in the Alboran Sea during the stadial periods for the penultimate climate cycle (Huguet et al., 2006). Thus, SST coolings in the westernmost Mediterranean could be triggered by two possible and non-contradictory mechanisms, an intensification of the westerlies and major WMDW formation reaching the Alboran area, and fresher Atlantic water inflows (AMW) during the H1, as it has been demonstrated by a δO^{18} anomaly in the Alboran basin (Sierro et al., 2005; Rodrigo-Gámiz et al., 2011).

Then a progressive warming trend is recorded in TEX^{H}_{86}-SST through the Oldest Dryas (15,070 – 14,670 yr cal. BP) reaching temperatures of 19.9ºC at the Bölling period onset, while $U^{k'}_{37}$-SST record a rapid and abrupt SST oscillation from 12.4ºC to 17.9ºC (Fig. 3).

The temperature evolution through the B-A period is recorded at the two sites, although major divergence between SSTs derived from both proxies is started to appear. In the eastern area, $U^{k'}_{37}$ and TEX^{H}_{86} proxies depict temperatures of 17.9ºC and 20.5ºC respectively (Fig. 3), while in the western Alboran SST-derived temperatures record of 17.0ºC with $U^{k'}_{37}$ and 19.4ºC with TEX^{H}_{86} (Fig. 4). A stable Mediterranean thermohaline circulation during this warm period is demonstrated with SST variations along the Alboran basin of ±1.0ºC. Moreover, stagnation of the water-column and low deep-water ventilation, as consequence of the global increase in the sea level following the deglaciation, higher productivity and/or increased river runoff, favoured the last Organic Rich Layer deposition (ORL1) in the Alboran Sea (e.g., Cacho et al., 2002; Rodrigo-Gámiz et al., 2011). In spite of a homogenous pattern is registered in the alkenone-434G record, short time fluctuations are evidenced in the alkenone-293G record (Figs. 3, 4). Comparable fluctuations have been illustrated with the oxygen isotope profile in this eastern record (Fig. 3).

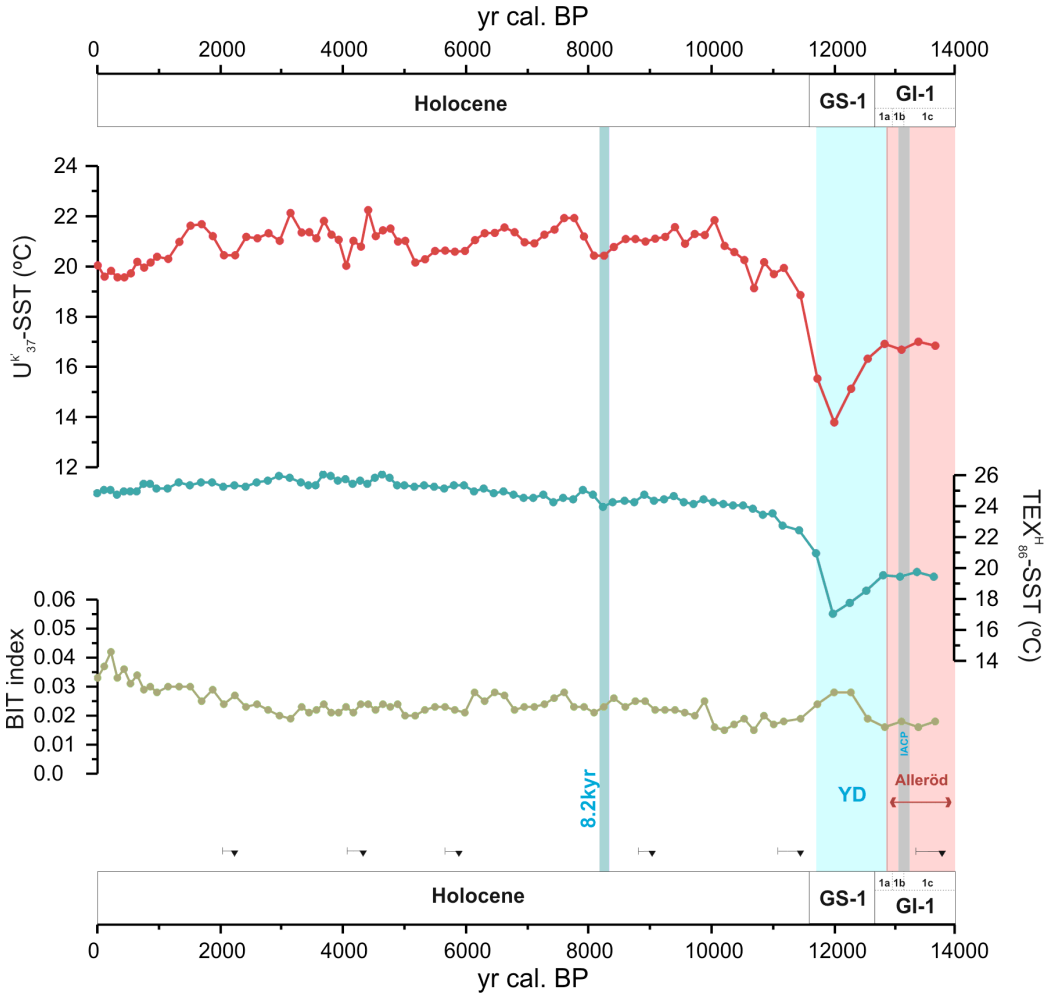

Figure 4. Age profiles of $U^{k'}_{37}$ and TEX^{H}_{86}-SST records, and BIT index from core 434G. Color-coded vertical bars indicate warm and cold periods as described in Fig. 3.

Nutrient availability fluctuations or salinity fluctuations and hence seasonal changes in the coccolith blooms in the East Alboran basin, could be an explanation for the rapid $U^{k'}_{37}$-SST oscillations and their incipient divergence from TEX^{H}_{86}-SST derived (Prahl et al., 2006). Salinity oscillations could affect also to the stable oxygen isotopes, although it could be discarded due the general stable thermohaline circulation during the B-A period. In contrast, more stable nutrient flux by the upwelling zone in the western Alboran basin could have led to a more regular $U^{k'}_{37}$-SST evolution (e.g., Rodríguez et al., 1998; García-Gorriz and Carr, 2001).

It is also important to note that the high-resolution in the eastern record during the B-A points out a rapid decrease in TEX^{H}_{86}-SST just during the cooler short period Older Dryas (14,090 – 14,010 yr cal. BP) (Fig. 3). This short-lived climate oscillation has been documented in circum-Atlantic records, being related with decreased in warm surface waters (e.g., Björck et al., 1996; Kroon et al., 1997).

Then, a progressive decreasing temperature trend during the Alleröd terminates in the YD onset (12,890 yr cal. BP), with SST-derived from $U^{k'}_{37}$ and TEX^{H}_{86} oscillating in the eastern between 12.8ºC and 16.1ºC respectively and 13.8ºC and 17.0ºC respectively in the western Alboran basin (Figs. 3, 4). In this case, major SST shift in the eastern Alboran basin could record the Mediterranean strengthening effect of Atlantic fresh-water inflow (Cacho et al., 2001).

The YD paleo-T evolution presents different patterns, in the eastern area $U^{k'}_{37}$-SST shows a tooth-saw increase reaching 18.2ºC at the offset, while TEX^{H}_{86}-SST depicts a sharp increase (21.4ºC) at 12,653 yr cal. BP with more stable values until the end of the YD (22.7ºC) at 11,650 yr cal. BP (Fig. 3). In contrast, paleo-T derived from both biomarkers in the western Alboran show a similar pattern with progressive SST raise with values of 18.9ºC (from $U^{k'}_{37}$) and 22.4ºC (from TEX^{H}_{86}) at the YD offset (Fig. 4). One again, $U^{k'}_{37}$ index in the eastern site present a more SST fluctuations probably related with nutrient availability, salinity or changes in preservation (Prahl et al., 2006; Mollenhauer et al., 2007, 2008). High productivity levels during the YD has been described previously in the eastern (Rodrigo-Gámiz et al., 2011) and western Alboran basins (Bárcena et al., 2001), suggesting that the meteorological conditions, with increased westerlies, intensified the hydrological flow to the east, driving an eastward migration of the WAG (Bárcena et al., 2001).

Furthermore, in both cases, the cold phase present a brief duration (around 700-800 yrs) according to previous Mediterranean records documented (Cacho et al., 2001), with earlier warming in the SST Mediterranean than over the Greenland (Grootes et al., 1993). In the eastern Mediterranean, the YD termination also documented a delayed warming with a gradual transition into the Holocene (Castañeda et al., 2010). The atmospheric circulation, such as southward displacement of the North Atlantic polar front winter storm tracks, might also have played an important role in the southward propagation of the cold YD period (e.g., Renssen et al., 1996).

During the Holocene (11,650 yr cal. BP – present) the eastern-western SST evolution ranges of 18.2-20.4ºC, and 18.9-22.3ºC in $U^{k'}_{37}$-SST, and 22.7-26ºC and 22.4-26ºC in TEX^{H}_{86}-SST in the respective basins (Figs. 3, 4). Thus, the TEX^{H}_{86} proxy have revealed a homogenous SST values in both regions, although with absolute values higher than those inferred from $U^{k'}_{37}$, while $U^{k'}_{37}$ index present warmer SST reached in the western site. An inversion in the main season of production for the

thaumarchaeota (e.g., from winter to summer) could be a plausible explanation for the notable TEX^{H}_{86}-SST shift from the LGM to the Holocene.

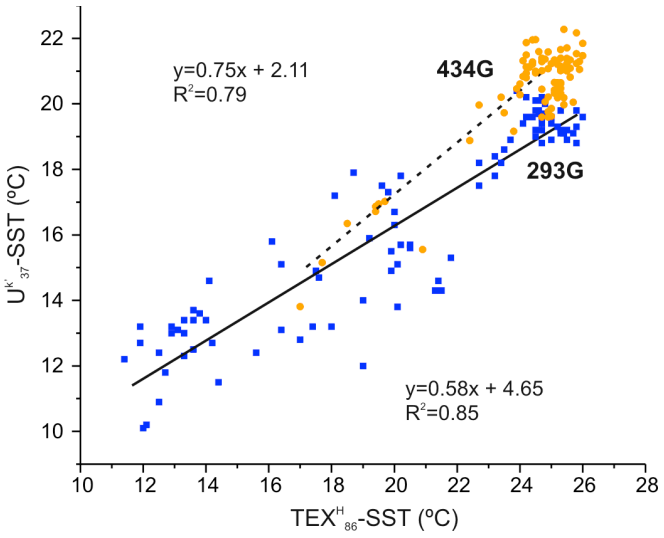

Figure 5. Correlations between TEX^{H}_{86}-SST and $U^{k'}_{37}$-SST in both records, 293G (blue squares) and 434G (orange circles).

The $U^{k'}_{37}$-SST in the eastern Alboran range between 18º and 20ºC in agreement with previous alkenone records and average summer SST (21ºC) during the early Holocene inferred from MAT (Cacho et al., 2001; Jiménez-Espejo et al., 2008), whereas that $U^{k'}_{37}$-SST in the westernmost Alboran are similar to the alkenone record in the Gulf of Cadiz (19º-22ºC) (Cacho et al., 2001). This Holocene variability was proposed as an Atlantic cooling amplification signal by winter continental winds through out the Mediterranean (Cacho et al., 2001).

The superficial oceanographic circulation in the 434G core site influenced by the WAG, and the major influence of the Mediterranean deeper water masses in the 293G core site would also cause these differences in maximum $U^{k'}_{37}$-SSTs between eastern and western Alboran basins (Millot, 1999).

4.2. SST evolution from the West to the East Alboran basin

The high-resolution of both marine records has allowed a SST assessment between the West and the East Alboran basin over the last 14,000 yrs. Then we will center in the Holocene SST-oscillations and their relationships with other nearby records.

As we mentioned above, both records register the SST decreasing trend from the B-A to the YD, and a developed difference in the absolute SST values obtained with both proxies is observed, with a possible inversion in the production season for the thaumarchaeota since the LGM. This major divergence in the absolute SSTs between both biomarkers was also obtained in the eastern

Mediterranean (Castañeda et al., 2010). However, in spite of the different paleo-T evolution in each area during the cold YD period, another interesting issue is the short cooling duration recorded at both sites (Fig. 6).

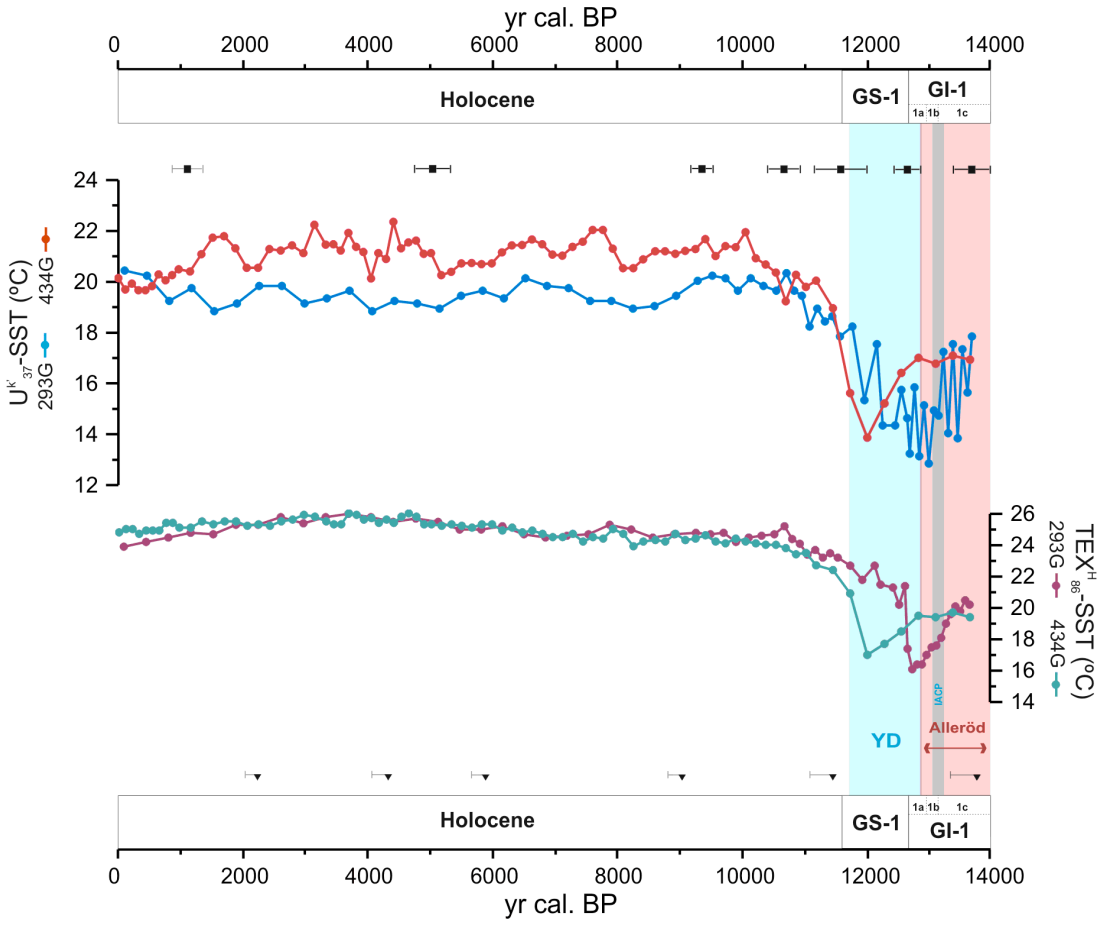

Figure 6. Comparison of $U^{k'}_{37}$ and TEX^{H}_{86}-SST records from both cores 293G and 434G for the last 14,000 yr cal. BP. Squares and inverted triangles correspond to AMS ^{14}C ages from cores 293G and 434G respectively. Color-coded vertical bars indicate warm and cold periods as described in Fig. 3.

The YD period has been recognized in the western Mediterranean as a period not as cold as has been recorded at higher latitudes (e.g., Maslin et al., 1995). Several records from the Iberian sector and western Mediterranean region have documented the occurrence of climatic changes during the YD, pointing to an early cold/dry phase with a warmer/more humid episode during the latter phase (e.g., Genty et al., 2006; Combourieu Nebout et al., 2009; Naughton et al., 2007; Rodrigo-Gámiz et

al., 2011). In the eastern Mediterranean and Red Sea, both proxies have experienced a gradual transition from the YD termination to the Holocene (Arz et al., 2003; Castañeda et al., 2010). Thus, the SST records obtained also seem to evidence the two YD phases in the oceanographic context.

Furthermore, the influence in the western basin of the surface WAG and the proximity to the Iberian margin could also reduce the YD cooling with SST-derived from $U^{k'}_{37}$ and TEX^{H}_{86} ranging in the eastern between 12.8ºC and 16.1ºC and in the western between 13.8ºC and 17.0ºC respectively (Fig. 6).

During the Holocene, the TEX^{H}_{86}-SST in both sub-basin sites present a quite similar trend with stable SSTs profiles presenting SSTs-onset of 23.2ºC in the eastern basin and 22.4ºC in the western, and reaching maximum values of 25.3ºC and 25ºC at 7.9 kyr cal. BP respectively (Fig. 6). In contrast, $U^{k'}_{37}$-SST derived from both cores, present notable differences in the magnitude of the SSTs oscillations as well as in the absolute temperature values (Fig. 6). In general, SSTs derived from alkenones in the eastern basin present fresher values than in the western basin, ranging between 20.4ºC and 17.8ºC, and between 22.3ºC and 18.9ºC in the respective sites (Fig. 6). Thus, the different responses between both biomarkers could suggest that the thaumarchaeota is less affected by the site localization of the cores than the haptophyte. Among the factors that could influence this discrepancy is the depth-influence of the alkenone production in the water column (e.g., Prahl et al., 2006). Haptophyte are light- and nutrient-organism dependents with dominant zone of production of 10-40 m in a stratified water column (e.g., Ternois et al., 1997; Bentaleb et al., 1999; Cacho et al., 2001) might reflect the SSTs of the maximum production zone. Conversely, the thaumarchaeota is a non-dependent light and nutrient organisms, which could life at depth up 100 m (Prahl et al., 2006), reflecting temperatures from these deeper water layers (Wutcher et al., 2005).

Another interesting observation is that the amplitude of SST changes for thaumarchaeota is substantially larger than for haptophyte in both regions (Fig. 5). An open question is concerning the seasonality impact in both biomarkers, reflecting annual mean vs. seasonal derived SSTs. This seasonality feature has been also documented in this region during the penultimate climate cycle and for the Late Holocene (Huguet et al., 2011; Nieto-Moreno et al., submitted).

Based on the temporal distribution of pigment concentrations in the Alboran Sea, two main regimes of primary production have been distinguished (García-Gorriz and Carr, 2001): the bloom regime (from November to March), linked to the winter mixing waters, and the non-bloom period (from May to September), when surface water stratification prevails in the Alboran Sea and nutrients are mostly supplied by the different upwelling zones.

Conversely thaumarchaeota might present a preferred growth season during summer-autumn with major export flux of GDGTs from the surface waters (Wutcher et al., 2006b).

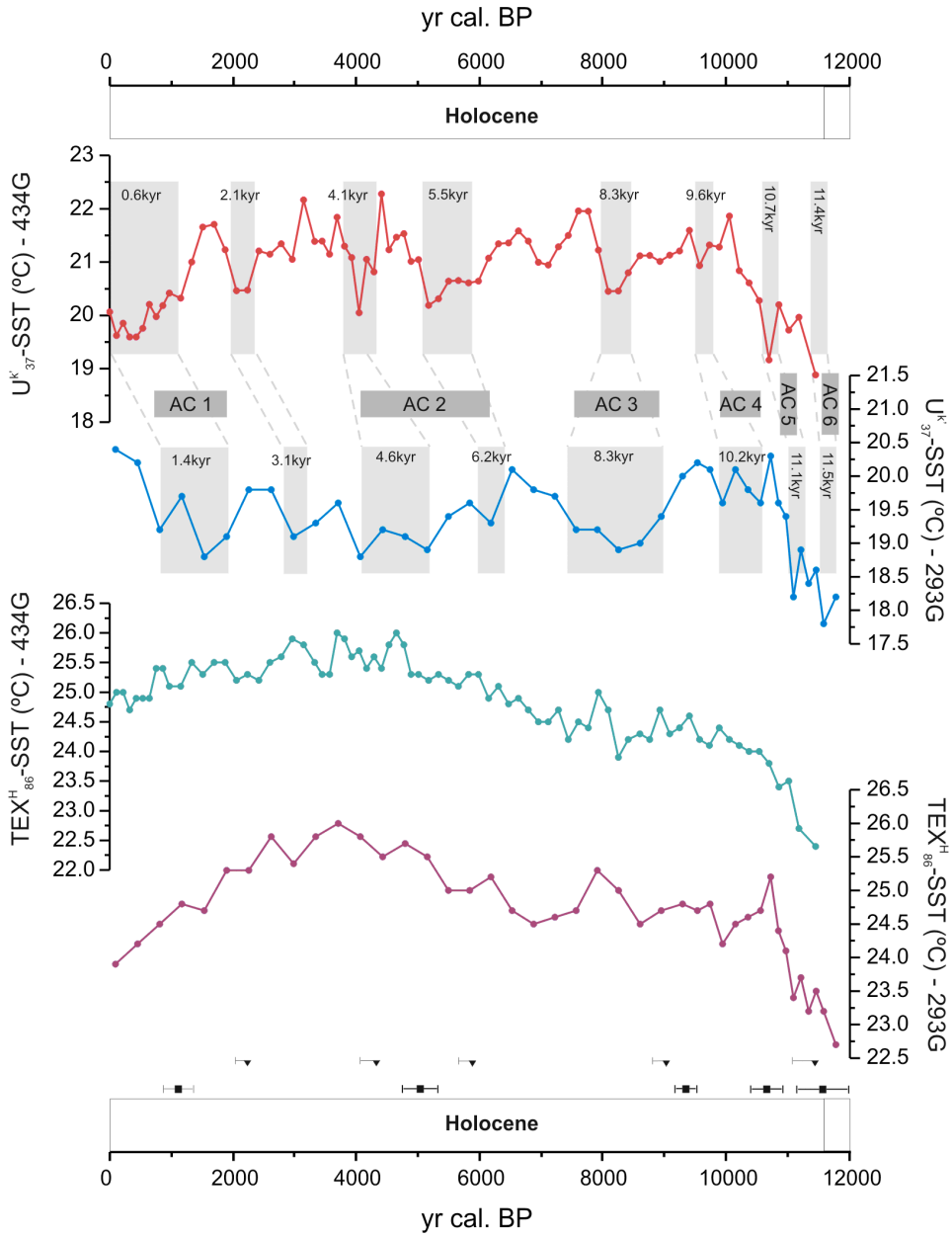

Figure 7. Holocene profiles of $U^{k'}_{37}$-SST and TEX^{H}_{86}-SST from 293G and 434G records. Squares and inverted triangles correspond to AMS ^{14}C ages from cores 293G and 434G respectively. AC6-AC1 corresponds to Alboran coolings described by Cacho et al., (2001) and grey bars indicate the different short-term cold events recognized in the two Alboran records.

Thus, coccolith fluxes of alkenone producing species *E. huxleyi* mainly could reflect spring SSTs due to its higher abundance is after turbulent winter conditions (Pérez-Folgado et al., 2003; Bárcena et al., 2004), while thaumarchaeota could reflect summer temperatures rather than mean SST as has been suggested in the Alboran basin (Huguet et al., 2011; Nieto-Moreno et al., submitted), in spite of both core top calibrations used to derive the SSTs in principle provide annual mean temperature estimate at surface level (Müller et al., 1998; Kim et al., 2010). Present-day average annual and summer temperatures at the upper water column are around 18ºC and 21ºC respectively, presenting both SST-derived higher values (MEDAR Group, Mediterranean Targeted Project II, Mass Transfer and Ecosystem Response, 2002, http://www.ieo.es).

Furthermore, several short-term cooling periods during the Holocene period (Fig. 7) registered in both alkenone records are in agreement with other abrupt climate events described in the North Atlantic region and Mediterranean nearby records (e.g., Bond et al., 1997; Cacho et al., 2001; Frigola et al., 2007; Combourieu Nebout et al., 2009). Some of these short-term cooling periods are also recognized in the thaumarcheota profiles, although with minor evidences in the western basin (Fig. 7).

Previous Alboran coolings (AC6-AC1) (Cacho et al., 2001) represented in Fig. 7 have also been recorded in our records although with a non-synchronous features. The two last cooling periods (AC6 and AC5) are almost synchronies in both sub-basins suggesting major divergence in the oceanographic response in both sub-basins since the deglaciation through out the Holocene (Fig. 7).

The most significant Holocene cooling documented previously is the 8.2 kyr period, broadly recognized in Greenland ice core records (e.g., Alley et al., 1997), as well as in western Mediterranean cores (AC3) (Cacho et al., 2001; Pérez-Folgado et al., 2003). This short-term cooling event was particularly significant during summer with an increase in cool-water species (*Globigerinoides ruber*), and a temperature drop of around 4ºC using MAT and $U^{k'}_{37}$ records (Pérez-Folgado et al., 2003).

This cold 8.2 kyr period is recorded in the western site as rapid oscillation with a decrease in temperature of about 0.6ºC, while in the eastern basin the cooling is recorded as more pronounced in terms of temperature and time period (about 1.3ºC) (Fig. 7). This amplification of the cooling signal transmitted by the Atlantic water inflow through the eastern Mediterranean areas, has been previously documented with oscillations in $U^{k'}_{37}$-SST of 1º-2ºC in the Alboran Sea and an intensification of 2.5-3ºC in the Tyrrhenian Sea (2.5º-3ºC) as consequence of stronger winter winds (Cacho et al., 2001). However, intense westerlies triggering major WMDW formation could also support the general cooling signal in the Alboran basin records.

However, a marked SST cooling event is observed between AC1 and AC2 dated at around 2.1 kyr cal. BP in the western basin and at around 3.1 kyr cal. BP in the eastern (Fig. 7), with $U^{k'}_{37}$-SST differences of 19.1ºC and 20.5ºC respectively (Fig. 7). This could suggest an enhance of upwelled cold-water in of the western Alboran (Fabres et al., 2002), which further supports our observation of the WAG influence in the western Alboran site. Moreover, a progressively SST-trend is observed for the Late Holocene in coherence with minimum SST-estimates during the Little Ice Age in core tops from the Alboran basin (Nieto-Moreno et al., submitted).

5. Conclusions

$U^{k'}_{37}$ and TEX^{H}_{86} SST records from the eastern and western Alboran Sea basins have provided a high-resolution temperature reconstruction for the last 20,000 and 14,000 yrs respectively. The last Heinrich event (H1) depict $U^{k'}_{37}$-SST of 12.2ºC and TEX^{H}_{86}-SST of 11.4ºC slightly lower than during the Last Glacial Maximum, influenced by the Atlantic meltwater inflow. Similar SST oscillations patterns in both haptophyte and thaumarchaeota records suggest similar seasonal or depth-life features. During the B-A warm period higher SST are evidenced in both marine records, although with different oscillations pattern, which suggests a more stable nutrient flux by the upwelling zone in the western basin. The YD is recorded as a brief and initial cold-phase with an abrupt SST increased to the Holocene in the eastern basin, and progressive increasing trend in the western. Several short-term cooling periods in both alkenone records during the Holocene are in coherence with other rapid events recorded in nearby regions.

Similar SST oscillations patterns in both haptophyte and thaumarchaeota records suggest similar seasonal or depth-life features from the LGM to the B-A, although an early discrepancy and progressive increased in the SST derived from both proxies during the Holocene is recorded. An inversion in the main season of production for the thaumarchaeota could be a plausible explanation for the notable TEX^{H}_{86}-SST shift from the LGM to the Holocene, indicating the TEX^{H}_{86} record summer temperatures. Higher absolute temperature values derived from haptophyta between the western and eastern sites are more accentuated through out the Late Holocene, suggesting major influence of the Alboran surface oceanographic circulation in the western basin.

Acknowledgements

This work was supported by Projects CGL2009-07603, CTM2009-07715, CSD2006-00041 (Ministerio de Ciencia e Innovación), 200800050084447 (MARM), Project RNM-5212, and Research Group RNM-179 (Junta de Andalucía). We would like thank the Training- Through-Research Programme (UNESCO-Moscow State University) regarding recovery of gravity cores 293G and 434G. We likewise thank to Anchelique Mets and Jort Ossebaar for their laboratory assistance.

8. Conclusions

The multi-proxy approach conducted on marine sediment records from the westernmost Mediterranean has provided a high-resolution time window reconstruction of paleoclimate and paleoceanographic oscillations since the LGM. The subsequent concluding remarks derive from the different specific objectives of this Thesis.

Concerning the paleoclimate conditions and the atmosphere response to climate variability over the last 20,000 yrs:

- The H1 has been characterized as the coldest and most arid period since the LGM offset, with increasing values of ratios used as eolian input proxies, such as Zr/Al, Ti/Al and Si/Al, as well as in palygorskite and quartz contents, also indicative of enhanced eolian supply.

- The B-A has been recognized as a generalized warm period implying progressively more humid conditions, denoted by a decrease in values of eolian detrital proxies, and a subsequent increase in typical fluvial proxies (Mg/Al, K/Al, Rb/Al ratios). A short-term IACP dry pulse has been also recognized

- During the YD, two distinct phases have been recorded; a slightly dry onset and more humid conditions towards the end of this time interval.

- The Holocene is characterized by apparent cycles of major humidity and aridity revealed by detrital proxies and a detailed comparison with nearby pollen records. Particularly, a significant shift in terrigenous input from 7.4 to 4.5 kyr cal. BP is recorded as decreased trend in the K/Al, Mg/Al and illite+chlorite/kaolinite ratios, suggesting an early decline of the African Humid Period (AHP).

- Radiogenic isotopes (Sr, Nd) evidence differences in the eolian dust provenance, separating a southern North Africa source area (Senegal and Guinea) during the cold period H1 and at around 8.9 kyr cal. BP and a dominant provenance from Morocco, Mali and Mauritania during warmer periods such as the B-A period. Furthermore, Pb isotopic signatures have shown a binary mixing between North Africa (less radiogenic) and European sources (more radiogenic).

Variations along the mixing line reflect enhanced inputs from North Africa during colder periods such as the last Heinrich event (16.7 kyr cal. BP), while prevailing European input (transported by river runoff) correspond to warm intervals such as Alleröd period (13.5 kyr cal. BP), and distinct Holocene phases (11.1, 9.4, 1.1 kyr cal. BP).

- Enhanced total detrital input during cold events were derived from the intensification of Saharan dust export across the western Mediterranean by southward migrations of the ITCZ over North Africa, also related with a predominant positive NAO index.

In terms of paleoceanographic conditions and oceanic climate responses the following remarks has been established:

- Cold events, such as the H1 and the early YD are characterized by enhanced productivity, which is supported by increased Ba/Al ratio, derived from biogenic barite and by higher TOC contents.

- The Last Organic Rich Layer deposition in the Alboran Sea occurred from the B-A onset to the demise at 8.9 kyr cal. BP. Such deposition appears to be related to aspiration forces between intermediate and deep water in the westernmost Mediterranean. Furthermore, Ba/Al ratios and TOC contents also indicate an organic enrichment prior to the ORL1 (pre-ORL1) during the H1.

- During the H1, an Atlantic freshwater influx from North Atlantic iceberg melting impacted the western Mediterranean, recorded by a strong shift toward lower $\delta^{18}O$ values.

- Major changes in the Mediterranean thermohaline circulation resulted in reoxidation events, as indicated by Mn/Al and Fe/Al peaks, involving variations in paleocurrents intensity just prior to H1. This suggests an active circulation during the GS-2a triggered by the WMDW formation induced by intensified northwesterlies, and followed by fresher AMW inflow during the H1. Conversely, diminished deep-water ventilation (high V/Al, Cu/Al and Zn/Al ratios) and paleocurrents intensity (low SS, and S/C ratio) were recognized during the B-A, which was

followed by a resumption of intense ventilation throughout the YD. A reactivation of the Mediterranean thermohaline circulation is also denoted at 8.9 yr cal. BP.

- Sea surface temperatures (SST) obtained from two molecular organic proxies ($U^{k'}_{37}$ and TEX^{H}_{86}) clearly reveal the transition from the LGM to the Holocene, showing SST increase of 7º ($U^{k'}_{37}$) and 12ºC (TEX^{H}_{86}). Minimum SSTs are reached at H1 (12.2ºC-$U^{k'}_{37}$ and 11.4ºC-TEX^{H}_{86}) whereas a progressive SST increase (17.9ºC) characterized the B-A period. During the YD, SST records have evidenced the two-YD phases; a short early cooling period and an abrupt SST increase into the Holocene in the eastern basin, while a more progressive increasing trend is recorded in the western basin. An inversion in the main season of production for the *Thaumarchaeota* (TEX^{H}_{86}) seems a plausible explanation for the notable SST shift from the LGM to the Holocene, indicating the TEX^{H}_{86} records summer temperatures. Differences in absolute temperature values, derived from *Haptophyta algae* ($U^{k'}_{37}$), between the western and eastern sites were more accentuated throughout the Late Holocene, suggesting major influence of the Alboran surface oceanographic circulation in the western basin.

The spectral analysis conducted on different paleonvironmental proxy records over the last 20,000 yrs has shown four main high-periodicity cycles related to different climate-forcing mechanisms: the 1,300 and 1,515 yr cycles appear to be linked to the North Atlantic climate and the African monsoon system; whereas obtained periodicities of 2,000 and 5,000 yrs correlate with records distributed around high-, mid-, and low-latitudes connected to solar activity and orbital forcing, sugesting similar forcing mechanism.

9. Conclusiones

La reconstrucción paleoclimática y paleoceanográfica de los últimos 20.000 años, llevada a cabo a partir del análisis de alta resolución e integración de numerosos indicadores procedentes de registros marinos del Mediterráneo más occidental, cuenca del mar de Alborán, ha permitido obtener las siguientes conclusiones en respuesta a los objetivos fundamentales inicialmente planteados en esta Tesis:

Respecto a las condiciones paleoclimáticas y la respuesta atmosférica a la variabilidad climática cabe señalar que:

- El último evento Heinrich (H1) se registra como el periodo más frío y seco desde el fin del Último Máximo Glacial, con un incremento en los valores de las relaciones geoquímicas indicadoras de aporte eólico, como son Zr/Al, Ti/Al y Si/Al, así como un incremento en los contenidos de minerales típicamente eólicos, cuarzo y paligorskita.

- El período Bölling-Alleröd (B-A) se ha reconocido generalmente como un intervalo de tiempo con unas condiciones más cálidas y con un incremento progresivo de la humedad. Se caracteriza por un descenso progresivo en el valor de los indicadores de aporte eólico y aumento de las relaciones geoquímicas correspondientes a indicadores fluviales (p. ej., Mg/Al, K/Al, Rb/Al). También se han registrado oscilaciones climáticas rápidas relacionadas con momentos de mayor aridez, como el “Intra-Alleröd Cold Period (IACP)”.

- Durante el Younger-Dryas (YD), han podido establecerse condiciones climáticas peculiares, identificándose una primera fase temprana más fría y seca, seguida por un periodo más húmedo hasta el final de este intervalo.

- Durante el Holoceno se han establecido oscilaciones climáticas rápidas que se han relacionado con cambios en la humedad y aridez, puestas de manifiesto por oscilaciones en los indicadores de aportes detríticos, tanto fluviales como eólicos, así como por su correlación con registros polínicos cercanos. En particular, cabe destacar el progresivo descenso en los aportes fluviales a partir de los 7.400 años BP, que sugiere un anticipado descenso de la terminación del “Periodo Húmedo Africano”, con un cambio hacia las condiciones semi-áridas y áridas actualmente reconocidas en el Norte de África.

- Los isótopos radiogénicos, como relaciones de Sr y Nd, han aportado una valiosa información sobre la procedencia del material eólico depositado en la cuenca del mar de Alborán. Se ha podido establecer que los aportes de material detrítico durante el periodo frío H1, y entorno a los 8.900 años BP, presentan una composición isotópica típica de materiales procedentes de las actuales regiones de Guinea y Senegal. Por el contrario, durante los periodos más cálidos, la composición isotópica indicaría un área fuente más próxima dentro del Norte de África, como serían materiales presentes en las regiones actuales de Marruecos, Mauritania y Mali. Además, las relaciones isotópicas de Pb también ofrecen información sobre la mezcla de material detrítico entre dos términos extremos; por un lado, los materiales con composiciones isotópicas de Pb equivalentes a las presentes en el Norte de África, mientras que en el otro extremo se encontrarían materiales con composición isotópica característica de procedencia Europea y del Sur de la Península Ibérica. Estos últimos habrían sido transportados por el sistema fluvial durante los períodos cálidos definidos como el Alleröd (hace unos 13.500 años BP), así como durante otros eventos cálidos reconocidos durante el Holoceno.

- Estas variaciones de material detrítico y mayor aporte eólico durante los eventos fríos en la cuenca del mar de Alborán, están principalmente condicionadas por las migraciones meridionales de la Zona de Convergencia Inter-Tropical y las consecuentes fluctuaciones en las trayectorias de circulación atmosférica sobre el Norte de África. Igualmente, con un índice positivo en la Oscilación del Atlántico Norte se favorecerían unas condiciones más áridas sobre el Sur de la Península Ibérica y Norte de África con un incremento en la intensidad de la circulación atmosférica y en consecuencia en el material eólico transportado.

Respecto a las variaciones en las condiciones paleoceanográficas, cabe señalar que:

- Durante los períodos fríos como el H1 y el YD se produjo un incremento en la productividad biológica, que se pone de manifiesto por el incremento en la relación Ba/Al derivado de la presencia de barita de origen biológico, así como por los altos contenidos en materia orgánica.

- El intervalo de tiempo correspondiente al depósito de la "última capa rica en materia orgánica" en la cuenca del mar de Alborán, abarca desde el comienzo del período cálido B-A hasta los 8.900 años BP. Además, un incremento en el contenido en carbono orgánico total así como en la relación Ba/Al durante el evento H1, sugieren el depósito de una capa rica en materia orgánica previa a la definida. El fin de este depósito puede relacionarse con fenómenos de aspiración entre masas de agua intermedias y profundas.

- Durante el evento H1 los isótopos estables de oxígeno presentan una marcada anomalía hacia valores de $\delta^{18}O$ menores, corroborando la entrada de aguas Atlánticas procedentes del deshielo de los glaciares.

- Cambios en la circulación termohalina dieron lugar a eventos de reventilación en el Mediterráneo más occidental antes del evento H1, tal y como han indicado las relaciones redox Fe/Al y Mn/Al, así como los indicadores de velocidad de corrientes de fondo. Esta mayor intensidad de la circulación termohalina estuvo favorecida por una intensificación de los vientos aliseos del noroeste, que caracterizó todo el periodo "stadial" de Groenlandia 2-a, seguido por una aminoración de la circulación debida a la entrada de aguas de origen Atlántico. Por otra parte, unas condiciones de circulación menos intensa de las aguas con menor oxigenación, como indican los altos valores en las relaciones geoquímicas V/Al, Cu/Al y Zn/Al y bajos valores en los indicadores de corrientes de fondo, se registraron durante el período B-A con una ligera interrupción durante el YD. Posteriormente, a los 8.900 años BP, comenzó la reactivación de la circulación termohalina Mediterránea .

- La reconstrucción de las temperaturas superficiales, basada en el análisis de dos testigos procedentes de las cuencas Este y Oeste del mar de Alborán, a partir del uso de dos indicadores de origen orgánico, índice $U^{k'}_{37}$ correspondiente a alquenonas biosintetizadas por *Hapthopyta algae*, e índice TEX^{H}_{86} basado en membranas lípidas isoprenoidales de *Thaumarchaeota* marinas, un nuevo filum de las Archaeas, ha puesto de manifiesto la transición climática desde el Último Máximo Glacial hasta el Holoceno. Se ha establecido una diferencia de temperatura de unos 7ºC mediante $U^{k'}_{37}$, y de 12ºC mediante TEX^{H}_{86}. Las temperaturas mínimas registradas correspondieron al evento H1 con valores de 12,2ºC-$U^{k'}_{37}$ y

11,4ºC-TEX^{H}_{86}, aumentando de manera progresiva hasta los 17,9ºC alcanzados durante el periodo B-A. La reconstrucción de paleotemperatura durante el evento YD también revela una primera fase de enfriamiento brusco, con un posterior incremento rápido de la temperatura en la cuenca Este del mar de Alboran, mientras que el incremento de temperatura hacia el Holoceno fue progresivo en la cuenca Oeste. Las diferencias en el valor absoluto de las temperaturas obtenidas con los dos indicadores orgánicos puede explicarse por una inversión en la estación de máxima producción de *Thaumarchaeota*, reflejando temperaturas de la estación de verano. Además, los valores de temperatura obtenidas con *Hapthopyta* son mayores en la cuenca Oeste de Alboran, sugiriendo una mayor influencia de la circulación oceánica superficial de Alboran en esta cuenca.

Finalmente, se integraron los distintos indicadores paleoclimáticos para llevar a cabo un análisis espectral que ha puesto de manifiesto la existencia de diferentes ciclicidades en la escala de las altas frecuencias y que se asocian a distintos mecanismos climáticos. Los ciclos de 1.300 y 1.515 años se relacionan con variaciones climáticas en el Atlántico Norte así como con las oscilaciones del sistema monzónico Africano; mientras que los ciclos de 2.000 y 5.000 años, también reconocidos en otros registros situados a latitudes altas, medias y bajas, parecen estar conectados con las variaciones de la actividad solar, así como con oscilaciones climáticas a escala orbital.

10. Perspectives and future works

The research work initiated with this Thesis will be completed with work in progress that will be summarized in upcoming manuscripts focused on:

(1) Development of a new mineralogical proxy for eolian input in marine sediments: A new methodology for identifying eolian Quartz in marine sediments will be based on grain size determination by spotty X-Ray diffraction rings. In general, quartz is known as a useful indication of eolian dust. In the particular case of the studied records, the analyses of quartz content has served to demonstrate an increase in grain-size and quartz contents during arid glacial periods compared to interglacial. For these mineralogical analyses, the use of XRD-2DScan is an ideal methodology, being a non-destructive, continuous and fast method to identify mineral phases where the mean intensity of the diffraction peaks integrated, i.e., spot-size of the diffraction rings, could be directly related with the grain size of the mineral particle. This enables a detailed characterization of eolian Saharan dust input in marine sediments from the western Mediterranean during major paleoclimate oscillations since the LGM.

(2) Further work in progress will consider a cyclostratigraphic approach through the study of the cyclic behavior of a group of proxies, since none of the proxies have a synchronous response to periodic climate oscillations. This study allows the identification of the leads and lags of different proxy records

(3) Another manuscript in preparation concentrates on the mineralogical and geochemical analysis of marine record 434G in order to reconstruct climate variability in the West Alboran Sea basin and their connection with the East Alboran basin, with special attention paid to detrital fluctuations during the YD and the early demise of the AHP during the Holocene.

(4) Furthermore, an East (Alboran Sea) – West (Gulf of Cadiz) transect is also being analyzed in terms of climate variability reconstruction since the LGM, which will improve the understanding of climate connections between the Mediterranean and the Atlantic.

(5) Post-doctoral contract at NIOZ (The Netherlands) will allow to extent my research field to marine organic biogeochemistry.

11. Agradecimientos/Acknowledgements

Llegado este punto, son muchas las personas a las que tengo que agradecer su colaboración y apoyo directo e indirecto, no menos importante, en este trabajo y al progreso del mismo durante todo este tiempo, sin los cuales hubiera sido más complicado llegar hasta aquí. Mi más profundo agradecimiento.

En primer lugar, mi más sincera y profunda gratitud a mi directora de tesis, Paqui, por su excepcional calidad profesional y humana, durante estos cortos y a la vez largos cuatro años de experiencias. Gracias por ofrecerme esta oportunidad y depositar tu confianza en mí para esta emprendedora etapa.

A mis padres y hermano, por vuestro ánimos y apoyo incondicional, gracias por todo lo que me habeis dado y por los valores que me habeis enseñado.

Lucas, ¡que paciencia la tuya! todas esas horas de ordenador junto a mí y esos descansos de paseo y reflexión…

Ramón, que puedo decir que no sepas, gracias por llevar "media vida" a mi lado, por tu paciencia y apoyo, fundamental en todo este tiempo. Gracias por estar ahí.

A todos mis compañeros del Instituto Andaluz de Ciencias de la Tierra, y en especial a aquellos con los que más he compartido horas de trabajo y discusiones (Alberto López Galindo, Menchu,…), al personal de apoyo técnico (Juan, Alpiste, Leti, Chari, Luisa, Manolo, …) y administrativo (Ana, Cristina, …), y cómo no a nuestro acogido Gert por su inolvidable e intensivo Paleoceanography Course, sus comentarios, bromas y sus wine and cheese tasting!

A Elisa, Carmen y Diana, no sólo gracias por esos cientos y cientos de molidos de muestras, ataques, etc., sino por ser unas personas maravillosas, y que os conste que sois parte importante de este trabajo.

A mis antecesores, Francis y David, y "scientific sisters" Vanesa, Carmina, Meri y Nieves, gracias por vuestros ánimos y ayuda.

Al Departamento de Mineralogía y Petrología, donde hasta hace poco he desarrollado este trabajo, su director Miguel Ortega y todos sus miembros (Isa, Emi, Jesús, Inés, Sandra, y un largo etc.), así como a Daniel Martín-Ramos y Alejandro Rodríguez-Navarro por las horas de trabajo y colaboraciones.

A Francis (Rodríguez-Tovar) un especial agradecimiento por compartir tu tiempo conmigo.

A "mis niñas" (Vero, Silvia, Pili, Rute, Carmen), y a Pedrito, por los momentos de alegría e ilusión, y por los no tan buenos, que sólo pueden ser fruto de la amistad y confianza que nos une.

A todos compañeros de despacho 29, antiguo y nuevo, que no son pocos los que han pasado o seguimos ligados a este gran número. Gracias Aitor, Juan, Erwin, Amel, Zoltan, Luis, Rita,…

A los compañeros de promoción, ¿quién nos iba a decir que nos volveríamos a encontrar? Carlos, Chema, Antonio, Maite, gracias por vuestro apoyo.

A los demás compañeros de las otras becarías y despachos: geodinámica (Vicente, Ana, Farida, John, Lourdes, …), mineralogía (Anna, Ana Luque, Pedro-pop, Iñaki, Maja, …), petrología (Anika, Sandra, Jose Alberto, Antonio,…), paleontología y estratigrafía (Gonzálo, Noel, …), etc.

11. Agradecimientos/Acknowledgements

A todo el personal del CIC (Olga, Mª del Mar, Alicia, Pepe, …) sin su coloboración no hubiera sido posible realizar todo esto.

A la sección de "Earth & Environmental Sciences" de la Universida de Ginebra, en especial a Dr. Daniel Ariztegui, Dr. Urs Schaltegger y Dr. Massimo Chiarada, por la acogida durante las estancias.

A "mis suizos" Paula, Adiela, Antoine, George, Cristina, Lisa… sin duda gracias por vuestra nobleza, por vuestro tiempo y por hacerme sentir como en casa (nunca mejor dicho) desde el primer hasta el último día!

Igualmente gracias al "Department of Marine Organic Biogeochemistry" de NIOZ, a su director Dr. Prof. Jaap Sinninghe Damsté por el recibimiento durante las dos estancias, al Dr. Stefan Schouten, Dr. Ellen Hopmans, y demás miembros del grupo (Anchelique, Jort, Sabine, Darcy, Nicole, Raquel, Claudia, Petra, etc.). De nuevo gracias Jaap por depositar tu confianza en mí para continuar en esta carrera investigadora.

A Julie y Craig, y muchas gracias Laura, por tu hospitalidad y disponibilidad durante el tiempo en Holanda.

A mis amigas de siempre!! todo un privilegio seguir unidas desde la infancia, con nuestros mejores y peores momentos que nos van haciendo mayores.

A mis ex-compañeros de Conanma, que me animaron a embarcarme en esta aventura.

A la gente de ASI-Granada por sus esfuerzos para un futuro mejor.

A Angela y Jean, por hacer del inglés una lengua algo más fácil.

Al resto de mi familia, y amigos, que de una u otra forma también me han ayudado y han confiado en mí.

Y cómo no, a todos los que se me olvida nombrar pero que saben que están en mi mente.

GRACIAS A TODOS por ser como sois!

12. References

Abouchami, W., Zabel, M., 2003. Climate forcing of the Pb isotope record of terrigenous input into the Equatorial Atlantic. Earth and Planetary Science Letters 213, 221-234.

Allen, J.R.M., Huntley, B., 2000. Weichselian palynological records from southern Europe: Correlation and chronology. Quaternary International 73-74, 111-125.

Alley, R.B., 2000. The Younger Dryas cold interval as viewed from central Greenland. Quaternary Science Reviews 19, 213-226.

Alley, R.B., Ágústsdóttir, A.M., 2005. The 8k event: Cause and consequences of a major Holocene abrupt climate change. Quaternary Science Reviews 24, 1123-1149.

Alley, R.B., Anandakrishnan, S., Dupont, T.K., Parizek, B.R., Pollard, D., 2007. Effect of sedimentation on ice-sheet grounding-line stability. Science 315, 1838-1841.

Alley, R.B., Mayewski, P.A., Sowers, T., Stuiver, M., Taylor, K.C., Clark, P.U., 1997. Holocene climatic instability: A prominent, widespread event 8200 yr ago. Geology 25, 483-486.

Alley, R.B., Meese, D.A., Shuman, C.A., Gow, A.J., Taylor, K.C., Grootes, P.M., White, J.W.C., Ram, M., Waddington, E.D., Mayewski, P.A., Zielinski, G.A., 1993. Abrupt increase in Greenland snow accumulation at the end of the Younger Dryas event. Nature 362, 527-529.

Andrews, J.T., Hardadottir, J., Stoner, J.S., Mann, M.E., Kristjansdottir, G.B., Koc, N., 2003. Decadal to millennial-scale periodicities in North Iceland shelf sediments over the last 12 000 cal yr: Long-term North Atlantic oceanographic variability and solar forcing. Earth and Planetary Science Letters 210, 453-465.

Arz, H.W., Pätzold, J., Müller, P.J., Moammar, M.O., 2003. Influence of Northern Hemisphere climate and global sea level rise on the restricted Red Sea marine environment during termination I. Paleoceanography 18, 31-31.

Asmerom, Y., Jacobsen, S.B., 1993. The Pb isotopic evolution of the Earth: inferences from river water suspended loads. Earth and Planetary Science Letters 115, 245-256.

Avila, A., Alarcón, M., Queralt, I., 1998. The chemical composition of dust transported in red rains - Its contribution to the biogeochemical cycle of a Holm Oak Forest in Catalonia (Spain). Atmospheric Environment 32, 179-191.

Bar-Or, R., Erlick, C., Gildor, H., 2008. The role of dust in glacial-interglacial cycles. Quaternary Science Reviews 27, 201-208.

Bárcena, M.A., Cacho, I., Abrantes, F., Sierro, F.J., Grimalt, J.O., Flores, J.A., 2001. Paleoproductivity variations related to climatic conditions in the Alboran Sea (western Mediterranean) during the last glacial-interglacial transition: The diatom record. Palaeogeography, Palaeoclimatology, Palaeoecology 167, 337-357.

Bárcena, M.A., Flores, J.A., Sierro, F.J., Pérez-Folgado, M., Fabres, J., Calafat, A., Canals, M., 2004. Planktonic response to main oceanographic changes in the Alboran Sea (Western Mediterranean) as documented in sediment traps and surface sediments. Marine Micropaleontology 53, 423-445.

Barker, S., Cacho, I., Benway, H., Tachikawa, K., 2005. Planktonic foraminiferal Mg/Ca as a proxy for past oceanic temperatures: A methodological overview and data compilation for the Last Glacial Maximum. Quaternary Science Reviews 24, 821-834.

Bassetti, M.A., Carbonel, P., Sierro, F.J., Pérez-Folgado, M., Jouët, G., Berné, S., 2010. Response of ostracods to abrupt climate changes in the Western Mediterranean (Gulf of Lions) during the last 30kyr. Marine Micropaleontology 77, 1-14.

Baudin, F., Combourieu-Nebout, N., Zahn, R., 2007. Signatures of rapid climatic changes in organic matter records in the western Mediterranean Sea during the last glacial period. Bulletin de la Société Géologique de France 178, 3-10.

12. References

Bea, F., 1996. Residence of REE, Y, Th and U in granites and crustal protoliths; implications for the chemistry of crustal melts. Journal of Petrology 37, 521-552.

Becker, J., Lourens, L.J., Hilgen, F.J., Van Der Laan, E., Kouwenhoven, T.J., Reichart, G.J., 2005. Late Pliocene climate variability on Milankovitch to millennial time scales: A high-resolution study of MIS100 from the Mediterranean. Palaeogeography, Palaeoclimatology, Palaeoecology 228, 338-360.

Beltagy, A.I., Chester, R., Padgham, R.C., 1972. The particle-size distribution of quartz in some North Atlantic deep-sea sediments. Marine Geology 13, 297-310.

Bentaleb, I., Grimalt, J.O., Vidussi, F., Marty, J.C., Martin, V., Denis, M., Hatte, C., Fontugne, M., 1999a. Erratum: The C37 alkenone record of seawater temperature during seasonal thermocline stratification (Marine Chemistry (1999) 64 (301-313) (PII: S030442039800079-6). Marine Chemistry 67, 145.

Bentaleb, I., Grimalt, J.O., Vidussi, F., Marty, J.C., Martin, V., Denis, M., Hatté, C., Fontugne, M., 1999b. The C37 alkenone record of seawater temperature during seasonal thermocline stratification. Marine Chemistry 64, 301-313.

Bergametti, G., Dutot, A.L., Buat-Menard, P., Losno, R., Remoudaki, E., 1989a. Seasonal variability of the elemental composition of atmospheric areosol particles over the northwestern Mediterranean. TELLUS, SER. B. CHEM. PHYS. METEOROL. 41, 353-361.

Bergametti, G., Gomes, L., Remoudaki, E., Desbois, M., Martin, D., Buat-Ménard, P., 1989b. Present transport and deposition patterns of African dusts to the north-western Mediterranean. In: Leinen, M., Sarnthein, M. (Eds.), Paleoclimatology and Paleometeorology: Modern and Past Patterns of Global Atmospheric Transport, NATO ASI Series, Mathematical and Physical Sciences 282, 227-250.

Berger, A., Loutre, M.F., 1991. Insolation values for the climate of the last 10 million years. Quaternary Science Reviews 10, 297-317.

Berger, A., Loutre, M.F., Mélice, J.L., 2006. Equatorial insolation: From precession harmonics to eccentricity frequencies. Climate of the Past Discussions 2, 519-533.

Berner, K.S., Ko, N., Godtliebsen, F., Divine, D., 2011. Holocene climate variability of the Norwegian Atlantic Current during high and low solar insolation forcing. Paleoceanography 26.

Béthoux, J.P., 1979. Budgets of the Mediterranean Sea. Their dependence on the local climate and on the characteristics of the Atlantic waters. Oceanologica Acta 2, 157-163.

Béthoux, J.P., 1980. Mean water fluxes across sections in the Mediterranean Sea, evaluated in the basis of water and salt budgets and of observed salinities. Oceanologica Acta 3, 79-88.

Bianchi, G.G., McCave, I.N., 1999. Holocene periodicity in North Atlantic climate and deep-ocean flow south of Iceland. Nature 397, 515-517.

Björck, S., Kromer, B., Johnsen, S., Bennike, O., Hammarlund, D., Lemdahl, G., Possnert, G., Rasmussen, T.L., Wohlfarth, B., Hammer, C.U., Spurk, M., 1996. Synchronized terrestrial-atmospheric deglacial records around the North Atlantic. Science 274, 1155-1160.

Blum, J.D., Erel, Y., 1997. Rb-Sr isotope systematics of a granitic soil chronosequence: The importance of biotite weathering. Geochimica et Cosmochimica Acta 61, 3193-3204.

Bond, G., Broecker, W., Johnsen, S., McManus, J., Labeyrie, L., Jouzel, J., Bonani, G., 1993. Correlations between climate records from North Atlantic sediments and Greenland ice. Nature 365, 143-147.

Bond, G., Heinrich, H., Broecker, W., Labeyrie, L., McManus, J., Andrews, J., Huon, S., Jantschik, R., Glasen, S., Simet, C., Tedesco, K., Klas, M., Bonanitt, G., Ivy, S., 1992. Evidence for massive discharges of icebergs into the North Atlantic ocean during the last glacial period. Nature 360, 245-XIII.

Bond, G., Kromer, B., Beer, J., Muscheler, R., Evans, M.N., Showers, W., Hoffmann, S., Lotti-Bond, R., Hajdas, I., Bonani, G., 2001. Persistent solar influence on north atlantic climate during the Holocene. Science 294, 2130-2136.

Bond, G., Showers, W., Cheseby, M., Lotti, R., Almasi, P., DeMenocal, P., Priore, P., Cullen, H., Hajdas, I., Bonani, G., 1997. A pervasive millennial-scale cycle in North Atlantic Holocene and glacial climates. Science 278, 1257-1266.

Bond, G., Lotti, R., 1995. Iceberg discharges into the North Atlantic on millennial time scales during the last glaciation. Science 267, 1005-1010. (ESTE ES EL MISMO AUTOR???)

Böttcher, M.E., Rinna, J., Warning, B., Wehausen, R., Howell, M.W., Schnetger, B., Stein, R., Brumsack, H.J., Rullkötter, J., 2003. Geochemistry of sediments from the connection between the western and the eastern Mediterranean Sea (Strait of Sicily, ODP Site 963). Palaeogeography, Palaeoclimatology, Palaeoecology 190, 165-194.

Bout-Roumazeilles, V., Combourieu Nebout, N., Peyron, O., Cortijo, E., Landais, A., Masson-Delmotte, V., 2007. Connection between South Mediterranean climate and North African atmospheric circulation during the last 50,000 yr BP North Atlantic cold events. Quaternary Science Reviews 26, 3197-3215.

Brassell, S.C., Eglinton, G., Marlowe, I.T., Pflaumann, U., Sarnthein, M., 1986. Molecular stratigraphy: a new tool for climatic assessment. Nature 320, 129-133.

Brauer, A., Günter, C., Johnsen, S.J., Negendank, J.F.W., 2000. Land-ice teleconnections of cold climatic periods during the last Glacial/Interglacial transition. Climate Dynamics 16, 229-239.

Braun, J.J., Viers, J., Dupré, B., Polve, M., Ndam, J., Muller, J.P., 1998. Solid/liquid REE fractionation in the lateritic system of Goyoum, East Cameroon: The implication for the present dynamics of the soil covers of the humid tropical regions. Geochimica et Cosmochimica Acta 62, 273-299.

Brochier-Armanet, C., Boussau, B., Gribaldo, S., Forterre, P., 2008. Mesophilic crenarchaeota: Proposal for a third archaeal phylum, the Thaumarchaeota. Nature Reviews Microbiology 6, 245-252.

Broecker, W.S., 1994. Massive iceberg discharges as triggers for global climate change. Nature 372, 421-424.

Broecker, W.S., 2000. Abrupt climate change: Causal constraints provided by the paleoclimate record. Earth Science Reviews 51, 137-154.

Broecker, W.S., Denton, G.H., Edwards, R.L., Cheng, H., Alley, R.B., Putnam, A.E., 2010. Putting the Younger Dryas cold event into context. Quaternary Science Reviews 29, 1078-1081.

Brumsack, H.J., 2006. The trace metal content of recent organic carbon-rich sediments: Implications for Cretaceous black shale formation. Palaeogeography, Palaeoclimatology, Palaeoecology 232, 344-361.

Brumsack, H.J., Wehausen, R., 1999. A geochemical record of precession-induced cyclic eastern Mediterranean sedimentation: Implications for northern Sahara humidity during the Pliocene. Naturwissenschaften 86, 281-286.

Bütikofer, J., 2007. Millennial scale climate variability during the last 6000 years–tracking down the Bond cycles. Diploma thesis. University of Bern, Switzerland. http://www.giub.unibe.ch/klimet/docs/diplom_jbuetikofer.pdf

Cacho, I., Grimalt, J.O., Canals, M., 2002. Response of the Western Mediterranean Sea to rapid climatic variability during the last 50,000 years: A molecular biomarker approach. Journal of Marine Systems 33-34, 253-272.

Cacho, I., Grimalt, J.O., Canals, M., Sbaffi, L., Shackleton, N.J., Schönfeld, J., Zahn, R., 2001. Variability of the Western Mediterranean sea surface temperature during the last 25,000 years and its connection with the Northern Hemisphere climatic changes. Paleoceanography 16, 40-52.

Cacho, I., Grimalt, J.O., Pelejero, C., Canals, M., Sierro, F.J., Flores, J.A., Shackleton, N., 1999. Dansgaard-Oeschger and Heinrich event imprints in Alboran Sea paleotemperatures. Paleoceanography 14, 698-705.

12. References

Cacho, I., Grimalt, J.O., Sierro, F.J., Shackleton, N., Canals, M., 2000. Evidence for enhanced Mediterranean thermohaline circulation during rapid climatic coolings. Earth and Planetary Science Letters 183, 417-429.

Cacho, I., Shackleton, N., Elderfield, H., Sierro, F.J., Grimalt, J.O., 2006. Glacial rapid variability in deep-water temperature and δ18O from the Western Mediterranean Sea. Quaternary Science Reviews 25, 3294-3311.

Cai, Y., Tan, L., Cheng, H., An, Z., Edwards, R.L., Kelly, M.J., Kong, X., Wang, X., 2010. The variation of summer monsoon precipitation in central China since the last deglaciation. Earth and Planetary Science Letters 291, 21-31.

Calvert, S.E., Pedersen, T.F., 2007. Chapter Fourteen Elemental Proxies for Palaeoclimatic and Palaeoceanographic Variability in Marine Sediments: Interpretation and Application, In: Hillaire-Marcel, C., De Vernal, A. (Eds.), pp. 567-644.

Caquineau, S., Gaudichet, A., Gomes, L., Legrand, M., 2002. Mineralogy of Saharan dust transported over northwestern tropical Atlantic Ocean in relation to source regions. Journal of Geophysical Research D: Atmospheres 107, 4-1-4-12.

Caquineau, S., Gaudichet, A., Gomes, L., Magonthier, M.C., Chatenet, B., 1998. Saharan dust: clay ratio as a relevant tracer to assess the origin of soil-derived aerosols. Geophysical Research Letters 25, 983-986.

Carrión, J.S., 2002. Patterns and processes of Late Quaternary environmental change in a montane region of southwestern Europe. Quaternary Science Reviews 21, 2047-2066.

Carrión, J.S., Andrade, A., Bennett, K.D., Navarro, C., Munuera, M., 2001a. Crossing forest thresholds: Inertia and collapse in a Holocene sequence from south-central Spain. Holocene 11, 635-653.

Carrión, J.S., Fernández, S., Jiménez-Moreno, G., Fauquette, S., Gil-Romera, G., González-Sampériz, P., Finlayson, C., 2010. The historical origins of aridity and vegetation degradation in southeastern Spain. Journal of Arid Environments 74, 731-736.

Carrión, J.S., Fuentes, N., González-Sampériz, P., Sánchez Quirante, L., Finlayson, J.C., Fernández, S., Andrade, A., 2007. Holocene environmental change in a montane region of southern Europe with a long history of human settlement. Quaternary Science Reviews 26, 1455-1475.

Carrión, J.S., Munuera, M., Dupré, M., Andrade, A., 2001b. Abrupt vegetation changes in the Segura mountains of southern Spain throughout the Holocene. Journal of Ecology 89, 783-797.

Carrión, J.S., Van Geel, B., 1999. Fine-resolution Upper Weichselian and Holocene palynological record from Navarres (Valencia, Spain) and a discussion about factors of Mediterranean forest succession. Review of Palaeobotany and Palynology 106, 209-236.

Cartes, J.E., Maynou, F., Fanelli, E., 2011. Nile damming as plausible cause of extinction and drop in abundance of deep-sea shrimp in the western Mediterranean over broad spatial scales. Progress in Oceanography 91, 286-294.

Castañeda, I.S., Schefuß, E., Pätzold, J., Sinninghe Damsté, J.S., Weldeab, S., Schouten, S., 2010. Millennial-scale sea surface temperature changes in the eastern Mediterranean (Nile River Delta region) over the last 27,000 years. Paleoceanography 25, PA1208.

Chamley H. 1989. Clay Sedimentology. Springer-Verlag, Berlin and New York.

Chen, W., Dong, B., Lu, R., 2010. Impact of the Atlantic Ocean on the multidecadal fluctuation of El Niño-Southern Oscillation-South Asian monsoon relationship in a coupled general circulation model. J. Geophys. Res. 115, D17109.

Chester, R., Baxter, G.G., Behairy, A.K.A., Connor, K., Cross, D., Elderfield, H., Padgham, R.C., 1977. Soil-sized eolian dusts from the lower troposphere of the eastern Mediterranean Sea. Marine Geology 24, 201-217.

Chester, R., Elderfield, H., Griffin, J.J., 1971. Dust transported in the North-East and South-East trade winds in the Atlantic Ocean. Nature 233, 474-476.

Chester, R., Sharples, E.J., Sanders, G.S., Saydam, A.C., 1984. Saharan dust incursion over the Tyrrhenian Sea. Atmospheric Environment - Part A General Topics 18, 929-935.

Chondrogianni, C., Ariztegui, D., Rolph, T., Juggins, S., Shemesh, A., Rietti-Shati, M., Niessen, F., Guilizzoni, P., Lami, A., McKenzie, J.A., Oldfield, F., 2004. Millennial to interannual climate variability in the Mediterranean during the Last Glacial Maximum. Quaternary International 122, 31-41.

Clemens, S.C., Prell, W.L., 1990. Late Pleistocene variability of Arabian Sea summer monsoon winds and continental aridity: eolian records from the lithogenic component of deep-sea sediments. Paleoceanography 5, 109-145.

CLIMAP Project Members, 1976. The surface of the ice-age earth. Science 191, 1138–1144.

CLIMAP Project Members, 1981. Seasonal reconstructions of the Earth's surface at the last glacial maximum. Geological Society of America Map and Chart Series MC-36.

Cole, J.M., Goldstein, S.L., deMenocal, P.B., Hemming, S.R., Grousset, F.E., 2009. Contrasting compositions of Saharan dust in the eastern Atlantic Ocean during the last deglaciation and African Humid Period. Earth and Planetary Science Letters 278, 257-266.

Comas, M.C., Ivanov, M.K., 2003. Alboran basin (Leg 3). In: Kenyon, H., Ivanov, M.K., Akhmetzhanov, A.M., Akhmanov. G.G. (Eds.), Interdisciplinary geoscience research on the North East Atlantic margin, Mediterranean Sea and Mid-Atlantic Ridge. IOC Technical Series UNESCO, pp. 51-71.

Comas, M.C., Zahn, R., Klaus, A., et al., 1996. Proceedings of the Ocean Drilling Program (ODP), Initial Reports, Leg 161, Mediterranean Sea II, the western Mediterranean. Ocean Drilling Program, College Station, TX.

Combourieu Nebout, N., Peyron, O., Dormoy, I., Desprat, S., Beaudouin, C., Kotthoff, U., Marret, F., 2009. Rapid climatic variability in the west Mediterranean during the last 25 000 years from high resolution pollen data. Climate of the Past 5, 503-521.

Combourieu Nebout, N., Turon, J.L., Zahn, R., Capotondi, L., Londeix, L., Pahnke, K., 2002. Enhanced aridity and atmospheric high-pressure stability over the western Mediterranean during the North Atlantic cold events of the past 50 k.y. Geology 30, 863-866.

Coude-Gaussen, G., 1987. Saharan dust on Fuerteventura Island (Canaries): chemical and mineralogical characteristics, air mass trajectories, and probable sources. Journal of Geophysical Research 92, 9753-9771.

Coude-Gaussen, G., Rognon, P., Bergametti, G., Gomes, I., Strauss, B., Gros, J.M., 1987. Saharan dust on Fuerteventura Island (Canaries): chemical and mineralogical characteristics, air mass trajectories, and probable sources. Journal of Geophysical Research 92, 9753-9771.

Dansgaard, W., Johnsen, S.J., Clausen, H.B., Dahl-Jensen, D., Gundestrup, N.S., Hammer, C.U., Hvidberg, C.S., Steffensen, J.P., Sveinbjörnsdottir, A.E., Jouzel, J., Bond, G., 1993. Evidence for general instability of past climate from a 250-kyr ice-core record. Nature 364, 218-220.

Dansgaard, W., White, J.W.C., Johnsen, S.J., 1989. The abrupt termination of the Younger Dryas climate event. Nature 339, 532-534.

Debret, M., Bout-Roumazeilles, V., Grousset, F., Desmet, M., McManus, J.F., Massei, N., Sebag, D., Petit, J.R., Copard, Y., Trentesaux, A., 2007. The origin of the 1500-year climate cycles in holocene north-atlantic records. Climate of the Past 3, 569-575.

12. References

Debret, M., Sebag, D., Crosta, X., Massei, N., Petit, J.R., Chapron, E., Bout-Roumazeilles, V., 2009. Evidence from wavelet analysis for a mid-Holocene transition in global climate forcing. Quaternary Science Reviews 28, 2675-2688.

Dehairs, F., Chesselet, R., Jedwab, J., 1980. Discrete suspended particles of barite and the barium cycle in the open ocean. Earth and Planetary Science Letters 49, 528-550.

Dehairs, F., Lambert, C.E., Chesselet, R., Risler, N., 1987. The biological production of marine suspended barite and the barium cycle in the Western Mediterranean Sea. Biogeochemistry 4, 119-140.

de Leeuw, J . W., V. D. Meer F. W., Rijpstra W. I. C. and Schenck P. A. (1980). On the occurrence and structural identification of long chain unsaturated ketones and hydrocarbons in sediments. In: Douglas, A.G., Maxwell, J.R. (Eds.), Advances in Organic Geochemistry 1979. Pergamon Press, pp. 211-217.

deMenocal, P.B., 1995. Plio-Pleistocene African climate. Science 270, 53-59.

deMenocal, P.B., 2004. African climate change and faunal evolution during the Pliocene-Pleistocene. Earth and Planetary Science Letters 220, 3-24

deMenocal, P.B., Ortiz, J., Guilderson, T., Adkins, J., Sarnthein, M., Baker, L., Yarusinsky, M., 2000. Abrupt onset and termination of the African Humid Period: Rapid climate responses to gradual insolation forcing. Quaternary Science Reviews 19, 347-361.

deMenocal, P.B., Rind, D., 1993. Sensitivity of Asian and African climate to variations in seasonal insolation, glacial ice cover, sea surface temperature, and Asian orography. Journal of Geophysical Research 98, 7265-7287.

Denton, G.H., Broecker, W., Alley, R.B., 2006. The mystery interval 17.5 to 14.5 kyr ago. In: Brigham-Grette, J., Kull, C., Kiefer, T. (Eds.), PAGES News, pp. 14-16.

Denton, G.H., Karlén, W., 1973. Holocene climatic variations-Their pattern and possible cause. Quaternary Research 3, 155-205.

Díaz-Hernández, J.L., Martín-Ramos, J.D., López-Galindo, A., Corrigendum to "Quantitative analysis of mineral phases in atmospheric dust deposited in the south-eastern Iberian Peninsula" [Atmos. Environ. 45 (2011) 3013-3024] (DOI:10.1016/j.atmosenv.2011.03.024). Atmospheric Environment.

Díaz-Hernández, J.L., Martín-Ramos, J.D., López-Galindo, A., 2011. Quantitative analysis of mineral phases in atmospheric dust deposited in the south-eastern Iberian Peninsula. Atmospheric Environment 45, 3015-3024.

Dickin, A., 1997. Radiogenic Isotope Geology, second ed. Cambridge University Press, Cambridge.

Dulac, F., Tanre, D., Bergametti, G., Buat-Menard, P., Desbois, M., Sutton, D., 1992. Assessment of the African airborne dust mass over the western Mediterranean Sea using Meteosat data. Journal of Geophysical Research 97, 2489-2506.

Dymond, J., Suess, E., Lyle, M., 1992. Barium in deep-sea sediment: a geochemical proxy for paleoproductivity. Paleoceanography 7, 163-181.

Eagle, M., Paytan, A., Arrigo, K.R., van Dijken, G., Murray, R.W., 2003. A comparison between excess barium and barite as indicators of carbon export. Paleoceanography 18, 21-21.

Elenga, H., Peyron, O., Bonnefille, R., Jolly, D., Cheddadi, R., Guiot, J., Andrieu, V., Bottema, S., Buchet, G., De Beaulieu, J.L., Hamilton, A.C., Maley, J., Marchant, R., Pérez-Obiol, R., Reille, M., Riollet, G., Scott, L., Straka, H., Taylor, D., Van Campo, E., Vincens, A., Laarif, F., Jonson, H., 2000. Pollen-based biome reconstruction for southern Europe and Africa 18,000 yr BP. Journal of Biogeography 27, 621-634.

El Mouden, A., Bouchaou, L., Snoussi, M., 2005. Constraints on alluvial clay mineral assemblages in semiarid regions. The Souss Wadi Basin (Morocco, Northwestern Africa). Geologica Acta 3, 3–13.

Hamroush, H.A., Stanley, A.D.J., 1990. Paleoclimatic oscillations in East Africa interpreted by analysis of trace elements in Nile delta sediments. Episodes 13, 264–269.

Emeis, K.C., Struck, U., Schulz, H.M., Rosenberg, R., Bernasconi, S., Erlenkeuser, H., Sakamoto, T., Martínez-Ruiz, F., 2000. Temperature and salinity variations of Mediterranean Sea surface waters over the last 16,000 years from records of planktonic stable oxygen isotopes and alkenone unsaturation ratios. Palaeogeography, Palaeoclimatology, Palaeoecology 158, 259-280.

Erel, Y., Torrent, J., 2010. Contribution of Saharan dust to Mediterranean soils assessed by sequential extraction and Pb and Sr isotopes. Chemical Geology 275, 19-25.

Fabres, J., Calafat, A., Sanchez-Vidal, A., Canals, M., Heussner, S., 2002. Composition and spatio-temporal variability of particle fluxes in the Western Alboran Gyre, Mediterranean Sea. Journal of Marine Systems 33-34, 431-456.

Fagel, N., Hillaire-Marcel, C., Humblet, M., Brasseur, R., Weis, D., Stevenson, R., 2004. Nd and Pb isotope signatures of the clay-size fraction of Labrador Sea sediments during the Holocene: Implications for the inception of the modern deep circulation pattern. Paleoceanography 19, PA3002 3001-3016.

Fernández de Puelles, M.L., Alemany, F., Jansá, J., 2007. Zooplankton time-series in the Balearic Sea (Western Mediterranean): Variability during the decade 1994-2003. Progress in Oceanography 74, 329-354.

Fleitmann, D., Burns, S.J., Mudelsee, M., Neff, U., Kramers, J., Mangini, A., Matter, A., 2003. Holocene forcing of the Indian monsoon recorded in a stalagmite from Southern Oman. Science 300, 1737-1739.

Fletcher, W.J., Sánchez Goñi, M.F., 2008. Orbital- and sub-orbital-scale climate impacts on vegetation of the western Mediterranean bM.Fasin over the last 48,000 yr. Quaternary Research 70, 451-464.

Fletcher, W.J., Sánchez Goñi, M.F., Peyron, O., Dormoy, I., 2010. Abrupt climate changes of the last deglaciation detected in a Western Mediterranean forest record. Climate of the Past 6, 245-264.

Foucault, A., Mélières, F., 2000. Palaeoclimatic cyclicity in central Mediterranean Pliocene sediments: the mineralogical signal. Palaeogeography, Palaeoclimatology, Palaeoecology 158, 311-323.

Frigola, J., Moreno, A., Cacho, I., Canals, M., Sierro, F.J., Flores, J.A., Grimalt, J.O., 2008. Evidence of abrupt changes in Western Mediterranean Deep Water circulation during the last 50 kyr: A high-resolution marine record from the Balearic Sea. Quaternary International 181, 88-104.

Frigola, J., Moreno, A., Cacho, I., Canals, M., Sierro, F.J., Flores, J.A., Grimalt, J.O., Hodell, D.A., Curtis, J.H., 2007. Holocene climate variability in the western Mediterranean region from a deepwater sediment record. Paleoceanography 22.

Gaetani, M., Fontaine, B., Roucou, P., Baldi, M., 2010. Influence of the Mediterranean Sea on the West African monsoon: Intraseasonal variability in numerical simulations. Journal of Geophysical Research D: Atmospheres 115.

Gallego-Torres, D., Martínez-Ruiz, F., Meyers, P.A., Paytan, A., Jiménez-Espejo, F.J., Ortega-Huertas, M., 2011. Productivity patterns and N-fixation associated with Pliocene-Holocene sapropels: Paleoceanographic and paleoecological significance. Biogeosciences 8, 415-431.

Gallego-Torres, D., Martínez-Ruiz, F., Paytan, A., Jiménez-Espejo, F.J., Ortega-Huertas, M., 2007. Pliocene-Holocene evolution of depositional conditions in the eastern Mediterranean: Role of anoxia vs. productivity at time of sapropel deposition. Palaeogeography, Palaeoclimatology, Palaeoecology 246, 424-439.

Ganopolski, A., Kubatzki, C., Claussen, M., Brovkin, V., Petoukhov, V., 1998. The influence of vegetation-atmosphere-cean interaction on climate during the mid-holocene. Science 280, 1916-1919.

12. References

García-Gorriz, E., Carr, M.E., 2001. Physical control of phytoplankton distributions in the Alboran Sea: A numerical and satellite approach. Journal of Geophysical Research C: Oceans 106, 16795-16805.

Gasse, F., 2000. Hydrological changes in the African tropics since the Last Glacial Maximum. Quaternary Science Reviews 19, 189-211.

Gasse, F., 2002. Diatom-inferred salinity and carbonate oxygen isotopes in Holocene waterbodies of the western Sahara and Sahel (Africa). Quaternary Science Reviews 21, 737-767.

Gasse, F., Van Campo, E., 1994. Abrupt post-glacial climate events in West Asia and North Africa monsoon domains. Earth and Planetary Science Letters 126, 435-456.

Genty, D., Blamart, D., Ghaleb, B., Plagnes, V., Causse, C., Bakalowicz, M., Zouari, K., Chkir, N., Hellstrom, J., Wainer, K., Bourges, F., 2006. Timing and dynamics of the last deglaciation from European and North African δ13C stalagmite profiles-comparison with Chinese and South Hemisphere stalagmites. Quaternary Science Reviews 25, 2118-2142.

Gerstenberger, H., Haase, G., 1997. A highly effective emitter substance for mass spectrometric Pb isotope ratio determinations. Chemical Geology 136, 309-312.

Giraudeau, J., Grelaud, M., Solignac, S., Andrews, J.T., Moros, M., Jansen, E., 2010. Millennial-scale variability in Atlantic water advection to the Nordic Seas derived from Holocene coccolith concentration records. Quaternary Science Reviews 29, 1276-1287.

González-Donoso, J.M., Serrano, F., Linares, D., 2000. Sea surface temperature during the Quaternary at ODP Sites 976 and 975 (western Mediterranean). Palaeogeography, Palaeoclimatology, Palaeoecology 162, 17-44.

González-Sampériz, P., Valero-Garcés, B.L., Moreno, A., Jalut, G., García-Ruiz, J.M., Martí-Bono, C., Delgado-Huertas, A., Navas, A., Otto, T., Dedoubat, J.J., 2006. Climate variability in the Spanish Pyrenees during the last 30,000 yr revealed by the El Portalet sequence. Quaternary Research 66, 38-52.

Goudie, A.S., Middleton, N.J., 2001. Saharan dust storms: Nature and consequences. Earth-Science Reviews 56, 179-204.

Grootes, P.M., Stuiver, M., 1997. Oxygen 18/16 variability in Greenland snow and ice with 10-3- to 105-year time resolution. Journal of Geophysical Research 102, 26455-26470.

Grootes, P.M., Stuiver, M., White, J.W.C., Johnsen, S., Jouzel, J., 1993. Comparison of oxygen isotope records from the GISP2 and GRIP Greenland ice cores. Nature 366, 552-554.

Grousset, F.E., 1993. Patterns of ice-rafted detritus in the glacial North Atlantic (40- 55°N). Paleoceanography 8, 175-192.

Grousset, F.E., Biscaye, P.E., 2005. Tracing dust sources and transport patterns using Sr, Nd and Pb isotopes. Chemical Geology 222, 149-167.

Grousset, F.E., Biscaye, P.E., Revel, M., Petit, J.R., Pye, K., Joussaume, S., Jouzel, J., 1992. Antarctic (Dome C) ice-core dust at 18 k.y. B.P.: Isotopic constraints on origins. Earth and Planetary Science Letters 111, 175-182.

Grousset, F.E., Biscaye, P.E., Zindler, A., Prospero, J., Chester, R., 1988a. Neodymium isotopes as tracers in marine sediments and aerosols: North Atlantic. Earth and Planetary Science Letters 87, 367-378.

Grousset, F.E., Joron, J.L., Biscaye, P.E., Latouche, C., Treuil, M., Maillet, N., Faugères, J.C., Gonthier, E., 1988b. Mediterranean outflow through the Strait of Gibraltar since 18,000 Years B.P.: Mineralogical and geochemical arguments. Geo-Marine Letters 8, 25-34.

Grousset, F.E., Buat-Menard, P., Boust, D., Tian, R.C., Baudel, S., Pujol, C., Vergnaud-Grazzini, C., 1989. Temporal changes of aeolian Saharan input in the Cape Verde abyssal plain since that last Glacial period. Oceanologica Acta 12, 177-185.

Grousset, F.E., Parra, M., Bory, A., Martínez, P., Bertrand, P., Shimmield, G., Ellam, R.M., 1998. Saharan wind regimes traced by the Sr-Nd isotopic composition of subtropical Atlantic sediments: Last Glacial Maximum vs today. Quaternary Science Reviews 17, 395-409.

Guerzoni, S., Molinaroli, E., Chester, R., 1997. Saharan dust inputs to the western Mediterranean Sea: Depositional patterns, geochemistry and sedimentological implications. Deep-Sea Research Part II: Topical Studies in Oceanography 44, 631-654.

Gupta, A.K., Das, M., Anderson, D.M., 2005. Solar influence on the Indian summer monsson during the Holocene. Geophysical Research Letters 32, 1-4.

Hall, I.R., McCave, I.N., 2000. Palaeocurrent reconstruction, sediment and thorium focussing on the Iberian margin over the last 140 ka. Earth and Planetary Science Letters 178, 151-164.

Hall, N.M.J., Peyrillé, P., 2006. Dynamics of the West African monsoon, Grenoble, pp. 81-99.

Haug, G.H., Hughen, K.A., Sigman, D.M., Peterson, L.C., Röhl, U., 2001. Southward migration of the intertropical convergence zone through the holocene. Science 293, 1304-1308.

Heinrich, H., 1988. Origin and consequences of cyclic ice rafting in the Northeast Atlantic Ocean during the past 130,000 years. Quaternary Research 29, 142-152.

Hemming, S.R., Broecker, W.S., Sharp, W.D., Bond, G.C., Gwiazda, R.H., McManus, J.F., Klas, M., Hajdas, I., 1998. Provenance of Heinrich layers in core V28-82, northeastern Atlantic: 40Ar/39Ar ages of ice-rafted hornblende, Pb isotopes in feldspar grains, and Nd-Sr-Pb isotopes in the fine sediment fraction. Earth and Planetary Science Letters 164, 317-333.

Henry, F., Jeandel, C., Dupré, B., Minster, J.F., 1994. Particulate and dissolved Nd in the western Mediterranean Sea: Sources, fate and budget. Marine Chemistry 45, 283-305.

Hoefs, M.J.L., Schouten, S., De Leeuw, J.W., King, L.L., Wakeham, S.G., Sinninghe Damsté, J.S., 1997. Ether lipids of planktonic archaea in the marine water column? Applied and Environmental Microbiology 63, 3090-3095.

Hoelzmann, P., Gasse, F., Dupont, L.M., Salzmann, U., Staubwasser, M., Leuchner, D.C., Sirocko, F., 2004. Palaeoenvironmental changes in the arid and subarid belt (Sahara–Sahel–Arabian Peninsula) from 150 ka to present. In: Battarbee, R.W., Gasse, F., Stickley, C.S. (Eds.), Past Climate through Europe and Africa. Kluwer Academic, Dordrecht, pp. 219-256.

Holz, C., 2004. Climate-induced variability of fluvial and aeolian sediment supply and gravity-driven sediment transport off northwest Africa, Ph.D. dissertation, University of Bremen, Bremen, Germany.

Hoogakker, B.A.A., Rothwell, R.G., Rohling, E.J., Paterne, M., Stow, D.A.V., Herrle, J.O., Clayton, T., 2004. Variations in terrigenous dilution in western Mediterranean Sea pelagic sediments in response to climate change during the last glacial cycle. Marine Geology 211, 21-43.

Hopmans, E.C., Weijers, J.W.H., Schefuß, E., Herfort, L., Sinninghe Damsté, J.S., Schouten, S., 2004. A novel proxy for terrestrial organic matter in sediments based on branched and isoprenoid tetraether lipids. Earth and Planetary Science Letters 224, 107-116.

Huguet, C., Kim, J.H., Damsté, J.S.S., Schouten, S., 2006. Reconstruction of sea surface temperature variations in the Arabian Sea over the last 23 kyr using organic proxies (TEX86 and U 37K′). Paleoceanography 21.

12. References

Huguet, C., Martrat, B., Grimalt, J.O., Sinninghe Damsté, J.S., Schouten, S., 2011. Coherent millennial-scale patterns in U37k and TEX86H temperature records during the penultimate interglacial-to-glacial cycle in the western Mediterranean. Paleoceanography 26.

Hurrell, J.W., 1995. Decadal trends in the North Atlantic Oscillation: Regional temperatures and precipitation. Science 269, 676-679.

IPCC, 2007. Climate Change 2007: The Physical Science Basis. In: Solomon, S., Qin, D., Manning, M., Chen, Z., Marquis, M., Averyt, K.B., Tignor, M., Miller, H.L. (Eds.), Contribution of Working Group I to the Fourth Assessment Report of the Intergovernmental Panel on Climate Change. Cambridge University Press, Cambridge and New York.

Jansen, E., Overpeck, J., Briffa, K.R., Duplessy, J.-C., Joos, F., Masson-Delmotte, V., Olago, D., Otto-Bliesner, B., Peltier, W.R., Rahmstorf, S., Ramesh, R., Raynaud, D., Rind, D., Solomina, O., Villalba, R., Zhang, D., 2007. Palaeoclimate. In: Solomon, S., Qin, D., Manning, M., Chen, Z., Marquis, M., Averyt, K.B., Tignor, M., Miller, H.L. (Eds.), Climate Change 2007: The Physical Science Basis. Contribution of Working Group I to the Fourth Assessment Report of the Intergovernmental Panel on Climate Change. Cambridge University Press, pp. 433-497.

Jeandel, C., Arsouze, T., Lacan, F., Téchiné, P., Dutay, J.C., 2007. Isotopic Nd compositions and concentrations of the lithogenic inputs into the ocean: A compilation, with an emphasis on the margins. Chemical Geology 239, 156-164.

Jiménez-Espejo, F.J., Martínez-Ruiz, F., Rogerson, M., González-Donoso, J.M., Romero, O.E., Linares, D., Sakamoto, T., Gallego-Torres, D., Ruiz, J.L.R., Ortega-Huertas, M., Claros, J.A.P., 2008. Detrital input, productivity fluctuations, and water mass circulation in the westernmost Mediterranean Sea since the Last Glacial Maximum. Geochemistry, Geophysics, Geosystems 9. Q11U02.

Jiménez-Espejo, F.J., Martínez-Ruiz, F., Sakamoto, T., Iijima, K., Gallego-Torres, D., Harada, N., 2007. Paleoenvironmental changes in the western Mediterranean since the last glacial maximum: High resolution multiproxy record from the Algero-Balearic basin. Palaeogeography, Palaeoclimatology, Palaeoecology 246, 292-306.

Jiménez-Moreno, G., Aziz, H.A., Rodríguez-Tovar, F.J., Pardo-Igúzquiza, E., Suc, J.P., 2007. Palynological evidence for astronomical forcing in Early Miocene lacustrine deposits from Rubielos de Mora Basin (NE Spain). Palaeogeography, Palaeoclimatology, Palaeoecology 252, 601-616.

Jullien, E., Grousset, F., Malaizé, B., Duprat, J., Sanchez-Goni, M.F., Eynaud, F., Charlier, K., Schneider, R., Bory, A., Bout, V., Flores, J.A., 2007. Low-latitude "dusty events" vs. high-latitude "icy Heinrich events". Quaternary Research 68, 379-386.

Jung, S.J.A., Davies, G.R., Ganssen, G.M., Kroon, D., 2004. Stepwise Holocene aridification in NE Africa deduced from dust-borne radiogenic isotope records. Earth and Planetary Science Letters 221, 27-37.

Juteau, M., Michard, A., Albarede, F., 1986. The Pb-Sr-Nd isotope geochemistry of some recent circum-Mediterranean granites. Contributions to Mineralogy and Petrology 92, 331-340.

Kageyama, M., Combourieu Nebout, N., Sepulchre, P., Peyron, O., Krinner, G., Ramstein, G., Cazet, J.P., 2005. The Last Glacial Maximum and Heinrich Event 1 in terms of climate and vegetation around the Alboran Sea: A preliminary model-data comparison. Le dernier maximum glaciaire et l'événement de Heinrich 1 en termes de climat et de végétation autour de la mer d'Alboran: Une comparaison préliminaire entremodèles et données 337, 983-992.

Kalu, A.E., 1979. The African Dust Plume: its characteristics and propagation across West Africa in winter. In: Morales, C. (Ed.), Saharan Dust: Mobilisation, Transport, Deposition. SCOPE Report 14, John Wiley & Sons, New York, pp. 95-118.

Karner, M.B., Delong, E.F., Karl, D.M., 2001. Archaeal dominance in the mesopelagic zone of the Pacific Ocean. Nature 409, 507-510.

Kim, J.H., Schouten, S., Hopmans, E.C., Donner, B., Sinninghe Damsté, J.S., 2008. Global sediment core-top calibration of the TEX86 paleothermometer in the ocean. Geochimica et Cosmochimica Acta 72, 1154-1173.

Kisch, H.J., 1991. Illite crystallinity: recommendations on sample preparation, X-ray diffraction settings, and interlaboratory samples. Journal of Metamorphic Geology 9, 665-670.

Kloosterboer-Van Hoeve, M.L., Steenbrink, J., Visscher, H., Brinkhuis, H., 2006. Millennial-scale climatic cycles in the Early Pliocene pollen record of Ptolemais, northern Greece. Palaeogeography, Palaeoclimatology, Palaeoecology 229, 321-334.

Kodera, K., Kuroda, Y., 2005. A possible mechanism of solar modulation of the spatial structure of the North Atlantic Oscillation. Journal of Geophysical Research D: Atmospheres 110, 1-9.

Kolla, V., Biscaye, P.E., Hanley, A.F., 1979. Distribution of quartz in late Quaternary Atlantic sediments in relation to climate. Quaternary Research 11, 261-277.

Kroon, D., Austin, W.E.N., Chapman, M.R., Ganssen, G.M., 1997. Deglacial surface circulation changes in the northeastern Atlantic: Temperature and salinity records off NW Scotland on a century scale. Paleoceanography 12, 755-763.

Kröpelin, S., Verschuren, D., Lézine, A.M., Eggermont, H., Cocquyt, C., Francus, P., Cazet, J.P., Fagot, M., Rumes, B., Russell, J.M., Darius, F., Conley, D.J., Schuster, M., Von Suchodoletz, H., Engstrom, D.R., 2008. Climate-driven ecosystem succession in the Sahara: The past 6000 years. Science 320, 765-768.

Kuhlmann, H., Meggers, H., Freudenthal, T., Wefer, G., 2004. The transition of the monsoonal and the N Atlantic climate system off NW Africa during the Holocene. Geophysical Research Letters 31, 1-4.

Kutzbach, J., Bonan, G., Foley, J., Harrison, S.P., 1996. Vegetation and soil feedbacks on the response of the African monsoon to orbital forcing in the early to middle Holocene. Nature 384, 623-626.

Lacombe, H., Gascard, J.C., Cornella, J., Béthoux, J.P., 1981. Response of the Mediterranean to the water and energy fluxes across its surface, on seasonal and interannual scales. Oceanologica Acta 4, 247-255.

La-Violette, P.E., 1986. Short-term measurements of surface currents associated with the Alboran Sea Gyre. Journal of Physical Oceanography 16, 262-279.

Lee, S.-Y., Chiang, J.C.H., Matsumoto, K., Tokos, K.S., 2011. Southern Ocean wind response to North Atlantic cooling and the rise in atmospheric CO2: Modeling perspective and paleoceanographic implications. Paleoceanography 26, PA1214.

Liu, Z., Otto-Bliesner, B.L., He, F., Brady, E.C., Tomas, R., Clark, P.U., Carlson, A.E., Lynch-Stieglitz, J., Curry, W., Brook, E., Erickson, D., Jacob, R., Kutzbach, J., Cheng, J., 2009. Transient simulation of last deglaciation with a new mechanism for bolling-allerod warming. Science 325, 310-314.

Lomb, N.R., 1976. Least-squares frequency analysis of unequally spaced data. Astrophysics and Space Science 39, 447-462.

Lowe, J.J., Rasmussen, S.O., Björck, S., Hoek, W.Z., Steffensen, J.P., Walker, M.J.C., Yu, Z.C., 2008. Synchronisation of palaeoenvironmental events in the North Atlantic region during the Last Termination: a revised protocol recommended by the INTIMATE group. Quaternary Science Reviews 27, 6-17.

Loÿe-Pilot, M.D., Martin, J.M., 1996. Saharan dust inputs to the western Mediterranean: an eleven year record in Corsica. In: Guerzoni, S., Chester, R. (Eds.), The impact of desert dust across the Mediterranean. Kluwer Academic, Dordrecht, pp. 191-199.

Loÿe-Pilot, M.D., Martin, J.M., Morelli, J., 1986. Influence of Saharan dust on the rain acidity and atmospheric input to the Mediterranean. Nature 321, 427-428.

12. References

Loÿe-Pilot, M.D., Martin, J.M., Morelli, J., 1989. Atmospheric input of particulate matter and inorganic nitrogen to the northwestern Mediterranean. Water Pollution Research Report 13, 368-376.

Magny, M., Aalbersberg, G., Bégeot, C., Benoit-Ruffaldi, P., Bossuet, G., Disnar, J.R., Heiri, O., Laggoun-Defarge, F., Mazier, F., Millet, L., Peyron, O., Vannière, B., Walter-Simonnet, A.V., 2006. Environmental and climatic changes in the Jura mountains (eastern France) during the Lateglacial-Holocene transition: A multi-proxy record from Lake Lautrey. Quaternary Science Reviews 25, 414-445.

Mangini, A., Jung, M., Laukenmann, S., 2001. What do we learn from peaks of uranium and of manganese in deep sea sediments? Marine Geology 177, 63.

Mangini, A., Verdes, P., Spötl, C., Scholz, D., Vollweiler, N., Kromer, B., 2007. Persistent influence of the North Atlantic hydrography on central European winter temperature during the last 9000 years. Geophysical Research Letters 34.

Marchitto, T.M., Muscheler, R., Ortiz, J.D., Carriquiry, J.D., Van Geen, A., 2010. Dynamical response of the tropical pacific ocean to solar forcing during the early holocene. Science 330, 1378-1381.

Marlowe, I.T., Green, J.C., Neal, A.C., Brassell, S.C., Eglinton, G., Course, P.A., 1984. Long chain (n-C37–C39) alkenones in the Prymnesiophyceae. Distribution of alkenones and other lipids and their taxonomic significance. British Phycological Journal 19, 203-216.

Marshall, J., Kushnir, Y., Battisti, D., Chang, P., Czaja, A., Dickson, R., Hurrell, J., McCartney, M., Saravanan, R., Visbeck, M., 2001. North Atlantic climate variability: Phenomena, impacts and mechanisms. International Journal of Climatology 21, 1863-1898.

Martin, J.D., 2004. Using XPowder: A software package for Powder X-Ray diffraction analysis. http://www.xpowder.com D.L. GR 1001/04.ISBN 84-609-1497-6. 105 p. Spain.

Martín-Puertas, C., Jiménez-Espejo, F., Martínez-Ruiz, F., Nieto-Moreno, V., Rodrigo, M., Mata, M.P., Valero-Garcés, B.L., 2010. Late Holocene climate variability in the southwestern Mediterranean region: An integrated marine and terrestrial geochemical approach. Climate of the Past Discussions 6, 1655-1683.

Martínez-Ruiz, F., Kastner, M., Paytan, A., Ortega-Huertas, M., Bernasconi, S.M., 2000. Geochemical evidence for enhanced productivity during S1 sapropel deposition in the eastern Mediterranean. Paleoceanography 15, 200-209.

Martínez-Ruiz, F., Paytan, A., Kastner, M., González-Donoso, J.M., Linares, D., Bernasconi, S.M., Jiménez-Espejo, F.J., 2003. A comparative study of the geochemical and mineralogical characteristics of the S1 sapropel in the western and eastern Mediterranean. Palaeogeography, Palaeoclimatology, Palaeoecology 190, 23-37.

Martrat, B., Grimalt, J.O., Lopez-Martínez, C., Cacho, I., Sierro, F.J., Flores, J.A., Zahn, R., Canals, M., Curtis, J.H., Hodell, D.A., 2004. Abrupt temperature changes in the Western Mediterranean over the past 250,000 years. Science 306, 1762-1765.

Martrat, B., Grimalt, J.O., Shackleton, N.J., De Abreu, L., Hutterli, M.A., Stocker, T.F., 2007. Four climate cycles of recurring deep and surface water destabilizations on the Iberian margin. Science 317, 502-507.

Maslin, M.A., Shackleton, N.J., Pflaumann, U., 1995. Surface water temperature, salinity, and density changes in the northeast Atlantic during the last 45 000 years: Heinrich events, deep water formation, and climatic rebounds. Paleoceanography 10, 527-544.

Masqué, P., Fabres, J., Canals, M., Sanchez-Cabeza, J.A., Sanchez-Vidal, A., Cacho, I., Calafat, A.M., Bruach, J.M., 2003. Accumulation rates of major constituents of hemipelagic sediments in the deep Alboran Sea: A centennial perspective of sedimentary dynamics. Marine Geology 193, 207-233.

Massana, R., Delong, E.F., Pedrós-Alió, C., 2000. A few cosmopolitan phylotypes dominate planktonic archaeal assemblages in widely different oceanic provinces. Applied and Environmental Microbiology 66, 1777-1787.

Matthewson, A.P., Shimmield, G.B., Kroon, D., Fallick, A.E., 1995. A 300 kyr high-resolution aridity record of the North African continent. Paleoceanography 10, 677-692.

Mayewski, P.A., Meeker, L.D., Twickler, M.S., Whitlow, S., Qinzhao, Y., Berry Lyons, W., Prentice, M., 1997. Major features and forcing of high-latitude Northern Hemisphere atmospheric circulation using a 110 000-year-long glaciochemical series. Journal of Geophysical Research 102, 26345-26366.

Mayewski, P.A., Meeker, L.D., Whitlow, S., Twickler, M.S., Morrison, M.C., Bloomfield, P., Bond, G.C., Alley, R.B., Gow, A.J., Grootes, P.M., Meese, D.A., Ram, M., Taylor, K.C., Wumkes, W., 1994. Changes in atmospheric circulation and ocean ice cover over the North Atlantic during the last 41,000 years. Science 263, 1747-1751.

Mayewski, P.A., Rohling, E.E., Curt Stager, J., Karlén, W., Maasch, K.A., David Meeker, L., Meyerson, E.A., Gasse, F., van Kreveld, S., Holmgren, K., Lee-Thorp, J., Rosqvist, G., Rack, F., Staubwasser, M., Schneider, R.R., Steig, E.J., 2004a. Holocene climate variability. Quaternary Research 62, 243-255.

Mayewski, P.A., Rohling, E.E., Stager, J.C., Karlén, W., Maasch, K.A., Meeker, L.D., Meyerson, E.A., Gasse, F., van Kreveld, S., Holmgren, K., Lee-Thorp, J., Rosqvist, G., Rack, F., Staubwasser, M., Schneider, R.R., Steig, E.J., 2004b. Holocene climate variability. Quaternary Research 62, 243-255.

McCave, I.N., Manighetti, B., Robinson, S.G., 1995. Sortable silt and fine sediment size/composition slicing: parameters for palaeocurrent speed and palaeoceanography. Paleoceanography 10, 593-610.

McGowan, H.A., Marx, S.K., Soderholm, J., Denholm, J., 2010. Evidence of solar and tropical-ocean forcing of hydroclimate cycles in southeastern Australia for the past 6500 years. Geophysical Research Letters 37.

MEDAR Group, 2002. MEDATLAS/2002 Database. Mediterranean and Black Sea Database of Temperature Salinity and Bio-chemical Parameters. Climatological Atlas. Institut Français de Recherche pour L'Exploitation de la Mer, (IFREMER) Edition/Instituto Nazionale di Oceanografia e di Geofisica Sperimentale (OGS).

Menviel, L., Timmermann, A., Timm, O.E., Mouchet, A., 2011. Deconstructing the Last Glacial termination: The role of millennial and orbital-scale forcings. Quaternary Science Reviews 30, 1155-1172.

Meunier, A., Velde, B., 2004. Illite: Origins, evolution and metamorphism. Springer-Verlag, Berlin.

Millot, C., 1999. Circulation in the Western Mediterranean Sea. Journal of Marine Systems 20, 423-442.

Mix, A.C., Bard, E., Schneider, R., 2001. Environmental processes of the ice age: Land, oceans, glaciers (EPILOG). Quaternary Science Reviews 20, 627-657.

Molinaroli, E., 1996. Mineralogical characterization of Saharan dust with a view to its final destination in Mediterranean sediemtns. In: Guerzoni, S., Chester, R. (Eds.), The impact of desert dust across the Mediterranean. Kluwer Academic, Dordrecht, pp. 153-162.

Mollenhauer, G., Eglinton, T.I., Hopmans, E.C., Sinninghe Damsté, J.S., 2008. A radiocarbon-based assessment of the preservation characteristics of crenarchaeol and alkenones from continental margin sediments. Organic Geochemistry 39, 1039-1045.

Mollenhauer, G., Inthorn, M., Vogt, T., Zabel, M., Sinninghe Damsté, J.S., Eglinton, T.I., 2007. Aging of marine organic matter during cross-shelf lateral transport in the Benguela upwelling system revealed by compound-specific radiocarbon dating. Geochemistry, Geophysics, Geosystems 8.

Morellón, M., Valero-Garcés, B., Moreno, A., González-Sampériz, P., Mata, P., Romero, O., Maestro, M., Navas, A., 2008. Holocene palaeohydrology and climate variability in northeastern Spain: The sedimentary record of Lake Estanya (Pre-Pyrenean range). Quaternary International 181, 15-31.

12. References

Morellón, M., Valero-Garcés, B., Vegas-Vilarrúbia, T., González-Sampériz, P., Romero, O., Delgado-Huertas, A., Mata, P., Moreno, A., Rico, M., Corella, J.P., 2009. Lateglacial and Holocene palaeohydrology in the western Mediterranean region: The Lake Estanya record (NE Spain). Quaternary Science Reviews 28, 2582-2599.

Moreno, A., Cacho, I., Canals, M., Grimalt, J.O., Sánchez-Goñi, M.F., Shackleton, N., Sierro, F.J., 2005. Links between marine and atmospheric processes oscillating on a millennial time-scale. A multi-proxy study of the last 50,000 yr from the Alboran Sea (Western Mediterranean Sea). Quaternary Science Reviews 24, 1623-1636.

Moreno, A., Cacho, I., Canals, M., Grimalt, J.O., Sanchez-Vidal, A., 2004. Millennial-scale variability in the productivity signal from the Alboran Sea record, Western Mediterranean Sea. Palaeogeography, Palaeoclimatology, Palaeoecology 211, 205-219.

Moreno, A., Cacho, I., Canals, M., Prins, M.A., Sánchez-Goni, M.F., Grimalt, J.O., Weltje, G.J., 2002. Saharan dust transport and high-latitude glacial climatic variability: The Alboran Sea record. Quaternary Research 58, 318-328.

Moreno, A., González-Sampériz, P., Morellón, M., Valero-Garcés, B.L., Fletcher, W.J., 2011b. Northern Iberian abrupt climate change dynamics during the last glacial cycle: A view from lacustrine sediments. Quaternary Science Reviews. doi:10.1016/j.quascirev.2010.06.031

Moreno, A., López-Merino, L., Leira, M., Marco-Barba, J., González-Sampériz, P., Valero-Garcés, B.L., López-Sáez, J.A., Santos, L., Mata, P., Ito, E., 2011. Revealing the last 13,500 years of environmental history from the multiproxy record of a mountain lake (Lago Enol, northern Iberian Peninsula). Journal of Paleolimnology 46, 327-349.

Moreno, A., Stoll, H., Jiménez-Sánchez, M., Cacho, I., Valero-Garcés, B., Ito, E., Edwards, R.L., 2010. A speleothem record of glacial (25-11.6 kyr BP) rapid climatic changes from northern Iberian Peninsula. Global and Planetary Change 71, 218-231.

Moulin, C., Lambert, C.E., Dayan, U., Masson, V., Ramonet, M., Bousquet, P., Legrand, M., Balkanski, Y.J., Guelle, W., Marticorena, B., Bergametti, G., Dulac, F., 1998. Satellite climatology of African dust transport in the Mediterranean atmosphere. Journal of Geophysical Research D: Atmospheres 103, 13137-13144.

Moulin, C., Lambert, C.E., Dulac, F., Dayan, U., 1997. Control of atmospheric export of dust from North Africa by the North Atlantic Oscillation. Nature 387, 691-694.

Mulitza, S., Prange, M., Stuut, J.B., Zabel, M., Von Dobeneck, T., Itambi, A.C., Nizou, J., Schulz, M., Wefer, G., 2008. Sahel megadroughts triggered by glacial slowdowns of Atlantic meridional overturning. Paleoceanography 23, PA4206.

Müller, P.J., Kirst, G., Ruhland, G., von Storch, I., Rosell-Melé, A., 1998. Calibration of the alkenone paleotemperature index U37K′ based on core-tops from the eastern South Atlantic and the global ocean (60°N-60°S). Geochimica et Cosmochimica Acta 62, 1757-1772.

Nagao, S., Nakashima, S., 1992. Possible complexation of uranium with dissolved humic substances in pore water of marine sediments. Science of the Total Environment 117-118, 439-447.

Naughton, F., Sanchez Goñi, M.F., Desprat, S., Turon, J.L., Duprat, J., Malaizé, B., Joli, C., Cortijo, E., Drago, T., Freitas, M.C., 2007. Present-day and past (last 25 000 years) marine pollen signal off western Iberia. Marine Micropaleontology 62, 91-114.

Naughton, F., Sánchez Goñi, M.F., Kageyama, M., Bard, E., Duprat, J., Cortijo, E., Desprat, S., Malaizé, B., Joly, C., Rostek, F., Turon, J.L., 2009. Wet to dry climatic trend in north-western Iberia within Heinrich events. Earth and Planetary Science Letters 284, 329-342.

Nederbragt, A.J., Thurow, J., 2005. Geographic coherence of millennial-scale climate cycles during the Holocene. Palaeogeography, Palaeoclimatology, Palaeoecology 221, 313-324.

Nesbitt, H.W., Markovics, G., Price, R.G., 1980. Chemical processes affecting alkalis and alkaline earths during continental weathering. Geochimica et Cosmochimica Acta 44, 1659-1666.

Nicholson, S.E., 2009. A revised picture of the structure of the "monsoon" and land ITCZ over West Africa. Climate Dynamics 32, 1155-1171.

Nieto-Moreno, V., Martínez-Ruiz, F., Giralt, S., Jiménez-Espejo, F., Gallego-Torres, D., Rodrigo-Gámiz, M., García-Orellana, J., Ortega-Huertas, M., De Lange, G.J., 2011. Tracking climate variability in the western Mediterranean during the Late Holocene: A multiproxy approach. Climate of the Past 7, 1-20.

Nieto-Moreno, V, Martínez-Ruiz, F., Willmott, V., García-Orellana, J., Masqué, P., Sinninghe Damsté, J.S. Climate conditions in the westernmost Mediterranean over the last two millennia: an integrated biomarker approach. Submitted to Organic Geochemistry.

O'Brien, S.R., Mayewski, P.A., Meeker, L.D., Meese, D.A., Twickler, M.S., Whitlow, S.I., 1995. Complexity of Holocene climate as reconstructed from a Greenland Ice Core. Science 270, 1962-1964.

Overpeck, J.T., Cole, J.E., 2006. Abrupt change in earth's climate system, In: Matson, P.A., Kammen, D.M., Gadil, A. (Eds.), pp. 1-31.

Packard, T.T., Minas, H.J., Coste, B., Martínez, R., Bonin, M.C., Gostan, J., Garfield, P., Christensen, J., Dortch, Q., Minas, M., Copin-Montegut, G., Copin-Montegut, C., 1988. Formation of the Alboran oxygen minimum zone. Deep Sea Research Part A, Oceanographic Research Papers 35, 1111-1118.

Paillard, D., Labeyrie, L., 1994. Role of the thermohaline circulation in the abrupt warming after Heinrich events. Nature 372, 162-164.

Pardo-Igúzquiza, E., Rodríguez-Tovar, F.J., 2000. The permutation test as a non-parametric method for testing the statistical significance of power spectrum estimation in cyclostratigraphic research. Earth and Planetary Science Letters 181, 175-189.

Pardo-Igúzquiza, E., Rodríguez-Tovar, F.J., 2005. MAXENPER: A program for maximum entropy spectral estimation with assessment of statistical significance by the permutation test. Computers and Geosciences 31, 555-567.

Pastouret, L., Chamley, H., Delibrias, G., Duplessy, J.C., Thiede, J., 1978. Late Quaternary climatic changes in western tropical Africa deduced from deep-sea sedimentation off the Niger delta. Oceanologica Acta 1, 217-232.

Paterne, M., Kallel, N., Labeyrie, L., Vautravers, M., Duplessy, J.C., Rossignol-Strick, M., Cortijo, E., Arnold, M., Fontugne, M., 1999. Hydrological relationship between the North Atlantic Ocean and the Mediterranean Sea during the past 15 - 75 kyr. Paleoceanography 14, 626-638.

Patton, G.M., Martin, P.A., Voelker, A., Salgueiro, E., 2011. Multiproxy comparison of oceanographic temperature during Heinrich Events in the eastern subtropical Atlantic. Earth and Planetary Science Letters 310, 45-58.

Paytan, A., Kastner, M., Chavez, F.P., 1996. Glacial to interglacial fluctuations in productivity in the equatorial pacific as indicated by marine barite. Science 274, 1355-1357.

Paytan, A., Martínez-Ruiz, F., Eagle, M., Ivy, A., Wankel, S.D., 2004. Using sulfur isotopes to elucidate the origin of barite associated with high organic matter accumulation events in marine sediments. Geological Society of America Special Papers 379, 151-160.

Paytan, A., Mearon, S., Cobb, K., Kastner, M., 2002. Origin of marine barite deposits: Sr and S isotope characterization. Geology 30, 747-750.

Pérez-Folgado, M., Sierro, F.J., Flores, J.A., Cacho, I., Grimalt, J.O., Zahn, R., Shackleton, N., 2003. Western Mediterranean planktonic foraminifera events and millennial climatic variability during the last 70 kyr. Marine Micropaleontology 48, 49-70.

Peteet, D., 1995. Global Younger Dryas? Quaternary International 28, 93-104.

Peyrillé, P., Lafore, J.P., 2007. An idealized two-dimensional framework to study the West African Monsoon. Part II: Large-scale advection and the diurnal cycle. Journal of the Atmospheric Sciences 64, 2783-2803.

Pin, C., Briot, D., Bassin, C., Poitrasson, F., 1994. Concomitant separation of strontium and samarium-neodymium for isotopic analysis in silicate samples, based on specific extraction chromatography. Analytica Chimica Acta 298, 209-217.

Plewa, K., Meggers, H., Kasten, S., 2006. Barium in sediments off northwest Africa: A tracer for paleoproductivity or meltwater events? Paleoceanography 21.

Powell, W.G., Johnston, P.A., Collom, C.J., 2003. Geochemical evidence for oxygenated bottom waters during deposition of fossiliferous strata of the Burgess Shale Formation. Palaeogeography, Palaeoclimatology, Palaeoecology 201, 249-268.

Prahl, F.G., Mix, A.C., Sparrow, M.A., 2006. Alkenone paleothermometry: Biological lessons from marine sediment records off western South America. Geochimica et Cosmochimica Acta 70, 101-117.

Prahl, F.G., Muehlhausen, L.A., Zahnle, D.L., 1988. Further evaluation of long-chain alkenones as indicators of paleoceanographic conditions. Geochimica et Cosmochimica Acta 52, 2303-2310.

Prahl, F.G., Wakeham, S.G., 1987. Calibration of unsaturation patterns in long-chain ketone compositions for palaeotemperature assessment. Nature 330, 367-369.

Prospero, J.M., 1981. Aeolian transport to the world ocean. In: Emiliani, C. (Ed.), The Sea, The oceanic lithosphere. John Wiley and Sons, New York, pp. 801-874.

Prospero, J.M., 1996. The Atmospheric transport of particles to the ocean. In: Ittekkot, V., Schäfer, P., Honjo, S., Depetris, J.P. (Eds.), Particle Flux in the Ocean. SCOPE Report 57, John Wiley & Sons, New York, pp.19-52.

Prospero, J.M., 1999. Long-range transport of mineral dust in the global atmosphere: Impact of African dust on the environment of the southeastern United States. Proceedings of the National Academy of Sciences of the United States of America 96, 3396-3403.

Pye, K., 1987. Aeolian Dust and Dust Deposits. Academic Press, London, pp. 334.

Rahmstorf, S., 1995. Bifurcations of the Atlantic thermohaline circulation in response to changes in the hydrological cycle. Nature 378, 145-149.

Rahmstorf, S., 2001. Abrupt climate change. In: Steele, J., Thorpe, S., Turekian, K. (Eds.), Encyclopedia of Ocean Sciences. London: Academic, pp. 1–6.

Rasmussen, S.O., Vinther, B.M., Clausen, H.B., Andersen, K.K., 2007. Early Holocene climate oscillations recorded in three Greenland ice cores. Quaternary Science Reviews 26, 1907-1914.

Reader, M.C., Fung, I., McFarlane, N., 1999. The mineral dust aerosol cycle during the Last Glacial Maximum. Journal of Geophysical Research D: Atmospheres 104, 9381-9398.

Reimer, P.J., Baillie, M.G.L., Bard, E., Bayliss, A., Beck, J.W., Blackwell, P.G., Ramsey, C.B., Buck, C.E., Burr, G.S., Edwards, R.L., Friedrich, M., Grootes, P.M., Guilderson, T.P., Hajdas, I., Heaton, T.J., Hogg, A.G., Hughen, K.A., Kaiser, K.F., Kromer, B., McCormac, F.G., Manning, S.W., Reimer, R.W., Richards, D.A., Southon, J.R., Talamo, S., Turney, C.S.M., van der Plicht, J., Weyhenmeyer, C.E., 2009. INTCAL09 and MARINE09 radiocarbon age calibration curves, 0-50,000 years CAL BP. Radiocarbon 51, 1111-1150.

Renssen, H., Lautenschlager, M., Schuurmans, C.J.E., 1996. The atmospheric winter circulation during the Younger Dryas stadial in the Atlantic/European sector. Climate Dynamics 12, 813-824.

Revel, M., Sinko, J.A., Grousset, F.E., Biscaye, P.E., 1996. Sr and Nd isotopes as tracers of North Atlantic lithic particles: Paleoclimatic implications. Paleoceanography 11, 95-113.

Rimbu, N., Lohmann, G., Lorenze, S.J., Kim, J.H., Schneider, R.R., 2004. Holocene climate variability as derived from alkenone sea surface temperature and coupled ocean-atmosphere model experiments. Climate Dynamics 23, 215-227.

Rodó, X., Baert, E., Comin, F.A., 1997. Variations in seasonal rainfall in Southern Europe during the present century: Relationships with the North Atlantic Oscillation and the El Niño-Southern Oscillation. Climate Dynamics 13, 275-284.

Rodrigo-Gámiz, M., Martínez-Ruiz, F., Jiménez-Espejo, F.J., Gallego-Torres, D., Nieto-Moreno, V., Romero, O., Ariztegui, D., 2011. Impact of climate variability in the western Mediterranean during the last 20,000 years: Oceanic and atmospheric responses. Quaternary Science Reviews 30, 2018-2034.

Rodrigo-Gámiz, M., Martínez-Ruiz, F., Rodríguez-Tovar, F.J., Jiménez-Espejo, F.J., Pardo-Igúzquiza, E. Forcing mechanisms of climate variability in the western Mediterranean: millennial- to centennial-scale periodicities for the past 20,000 yrs. Submitted to Global and Planetary Change.

Rodríguez-Tovar, F.J., Reolid, M., Pardo-Igúzquiza, E., 2010. Planktonic versus benthic foraminifera response to Milankovitch forcing (Late Jurassic, Betic Cordillera): Testing methods for cyclostratigraphic analysis. Facies 56, 459-470.

Rodríguez, J., Blanco, J.M., Jiménez-Gómez, F., Echevarría, F., Gil, J., Rodríguez, V., Ruiz, J., Bautista, B., Guerrero, F., 1998. Patterns in the size structure of the phytoplankton community in the deep fluorescence maximum of the Alboran Sea (southwestern Mediterranean). Deep-Sea Research Part I: Oceanographic Research Papers 45, 1577-1593.

Rodríguez, S., Querol, X., Alastuey, A., Kallos, G., Kakaliagou, O., 2001. Saharan dust contributions to PM10 and TSP levels in Southern and Eastern Spain. Atmospheric Environment 35, 2433-2447.

Rogerson, M., Cacho, I., Jiménez-Espejo, F., Reguera, M.I., Sierro, F.J., Martínez-Ruiz, F., Frigola, J., Canals, M., 2008. A dynamic explanation for the origin of the western Mediterranean organic-rich layers. Geochemistry, Geophysics, Geosystems 9.

Rogerson, M., Rohlin, E.J., Weaver, P.P.E., 2006. Promotion of meridional overturning by Mediterranean-derived salt during the last deglaciation. Paleoceanography 21.

Rognon, P., Coudé-Gaussen, G., Bergametti, G., Gomes, L., 1989. Relationship between the characteristics of soils, the wind energy and dust near the ground in the western sandsea. In: Leinen, M., Sarnthein, M. (Eds.), Paleoclimatology and Paleometeorology: Modern and Past Patterns of Global Atmospheric Transport. Kluwer Academic Publishers, Dordrecht, The Netherlands, pp. 359-383.

Rohling, E.J., Hayes, A., De Rijk, S., Kroon, D., Zachariasse, W.J., Eisma, D., 1998. Abrupt cold spells in the northwest Mediterranean. Paleoceanography 13, 316-322.

Rohling, E.J., Mayewski, P.A., Abu-Zied, R., Casford, J., Hayes, A., 2002. Holocene atmosphere-ocean interactions: records from Greenland and the Aegean Sea. Climate Dynamics 18, 587-593.

Rohling, E.J., Mayewski, P.A., Challenor, P., 2003. On the timing and mechanism of millennial-scale climate variability during the last glacial cycle. Climate Dynamics 20, 257-267.

Rohling, E.J., Pälike, H., 2005. Centennial-scale climate cooling with a sudden cold event around 8,200 years ago. Nature 434, 975-979.

Rowell, D.P., 2003. The impact of Mediterranean SSTs on the Sahelian rainfall season. Journal of Climate 16, 849-862.

12. References

Ruddiman, W.F., 2001. Earth's Climate: Past and Future. Freeman, W.H., and company. New York, pp. 465.

Rutten, A., De Lange, G.J., 2003. Sequential extraction of iron, manganese and related elements in S1 sapropel sediments, eastern Mediterranean. Palaeogeography, Palaeoclimatology, Palaeoecology 190, 79-101.

Sánchez Goñi, M.F., Cacho, I., Turon, J., Guiot, J., Sierro, F., Peypouquet, J., Grimalt, J., Shackleton, N., 2002. Synchroneity between marine and terrestrial responses to millennial scale climatic variability during the last glacial period in the Mediterranean region. Climate Dynamics 19, 95-105.

Sánchez Goñi, M.F., Landais, A., Fletcher, W.J., Naughton, F., Desprat, S., Duprat, J., 2008a. Contrasting impacts of Dansgaard-Oeschger events over a western European latitudinal transect modulated by orbital parameters. Quaternary Science Reviews 27, 1136-1151.

Sánchez Goñi, M.F., Landais, A., Fletcher, W.J., Naughton, F., Desprat, S., Duprat, J., 2008b. Corrigendum to "Contrasting impacts of Dansgaars-Oeschger events over a western European latitudinal transect modulated by orbital parameters" [Quat. Sci. Rev. 27 (11-12) (2008) 1136-1151] (DOI:10.1016/j.quascirev.2008.03.003). Quaternary Science Reviews 27, 1789.

Sarnthein, M., Thiede, U., Pflaumann, H., Erlenkeuser, D., Fütterer, D., Koopmann, H., Lange, H., Seibold, E., 1982. Atmospheric circulation patterns off northwest Africa during the last 25 million years. In: von Rad, U., Hinz, K., Sarnthein, M., Seibold, E. (Eds.), Geology of the Northwest African Continental Margin. Springer, New York, pp. 584-604.

Sarkar, A., Ramesh, R., Somayajulu, B.L.K., Agnihotri, R., Jull, A.J.T., Burr, O.S., 2000. High resolution Holocene monsoon record from the eastern Arabian Sea. Earth and Planetary Science Letters 177, 209-218.

Scargle, J.D., 1982. Studies in astronomical time series analysis. II. Statistical aspects of spectral analysis of unevenly spaced data. Astrophysical Journal 263, 835-853.

Schmiedl, G., Kuhnt, T., Ehrmann, W., Emeis, K.C., Hamann, Y., Kotthoff, U., Dulski, P., Pross, J., 2010. Climatic forcing of eastern Mediterranean deep-water formation and benthic ecosystems during the past 22 000 years. Quaternary Science Reviews 29, 3006-3020.

Schouten, S., Hopmans, E.C., Schefuß, E., Sinninghe Damsté, J.S., 2002. Distributional variations in marine crenarchaeotal membrane lipids: A new tool for reconstructing ancient sea water temperatures? Earth and Planetary Science Letters 204, 265-274.

Schouten, S., Huguet, C., Hopmans, E.C., Kienhuis, M.V.M., Sinninghe Damsté, J.S., 2007. Analytical methodology for TEX86 paleothermometry by high-performance liquid chromatography/atmospheric pressure chemical ionization-mass spectrometry. Analytical Chemistry 79, 2940-2944.

Schulz, M., Prange, M., Klocker, A., 2007. Low-frequency oscillations of the Atlantic Ocean meridional overturning circulation in a coupled climate model. Climate of the Past 3, 97-107.

Seidov, D., Maslin, M., 1999. North-Atlantic deep water circulation collapse during Heinrich events. Geology 27, 23-26.

Send, U., Font, J., Krahmann, G., Millot, C., Rhein, M., Tintoré, J., 1999. Recent advances in observing the physical oceanography of the Western Mediterranean Sea. Progress in Oceanography 44, 37-64.

Serrano, F., González-Donoso, J.M., Palmqvist, P., Guerra-Merchán, A., Linares, D., Pérez-Claros, J.A., 2007. Estimating Pliocene sea-surface temperatures in the Mediterranean: An approach based on the modern analogs technique. Palaeogeography, Palaeoclimatology, Palaeoecology 243, 174-188.

Sierro, F.J., Hodell, D.A., Curtis, J.H., Flores, J.A., Reguera, I., Colmenero-Hidalgo, E., Bárcena, M.A., Grimalt, J.O., Cacho, I., Frigola, J., Canals, M., 2005. Impact of iceberg melting on Mediterranean thermohaline circulation during Heinrich events. Paleoceanography 20, 1-13.

Sirocko, F., 1996. Past and present subtropical summer monsoons. Science 274, 937-938.

Sirocko, F., Garbe-Schönberg, D., McIntyre, A., Molfino, B., 1996. Teleconnections between the subtropical monsoons and high-latitude climates during the last deglaciation. Science 272, 526-529.

Skliris, N., Sofianos, S., Lascaratos, A., 2007. Hydrological changes in the Mediterranean Sea in relation to changes in the freshwater budget: A numerical modelling study. Journal of Marine Systems 65, 400-416.

Solomon, S., Qin, D., Manning, M., Chen, Z., Marquis, M., Averyt, K.B., Tignor, M. and Miller, H.L., 2007. Climate Change 2007: The Physical Science Basis. Contribution of Working Group I to the Fourth Assessment Report of the Intergovenmental Panle on Climate chang. Cambridge Universtiy Press, Cambridge U.K, and New York, U.S.A.

Spang, A., Hatzenpichler, R., Brochier-Armanet, C., Rattei, T., Tischler, P., Spieck, E., Streit, W., Stahl, D.A., Wagner, M., Schleper, C., 2010. Distinct gene set in two different lineages of ammonia-oxidizing archaea supports the phylum Thaumarchaeota. Trends in Microbiology 18, 331-340.

Sparnocchia, S., Manzella, G.M.R., La Violette, P.E., 1994. The Interannual and Seasonal Variability of the MAW and LIW Core Properties in the Western Mediterranean Sea. In: La Violette, P.E. (Ed.), Seasonal and Interannual Variability of the Western Mediterranean Sea vol. 46. Coastal and Estuarine Studies, AGU, Washington, D.C., pp. 177-194.

Stager, J.C., Ryves, D.B., Chase, B.M., Pausata, F.S.R., 2011. Catastrophic drought in the Afro-Asian monsoon region during Heinrich event 1. Science 331, 1299-1302.

Stocker, T.F., 2000. Past and future reorganizations in the climate system. Quaternary Science Reviews 19, 301-319.

Stott, L., Cannariato, K., Thunell, R., Haug, G.H., Koutavas, A., Lund, S., 2004. Decline of surface temperature and salinity in the western tropical Pacific Ocean in the Holocene epoch. Nature 430, 56-59.

Stuiver, M., Grootes, P.M., 2000. GISP2 oxygen isotope ratios. Quaternary Research 53, 277-284.

Stuiver, M., Grootes, P.M., Braziunas, T.F., 1995. The GISP2 δ18O Climate Record of the Past 16,500 Years and the Role of the Sun, Ocean, and Volcanoes. Quaternary Research 44, 341-354.

Stuiver, M., Reimer, P.J., 1993. Extended 14C data base and revised CALIB 3.0 14C age calibration program. Radiocarbon 35, 215-230.

Stumpf, R., Frank, M., Schönfeld, J., Haley, B.A., Climatically driven changes in sediment supply on the SW Iberian shelf since the Last Glacial Maximum. Earth and Planetary Science Letters 312, 80-90.

Sumner, G., Homar, V., Ramis, C., 2001. Precipitation seasonality in eastern and southern coastal Spain. International Journal of Climatology 21, 219-247.

Swezey, C., 2001. Eolian sediment responses to late Quaternary climate changes: Temporal and spatial patterns in the Sahara. Palaeogeography, Palaeoclimatology, Palaeoecology 167, 119-155.

Tanaka, T., Togashi, S., Kamioka, H., Amakawa, H., Kagami, H., Hamamoto, T., Yuhara, M., Orihashi, Y., Yoneda, S., Shimizu, H., Kunimaru, T., Takahashi, K., Yanagi, T., Nakano, T., Fujimaki, H., Shinjo, R., Asahara, Y., Tanimizu, M., Dragusanu, C., 2000. JNdi-1: A neodymium isotopic reference in consistency with LaJolla neodymium. Chemical Geology 168, 279-281.

Tanaka, T., Chiba, M., 2006. A numerical study of the contributions of dust source regions to the global dust budget. Global and Planetary Change 52, 88-104.

Ternois, Y., Sicre, M.A., Boireau, A., Conte, M.H., Eglinton, G., 1997. Evaluation of long-chain nikenones as paleo-temperature indicators in the mediterranean sea. Deep-Sea Research Part I: Oceanographic Research Papers 44, 271-286.

Thomson, J., Higgs, N.C., Wilson, T.R.S., Croudace, I.W., De Lange, G.J., Van Santvoort, P.J.M., 1995. Redistribution and geochemical behaviour of redox-sensitive elements around S1, the most recent eastern Mediterranean sapropel. Geochimica et Cosmochimica Acta 59, 3487-3501.

Tierney, J.E., Russell, J.M., 2007. Abrupt climate change in southeast tropical Africa influenced by Indian monsoon variability and ITCZ migration. Geophysical Research Letters 34.

Todt, W., Cliff, R.A., Hanser, A., Hofmann, A.W., 1996. Evaluation of a 202Pb-205Pb double spike for high-precision lead isotope analysis. In: Basu, A., Hart, S.R. (Eds.), Earth Processes: Reading the Isotopic Code. Geophysical Monograph 95. American Geophysical Union, pp. 429-437.

Torres-Padrón, M.E., Gelado-Caballero, M.D., Collado-Sánchez, C., Siruela-Matos, V.F., Cardona-Castellano, P.J., Hernández-Brito, J.J., 2002. Variability of dust inputs to the CANIGO zone. Deep-Sea Research Part II: Topical Studies in Oceanography 49, 3455-3464.

Toucanne, S., Mulder, T., Schönfeld, J., Hanquiez, V., Gonthier, E., Duprat, J., Cremer, M., Zaragosi, S., 2007. Contourites of the Gulf of Cadiz: A high-resolution record of the paleocirculation of the Mediterranean outflow water during the last 50,000 years. Palaeogeography, Palaeoclimatology, Palaeoecology 246, 354-366.

Tribovillard, N., Algeo, T.J., Lyons, T., Riboulleau, A., 2006. Trace metals as paleoredox and paleoproductivity proxies: An update. Chemical Geology 232, 12-32.

Trigo, R.M., Osborn, T.J., Corte-Real, J.M., 2002. The North Atlantic Oscillation influence on Europe: Climate impacts and associated physical mechanisms. Climate Research 20, 9-17.

Trouet, V., Esper, J., Graham, N.E., Baker, A., Scourse, J.D., Frank, D.C., 2009. Persistent positive north atlantic oscillation mode dominated the medieval climate anomaly. Science 324, 78-80.

Tuenter, E., Weber, S.L., Hilgen, F.J., Lourens, L.J., 2003. The response of the African summer monsoon to remote and local forcing due to precession and obliquity. Global and Planetary Change 36, 219-235.

Tuenter, E., Weber, S.L., Hilgen, F.J., Lourens, L.J., 2007. Simulating sub-Milankovitch climate variations associated with vegetation dynamics. Climate of the Past 3, 169-180.

Tütken, T., Eisenhauer, A., Wiegand, B., Hansen, B.T., 2002. Glacial-interglacial cycles in Sr and Nd isotopic composition of Arctic marine sediments triggered by the Svalbard/Barents Sea ice sheet. Marine Geology 182, 351-372.

Van der Weijden, C.H., 2002. Pitfalls of normalization of marine geochemical data using a common divisor. Marine Geology 184, 167-187.

Van Geel, B., Raspopov, O.M., Renssen, H., Van der Plicht, J., Dergachev, V.A., Meijer, H.A.J., 1999. The role of solar forcing upon climate change. Quaternary Science Reviews 18, 331-338.

Viau, A.E., Gajewski, K., Sawada, M.C., Fines, P., 2006. Millennial-scale temperature variations in North America during the Holocene. Journal of Geophysical Research D: Atmospheres 111.

Voelker, A.H.L., Lebreiro, S.M., Schönfeld, J., Cacho, I., Erlenkeuser, H., Abrantes, F., 2006. Mediterranean outflow strengthening during northern hemisphere coolings: A salt source for the glacial Atlantic? Earth and Planetary Science Letters 245, 39-55.

Volkman, J.K., Eghnton, G., Corner, E.D.S., Sargent, J.R., 1980. Novel unsaturated straight-chain C37-C39 methyl and ethyl ketones in marine sediments and a coccolithophorid Emiliania huxleyi. In: Douglas, A.G., Maxwell, J.R. (Eds.), Advances in organic geochemistry 1979. Pergamon Press, Oxford, pp. 219-227.

von Grafenstein, R., Zahn, R., Tiedemann, R., Murat, A., 1999a. Planktonic δ18O records at Site 976 and 977, Alboran Sea: Stratigraphy, forcing, and paleoceanographic implications. Proceedings of the Ocean Drilling Program: Scientific Results 161, 469-479.

von Grafenstein, U., Erlenkeuser, H., Brauer, A., Jouzel, J., Johnsen, S.J., 1999b. A mid-European decadal isotope-climate record from 15,500 to 5000 years B.P. Science 284, 1654-1657.

Wang, L., Sarnthein, M., Erlenkeuser, H., Grootes, P.M., Grimalt, J.O., Pelejero, C., Linck, G., 1999. Holocene variations in Asian monsoon moisture: A bidecadal sediment record from the South China Sea. Geophysical Research Letters 26, 2889-2892.

Wang, Y.J., Cheng, H., Edwards, R.L., An, Z.S., Wu, J.Y., Shen, C.C., Dorale, J.A., 2001. A high-resolution absolute-dated late pleistocene monsoon record from Hulu Cave, China. Science 294, 2345-2348.

Wanner, H., Beer, J., Bütikofer, J., Crowley, T.J., Cubasch, U., Flückiger, J., Goosse, H., Grosjean, M., Joos, F., Kaplan, J.O., Küttel, M., Müller, S.A., Prentice, I.C., Solomina, O., Stocker, T.F., Tarasov, P., Wagner, M., Widmann, M., 2008. Mid- to Late Holocene climate change: an overview. Quaternary Science Reviews 27, 1791-1828.

Wanner, H., Brönnimann, S., Casty, C., Gyalistras, D., Luterbacher, J., Schmutz, C., Stephenson, D.B., Xoplaki, E., 2001. North Atlantic oscillation - Concepts and studies. Surveys in Geophysics 22, 321-382.

Wasserburg, G.J., Jacousen, S.B., DePaolo, D.J., McCulloch, M.T., Wen, T., 1981. Precise determination of Sm Nd ratios, Sm and Nd isotopic abundances in standard solutions. Geochimica et Cosmochimica Acta 45, 2311-2323.

Weber, S.L., Crowley, T.J., van der Schrier, G., 2004. Solar irradiance forcing of centennial climate variability during the Holocene. Climate Dynamics 22, 539-553.

Wehausen, R., Brumsack, H.J., 1999. Cyclic variations in the chemical composition of eastern Mediterranean Pliocene sediments: A key for understanding sapropel formation. Marine Geology 153, 161-176.

Wehausen, R., Brumsack, H.J., 2000. Chemical cycles in Pliocene sapropel-bearing and sapropel-barren eastern Mediterranean sediments. Palaeogeography, Palaeoclimatology, Palaeoecology 158, 325-352.

Weijers, J.W.H., Schouten, S., Spaargaren, O.C., Sinninghe Damsté, J.S., 2006. Occurrence and distribution of tetraether membrane lipids in soils: Implications for the use of the TEX86 proxy and the BIT index. Organic Geochemistry 37, 1680-1693.

Weldeab, S., Emeis, K.C., Hemleben, C., Siebel, W., 2002a. Provenance of lithogenic surface sediments and pathways of riverine suspended matter in the Eastern Mediterranean Sea: Evidence from 143Nd/144Nd and 87Sr/86Sr ratios. Chemical Geology 186, 139-149.

Weldeab, S., Emeis, K.C., Hemleben, C., Vennemann, T.W., Schulz, H., 2002b. Sr and Nd isotope composition of Late Pleistocene sapropels and nonsapropelic sediments from the Eastern Mediterranean Sea: Implications for detrital influx and climatic conditions in the source areas. Geochimica et Cosmochimica Acta 66, 3585-3598.

Weldeab, S., Siebel, W., Wehausen, R., Emeis, K.C., Schmiedl, G., Hemleben, C., 2003. Late Pleistocene sedimentation in the Western Mediterranean Sea: Implications for productivity changes and climatic conditions in the catchment areas. Palaeogeography, Palaeoclimatology, Palaeoecology 190, 121-137.

Willis, K.J., Kleczkowski, A., Briggs, K.M., Gilligan, C.A., 1999. The role of sub-Milankovitch climatic forcing in the initiation of the Northern Hemisphere glaciation. Science 285, 568-571.

Wuchter, C., Schouten, S., Coolen, M.J.L., Sinninghe Damsté, J.S., 2004. Temperature-dependent variation in the distribution of tetraether membrane lipids of marine Crenarchaeota: Implications for TEX86 paleothermometry. Paleoceanography 19, 1-10.

Wuchter, C., Schouten, S., Wakeham, S.G., Damsté, J.S., 2006. Archaeal tetraether membrane lipid fluxes in the northeastern Pacific and the Arabian Sea: Implications for TEX86 paleothermometry. Paleoceanography 21.

12. References

Wuchter, C., Schouten, S., Wakeham, S.G., Sinninghe Damsté, J.S., 2005. Temporal and spatial variation in tetraether membrane lipids of marine Crenarchaeota in particulate organic matter: Implications for TEX86 paleothermometry. Paleoceanography 20, 1-11.

13. Appendix I | Core photos and core log

Core photos

Core 293G

Core photo on deck right after recovery and splitting

Core 293G

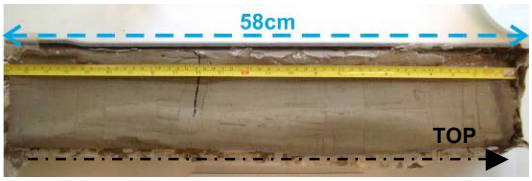

Section 1

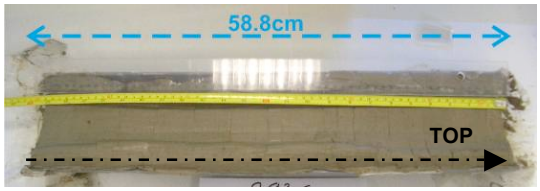

Section 2

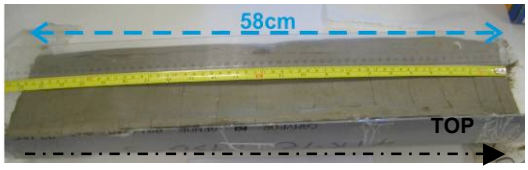

Section 3

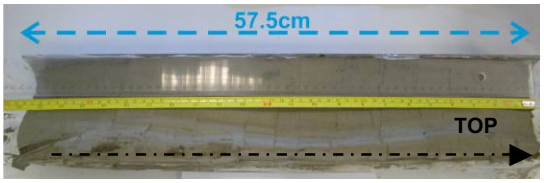

Section 4

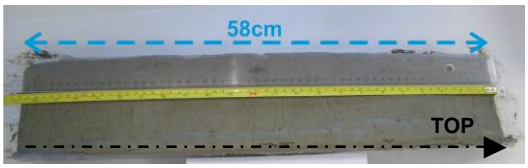

Section 5

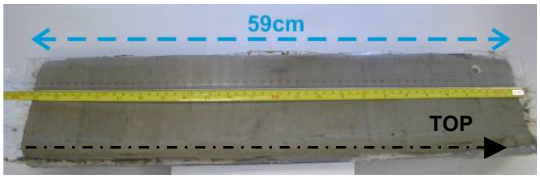

Section 6

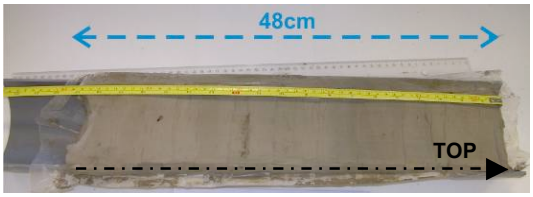

Section 7

Core sections photos taken before sampling

CORE LOG. R/V Professor Logachev TTR-12 Leg 3 (Alboran Sea).

Pelagic core 293G, Latitude 36´10.414N, Longitude 2`26.071W, Water Depth 1840m.

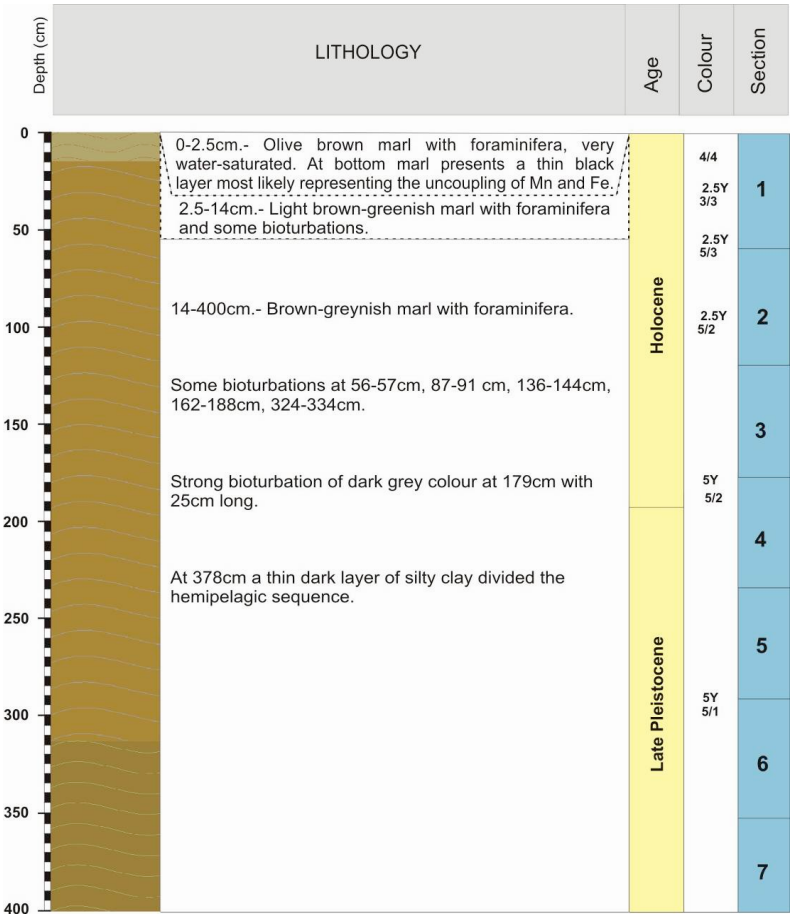

Core 434G

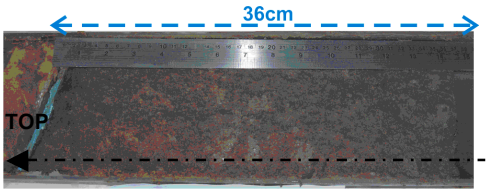

Section 0

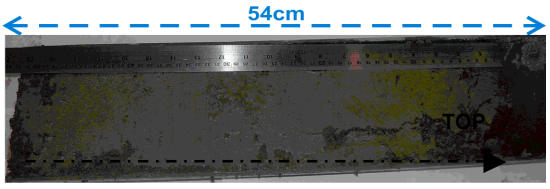

Section 1

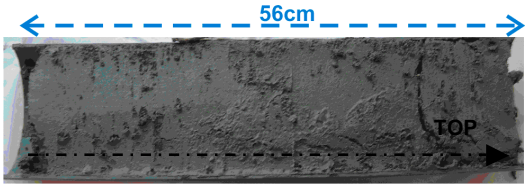

Section 2

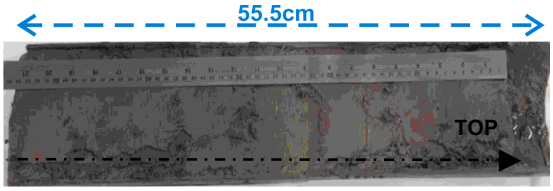

Section 3

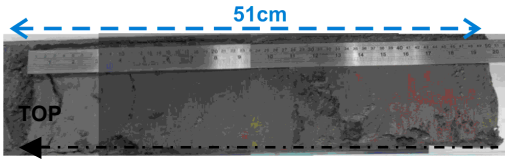

Section 4

Core sections photos taken before sampling

14. Appendix II | Electron microscope photographs from TEM and FESEM

TEM photographs showing sediment particles including palygorskite fibers. Both palygorskite and sepiolite are used as reliable proxies for eolian input from the African margin during arid periods.

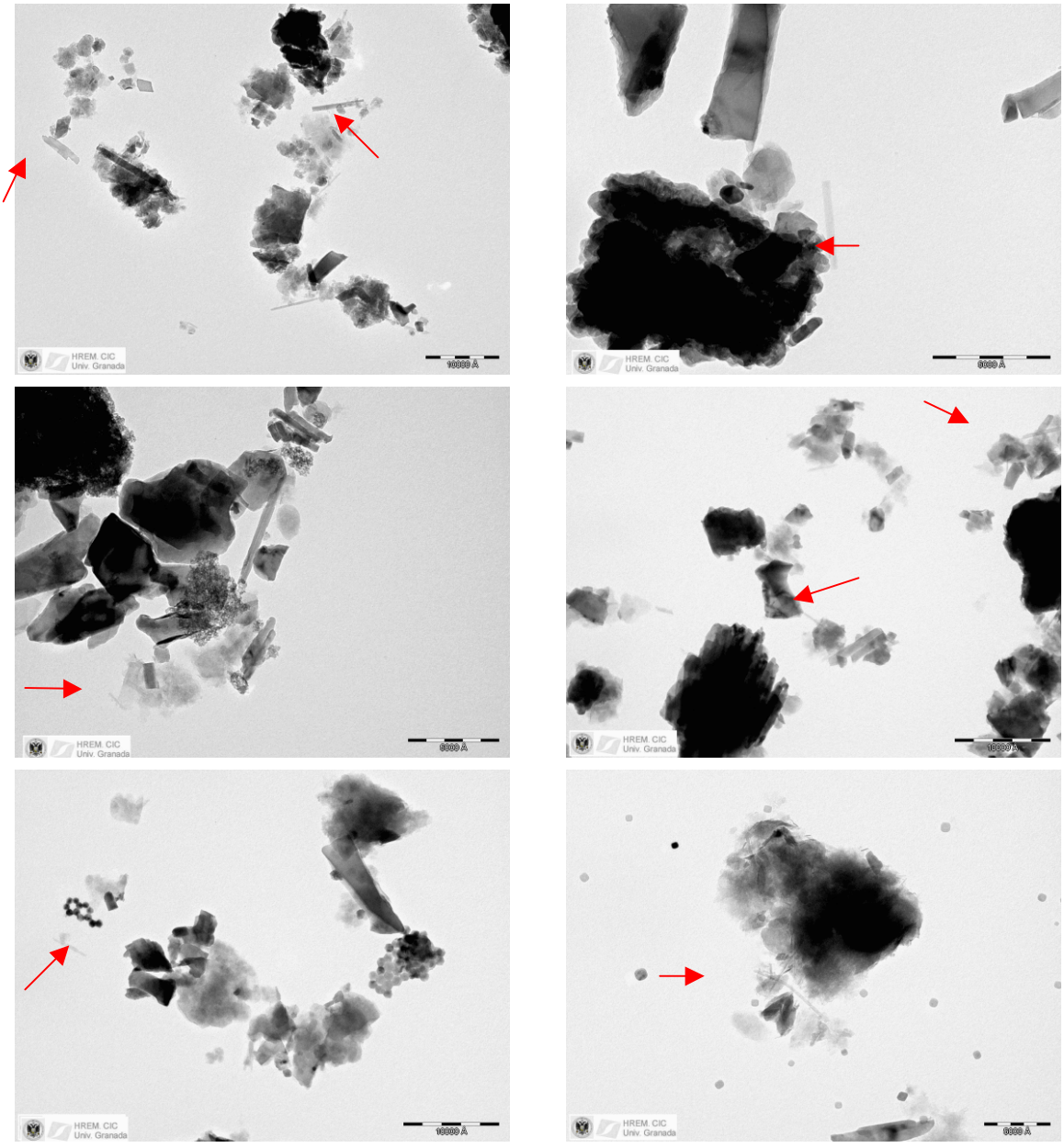

TEM photographs showing sediment particles including palygorskite fibers. Both palygorskite and sepiolite are used as reliable proxies for eolian input from the African margin during arid periods.

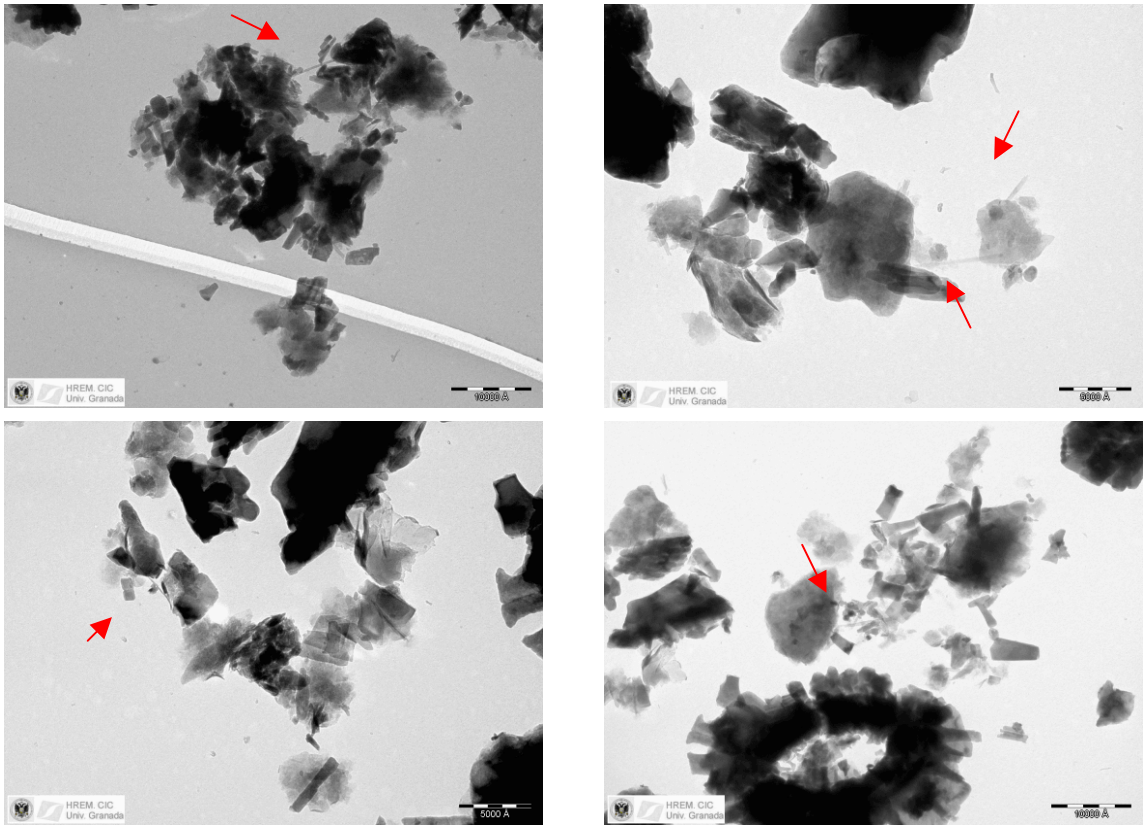

FESEM photographs showing authigenic marine barite from Ba-rich intervals, which shows size and morphologies corresponding to typical marine barite observed in high productivity regions.

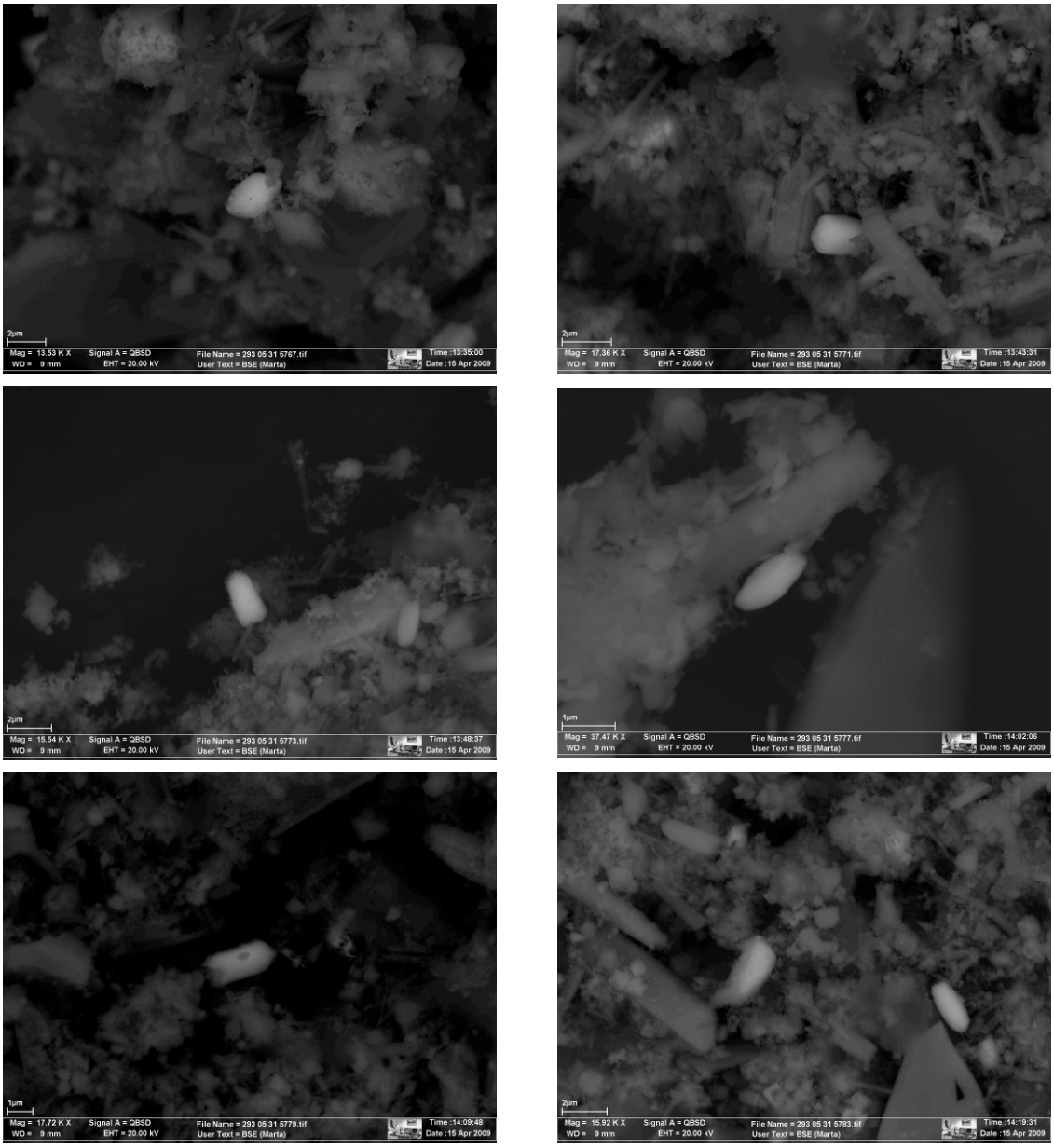

FESEM photographs showing authigenic marine barite from Ba-rich intervals, which shows size and morphologies corresponding to typical marine barite observed in high productivity regions.

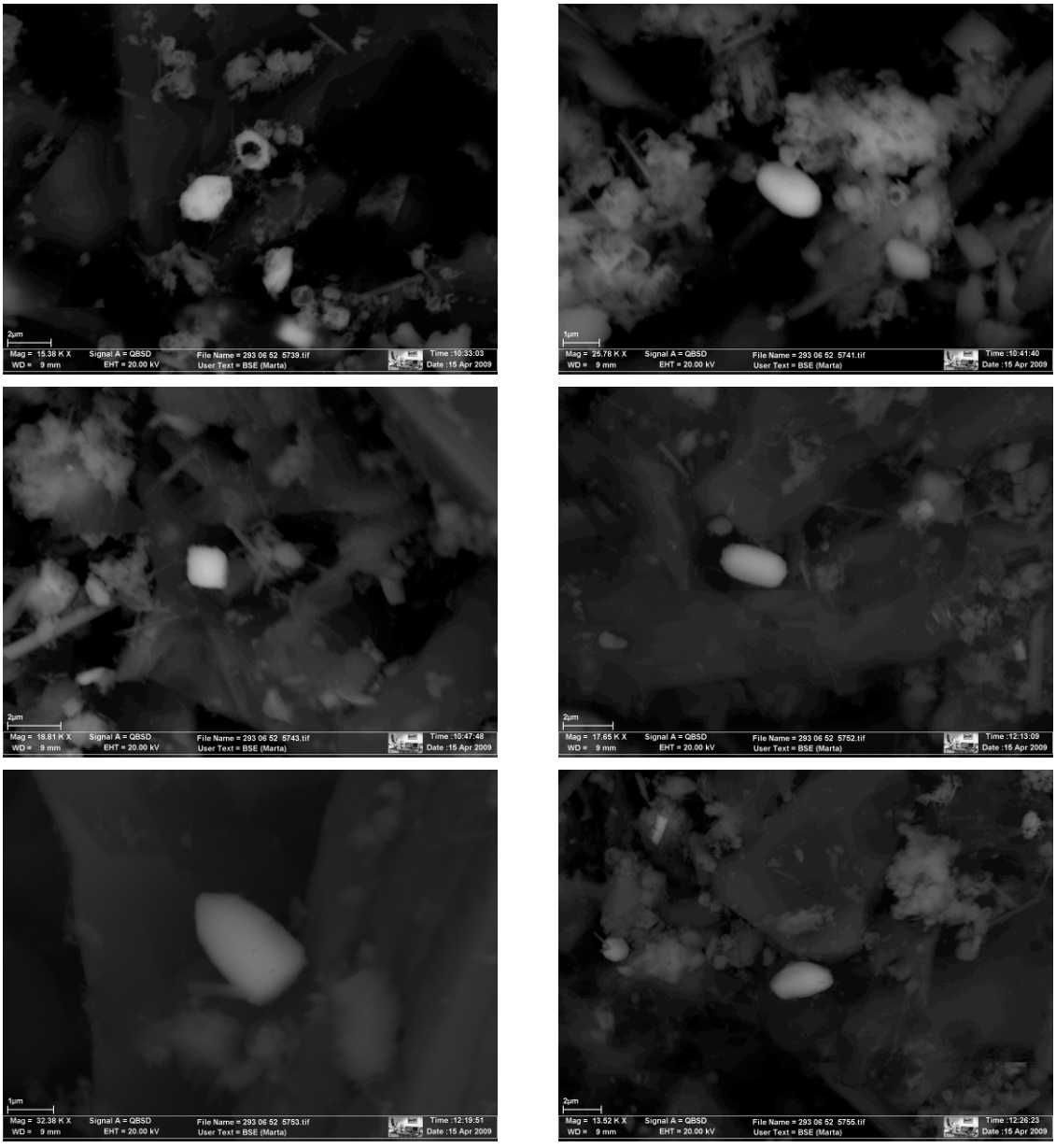

FESEM photographs showing main mineral components of the analyzed sediments: clay minerals, quartz, calcite/foraminifera and minor proportions of feldspars and pyrite framboids.

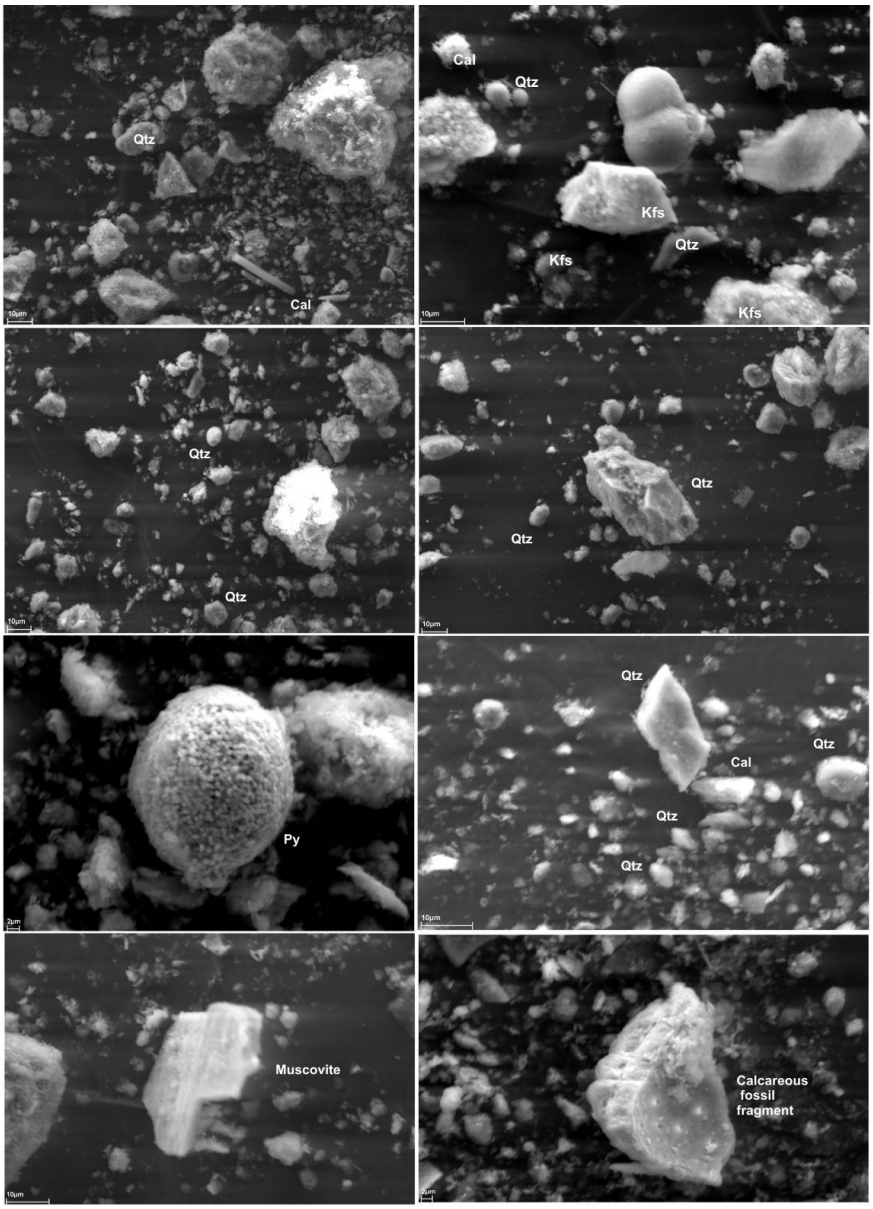

FESEM photographs showing main mineral components of the analyzed sediments: clay minerals, quartz, calcite/foraminifera and minor proportions of feldspars and pyrite framboids.

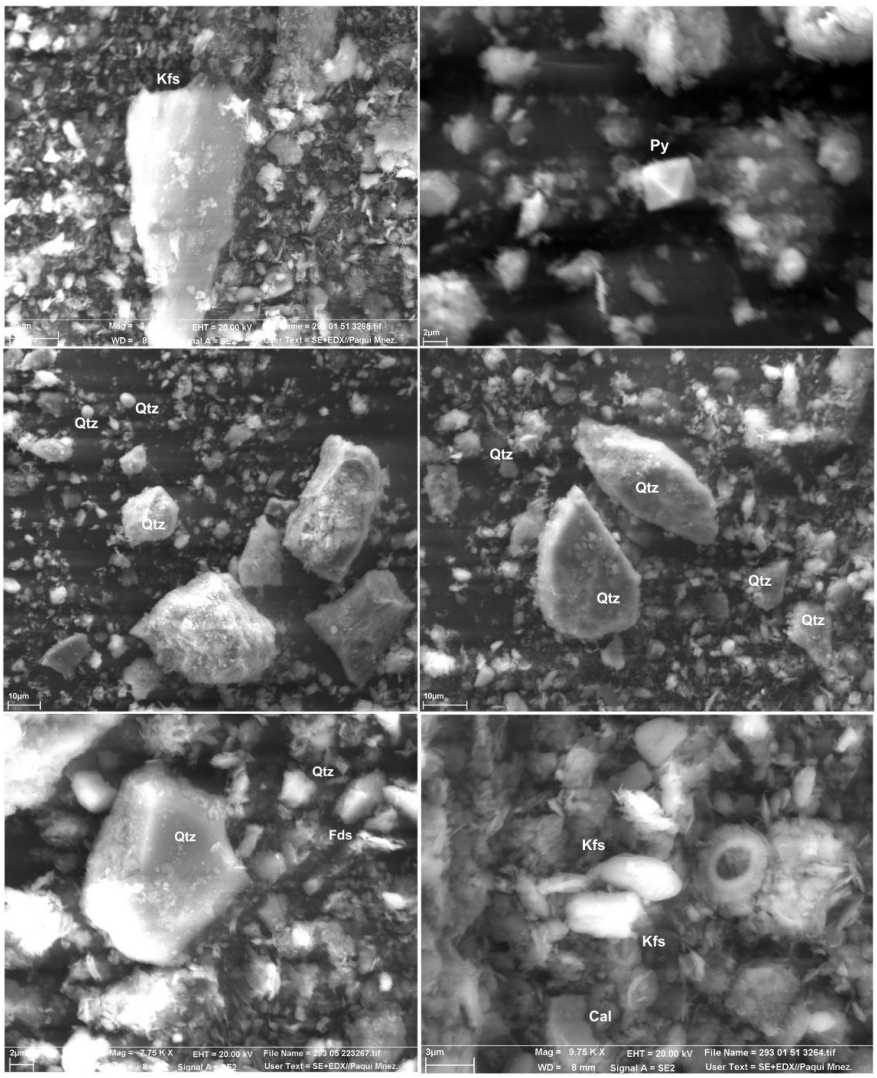

15. Appendix III | Other publications derived from this study

· Martín-Puertas, C., Jiménez-Espejo, F., Martínez-Ruiz, F., Nieto-Moreno, V., **Rodrigo, M.**, Mata, Valero-Garcés, B.L., 2010. Late Holocene climate variability in the southwestern Mediterranean region: an integrated marine and terrestrial geochemical approach. Climate of the Past 6, 807-816. doi:10.5194/cp-6-807-2010

· Cortés Sánchez, M., Morales Muñiz, A., Simón Vallejo, M.D., Lozano Francisco, M.C., Vera Peláez, J.L., Finlayson, C., Rodríguez Vidal, J., Delgado Huertas, A., Jiménez-Espejo, F.J., Martínez-Ruiz, F., Martínez Aguirre, M.A., Pascual Granged, A., Bergadà Zapata, M.M., Gibaja Bao, J.F., Riquelme Cantal, J.A., López Sáez, J.A., **Rodrigo-Gámiz, M.**, Sakai, S., Sugisaki, S., Finlayson, G., Fa, D.A., Bicho, N.F., 2011. Earliest Known Use of Marine Resources by Neanderthals. PLoS ONE 6(9), e24026. doi:10.1371/journal.pone.0024026

· Cortés Sánchez, M., Jiménez Espejo, F.J., Simón Vallejo, M.D., Gibaja Bao, J.F., Faustino Carvalho, A., Martínez-Ruiz, F., **Rodrigo-Gámiz, M.**, Flores, J.A., Paytan, A., López Sáez, J.A., Peña-Chocarro, L., Carrión, J.S., Morales Muñiz, A., Roselló Izquierdo, E., Riquelme Cantal, J.A., Dean, R.M., Salgueiro, E., Martínez Sánchez, R.M., De la Rubia de Gracia, J.J., Lozano Francisco, M.C., Vera Peláez, J.L., Bicho, N.F. The Mesolithic-Neolithic transition in southern Iberia. Quaternary Research, accepted (June 2011).

· Nieto-Moreno, V., Martínez-Ruiz, F., Giralt, S., Jiménez-Espejo, F., Gallego-Torres, D., **Rodrigo-Gámiz, M.**, García-Orellana, J., Ortega-Huertas, M., de Lange, G.J., 2011. Tracking climate variability in the western Mediterranean during the Late Holocene: a multiproxy approach. Climate of the Past 7, 1-20. doi:10.5194/cp-7-1-2011.

· Moreno, A., Pérez, A., Frigola, J., Nieto-Moreno, V., **Rodrigo-Gámiz, M.**, González-Sampériz, P., Morellón, M., Martín-Puertas, C., Corella, J.P., Belmonte, Á., Sancho, C., Cacho, I., Herrera, G., Canals, M., Jiménez-Espejo, F., Martínez-Ruiz, F., Vegas, T., Valero-Garcés, B.L. The Medieval Climate Anomaly in the Iberian Peninsula reconstructed from a compilation of marine and lake records. Quaternary Science Reviews, accepted (November 2011).

· Jiménez-Espejo, F.J., Rodríguez-Vidal, J., Finlayson, C., Martínez-Ruiz, F., Carrión, J.S., Paytan, A., Cortes-Sánchez, M., **Rodrigo-Gámiz, M.**, González-Donoso, J.M., Linares, M.D., Cáceres, L.M., Fernández, S., Iijima, K., Martínez Aguirre, A., Ortega Huertas, M. Environmental conditions during the transition between Homo sapiens neanderthalensis and Homo sapiens sapiens in the South Iberian Peninsula. Submitted to Quaternary Research.